Evolution of pyruvate kinase in the long-term evolution experiment of *Escherichia coli*:

A structure/function study

Tong Zhu

2008

Evolution of pyruvate kinase in the long-term evolution experiment of *Escherichia coli*: A structure/function study

A thesis presented in partial fulfilment of the requirements for the degree of

Master of Science

in

Biochemistry

at University of Canterbury, Christchurch, Canterbury

New Zealand

Tong Zhu

2008

Abstract

This thesis examines *Escherichia coli* pyruvate kinase type 1 (PK1), a regulatory enzyme core to energy metabolism. Specifically, this thesis characterises a series of mutations in PK1 that were found when populations of *E. coli* were evolved in a glucose-limited environment for 20,000 generations. The gene *pykF*, which codes for the PK1 enzyme, was found to have developed nonsynonymous mutations in all replicate populations. Although the mutations at the nucleotide level were not the same (i.e. not parallel), it is not clear whether parallel adaptation exists at the protein structure/function level. This study aimed to address this question by investigating the kinetic and biophysical properties of the wild-type and seven mutant enzymes.

The recombinant wild-type PK1 enzyme used in this study was found to have steady state kinetics consistent with those previously reported. Unlike the rabbit kidney PK enzyme, *E. coli* PK1 was shown to have a very tight tetrameric structure (picomolar range), which was not affected by the enzyme's substrates (PEP and ADP), or the allosteric effector (FBP), as judged by analytical ultracentrifugation with fluorescence detection.

The mutated residues were highly conserved, and found to fall loosely into three groups: those at the active site (P70T, P70Q and D127N); those at the subunit interface (I264F, A301T and A301S); and at the allosteric binding site (G381A). The seven mutated PK1 enzymes were obtained by mutagenesis followed by protein purification. Steady state kinetic analysis showed that the mutated enzymes displayed a variety of functional changes, suggesting that the populations had not evolved in a parallel manner at the enzyme structure/function level.

Mutations within the active site (P70T, P70Q and D127N) all showed a decrease in catalytic potency. P70 is located at the hinge connecting the A and B domains, which forms the active site. PK1-P70Q showed strong cooperative binding to PEP, similar to the wild-type enzyme, in the absence of FBP, whereas PK1-P70T had little cooperativity, suggesting changes in the active site. PK1-D127N showed severely attenuated activity, suggesting, for the first time, that this residue is essential for catalysis. Mutations at the subunit interface (I264F, A301T and A301S) all showed altered allosteric regulation, suggesting that this interface is important in the FBP allosteric response. PK1-I264F, which had lower activity, but greater affinity for PEP, displayed a decreased α-helix content (as judged by CD), indicating that a subunit interface helix that includes this residue had altered. Despite still having a similar response to FBP, PK1-G381A showed an increased affinity for PEP, which, together with an increased α-helix content, suggests that this mutation had changed the structure of the FBP binding domain. None of the mutated enzymes showed altered quaternary structure.

Although the populations evolved parallel changes with respect to cell physiology, fitness, and gene expression, this study suggests, for the first time, that the populations have not evolved in a parallel way with respect to protein structure and function.

Acknowledgement

Thank you to my supervisor Juliet Gerrard for all the help. You have provided great learning environment and introduced me to some great people along the way. Thanks for giving me the opportunity to do experiments in Melbourne last summer and to the Lorne conference (twice!). Also thanks for the wonderful finishing party.

Thank you to my associate-supervisor Renwick Dobson. You were always there to help. Thanks for introducing me to Perugini group in Bio21, University of Melbourne. I enjoyed working with you in Melbourne last summer and got many results. Thanks for the congratulation champagne!

Thank you to my associate-supervisors Tim Cooper and Jack Heinemann, for all the support and the advices gave in cell biology and evolution biology. Thanks to Tim for all the great ideas about this thesis topic, and to Jack for the critical comments.

Thanks to all the people in the Gerrard group (the purple team). It has been enjoyable to be able to work with the greatest team in the world. Special thanks to Sean Devenish for always be willing to help me out, be so patient to explain things, and much more.

Thanks to Matt Perugini who offered great opportunity for me to do research in Melbourne last summer. I really enjoyed working with people in the Perugini group and got heaps results. Special thanks to Michael Bailey who introduced me the amazing AUC-FDS technology and guided me all the way through the experiments.

Special thanks to Sean Devenish, for being patient to explain everything, for all the advices and numerous help.

Thanks to the purple team, Grant, Andy, Susie, Sophie, Shiva, Jackie, Jerrard and Laura. It is an honour to work with you. Also thanks Matt Walters for images and printing support.

Thanks to my family, mum and dad, for supporting me to live and study in this beautiful country to experience different culture. Whenever I need help, you are always there for me. Thank you to Gaoyuan, my husband, for taking care of me all the time, especially during those late working nights. You have always been supportive. Last but not least, thanks to my beloved dogs, Kaka and Tutu, for all the fun you have brought us in the past two years.

Table of contents

Abbreviations

amu	Atomic mass unit
A	Signal intensity in fluorescence detection system
A_{280}	Absorbance of the protein-dye conjugate at 280 nm
A_{max}	Maximal absorbance
$A_{protein}$	Protein absorbance
ADP	Adenosine diphosphate
Amp	Ampicillin
ATP	Adenosine triphosphate
AUC	Analytical ultracentrifugation
AUC-FDS	AUC coupled fluorescence detection system
bp	Base pair
c	Weight concentration of the solute
cm	Centimetre
c(s)	Sedimentation coefficient distribution
CD	Circular dichroism
°C	Degree Celsius
Da	Dalton
dH_2O	Distilled water
ddH_2O	Double distilled water (sterilised distilled water)
DNA	Deoxyribonucleic acid
dNTP	Deoxyribonucleotide triphosphate
DOL	Degree of labelling
EDTA	Ethylene diamine tetra-acetic acid (disodium salt)
DMF	Dimethylformamide
ESMS	Electrospray mass spectrometry

ε	Weight extinction coefficient of the solute
f/f_0	Friction ratio
F	The intensity of AUC-FDS
FBP	Fructose-1,6-biosphosphate
FC	Fluorescence count
FGA	Fixed gain amplifier
g	Gram
hokB/sokB	An *E. coli* locus (not discussed in this study)
H	Mass of a proton
HCl	Hydrochloric acid
HEPES	N-2-hydroxyethylpiperazine-N'-2-ethane-sulfonic acid
I_o	Intensity of the beam light
IPTG	Isopropyl-1-thio-β-D-galactopyranoside
kb	Kilo base
k_{cat}	Turnover number
KCl	Potassium chloride
kDa	Kilo Dalton
K_D	Dissociation coefficient
K_M	Michaelis coefficient
l	Sample pathlength
LDH	Lactate dehydrogenase
LB	Luria-Bertani
$MgCl_2$	Magnesium chloride
$MgSO_4$	Magnesium sulphate
mg	Milligram
min	Minute
ml/l	Millilitre per litre
µM	Micromolar
µmole	Micromole

µg	Microgram
mM	Millimolar
M	Molar
MES	2-(N-morpholino)ethanesulfonic acid
MOPS	3-(N-Morpholino) propanesulfonic acid
MW	Molecular weight
m/z	Mass to charge ratio
NaCl	Sodium chloride
NaN_3	Sodium azide
NaOH	Sodium hydroxide
n	Integer number of charges on ions
nadR	NAD biosynthesis regulator
nm	Nanometre
n.m.r.s.d.	Normalised root mean square deviation
$(NH_4)_2SO_4$	Ammonium sulphate
NAD	Nicotinamide adenine dinucleotide
NADH	Nicotinamide adenine dinucleotide, reduced form
NMR	Nuclear magnetic resonance
nadR	Gene codes for nadR in NAD biosynthesis
n_H	Hill coefficient
ŋ	Buffer viscosity
OD_{600}	Optical density at 600 nm
pbpA-rodA	An *E. coli* locus
P	Poise
PACT	pH-, anion- and cation-testing
PAGE	Polyacrylamide gel electrophoresis
PCR	Polymerase chain reaction
PEG	Polyethyleneglycol
PEP	Phosphoenolpyruvate

pI	Isoelectric point
P	Standard deviation
PK	Pyruvate kinase
PKM1	Mammalian muscle pyruvate kinase type 1
PKM2	Mammalian muscle pyruvate kinase type 2
PKRK	Rabbit kidney pyruvate kinase
PK1	Pyruvate kinase type 1
PK2	Pyruvate kinase type 2
PMT	Photomultiplier tube
Psi	Pounds per square inch
pykF	Gene codes for *E. coli* PK1
pykA	Gene codes for *E. coli* PK2
ρ	Density
Q	Quantum field
r.m.s.d.	Root mean square deviation
rpm	Runs per minute
R^2	Adjusted Chi-square
s_{min}	Minimal sedimentation coefficient
s_{max}	Maximal sedimentation coefficient
sec	Second
S	Svedberg, sedimentation coefficient
[S]	Substrate concentration
$S_{0.5}$	Substrate concentration at 1/2 V_{max} (Hill model)
$S_{0.5}^{ADP}$	ADP concentration at 1/2 V_{max}
$S_{0.5}^{PEP}$	PEP concentration at 1/2 V_{max}
SDS	Sodium dodecyl sulphate
SOB	Super Optimal Broth
SOC	Super Optimal broth with Catabolite repression
U	μmole NADH/sec

UV	Ultra violet
V	Volt
V_{max}	Maximum reaction velocity
v	Inital velocity
v-bar	Partial specific volume
v/v	Volume to volume
w/v	Weight to volume
X-gal	5-bromo-4-chloro-3-inolyl-β-D-galactopyranoside
λ_{max}	Maximal wavelength

Chapter 1

Introduction

The work presented in this thesis examines the role of the seven mutations in pyruvate kinase identified from an adaptive evolutionary experiment. The aim is to describe how the mutations have altered the catalytic and/or regulatory mechanisms of pyruvate kinase and relate these back to the adaptive evolution experiment. In this chapter, the background to both the evolution experiment and the structure and function of pyruvate kinase will be discussed. Firstly, the evolutionary background of this study is introduced, followed by an overview of pyruvate kinase from *Escherichia coli*. More detailed information on the structure and function of this enzyme, together with the regulatory pattern, which was core to this research, is then presented. Finally, the sequence and structural positions of the mutants studied in this research are illustrated.

1.1 Lenski's evolutionary experiment

Parallel and convergent changes across lineages are two main themes of evolution (Cooper *et al.* 2003). These different concepts are distinguished on the basis that parallelism describes the changes of homologous features among closely related organisms, whereas convergence occurs in antecedent features among less related organisms (Simpson 1953). Under these situations, derived similarity results from adaptation by natural selection, provided the base pool of all possible changes is so large that the similarity is unlikely to have evolved by a random process (Woods *et al.* 2006). The degree of parallelism is very hard to quantify in a natural system, as it involves the quantification of parallelism in nature (Pelosi *et al.* 2006; Woods *et al.* 2006). Bias in the estimated degree of the parallelism may exist, when the outcomes caused by parallelism are miscounted (downward bias), or the subtle changes in the environment are not included (upward bias) (Woods *et al.* 2006). On the other hand, well designed evolutionary experiments using fast evolving populations (usually viruses or bacteria) provide an excellent tool to study parallelism (Elena & Lenski 2003; Lenski *et al.* 1991; Wichman *et al.* 1999). The

advantage of these systems is that the environment is well controlled and is usually constant and identical for each evolving population (usually derived from a single ancestor to avoid initial genetic difference) and thus all the systematic differences are controlled (Lenski 1991; Lenski *et al.* 1991; Lenski & Travisano 1994).

Two decades ago, Lenski and colleagues began an ongoing evolution study using a bacterial strain of *Escherichia coli* B (Lenski *et al.* 1991). In the founder study, twelve populations of *E. coli* were evolved in a constant glucose-limited environment. The experimental system was designed such that no initial genetic variance existed among the populations, since all the strains arose from a single *E. coli* cell. The experimental environment was kept as uniform and identical as possible. Later studies examined this system for morphological, physiological and genetic changes and found altered morphology (i.e. cell size) and improved mean fitness (determined by competition assays with the ancestor) in all the evolved populations (Cooper & Lenski 2000; Lenski & Travisano 1994) (Figure 1.1).

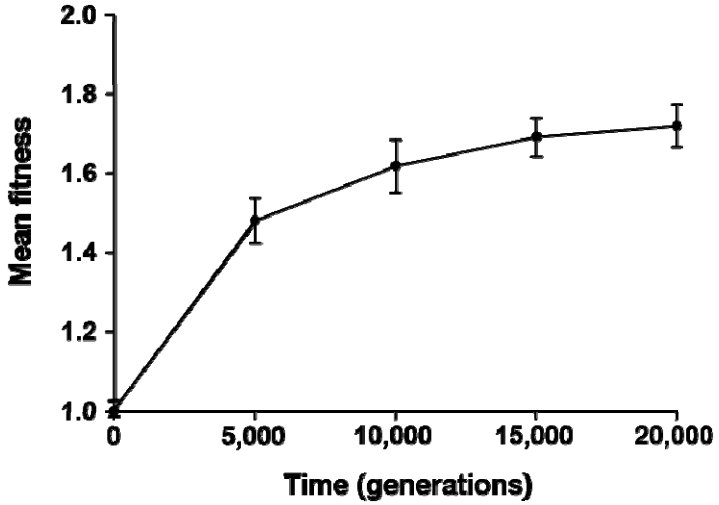

Figure 1.1 **Trajectory of mean fitness of *E. coli* during 20,000 generations in a glucose-limited environment.** Figure was regenerated from (Cooper & Lenski 2000).

The pattern in which the populations evolved also suggested that the independently derived genotypes adapted to the glucose-limited environment by similar changes in physiological mechanisms for glucose utilisation (Travisano & Lenski 1996). Thus, the populations appeared to be evolving in a parallel way.

DNA transcriptional profiles in two populations were examined by DNA expression arrays on all 4,290 genes from the *E. coli* genome (Cooper *et al.* 2003). This expression profile of the *E. coli* genome is a composite phenotype from which parallelism can be assessed (Cooper *et al.* 2003). Remarkably, this research found that the 59 genes with significantly changed expression profile were changed in the same direction relative to the ancestor, again implying parallelism.

A more recent genetic study compared the pattern of mutational substitutions in candidate genes and found that the *pykF* and *nadR* genes had substitutions in all twelve populations (Woods *et al.* 2006) (Figure 1.2). The *pykF* gene codes for the enzyme pyruvate kinase type 1 (PK1), which is a core regulatory enzyme in the glycolytic pathway. Glycolysis is an important pathway for bacterial survival, especially in the glucose-limited environment used in the evolutionary experimental system (Lenski *et al.* 1991). Thus, it would seem that at a genetic level the populations have developed changes in parallel (i.e. the same genes carry persistent mutations in all populations).

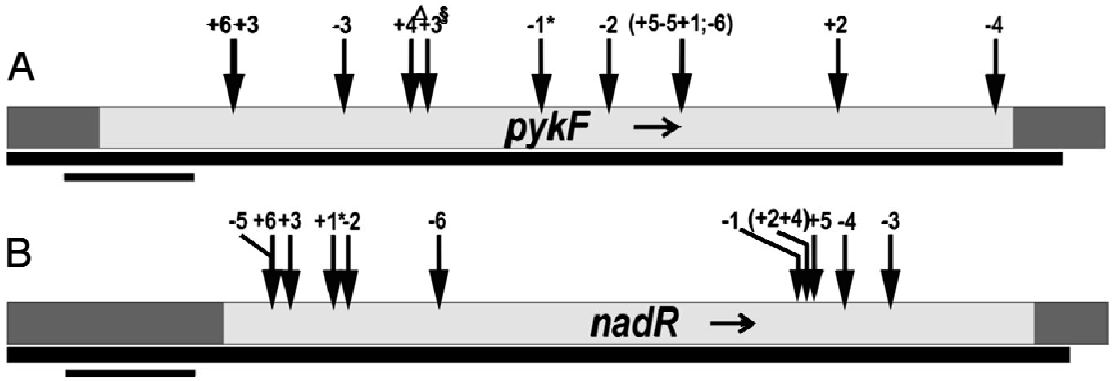

Figure 1.2 **Positions of the substituted amino acids mutated during 20,000 generations in candidate genes *pykF* and *nadR* in 12 experimental populations of *E. coli*.** Lighter regions indicate the protein-coding sequences for *pykF* (panel A) and *nadR* (panel B). Long bars below show the sequence range, short bars show the scale (200 bp). Each arrow marks a mutation, the number shows the population identity (+ means the population contained a mutual genetic marker, and – means the population did not have the marker): *, An *IS150* insertion; Δ, A 1-bp deletion; and §, A synonymous mutation. Figure was taken directly from (Woods *et al.* 2006).

Although the same genes sustained mutations, at the nucleotide level the mutations were different, changing residues throughout the enzyme. It could be concluded therefore that mutations were not parallel at the nucleotide level, but the affect of the mutations on

enzyme function is not known. Many studies have documented how the twelve populations adapted to the glucose limiting environment (i.e. with altered morphology, gene expression and improved fitness); however, it is not known *how* the genotypic changes affected phenotype. Here, this question is asked for the first time from a biochemical perspective by studying the affects of the mutations found in PK1.

1.2 Glycolysis

Glycolysis is the metabolic pathway that breaks down glucose to pyruvate and generates energy in the form of ATP and NADH. During the process, the six-carbon glucose is split into two three-carbon sugars which are then oxidised to form pyruvate by several enzyme-catalysed reactions.

There are three major regulatory enzymes in glycolysis: hexokinase, phophofructokinase and pyruvate kinase [ATP:pyruvate 2-*O*-phosphotransferase (E.C. 2.7.1.40), PK], which together control the metabolic flux in this pathway in virtually every cell type (Allert *et al.* 1991; Fothergill & Michels 1992) (Figure 1.3).

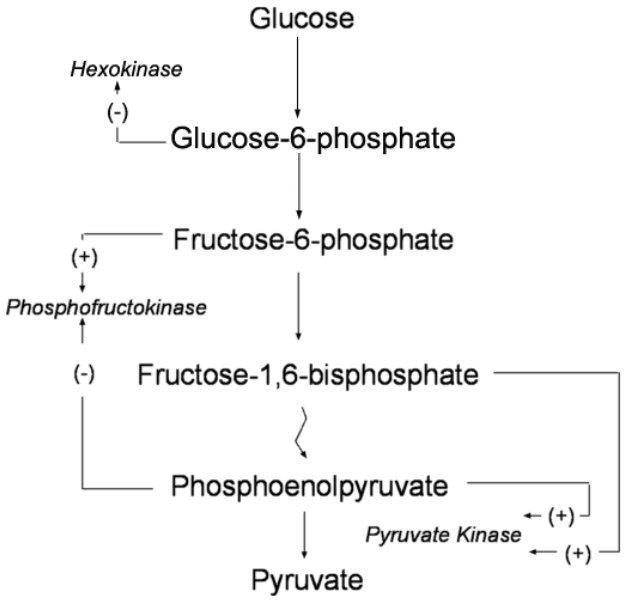

Figure 1.3 **An overview of the glycolysis.** Pyruvate kinase controls the second part of the pathway, and is activated by FBP and PEP. The figure was adapted from (Mattevi *et al.* 1996).

Pyruvate is the first non-phosphorylated sugar generated in this process and can feed into a number of metabolic processes (Campbell *et al.* 1999). This reaction is essentially

irreversible under physiological conditions, and PK is allosterically regulated by fructose-1,6-bisphosphate (FBP) in order to control metabolic flux. PK is thus at a primary metabolic regulation point (Mattevi *et al.* 1995).

1.3 Pyruvate kinase

1.3.1 Reaction

Pyruvate kinase is an ancient protein that existed before the split of eukaryotes and prokaryotes, as indicated by a similar glycolytic pathway in both eukaryotes and prokaryotes (Hattori *et al.* 1995). PK catalyses the transfer of a phosphoryl group from phosphoenolpyruvate (PEP) to adenosine diphosphate (ADP), generating ATP and pyruvate (Figure 1.4). It requires monovalent (K^+) and divalent cations (Mg^{2+}or Mn^{2+}) to assist its function.

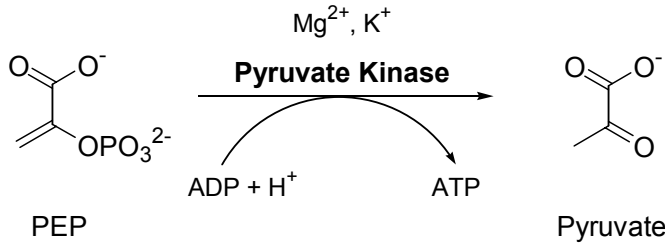

Figure 1.4 **Reaction catalysed by pyruvate kinase**

PK1 is regulated by its substrate PEP homotropically (i.e. the binding of one PEP molecule favours the binding of a second PEP) and kinetically characterised by sigmoidal activity in response to increased PEP concentrations. Most of the PK isozymes are also heterotropically regulated (i.e. binding of a ligand affects the binding of a different ligand, often at a distant position to the active site) by sugars with one or two phosphoryl groups (Fenton 2008). The nature of the heterotropic effector varies among isozymes from different sources (Mattevi *et al.* 1996; Munoz & Ponce 2003).

1.3.2 Kinetics

Kinetic studies of PK from different sources found that the substrate PEP binds cooperatively, with mammalian muscle PKM1 the only exception (Muirhead *et al.* 1986; Munoz & Ponce 2003). However, when an allosteric effector is present, the kinetic

pattern for PEP changes to Michaelis-Menten type behaviour, and the enzyme has a much greater affinity for PEP (Fenton & Blair 2002; Valentini *et al.* 2000; Valentini *et al.* 2002). Despite that, the maximal capacity of the enzyme does not change, as shown by the enzyme turnover number (k_{cat}) (Valentini *et al.* 2000; Valentini *et al.* 2002) or the maximal velocity (V_{max}) (Fenton & Blair 2002). ADP binding, on the other hand, was barely affected by the allosteric effector (Fenton & Blair 2002; Lovell *et al.* 1998; Valentini *et al.* 2000; Valentini *et al.* 2002).

PK requires monovalent (K^+, H^+) and divalent cations (Mg^{2+} or Mn^{2+}) for function (Mesecar & Nowak 1997a). It has been suggested that the divalent cation orients the phospho-groups of PEP and ADP in the active site, before the phosphotransfer takes place (Munoz & Ponce 2003). K^+ has a critical role to the random substrate binding pattern of PK. It has been reported that without K^+ present, ADP binding is dependent on the binding of PEP (Oria-Hernandez *et al.* 2005).

The *E. coli* PK1 investigated in this study is allosterically regulated by FBP (Mattevi *et al.* 1996; Mattevi *et al.* 1995; Valentini *et al.* 2000). In a previous study, it was found that FBP changed the enzyme affinity for PEP dramatically (PEP concentration at half of maximal velocity from 3.6 mM (FBP free) to 0.08 mM (FBP present)) (Valentini *et al.* 2000). Cooperative binding of PEP was abolished in the presence of FBP, with Hill constant changing from 3.2 (strong positive cooperativity) to 1.0 (no cooperativity) (Valentini *et al.* 2000).

1.3.3 Sequence alignment

Generally, PK consists of four identical (or very similar) subunits, each composed of approximately 500 residues (Muirhead *et al.* 1986). *E. coli* PK1 has three domains: A (residues 1-70, residues 171-345), B (residues 71-170) and C (residues 352-470) (Mattevi *et al.* 1995). In addition to these principal domains, an N-terminal domain is found in mammalian PK (residues 1-42 of cat muscle PK) (Muirhead *et al.* 1986), and a C-terminal domain is observed in some organisms (residues 476-587 of *Bacillus Stearothermophilus* PK) (Sakai & Ohta 1993); both are absent in *E. coli* PK1. Many *pyk* genes have been sequenced and some are cloned because of their important role in glycolysis regulation and

interesting properties (Munoz & Ponce 2003). The sequence alignment of some of the genes with known protein structures is shown in Figure 1.5, using the online multiple sequence alignment tool CLUSTALW (http://align.genome.jp/). The sequence differences are not randomly distributed, with the highest diversity observed in domain B, when domain A is highly conserved and domain C sequences are variable.

Figure 1.5 **Alignment of the PK sequences from different sources with structures solved.** The origins of these sequences are: *Escherichia coli* type 1 (bacterium); *Saccharomyces cerevisiae* (yeast); *Leishmania maxicana* (Leishmania); *Felis silvestris catus* (cat); *Oryctolagus cuniculus* M (rabbit); *Rattus norvegicus* M (rat); and *Homo sapiens* R/L (M15465). The residues thought to be involved in binding PEP and ADP/ATP are indicated with P and A, respectively. D and M indicate the ligands for divalent and monovalent cations. The vertical bars identify the domain boundaries and domains were labelled. Point mutations found in the evolutionary study (Woods *et al.* 2006) are identified are coloured. h and e indicate the residues belonged to α-helix and β-sheet. Conserved residues are marked with (*), conservative substitutions are marked with (:), and semi-conservative substitutions are marked with (.). The absolutely conserved Aα6' helix is highlighted with a border. The alignment used the online program CLUSTAL W. The mutated residues investigated in this study are coloured.

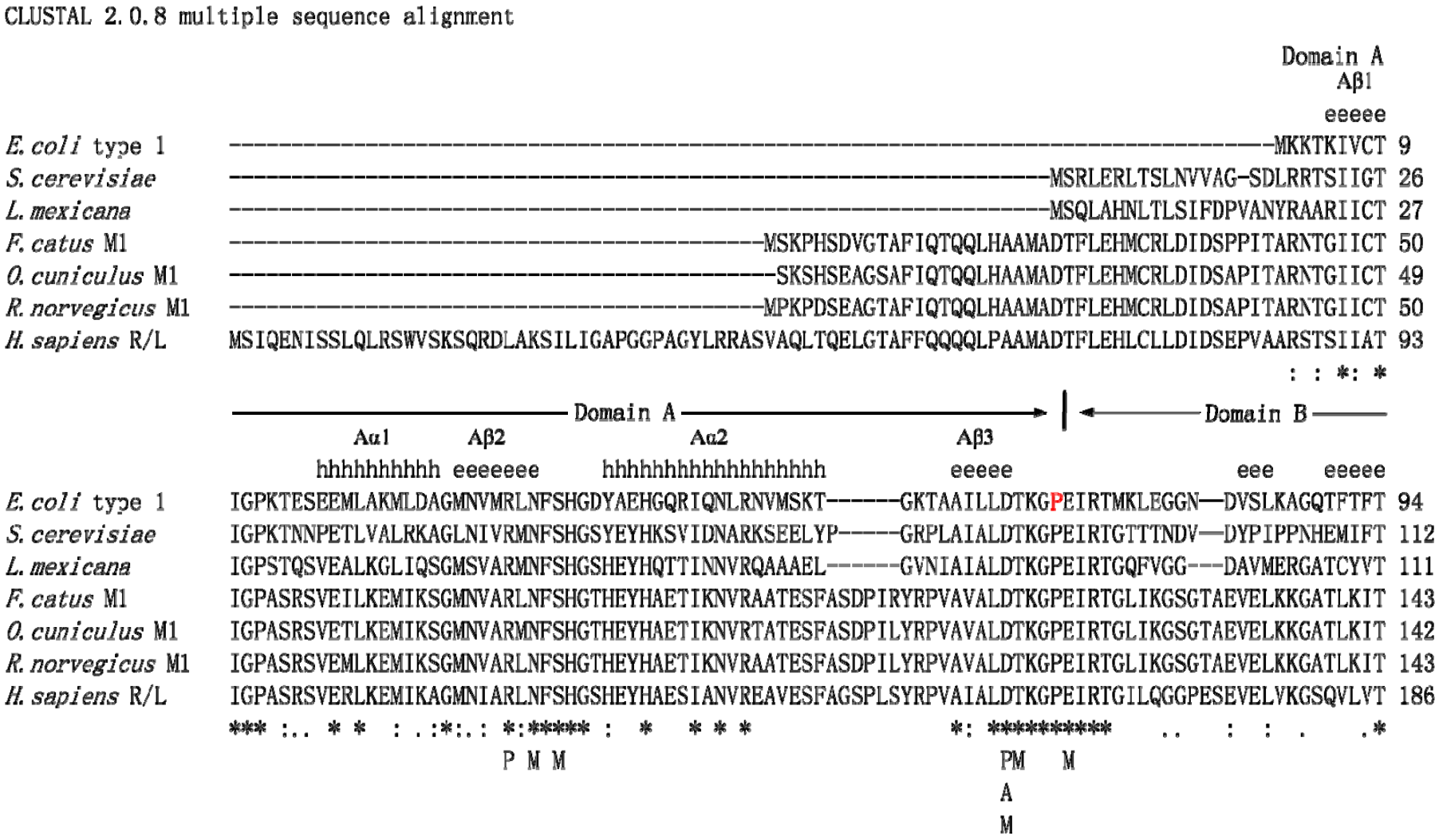
CLUSTAL 2.0.8 multiple sequence alignment
Domain A
Aβ1
eeeee
E.coli type 1 ----------MKKTKIVCT 9
S.cerevisiae ----------MSRLERLTSLNVVAG-SDLRRTSIIGT 26
L.mexicana ----------MSQLAHNLTLSIFDPVANYRAARIICT 27
F.catus M1 ----------MSKPHSDVGTAFIQTQQLHAAMADTFLEHMCRLDIDSPPITARNTGIICT 50
O.cuniculus M1 ----------SKSHSEAGSAFIQTQQLHAAMADTFLEHMCRLDIDSAPITARNTGIICT 49
R.norvegicus M1 ----------MPKPDSEAGTAFIQTQQLHAAMADTFLEHMCRLDIDSAPITARNTGIICT 50
H.sapiens R/L MSIQENISSLQLRSWVSKSQRDLAKSILIGAPGGPAGYLRRASVAQLTQELGTAFFQQQQLPAAMADTFLEHLCLLDIDSEPVAARSTSIIAT 93
: : *: *
Domain A
Domain B
Aα1
Aβ2
Aα2
Aβ3
hhhhhhhhhh eeeeeee hhhhhhhhhhhhhhhhhh eeeee eee eeeee
E.coli type 1 IGPKTESEEMLAKMLDAGMNVMRLNFSHGDYAEHGQRIQNLRNVMSKT------GKTAAILLDTKGPEIRTMKLEGGN--DVSLKAGQTFTFT 94
S.cerevisiae IGPKTNNPETLVALRKAGLNIVRMNFSHGSYEYHKSVIDNARKSEELYP-----GRPLAIALDTKGPEIRTGTTTNDV--DYPIPPNHEMIFT 112
L.mexicana IGPSTQSVEALKGLIQSGMSVARMNFSHGSHEYHQTTINNVRQAAAEL------GVNIAIALDTKGPEIRTGQFVGG---DAVMERGATCYVT 111
F.catus M1 IGPASRSVEILKEMIKSGMNVARLNFSHGTHEYHAETIKNVRAATESFASDPIRYRPVAVALDTKGPEIRTGLIKGSGTAEVELKKGATLKIT 143
O.cuniculus M1 IGPASRSVETLKEMIKSGMNVARMNFSHGTHEYHAETIKNVRTATESFASDPILYRPVAVALDTKGPEIRTGLIKGSGTAEVELKKGATLKIT 142
R.norvegicus M1 IGPASRSVEMLKEMIKSGMNVARLNFSHGTHEYHAETIKNVRAATESFASDPILYRPVAVALDTKGPEIRTGLIKGSGTAEVELKKGATLKIT 143
H.sapiens R/L IGPASRSVERLKEMIKAGMNIARLNFSHGSHEYHAESIANVREAVESFAGSPLSYRPVAIALDTKGPEIRTGILQGGPESEVELVKGSQVLVT 186
*** :.. * * : .:*:.: *:***** : * * * * *: ********** .. : : . .*
P M M
PM M
A
M

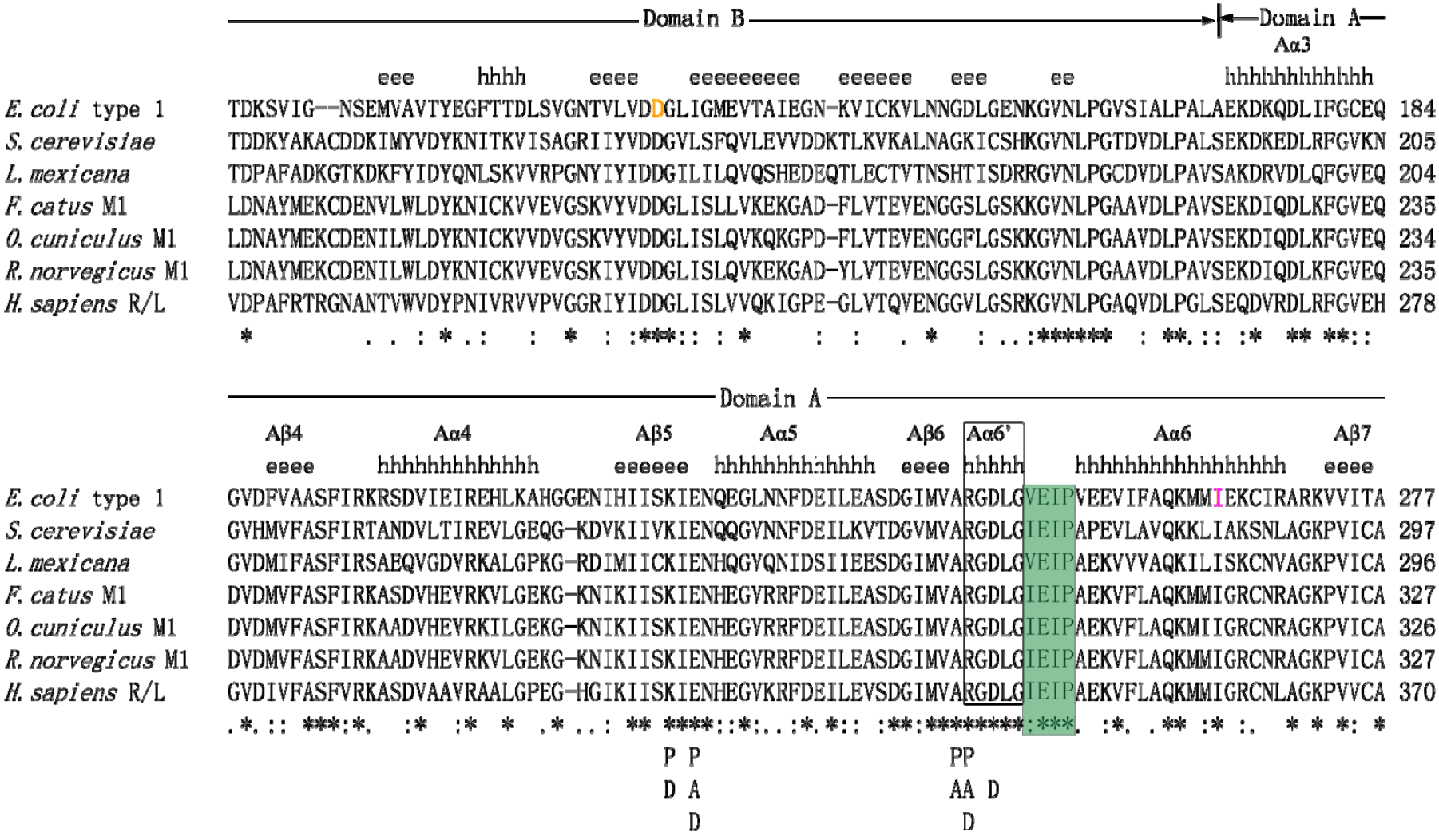
Domain B
Domain A
Aα3
eee hhhh eeee eeeeeeeee eeeeee eee ee hhhhhhhhhhhh
E. coli type 1 TDKSVIG--NSEMVAVTYEGFTTDLSVGNTVLVDDGLIGMEVTAIEGN-KVICKVLNNGDLGENKGVNLPGVSIALPALAEKDKQDLIFGCEQ 184
S. cerevisiae TDDKYAKACDDKIMYVDYKNITKVISAGRIIYVDDGVLSFQVLEVVDDKTLKVKALNAGKICSHKGVNLPGTDVDLPALSEKDKEDLRFGVKN 205
L. mexicana TDPAFADKGTKDKFYIDYQNLSKVVRPGNYIYIDDGILILQVQSHEDEQTLECTVTNSHTISDRRGVNLPGCDVDLPAVSAKDRVDLQFGVEQ 204
F. catus M1 LDNAYMEKCDENVLWLDYKNICKVVEVGSKVYVDDGLISLLVKEKGAD-FLVTEVENGGSLGSKKGVNLPGAAVDLPAVSEKDIQDLKFGVEQ 235
O. cuniculus M1 LDNAYMEKCDENILWLDYKNICKVVDVGSKVYVDDGLISLQVKQKGPD-FLVTEVENGGFLGSKKGVNLPGAAVDLPAVSEKDIQDLKFGVEQ 234
R. norvegicus M1 LDNAYMEKCDENILWLDYKNICKVVEVGSKIYVDDGLISLQVKEKGAD-YLVTEVENGGSLGSKKGVNLPGAAVDLPAVSEKDIQDLKFGVEQ 235
H. sapiens R/L VDPAFRTRGNANTVWVDYPNIVRVVPVGGRIYIDDGLISLVVQKIGPE-GLVTQVENGGVLGSRKGVNLPGAQVDLPGLSEQDVRDLRFGVEH 278
Domain A
Aβ4 Aα4 Aβ5 Aα5 Aβ6 Aα6' Aα6 Aβ7
eeee hhhhhhhhhhhhh eeeeee hhhhhhhhhhhhh eeee hhhhh hhhhhhhhhhhhhhhhh eeee
E. coli type 1 GVDFVAASFIRKRSDVIEIREHLKAHGGENIHIISKIENQEGLNNFDEILEASDGIMVARGDLGVEIPVEEVIFAQKMMIEKCIRARKVVITA 277
S. cerevisiae GVHMVFASFIRTANDVLTIREVLGEQG-KDVKIIVKIENQQGVNNFDEILKVTDGVMVARGDLGIEIPAPEVLAVQKKLIAKSNLAGKPVICA 297
L. mexicana GVDMIFASFIRSAEQVGDVRKALGPKG-RDIMIICKIENHQGVQNIDSIIEESDGIMVARGDLGVEIPAEKVVVAQKILISKCNVAGKPVICA 296
F. catus M1 DVDMVFASFIRKASDVHEVRKVLGEKG-KNIKIISKIENHEGVRRFDEILEASDGIMVARGDLGIEIPAEKVFLAQKMMIGRCNRAGKPVICA 327
O. cuniculus M1 DVDMVFASFIRKAADVHEVRKILGEKG-KNIKIISKIENHEGVRRFDEILEASDGIMVARGDLGIEIPAEKVFLAQKMIIGRCNRAGKPVICA 326
R. norvegicus M1 DVDMVFASFIRKAADVHEVRKVLGEKG-KNIKIISKIENHEGVRRFDEILEASDGIMVARGDLGIEIPAEKVFLAQKMMIGRCNRAGKPVICA 327
H. sapiens R/L GVDIVFASFVRKASDVAAVRAALGPEG-HGIKIISKIENHEGVKRFDEILEVSDGIMVARGDLGIEIPAEKVFLAQKMMIGRCNLAGKPVVCA 370
P P
D A
D
PP
AA D
D

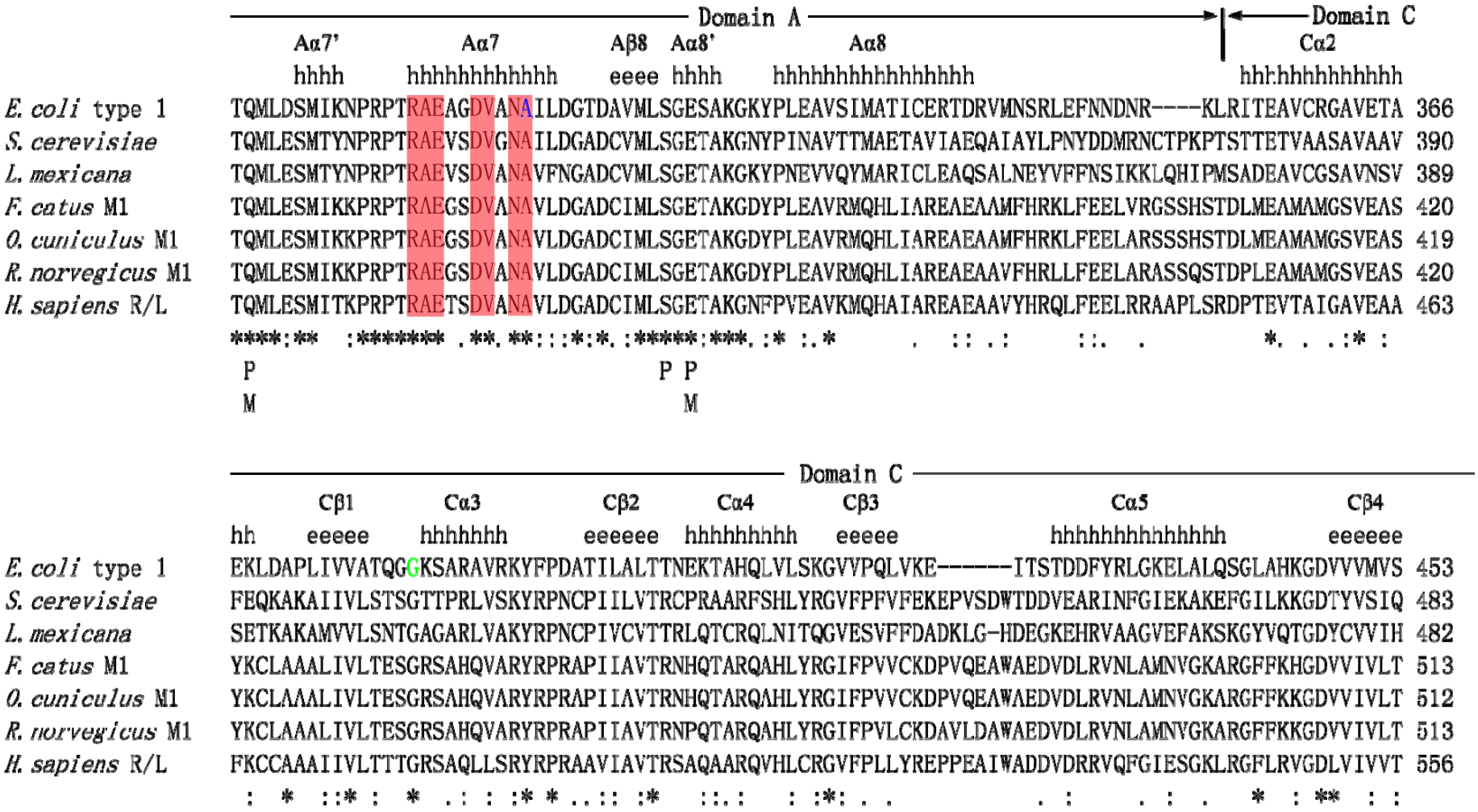
Domain A
Domain C
Aα7' Aα7 Aβ8 Aα8' Aα8 Cα2
hhhh hhhhhhhhhhh eeee hhhh hhhhhhhhhhhhhhhh hhhhhhhhhhhh
E. coli type 1 TQMLDSMIKNPRPTRAEAGDVANAILDGTDAVMLSGESAKGKYPLEAVSIMATICERTDRVMNSRLEFNNDNR----KLRITEAVCRGAVETA 366
S. cerevisiae TQMLESMTYNPRPTRAEVSDVGNAILDGADCVMLSGETAKGNYPINAVTTMAETAVIAEQAIAYLPNYDDMRNCTPKPTSTTETVAASAVAAV 390
L. mexicana TQMLESMTYNPRPTRAEVSDVANAVFNGADCVMLSGETAKGKYPNEVVQYMARICLEAQSALNEYVFFNSIKKLQHIPMSADEAVCGSAVNSV 389
F. catus M1 TQMLESMIKKPRPTRAEGSDVANAVLDGADCIMLSGETAKGDYPLEAVRMQHLIAREAEAAMFHRKLFEELVRGSSHSTDLMEAMAMGSVEAS 420
O. cuniculus M1 TQMLESMIKKPRPTRAEGSDVANAVLDGADCIMLSGETAKGDYPLEAVRMQHLIAREAEAAMFHRKLFEELARSSSHSTDLMEAMAMGSVEAS 419
R. norvegicus M1 TQMLESMIKKPRPTRAEGSDVANAVLDGADCIMLSGETAKGDYPLEAVRMQHLIAREAEAAVFHRLLFEELARASSQSTDPLEAMAMGSVEAS 420
H. sapiens R/L TQMLESMITKPRPTRAETSDVANAVLDGADCIMLSGETAKGNFPVEAVKMQHAIAREAEAAVYHRQLFEELRRAAPLSRDPTEVTAIGAVEAA 463
P
M
P P
M
Domain C
Cβ1 Cα3 Cβ2 Cα4 Cβ3 Cα5 Cβ4
hh eeeee hhhhhhh eeeeee hhhhhhhhh eeeee hhhhhhhhhhhhhhh eeeeee
E. coli type 1 EKLDAPLIVVATQGGKSARAVRKYFPDATILALTTNEKTAHQLVLSKGVVPQLVKE------ITSTDDFYRLGKELALQSGLAHKGDVVVMVS 453
S. cerevisiae FEQKAKAIIVLSTSGTTPRLVSKYRPNCPIILVTRCPRAARFSHLYRGVFPFVFEKEPVSDWTDDVEARINFGIEKAKEFGILKKGDTYVSIQ 483
L. mexicana SETKAKAMVVLSNTGAGARLVAKYRPNCPIVCVTTRLQTCRQLNITQGVESVFFDADKLG-HDEGKEHRVAAGVEFAKSKGYVQTGDYCVVIH 482
F. catus M1 YKCLAAALIVLTESGRSAHQVARYRPRAPIIAVTRNHQTARQAHLYRGIFPVVCKDPVQEAWAEDVDLRVNLAMNVGKARGFFKHGDVVIVLT 513
O. cuniculus M1 YKCLAAALIVLTESGRSAHQVARYRPRAPIIAVTRNHQTARQAHLYRGIFPVVCKDPVQEAWAEDVDLRVNLAMNVGKARGFFKKGDVVIVLT 512
R. norvegicus M1 YKCLAAALIVLTESGRSAHQVARYRPRAPIIAVTRNPQTARQAHLYRGIFPVLCKDAVLDAWAEDVDLRVNLAMNVGKARGFFKKGDVVIVLT 513
H. sapiens R/L FKCCAAAIIVLTTTGRSAQLLSRYRPRAAVIAVTRSAQAARQVHLCRGVFPLLYREPPEAIWADDVDRRVQFGIESGKLRGFLRVGDLVIVVT 556

```
                    ———Domain C——
                              Cβ5
                             eeeeeee
E.coli type 1       GALVPSGTTNTASVHVL- 470
S.cerevisiae        GFKAGAGHSNTLQVSTV- 500
L.mexicana          ADHKVKGYANQTRILLVE 499
F.catus M1          GWRPGSGFTNTMRVVPVP 531
O.cuniculus M1      GWRPGSGFTNTMRVVPVP 530
R.norvegicus M1     GWRPGSGFTNTMRVVPVP 531
H.sapiens R/L       GWRPGSGYTNIMRVLSIS 574
                    .     * :*   :  :
```

1.3.4 Structure

The monomeric molecular mass of PK is generally around 55 kDa (Aust & Suelter 1978; Malcovati & Valentini 1982). Although the majority of PK isozymes appear to be tetrameric (Mattevi *et al.* 1995; Rigden *et al.* 1999), many other forms, including a monomer, dimer and hexamer are also known (Munoz & Ponce 2003).

The crystal structure of pyruvate kinase has been obtained from various sources including rabbit muscle (Larsen *et al.* 1998), yeast *Saccharomyces cerevisiae* (Jurica *et al.* 1998), protozoan parasite *Leshmania mexicana* (Rigden *et al.* 1999), bacterial *E. coli* type 1 (Mattevi *et al.* 1995), human erythrocyte isozyme (Pendergrass *et al.* 2006; Valentini *et al.* 2002), and human tumor pyruvate kinase M2 (Dombrauckas *et al.* 2005). The overall structure of these pyruvate kinase isozymes is similar (Munoz & Ponce 2003).

E. coli PK1 is a homotetramer (Figure 1.6a). Each subunit can be divided into three domains: domain A forms a large $(\beta/\alpha)_8$-barrel structure, a fold common in enzymes (Mattevi *et al.* 1996); domain B, which is characterised by a small irregular β barrel; and domain C, which has an (α+β) open sheet topology (Figure 1.6b). The allosteric FBP binding site is located in domain C near the C/C' interface, and the active site lies within a cleft between domains A and B (Figure 1.6b) (Mattevi *et al.* 1995). Upon binding the effector FBP, the enzyme conformation changes from a low-affinity T-state to a high-affinity R-state for the substrates (Mattevi *et al.* 1995) (Section 1.3.6).

E. coli PK1 crystallises in the low affinity T-state and the addition of FBP has been shown to crack PK1 crystals (Mattevi *et al.* 1995), whereas yeast (*S. cerevisiae*) pyruvate kinase crystallises with FBP at the high-affinity R-state conformation (Jurica *et al.* 1998). Mammalian muscle PK (PKM1), an enzyme that lacks sigmoidal kinetics, is likely to adopt an active R-state conformation (Muirhead 1990; Walker *et al.* 1992). Data obtained from these X-ray crystallographic studies have been used to interpret the allosteric regulation of the enzyme, which is still not fully understood.

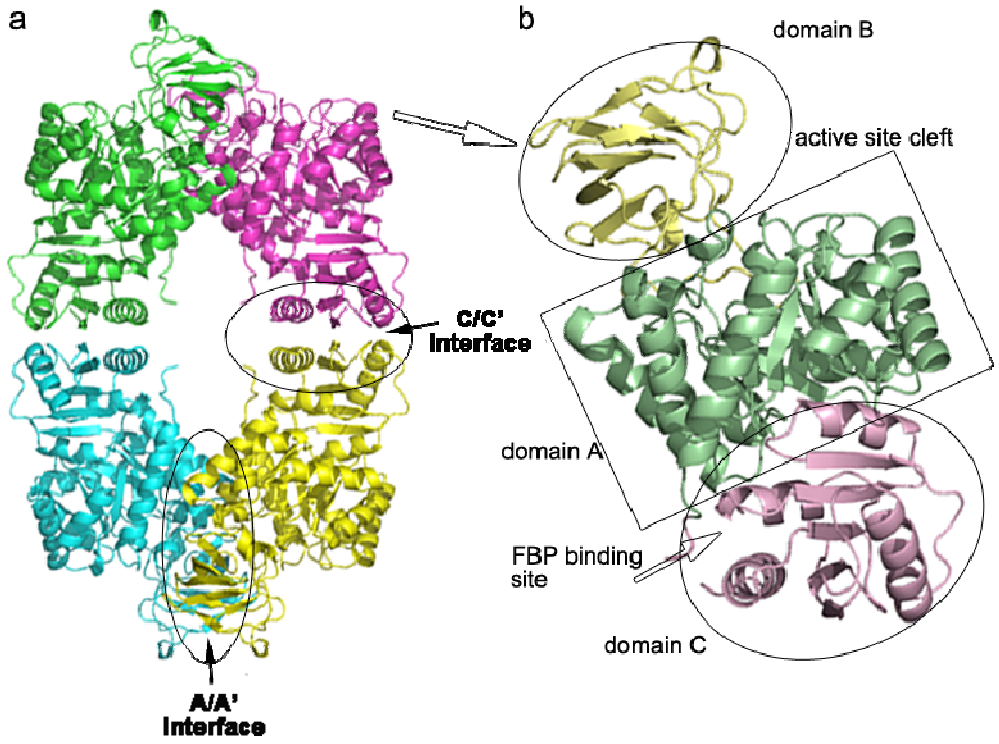

Figure 1.6 **Structure of *E. coli* PK1.** (a) the quaternary structure, and (b) the monomeric structure. The structure is generated by PDB file 1pky (Mattevi *et al.* 1995) using Pymol (DeLano 2002).

1.3.4.1 The active site

The active site lies in the pocket between domains A and B. A high degree of sequence identity among PK isozymes has been observed (Munoz & Ponce 2003) (Figure 1.5). The residues involved in constructing the active site have been identified in rabbit muscle PKM1 (Larsen *et al.* 1998; Larsen *et al.* 1994) and the corresponding residues in *E. coli* PK1 are shown in Figure 1.7.

1.3.4.2 The FBP binding site

The FBP binding site is in domain C, near the A/C domain interface (Figure 1.8). The site is clearly shown in the structure of yeast PK co-crystallised with FBP (Jurica *et al.* 1998). The 6'-phosphate fits in a pocket with residues with positive side chains (residues 402-407 in yeast PK), which are not completely conserved. In *E. coli* PK1, a similar pocket is observed (Figure 1.8); however, it is not clear whether FBP binds at the same position, due to the absence of crystal structures with FBP bound.

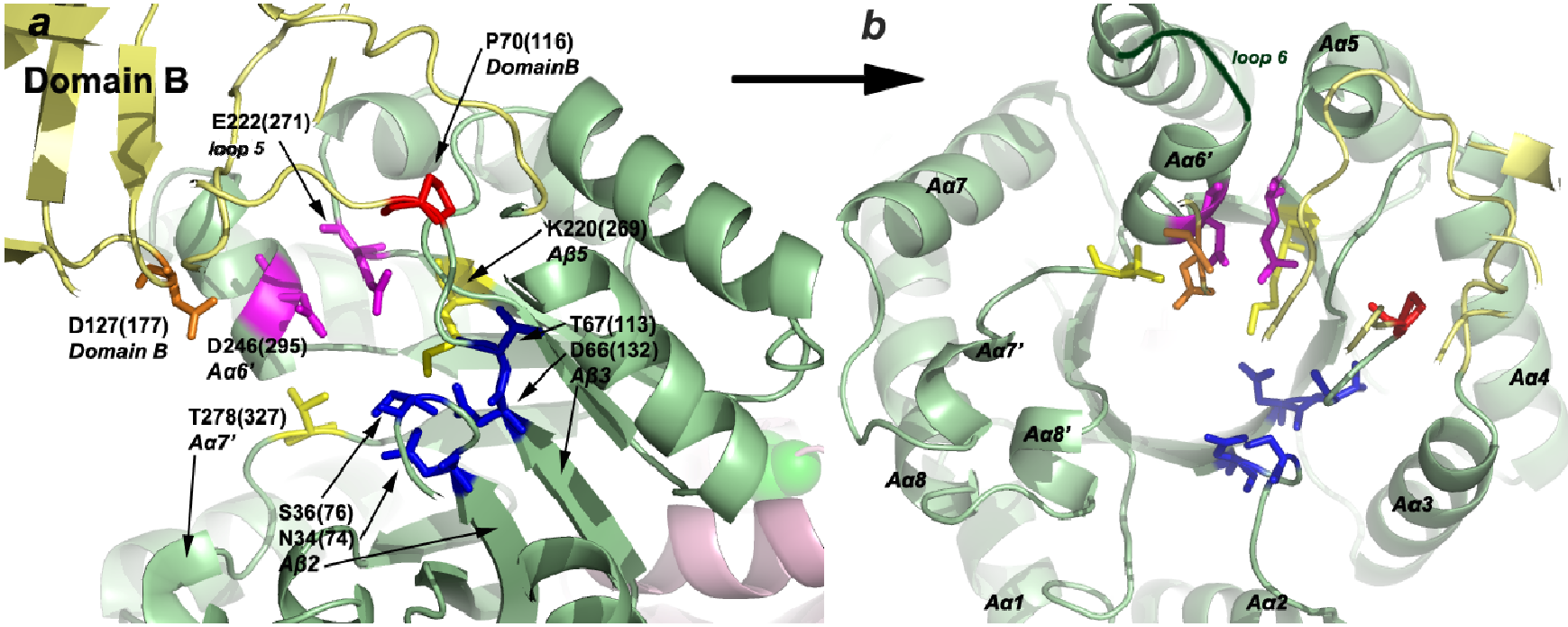

Figure 1.7 **Schematic drawing of the proposed residues at the active site and involved in cation binding in *E. coli* PK1.** Drawing was based on residues at the corresponding positions of the rabbit muscle PKM1 (Larsen *et al.* 1994). (a) A side view of the active site. The residues that bind to divalent cations (D246 and E222) are shown in purple sticks; the residues involved in pyruvate binding (K220 and T278) are shown in yellow sticks; the residues that directly bind to the monovalent cation (N34, S36, D66 and T67) are shown in blue sticks. P70 and D127N, which were mutated in this study, are shown in red and orange sticks respectively. The helices to which the residues belong are marked in *italics*. (b) A top view of the active site with all residues labelled as in (a), and all α-helices labelled in *italics*. Loop 6 is shaded in dark green and labelled. This picture was generated using PDB file 1pky (Mattevi *et al.* 1995) by Pymol (DeLano 2002).

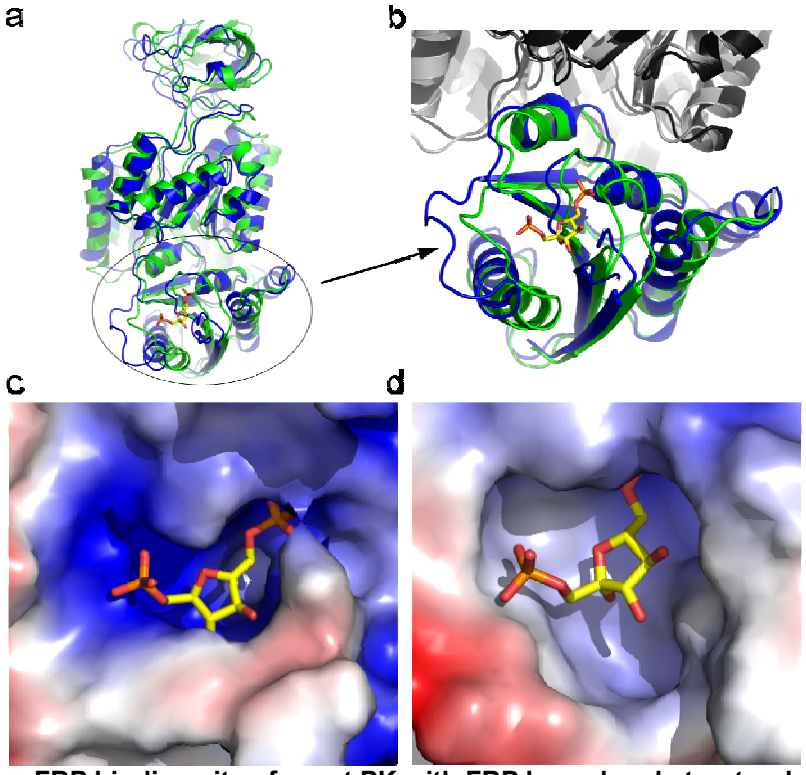

Figure 1.8 **FBP binding site of yeast PK with FBP bound and structural alignment with *E. coli* PK1.** (a) The structural alignment between yeast PK and *E. coli* PK1; (b) An expanded view at the FBP binding site; (c) Surface image of the FBP binding pocket in yeast PK, with FBP bound; (d) proposed FBP binding pocket in *E. coli* PK1, with FBP placed at the same orientation as in yeast PK. The *E. coli* PK1 structure is shown in green and yeast PK in blue. FBP is represented in yellow and orange sticks. The r.m.s.d. value for the Cα overlay is 1.7 Å. Figure was generated using PDB files 1pky (*E. coli* PK1) (Mattevi *et al.* 1995) and 1a3w (yeast PK) (Jurica *et al.* 1998) by Pymol (DeLano 2002).

1.3.5 Structural changes upon catalysis

Comparison between the tertiary structures of *E. coli* PK1 and rabbit PKM1 obtained from crystallographic studies revealed large variations in the domain orientations, while the structure within each domain is highly conserved (Larsen *et al.* 1994; Mattevi *et al.* 1995). When taking domain A as a reference, a rotation of 17° in domain B was observed, which caused a narrowing of the active-site cleft in the rabbit PKM1 model. This movement is achieved through a hinge-bending action. P70, which is located on this flexible hinge as a domain linker, may play a crucial role in this conformation change (Mattevi *et al.* 1996). Structural studies have demonstrated this for the rabbit PKM1 enzyme (Larsen *et al.* 1997) (Figure 1.9), where causes the opening or closing of the active site. The residue is mutated in this study.

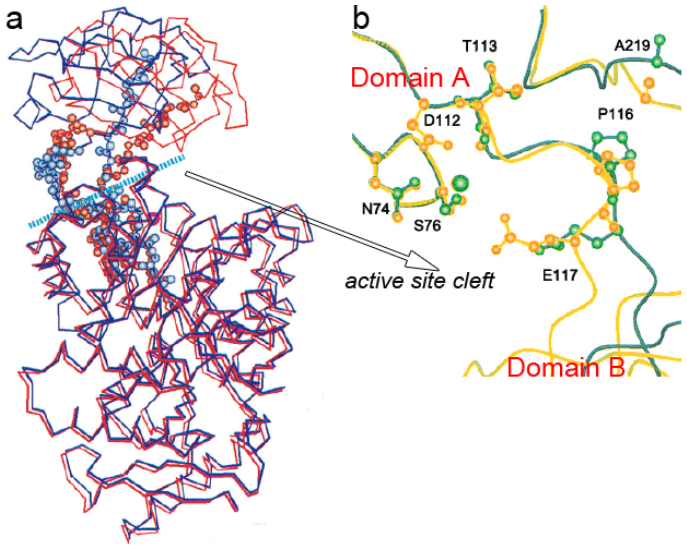

Figure 1.9 **Schematic drawing of the hinge-bending action between domains A and B in rabbit PKM1.** (a) Overlay of the α-carbons of subunit 1 (red, closed active site cleft) and 2 (blue, open active site cleft). The spheres represent the linkers. (b) A ball-and-stick model of the K^+ binding site for the open (green) and closed (yellow) cleft. K^+ is shown as a green sphere. Figure was directly copied from Larsen *et al*. (1997).

Residue D127 is located on a loop at domain B in *E. coli* PK1 (Figure 1.5). D177 in the rabbit muscle PK, which corresponds to D127 in *E. coli* PK1, pokes into the active site in the rabbit muscle PK enzyme upon the hinge-bending motion (Mattevi *et al.* 1995). D127N is also mutated in this study.

1.3.6 Regulation

The kinetic properties of pyruvate kinase have been extensively studied, together with site-directed mutagenesis and crystallographic data, to elucidate the regulation mechanism of the enzyme (Bond *et al.* 2000; Fenton & Blair 2002; Friesen *et al.* 1998b; Jurica *et al.* 1998; Lovell *et al.* 1998; Mattevi *et al.* 1996; Valentini *et al.* 2000; Wooll *et al.* 2001). Thus far, a definitive mechanism has been elusive, although a number of allosteric regulation models have been proposed.

1.3.6.1 The Domain Rotation model

As an allosterically regulated enzyme, PK undergoes a transition from a low-affinity T-(tensed) state to a high-affinity R-(relaxed) state. The R-state subunits bind to substrate more readily than those in the T-state (Monod *et al.* 1965).

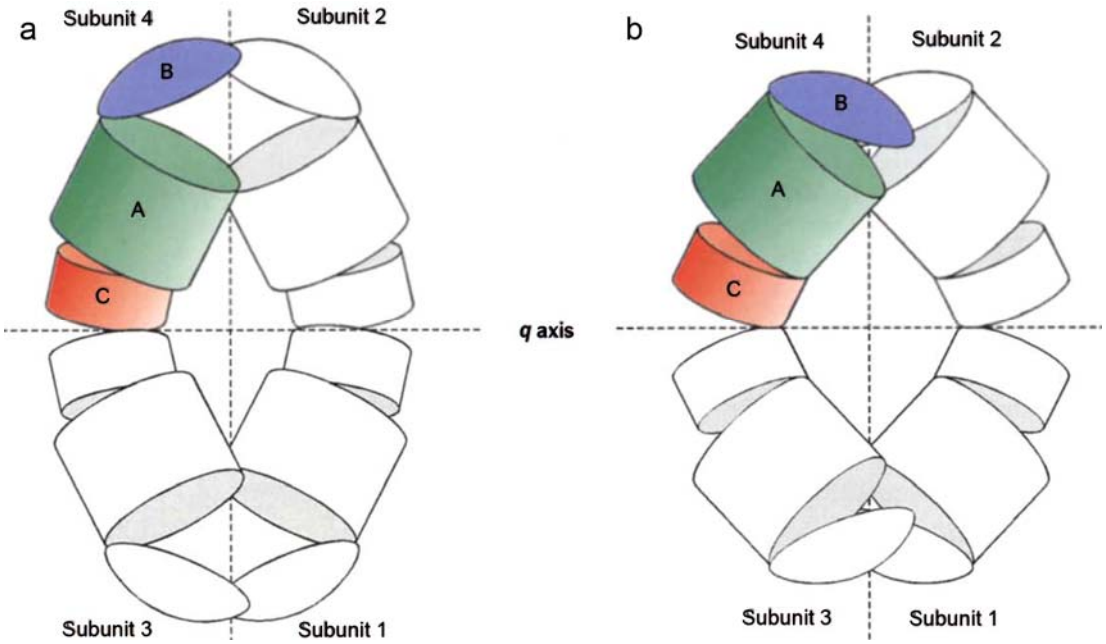

Figure 1.10 **Schematic comparisons of the T-state (a, *E. coli* PK1 (Mattevi *et al.* 1995)) and R-state (b, rabbit M1 PK (Larsen *et al.* 1994)) tetramers.** The set of motions that affect domain and subunit orientations are outlined. Figure was taken from (Mattevi *et al.* 1995).

In *E. coli* PK1, the FBP binding site is distal to the active site and the allosteric signal needs to be transmitted across the domain interface to reach the active site (Jurica *et al.* 1998; Valentini *et al.* 2002). In the "domain rotation model", Mattevi and colleagues (studying *E. coli* PK1) argued that the transition between T- and R-states requires little motion within domains, but rather involves rigid body motion between domains and within the subunits (Mattevi *et al.* 1996; Mattevi *et al.* 1995; Valentini *et al.* 2000). By comparing the crystal structures of *E. coli* PK1 in the T-state with the rabbit muscle M1 isozyme (which resembles the R-state conformation (Mattevi *et al.* 1995)) (Figure 1.10), large orientation differences were found between domains. These were functionally relevant since they affected the shape and space of the domain interfaces in which the active site and the allosteric site lie (Mattevi *et al.* 1995). Structural elements must exist for the coupling of domain movements to the conformational change at the active site (Mattevi *et al.* 1996; Mattevi *et al.* 1995). It was found that loop 6 of the $(\beta/\alpha)_8$-barrel (shaded green in Figure 1.5 and Figure 1.7b), which takes part in PEP binding, appears to be in a conformation that distorts the active site, as observed in the T-state crystal (Mattevi *et al.* 1995). This implies that the domain rotation upon FBP binding may restore the active site and therefore assist PEP binding. Structural information regarding the R-state of PK1 in complex with the activator FBP, and with substrates PEP and ADP, is still not

available for the *E. coli* enzyme to support this regulation mechanism. These structural studies need to be complemented with mutagenesis studies of PK1 enzymes with altered allosteric regulation, such as reported in this work.

1.3.6.2 "Network mechanism" model

An alternative model, the so called network mechanism, was proposed by Friesen and colleagues, in their studies of recombinant rabbit muscle (rRMPK) and kidney (rRKPK) pyruvate kinases (Friesen *et al.* 1998a; Friesen *et al.* 1998b). rRMPK shows non-allosteric kinetic behaviour whereas rRKPK shows allostery with respect to phenylalanine and FBP, even though they differ by only 22 residues (Friesen *et al.* 1998a). Friesen *et al.* (1998b) show that for the rRKPK enzyme, the tetramer dissociates to a (presumably less active) dimer at the C/C' subunit interface and that this process is modulated by FBP (which promotes tetramer formation) and phenylalanine and the substrate ADP (which promote dimer formation). However, this work did not consider how the signal was transferred from the allosteric binding site to the active site.

Using both molecular modelling and site-directed mutagenesis, coupled with enzyme kinetics, it was hypothesised that all the substrates and effectors of pyruvate kinase communicated through the C/C' subunit interface (Friesen *et al.* 1998b), and the allosteric signal is transmitted from the C/C' subunit interface to the active site through a hydrogen bonding network (Friesen *et al.* 1998a). This mechanism proposed that only a few residues serve pivotal roles in coupling a conformational change in the C/C' subunit interfacial region to the active site (Friesen *et al.* 1998a). K421 (K368 in *E. coli*) forms a salt bridge with Y443 (Y390), which in turn interacts with A319 (A301) at the C-terminal of Aα6. This helix spans the length of the subunit and the loop at the N-terminal end of this helix makes up part of the PEP binding site (Friesen *et al.* 1998a). A further structural study suggested that in the mammalian enzymes the R- and T-states are somewhat modulated by an intersubunit salt bridge between D127 and R289 (*E. coli* numbering), a connection which is not evident in the *E. coli* structures. The mechanism involved in this model is still under investigation.

Despite the two models, no conclusion about the allosteric signal transfer mechanism of *E. coli* PK1 has yet been drawn.

1.3.6.3 Phosphotyrosine peptide binding

Recently, Christofk and colleagues proposed a third mechanism of regulation, by which the mammalian tumour isozyme (PKM2) binds phosphotyrosine peptides, which results in loss of FBP binding, thus releasing the enzyme from activation (Christofk *et al.* 2008a; Christofk *et al.* 2008b). The phosphotyrosine peptide binds near the FBP-binding site (unique in PKM2) and lysine 433 was found to be important for the interaction. A similar mechanism was not found in other mammalian PK isozyme (Christofk *et al.* 2008b). No study has reported whether *E. coli* PK1 is regulated in this fashion *in vitro* or *in vivo*.

1.4 The PK1 mutants

The seven PK1 mutants investigated in this study were identified by Woods and colleagues (Woods *et al.* 2006). They identified two genes (*nadR* and *pykF*) that had mutations in all twelve evolved populations (Section 1.2), another that had mutations in six populations (*pbpA-radA*) and the fourth mutated gene (*hokB*/*socB*) was found in three populations (Woods *et al.* 2006). The position of each PK1 mutation in the populations is shown in Figure 1.2. Interestingly, four separately evolved populations showed mutations at the same residue of PK1: A301. In theory, after just 10,000 generations, each base pair in the genome was, on average, mutated over a 100 times, although genetic drift eliminates most changes immediately (Elena & Lenski 2003; Lenski *et al.* 1991). It is therefore likely that the mutations found in *pykF* were selected for.

The positions of the seven mutations were mapped onto the known *E. coli* PK1 structure (Figure 1.11). They fall loosely into three groups: those in or near the active site (P70T, P70Q and D127N); those in or near to the subunit interface between the A domains (A/A' interface, I264F, A301T and A301S); and that within the FBP binding site (G381A). While the mutations at the active site were predicted to affect catalysis, several studies have found that PK1 enzymes with mutations at both the FBP binding site and the subunit interfaces lead to changes of kinetic behaviour or allosteric regulation pattern (Christofk *et al.* 2008b; Collins *et al.* 1995; Friesen *et al.* 1998a; Mattevi *et al.* 1996; Valentini *et al.* 2000). Therefore, mutations in the FBP and subunit interfaces (as predicted by the domain rotation model of allostery) were predicted to alter regulation.

1.4.1 Active site mutations

Residue P70 is highly conserved across species (Munoz & Ponce 2003) (Figure 1.5). Interestingly, the adjacent residue E71 (in domain B) belongs to a group of residues highly conserved across species and involved in the construction of the active site (Figure 1.5) (Munoz & Ponce 2003). Structural studies suggest that E71 has an critical role in binding the monovalent cation (K^+) and, interestingly, is replaced by lysine in PK enzymes that lack a dependence on monovalent cation (Munoz & Ponce 2003).

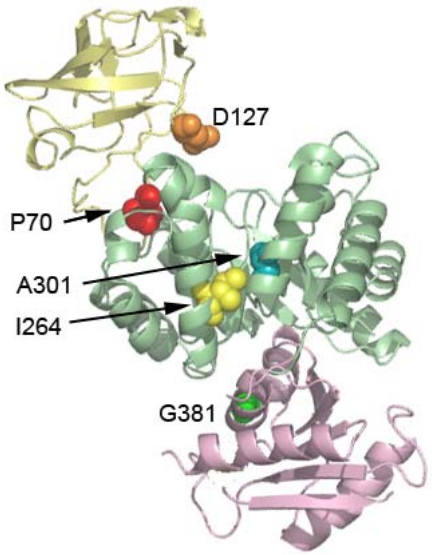

Figure 1.11 **View of the PK1 mutations with respect to their spatial positions.** The monomeric structure embedding the seven mutations is shown. The mutated residues are illustrated as coloured spheres. P70 was mutated to threonine and glutamine. D127 was mutated to asparagine, I264 was mutated to phenylalanine, A301 was mutated to threonine and serine, and G381 was mutated to alanine. Image was created using PDB:1pky (Mattevi *et al.* 1995).

Cation binding is essential for function for the majority of PK isozymes investigated to date (Munoz & Ponce 2003). Enzymatic activity is stimulated upon binding to the monovalent cation K^+ (Boyer *et al.* 1942; Oria-Hernandez *et al.* 2005). In yeast PK, regulation of FBP to PEP requires the presence of a divalent cation in the active site (Mesecar & Nowak 1997a; b). All these studies have implied the significant role of residue P70, suggesting that the mutation at this position will affect catalysis and allosteric regulation.

The residue D127 is situated on a loop that folds into the active site cleft upon ADP binding and is strictly conserved among PK sequences (Mattevi *et al.* 1995). When comparing the *E. coli* PK1 T-state with the rabbit PKM1 model (R-state) it was found that in the T-state, the side chain of D297 forms a salt-bridge with R292 from the adjacent subunit; however, in the R-state, R292 makes a salt bridge with D127 of the adjacent subunit and changes conformation (Figure 1.12). It is proposed that this transition represents the real transition process of PK1 from the T-state to R-state during catalysis (Mattevi *et al.* 1995). This transition is crucial for PEP binding at helix α6 in domain A, as it reconstructs the subunit interface and forces helix Aα6' on loop 6 to move towards the inner part of the active site for PEP binding (Mattevi *et al.* 1995) and locks the cleft between domain A and B in a closed conformation. A mutagenesis study found that R292D caused PK1 to be inactive, though it was able to retain the T-state quaternary structure (Valentini *et al.* 2000). It is possible that the R292D mutant is unable to bind to D127 to "lock the cleft". Therefore, the transition for the enzyme from T-state to R-state could not occur.

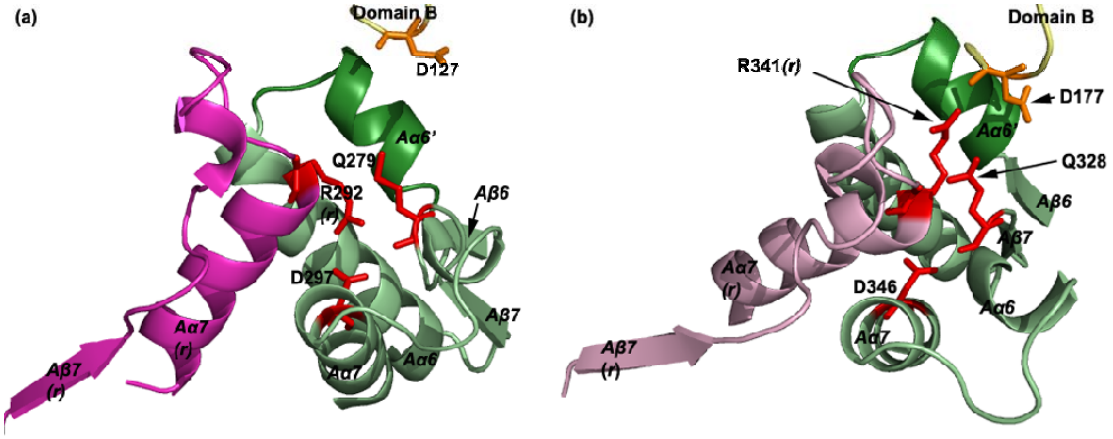

Figure 1.12 **Close-up view of the cleft between domain A and B with relevant interactions. (a) in the *E. coli* T-state PK1 and (b) in the rabbit PKM1.** Secondary structure elements and the residues belonging to the adjacent subunit (subunit 2) are labeled (*r*). Residues involved in the *E. coli* PK1 A/A' interface connections are illustrated with red sticks and labeled (D297 and R292*(r)*) in (a). The residues at the corresponding positions in rabbit PKM1 are illustrated with red sticks and labeled (D346 and R341*(r)*). D127 on the loop of domain B is labelled in orange stick in both figures. Each monomer across the A/A' interface in both structures is pale green, and purple for the *E. coli* structure (a) and pale purple for the rabbit muscle structure (b). The secondary structure is labeled in *italics*. Figure was adapted from (Mattevi *et al.* 1995), PDB 1pky (*E. coli* PK1) and 1a49 (rabbit PKM1).

Given the putative role of D127, altered catalytic function (*via* interactions with the active site upon ADP binding as seen in the rabbit muscle PK1, PDB: 1a49) and altered regulation (*via* interactions with the adjacent subunit as discussed above) were thus predicted for PK1-D127N in this study.

1.4.2 A/A' interface mutations

The residues I264 and A301 are situated at the A/A' interface and are close together in space (Figure 1.13). Sequence analysis among PK1 enzymes from a variety of organisms showed that I264 and A301 were well conserved across species (Figure 1.5). Mutations at these positions were of particular interest, since allosteric binding is thought to promote domain movements, interface rearrangements, or changes in oligomeric states (Fenton & Blair 2002) and thus the PK mutants in this category may inform a new allosteric mechanism.

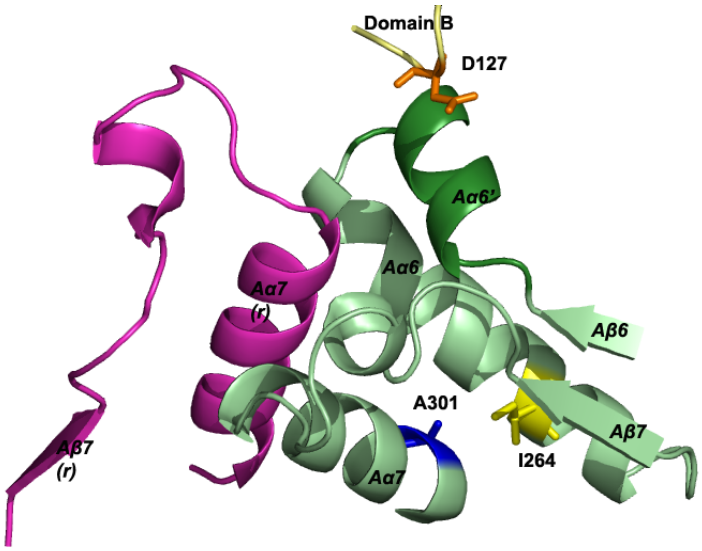

Figure 1.13 **Position of A301, I264 and D127 relative to the catalytic helices (Aα6 – Aα8).** A301 is illustrated in blue sticks, I264 in yellow sticks and D127 in orange sticks. Subunit 1 loops are illustrated in pale green; the *r*-related subunit loops are in purple. Aα6' and loop 6 are illustrated in dark green. The loops are labelled in *italics*.

The mutations A301T and A301S were found in 4 of the 12 evolved populations in the microevolutionary study (1 population showed the mutation A301T and 3 populations showed the mutation A301S) (Cooper *et al.* 2003; Lenski *et al.* 1998; Lenski & Travisano

1994). Why is this residue in PK1, over all others, a locus for mutation in a low glucose environment? Residues involved in the A/A' interface contacts are highly conserved among PK sequences, with a strikingly high sequence identity (76%) between *E. coli* PK1 and rabbit PKM1 in segments Aβ6 to Aα8 (Mattevi *et al.* 1995). Residue A301 belongs to helix Aα7 (Figure 1.13). Among the twelve residues that constitute this helix, nine are strictly conserved (Figure 1.5, highlighted in red). Moreover, A301 showed close proximity to D297 and R292 in helix Aα7 of the adjacent subunit (Figure 1.14), which are critical for the function of PK1 (Mattevi *et al.* 1996; Mattevi *et al.* 1995; Valentini *et al.* 2000).

Inter-subunit communications were shown to be critical for the allosteric regulation of PK (Fenton & Blair 2002); therefore, these two mutations were thus predicted to affect the allosteric regulation pattern of *E. coli* PK1.

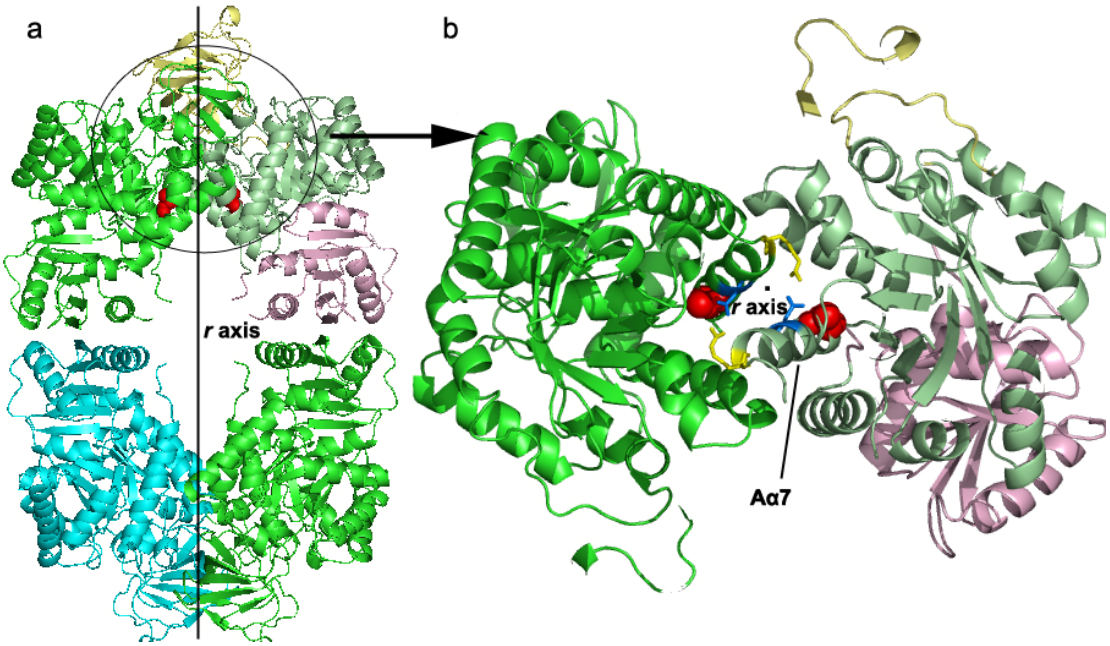

Figure 1.14 **Schematic drawing of the spatial position of A301.** (a) in quaternary structure and b) at the A/A' interface along the *r* axis away from the centre of the molecule. A301 is illustrated in red spheres, R292 is illustrated in yellow sticks and D297 is in blue sticks.

1.4.3 FBP binding site mutations

The residue G381 was the only position in the FBP binding domain to be investigated in this study. G381 belongs to a stretch of conserved residues involved in the formation of

the putative FBP binding site (Munoz & Ponce 2003).

Only a subtle change is achieved by changing the glycine residue to an alanine residue, leaving the polarity of the residue unaltered. G381 belongs to the loop connecting strand Cβ1 and helix Cα3 (residues 377-383) in PK1, both of which are thought to be involved in the binding of FBP at the 6'-phosphate position (Valentini *et al.* 2000) (Figure 1.15).

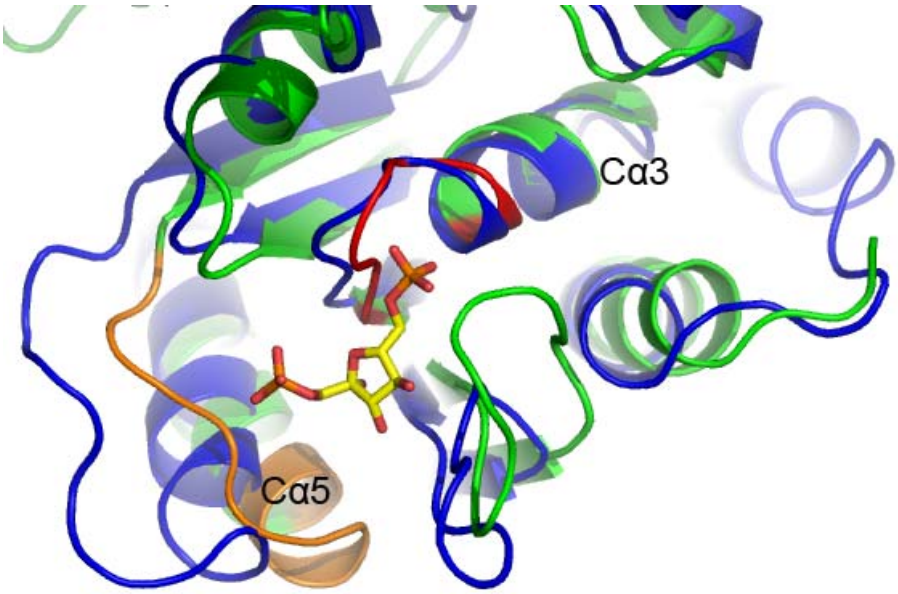

Figure 1.15 **Structure alignments between *E. coli* PK1 and yeast PK at the FBP binding site (domain C).** *E. coli* PK1 is shown in green, and yeast PK in blue. FBP is shown in red and orange sticks. The corresponding loop in *E. coli* PK1 in contact with the 6'-phosphate of FBP is shown in red, and the corresponding loop in contact with the 1'-phosphate of FBP is shown in orange. Figure was generated using PDB files 1pky (Mattevi *et al.* 1995) and 1a3w (Jurica *et al.* 1998).

G381 is in close proximity to K382 (Figure 1.16), which was found to be in close proximity to R271 across the A/C domain interface that may be involved in the allosteric signal transition, and was shown to be involved in the binding of FBP in chemical modification studies (Mattevi *et al.* 1995). This was further supported by the fact that T406 in the yeast PK, which is structurally analogous to K382 (*E. coli* numbering), is directly in contact with the 1'-phosphate of FBP (Jurica *et al.* 1998). A previous study of the *E. coli* PK1-K382Q mutant enzyme resulted in a drastic alteration of enzyme functional properties with a 70-fold increase in $S_{0.5}$ (substrate concentration at 1/2 V_{max} in Hill cooperative model (Hill 1910)) for FBP and decreases in the $k_{cat}/S_{0.5}$ for PEP in the absence

and presence of FBP (Valentini *et al.* 2000). They concluded that K382 is crucial for both FBP binding and the allosteric equilibrium (Valentini *et al.* 2000). Another residue, Q379, which is in close proximity to G381, was proposed to be crucial for FBP binding in allosterically regulated PK. A study of rat PKM1, which exhibited a hyperbolic kinetic profile with respect to PEP had glutamate at the corresponding position (E432) to Q379 in *E. coli* PK1 (Ikeda *et al.* 2000). This suggested the role of E432 in preventing FBP binding by repulsive electrostatic interaction (Ikeda *et al.* 2000). Thus it is possible that a subtle change at G381 alters the kinetic properties of PK1, *via* changes in the FBP binding site.

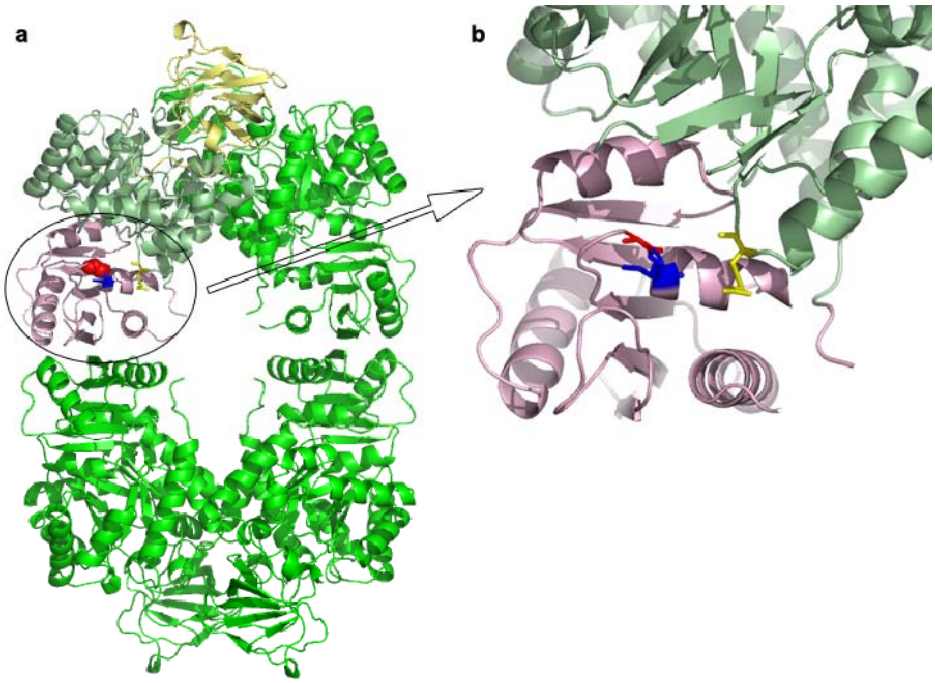

Figure 1.16 **Schematic drawing shows the position of G381 in the *E. coli* PK1 dimer.** (a) the positions of G381, K382 and R271 relative to the tetramer; (b) An expanded view of G381 , K382 and R271 at domain C. G381 is illustrated in red; K382 in blue and R271 across the cleft on domain A in yellow.

1.5 Aim of this project

The aim of this study was to define the changes found in the enzyme pyruvate kinase in Lenski's evolution experiment at a molecular level. Although Lenski's evolved populations have been studied from a genetic, physiological and evolutionary perspective, no study has looked into the molecular basis of the parallelism observed in the system.

This work, therefore, is fundamentally important in understanding how organisms adapt to a stable environment at the protein structural-functional level, and is a pivotal step in Lenski's long-term evolution experiment (Lenski *et al.* 1991). In addition, the current view of the mechanisms of allosteric regulation operating in pyruvate kinase is reviewed. The molecular details of the allosteric activation in PK1 have also been studied. Specifically, it is hypothesised that the adaptive mutations are altering the regulation of PK1.

This work seeks to address the following questions:

(a) Although the replicate populations show parallel evolution at a physiological and genetic level, do they also show parallel evolution at a biochemical level?
(b) Have the mutations affected PK1 regulation or catalytic function? Can these mutations allow us to further understand the mechanisms of allosteric regulation in PK1?

The aims of this study are, therefore, to:

1. Obtain the wild-type PK1 enzyme by transforming the plasmid encoding the enzyme into *E. coli* BL21, over-express and purify the protein (Chapter 2).
2. Characterise the wild-type enzyme using kinetics and structural analysis (secondary and quaternary) (Chapter 2) to determine whether *E. coli* PK1 is in a dimer-tetramer equilibrium and whether the substrates and FBP affect this equilibrium.
3. Obtain PK1 bearing each of the 7 mutations by mutagenesis, transformation, over-expression and purification (Chapter 3).
4. Characterise the seven mutant enzymes using enzyme kinetics (Chapter 3) and structural analysis (secondary, quaternary) (Chapter 4).
5. Relate any experimentally determined altered function back to the evolutionary observations of Lenski and others (Chapter 5).

1.6 References

Allert S, Ernest I, Poliszczak A, Opperdoes FR, Michels PA. 1991. Molecular cloning and analysis of two tandemly linked genes for pyruvate kinase of *Trypanosoma brucei*. *Eur J Biochem* 200:19-27

Aust AE, Suelter CH. 1978. Homogeneous pyruvate kinase isolated from yeast by two different methods is

indistinguishable from pyruvate kinase in cell-free extract. *J Biol Chem* 253:7508-12

Bond CJ, Jurica MS, Mesecar A, Stoddard BL. 2000. Determinants of allosteric activation of yeast pyruvate kinase and identification of novel effectors using computational screening. *Biochemistry* 39:15333-43

Boyer PD, Lardy HA, Phillips PH. 1942. The role of potassium in muscle phosphorylations. *J Mol Biol* 146:673-82

Campbell NA, Reece JB, Mitchell LG. 1999. *Biology 5th ed*. New York: Addison-Wesley

Christofk HR, Vander Heiden MG, Harris MH, Ramanathan A, Gerszten RE, Wei R, Fleming MD, Schreiber SL, Cantley LC. 2008a. The M2 splice isoform of pyruvate kinase is important for cancer metabolism and tumour growth. *Nature* 452:230-3

Christofk HR, Vander Heiden MG, Wu N, Asara JM, Cantley LC. 2008b. Pyruvate kinase M2 is a phosphotyrosine-binding protein. *Nature* 452:181-6

Collins RA, McNally T, Fothergill-Gilmore LA, Muirhead H. 1995. A subunit interface mutant of yeast pyruvate kinase requires the allosteric activator fructose 1,6-bisphosphate for activity. *Biochem J* 310 (Pt 1):117-23

Cooper TF, Rozen DE, Lenski RE. 2003. Parallel changes in gene expression after 20,000 generations of evolution in *Escherichia coli*. *Proc Natl Acad Sci U S A* 100:1072-7

Cooper VS, Lenski RE. 2000. The population genetics of ecological specialization in evolving *Escherichia coli* populations. *Nature* 407:736-9

DeLano WL. 2002. *The PyMOL molecular graphics system.* SanCarlos, CA, USA: DeLano Scientific

Dombrauckas JD, Santarsiero BD, Mesecar AD. 2005. Structural basis for tumor pyruvate kinase M2 allosteric regulation and catalysis. *Biochemistry* 44:9417-29

Elena SF, Lenski RE. 2003. Evolution experiments with microorganisms: the dynamics and genetic bases of adaptation. *Nat Rev Genet* 4:457-69

Fenton AW. 2008. Allostery: an illustrated definition for the 'second secret of life'. *Trends Biochem Sci*

Fenton AW, Blair JB. 2002. Kinetic and allosteric consequences of mutations in the subunit and domain interfaces and the allosteric site of yeast pyruvate kinase. *Arch Biochem Biophys* 397:28-39

Fothergill LA, Michels PA. 1992. Evolution of glycolysis. *Progr Mol Biol Biophys* 59:105-227

Friesen RH, Castellani RJ, Lee JC, Braun W. 1998a. Allostery in rabbit pyruvate kinase: development of a strategy to elucidate the mechanism. *Biochemistry* 37:15266-76

Friesen RH, Chin AJ, Ledman DW, Lee JC. 1998b. Interfacial communications in recombinant rabbit kidney pyruvate kinase. *Biochemistry* 37:2949-60

Hattori J, Baum BR, McHugh SG, Blakeley SD, Dennis DT, Miki BL. 1995. Pyruvate kinase isozymes: ancient diversity retained in modern plant cells. *Biochem Syst Ecol* 23:773-87

Hill AV. 1910. The possible effects of the aggregation of the molecules of hemoglobin on its dissociation curves. *J Physiol (Lond)* 40:iv-vii

Ikeda Y, Taniguchi N, Noguchi T. 2000. Dominant negative role of the glutamic acid residue conserved in the pyruvate kinase M(1) isozyme in the heterotropic allosteric effect involving fructose-1,6-bisphosphate. *J Biol Chem* 275:9150-6

Jurica MS, Mesecar A, Heath PJ, Shi W, Nowak T, Stoddard BL. 1998. The allosteric regulation of pyruvate

kinase by fructose-1,6-bisphosphate. *Structure* 6:195-210

Larsen TM, Benning MM, Rayment I, Reed GH. 1998. Structure of the bis(Mg^{2+})-ATP-oxalate complex of the rabbit muscle pyruvate kinase at 2.1 A resolution: ATP binding over a barrel. *Biochemistry* 37:6247-55

Larsen TM, Benning MM, Wesenberg GE, Rayment I, Reed GH. 1997. Ligand-induced domain movement in pyruvate kinase: structure of the enzyme from rabbit muscle with Mg^{2+}, K^{+}, and L-phospholactate at 2.7 A resolution. *Arch Biochem Biophys* 345:199-206

Larsen TM, Laughlin LT, Holden HM, Rayment I, Reed GH. 1994. Structure of rabbit muscle pyruvate kinase complexed with Mn^{2+}, K^{+}, and pyruvate. *Biochemistry* 33:6301-9

Lenski RE. 1991. Quantifying fitness and gene stability in microorganisms. *Biotechnology* 15:173-92

Lenski RE, Mongold JA, Sniegowski PD, Travisano M, Vasi F, Gerrish PJ, Schmidt TM. 1998. Evolution of competitive fitness in experimental populations of *E. coli*: what makes one genotype a better competitor than another? *A. V. Leeuwenhoek* 73:35-47

Lenski RE, Rose MR, Simpson SC, Tadler SC. 1991. Long-term experimental evolution in *Escherichia coli*. I. Adaptation and divergence during 2,000 generations. *Am Nat* 138:1315-41

Lenski RE, Travisano M. 1994. Dynamics of adaptation and diversification: a 10,000-generation experiment with bacterial populations. *Proc Natl Acad Sci U S A* 91:6808-14

Lovell SC, Mullick AH, Muirhead H. 1998. Cooperativity in *Bacillus stearothermophilus* pyruvate kinase. *J Mol Biol* 276:839-51

Malcovati M, Valentini G. 1982. AMP- and fructose 1,6-bisphosphate-activated pyruvate kinases from *Escherichia coli*. *Methods Enzymol* 90 Pt E:170-9

Mattevi A, Bolognesi M, Valentini G. 1996. The allosteric regulation of pyruvate kinase. *FEBS Lett* 389:15-9

Mattevi A, Valentini G, Rizzi M, Speranza ML, Bolognesi M, Coda A. 1995. Crystal structure of *Escherichia coli* pyruvate kinase type I: molecular basis of the allosteric transition. *Structure* 3:729-41

Mesecar AD, Nowak T. 1997a. Metal-ion-mediated allosteric triggering of yeast pyruvate kinase. 1. A multidimensional kinetic linked-function analysis. *Biochemistry* 36:6792-802

Mesecar AD, Nowak T. 1997b. Metal-ion-mediated allosteric triggering of yeast pyruvate kinase. 2. A multidimensional thermodynamic linked-function analysis. *Biochemistry* 36:6803-13

Monod J, Wyman J, Changeux JP. 1965. On the nature of allosteric transitions: a plausible model. *J Mol Biol* 12:88-118

Muirhead H. 1990. Isoenzymes of pyruvate kinase. *Biochem Soc Trans* 18:193-6

Muirhead H, Clayden DA, Barford D, Lorimer CG, Fothergill-Gilmore LA, Schiltz E, Schmitt W. 1986. The structure of cat muscle pyruvate kinase. *EMBO J* 5:475-81

Munoz ME, Ponce E. 2003. Pyruvate kinase: current status of regulatory and functional properties. *Comp Biochem Physiol B Biochem Mol Biol* 135:197-218

Oria-Hernandez J, Cabrera N, Perez-Montfort R, Ramirez-Silva L. 2005. Pyruvate kinase revisited: the activating effect of K^{+}. *J Biol Chem* 280:37924-9

Pelosi L, Kuhn L, Guetta D, Garin J, Geiselmann J, Lenski RE, Schneider D. 2006. Parallel changes in global protein profiles during long-term experimental evolution in *Escherichia coli*. *Genetics* 173:1851-69

Pendergrass DC, Williams R, Blair JB, Fenton AW. 2006. Mining for allosteric information: natural

mutations and positional sequence conservation in pyruvate kinase. *IUBMB Life* 58:31-8

Rigden DJ, Phillips SE, Michels PA, Fothergill-Gilmore LA. 1999. The structure of pyruvate kinase from *Leishmania mexicana* reveals details of the allosteric transition and unusual effector specificity. *J Mol Biol* 291:615-35

Sakai H, Ohta T. 1993. Molecular cloning and nucleotide sequence of the gene for pyruvate kinase of *Bacillus stearothermophilus* and the production of the enzyme in *Escherichia coli*. Evidence that the genes for phosphofructokinase and pyruvate kinase constitute an operon. *Eur J Biochem* 211:851-9

Simpson GG. 1953. *The major features of evolution*. New York Columbia University Press

Travisano M, Lenski RE. 1996. Long-term experimental evolution in *Escherichia coli*. IV. Targets of selection and the specificity of adaptation. *Genetics* 143:15-26

Valentini G, Chiarelli L, Fortin R, Speranza ML, Galizzi A, Mattevi A. 2000. The allosteric regulation of pyruvate kinase. *J Biol Chem* 275:18145-52

Valentini G, Chiarelli LR, Fortin R, Dolzan M, Galizzi A, Abraham DJ, Wang C, Bianchi P, Zanella A, Mattevi A. 2002. Structure and function of human erythrocyte pyruvate kinase. Molecular basis of nonspherocytic hemolytic anemia. *J Biol Chem* 277:23807-14

Walker D, Chia WN, Muirhead H. 1992. Key residues in the allosteric transition of *Bacillus stearothermophilus* pyruvate kinase identified by site-directed mutagenesis. *J Mol Biol* 228:265-76

Wichman HA, Badgett MR, Scott LA, Boulianne CM, Bull JJ. 1999. Different trajectories of parallel evolution during viral adaptation. *Science* 285:422-4

Woods R, Schneider D, Winkworth CL, Riley MA, Lenski RE. 2006. Tests of parallel molecular evolution in a long-term experiment with *Escherichia coli*. *Proc Natl Acad Sci U S A* 103:9107-12

Wooll JO, Friesen RH, White MA, Watowich SJ, Fox RO, Lee JC, Czerwinski EW. 2001. Structural and functional linkages between subunit interfaces in mammalian pyruvate kinase. *J Mol Biol* 312:525-40

Chapter 2

Functional and structural characterisation of the *E. coli* PK1: wild-type

2.1 Introduction

Pyruvate kinase type 1 (PK1) from *E. coli* has been well studied with respect to its role in glycolysis and in terms of its structure and function (Mattevi *et al.* 1996; Mattevi *et al.* 1995; Munoz & Ponce 2003; Ponce *et al.* 1995). In this chapter, the biochemical characterisations of the wild-type PK1 were presented, to ensure the clone used in this study is consistent with published results and to allow the direct comparison of these data with those observed for the later introduced mutants. The kinetic properties of the enzyme were examined using the LDH-coupled assay (Section 6.4.1). Circular dichroism was used to examine the secondary structure of PK1. In addition, analytical ultracentrifugation (AUC) and fluorescence detection coupled with AUC (AUC-FDS) were utilised to assess the quaternary structure of this enzyme. A previous paper reported that FBP assisted tetramer assembly in rabbit kidney PKRK, whereas ADP prompted the tetramer to disassemble into dimers (Friesen *et al.* 1998b). Therefore, the protein association in the presence of substrates PEP and ADP and the effector FBP were also tested in this chapter.

2.2 Expression and purification of the wild-type PK1

The rigorous biochemical and biophysical characterisation of the wild-type enzyme required production and purification of the enzyme in milligram scales. A high copy-number plasmid carrying the gene for *E. coli* PK1 (*pykF*) was utilised in this study,

which facilitated purification of the enzyme from *E. coli* BL21 cultures, a common bacterial expression system.

2.2.1 Enzyme expression

The plasmid pGV5A (Valentini *et al.* 1997), which is a modified pBlueScriptII KS+ vector carrying the wild-type PK1 gene (*pykF*) was kindly donated by Professor Andrea Mattevi (University of Pavia, Italy). This plasmid was transformed into *E. coli* BL21 (DE3) competent cells by the calcium chloride method (Section 6.2.15). The plasmid conferred ampicillin resistance to transformed cells. Transformed cells were cultured on a LB plate with ampicillin and incubated overnight. Colonies were subcultured and stored in LB-glycerol media at -80 °C.

E. coli BL21 (DE3) cells transformed with pGV5A were cultured in 10 ml of LB-ampicillin medium, which was used to inoculate 1 litre of LB-ampicillin medium overnight. Over-expression of the enzyme was induced by the addition of isopropyl-1-thio-β-D-galactopyranoside (IPTG). A cell-free lysate was produced by ultrasonication followed with centrifugation (Section 6.3.3.3).

2.2.2 Enzyme purification

The protocol for purification of the wild-type PK1 was adapted from the procedure used by Mattevi and colleagues (Mattevi *et al.* 1996). In each step, the activity of the fractions containing the PK1 enzyme was examined using a lactate dehydrogenase (LDH) coupled assay (Malcovati & Valentini 1982) (Section 6.4.1). In this assay, pyruvate, one of the products of the pyruvate kinase catalysed reaction, was utilised as a substrate for LDH. This reaction leads to loss of NADH. Therefore, activity of a fraction is correlated to the decrease in absorbance of NADH in the spectrometer at 340 nm.

The purification procedure contained three steps (Section 6.3.3). Initially, the cell free

crude extract was subjected to anion exchange chromatography with an increasing salt gradient of KCl. The active fractions were then analysed by SDS-PAGE (section 6.3.2) (Figure 2.1, lane 3). The pooled fractions contained PK1 (~55 kDa), as judged by SDS-PAGE, with highly improved purity as compared to the cell lysate (Figure 2.1, lane 2). The pooled fractions containing PK1 were then applied to a phenyl-Sepharose column for hydrophobic interaction chromatography and eluted with a decreasing ammonium sulphate gradient (Section 6.3.3). This step further improved the purity of the PK1 enzyme (Figure 2.1, lane 4). Finally, the pooled active fractions from the hydrophobic interaction chromatographic step were concentrated by centrifugation and purified and desalted by size-exclusion chromatography (Section 6.3.3). The enzyme was stored in the desalt buffer containing 10 mM Tris, pH 7.5, with ethylene diamine tetra-acetic acid (EDTA, 1 mM) and β-mercaptoethanol (2 mM). The eluent was analysed by both the LDH coupled assay and the SDS-PAGE for purity (Figure 2.1, lanes 5 & 6).

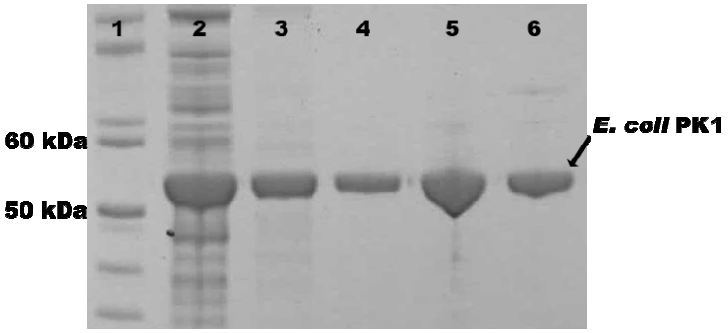

Figure 2.1 **SDS-PAGE of the wild-type PK1 purification.** Lane 1 shows the molecular weight markers with relevant bands indicated. Lane 2 shows the crude extract, lane 3 shows pooled fractions after ion exchange chromatography, lane 4 shows pooled fractions after phenyl-Sepharose chromatography, lane 5 and 6 show the protein after size exclusion chromatography (with 5 µl and 2 µl loaded, respectively).

The protein concentration after each purification step was determined by the Bio-Rad protein assay (Section 6.3.1), a modification of the method developed by Bradford, using bovine serum albumin (BSA) as a standard (Bradford 1976). Coupled with the activities of the eluents determined by the LDH coupled assay, the specific PK1 activities

were calculated. The purification table (Table 2.1) showed that the specific activity increased throughout the purification. A high yield of enzyme was recovered following purification (40%), consistent with the yield achieved in an early study (Valentini *et al.* 2000).

Table 2.1 **Purification of the wild-type PK1 from *E. coli* BL21 (DE3)-pGV5A**

	Protein[a] (mg)	**Total Activity**[b] (U[c])	**Specific Activity** (U/mg)	**Yield** (%)	**Degree of purification** (fold)
Crude extract	236	231	1.0	-	-
Ion exchange	59	197	3.3	85	3.3
Phenyl-Sepharose	32	142	4.4	61	4.4
Size exclusion	21	95	4.5	41	4.5

[a] Protein obtained per litre culture
[b] Activity was determined using the LDH coupled assay.
[c] 1 U is defined as the oxidation of 1 μmole of NADH per second.

The pure PK1 enzyme was stored in Tris buffer (10 mM Tris, pH 7.5, with 1 mM EDTA and 2 mM β-mercaptoethanol) at -20 °C at equal or less than10 mg/ml without loss of activity for up to 9 months (Malcovati & Valentini 1982).

2.3 Residual PK1 activity in *E. coli* BL21 (DE3) cells

The residual PK1 activity of *E. coli* BL21 (DE3) strain was examined. This was important since some of the mutated enzymes examined in Chapter 3 may have low activity, in which case contamination by wild-type PK1 may be a confounding factor. Therefore, it was necessary to measure the residual PK1 activity as a control for the kinetic study.

BL21 (DE3) bacteria (without pGV5A) were cultured in similar conditions to those used to grow BL21 (DE3)-pGV5A in a medium without antibiotics, but including IPTG (Sections 6.2.7 & 6.3.3). After ultrasonication and the removal of all cell debris, the whole cell lysate was subjected to the LDH coupled assay for the PK1 activity test (Section 6.4.1). Protein concentration was determined by the Bio-Rad protein assay.

The *E. coli* BL21 (DE3) cells had a residual PK1 activity of 0.5 U/l (unit activity per litre of culture harvested in the same conditions as the cultures transformed with the plasmid pGV5A), which is about 0.2% of the activity of the wild-type PK1 (with FBP added). This is equal to less than 0.1 mg of endogenous PK1 activity in every litre of BL21 (DE3) cell culture. At this low level of activity, the residual PK1 activity should not be a concern when studying the kinetics of the mutants that are reasonably active. Moreover, the small portion of PK1 activity observed in crude extract (Table 2.1) may be due to the function of other pyruvate, PEP and NADH utilising enzymes in the cell lysate.

2.4 Kinetic study of the wild-type PK1

2.4.1 pH optimisation and buffer strength

The pH tolerance of *E. coli* PK1 was tested. The enzyme was active over a broad pH range (pH 5.4-8.2) with the highest activity achieved between pH 6.0 and pH 7.5 (Figure 2.2). All subsequent assays for characterisation of the PK1 wild-type and the mutants were performed at pH 7.5.

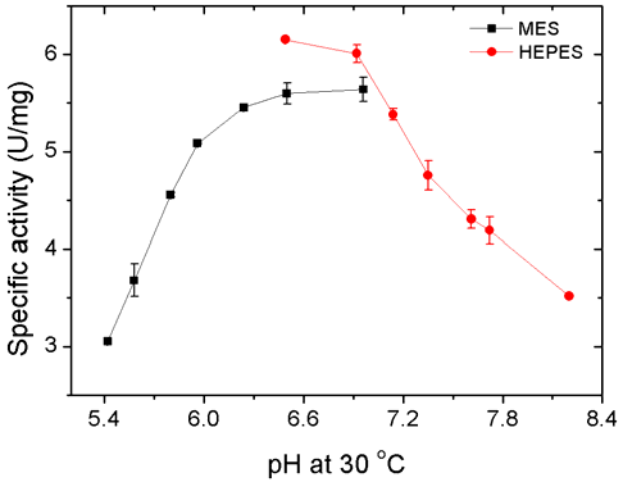

Figure 2.2 **The activity of *E. coli* PK1 (wild-type) at different pH.** One unit (U) is equal to the oxidation of 1 µmole NADH/sec under the assay conditions in Section 6.4.1. MES buffer (■, 10 mM) was used for assays between pH 5.4 and pH 7.0, HEPES buffer (□, 10 mM) was used for assays between pH 6.5 and pH 8.2. Error bars represent the standard error of the mean between two replicates.

HEPES buffer (10 mM) was used in the kinetic assay, following Valentini (2000). However, this buffer strength was too weak to keep the reaction mixture at a constant pH when a high substrate concentration (i.e. > 2 mM) of phosphoenolpyruvate (PEP) monosodium salt was added into the reaction solution. Enzyme activity changed steeply about pH 7.5 (Figure 2.2), affecting trial experiments. To solve this problem, higher HEPES concentrations were used and the activity of the wild-type PK1 with respect to buffer concentration was tested.

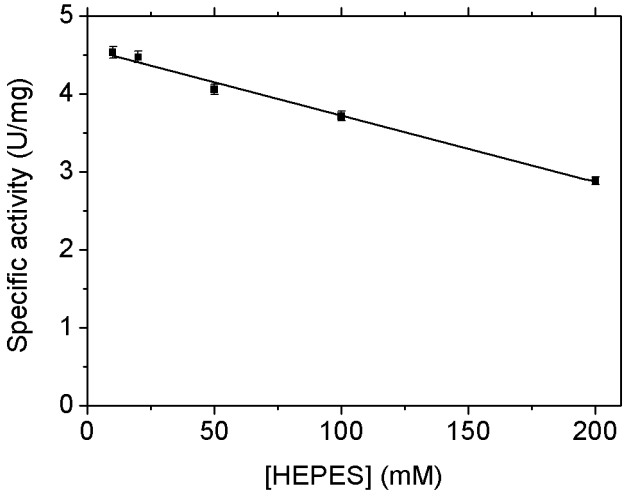

Figure 2.3 **The activity of wild-type PK1 with respect to HEPES buffer concentration.** The activity of the wild-type PK1 was tested under the standard assay conditions (Section 6.4.1), with various buffer concentrations. Error bars represent the standard error of the mean specific activity of two replicates.

Figure 2.3 shows that at high concentrations of HEPES buffer, the enzyme was moderately inhibited. About 80% of the activity of the enzyme was retained when a concentration of 100 mM HEPES was used. The activity further decreased to ~60% when a 200 mM HEPES buffer was used in the assay. Given the decrease in activity with increasing HEPES concentrations, the buffer concentration was kept standard. As an alternative strategy of solving the pH problem, the PEP monosodium stock solution at 200 mM was pre-adjusted to a neutral pH (as judged by universal pH testing strips) using concentrated potassium hydroxide, so that the pH of the reaction mixture was not altered

on addition of PEP.

2.4.2 Coupling efficiency of LDH

When utilising coupled reactions to monitor enzyme activity, a necessary control is to show that the coupling enzyme (in this case LDH) is in excess and does not limit the rate of the enzyme catalysed reaction being measured (see Figure 2.4 for the chemistry of the LDH catalysed reaction).

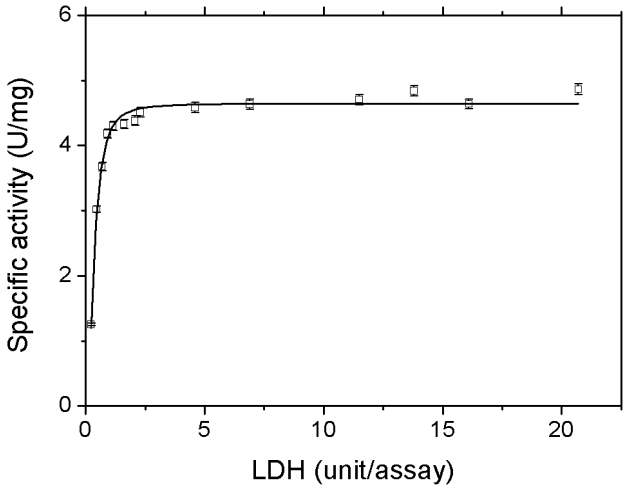

Figure 2.5 **LDH titration curve with respect to PK1 activity as measured by the coupled assay.** The activity of the wild-type PK1 was tested under the standard assay conditions (Section 6.4.1) and various amounts of lactate dehydrogenase (LDH) in a total volume of 1 ml. The reaction was performed at 30 °C and was initiated by adding pure wild-type PK1 into the reaction mixture. Error bars represent the standard error of the mean of the specific activity between two replicates.

Figure 2.5 shows the coupling efficiency of LDH at increasing concentrations. The amount of LDH in the coupled reaction should be in excess, so that the overall reaction rate is only limited by the rate of the PK1 catalysed reaction. In this way, the decrease in NADH will accurately reflect the initial rate of the PK1 enzyme (Bücher & Pfeiderer 1955).

The assay result suggested that approximately 2.5 units of LDH per assay were sufficient to ensure that the coupling enzyme was in excess and that the measured rate represented the PK1 catalysed reaction (Figure 2.5). In this study, 23 units of LDH (~10 times excess) were used in each kinetic assay to ensure that the LDH was in excess under all conditions tested.

2.4.3 Steady-state kinetic analysis of the PK1 wild-type

Steady state kinetic analysis of the wild-type PK1 was performed by measuring the initial velocity at various PEP and ADP concentrations (Section 6.4.2). Two approaches have been successfully used in assaying PK1 kinetics. The most widely used is the "coupled" assay, in which the oxidation of NADH is monitored in an UV-vis spectrophotomer at 340 nm (Bücher & Pfeiderer 1955). Alternatively, the analysis can be performed "directly" by monitoring the spectrophotometric recording of the decrease in absorbance at 230 nm due to PEP loss (Malcovati & Valentini 1982). In this thesis, the LDH coupled assay (Section 6.4.1) was used, as it required a minimal amount of enzyme and the loss of NADH absorbance signal was directly related to PK1 activity. Therefore, the enzyme activity was expressed as the spectral reading of the loss of the NADH, where one unit equals to the consumption of 1 μmole NADH per second per milligram of protein in a 1 ml assay (Valentini *et al.* 2000), and the turnover number k_{cat} (s^{-1}) was used to interpret the kinetic data. Data were processed with the program Origin (OriginLab, version 8E) to determine the mode of catalysis and various parameters, such as k_{cat}, $S_{0.5}$ and the Hill coefficient (n_H).

PK1 is an allosterically regulated protein. It is homotropically regulated (ligand binding affects the binding of an identical ligand) by the substrate PEP and heterotropically regulated (binding of ligand affects the binding of a different ligand) by FBP (Lovell *et al.* 1998). Previous studies found that in the presence of FBP and with respect to varying PEP concentrations, the enzyme showed a typical Michaelis-Menten type kinetic pattern; whereas when FBP is absent, the Hill cooperative model (Hill 1910) applied (Mattevi *et*

al. 1996; Valentini *et al.* 2000). A typical Michaelis-Menten model is achieved when the Hill coefficient is 1 (Equation 2.1b, when n = 1), in which case no cooperativity is observed. Equations for the Michaelis-Menten and Hill cooperative model are shown below:

Michaelis-Menten model: $\upsilon = (k_{cat}\,[S]) / (K_M + [S])$ (Equation 2.1a),

Hill cooperativity model: $\upsilon = (k_{cat}\,[S]^n / ((S_{0.5}{}^n) + ([S]^n))$ (Equation 2.1b),

where k_{cat} is the turnover number; [S] is the substrate concentration; K_M is the Michaelis–Menten coefficient for substrate [S]; $S_{0.5}$ is the substrate concentration when half of the V_{max} is reached under Hill cooperativity model; n_H is Hill coefficient; and υ is the initial velocity. In this study, the kinetic data were fitted to the best of the above two models by comparing the R^2 value of the non-linear regression and standard error associated with the kinetic parameters. $S_{0.5}$ was further defined at $S_{0.5}{}^{PEP}$ and $S_{0.5}{}^{ADP}$ in this study.

The steady state kinetic parameters for purified wild-type PK1 were measured by following the signal loss of NADH at pH 7.5 at 30 °C (Section 6.4.2). Parameters for the substrates PEP and ADP were determined, as well as the allosteric effector FBP. For PEP and ADP, the initial velocity values were determined at varying concentrations of one substrate at a fixed concentration of the other, and in the presence and absence of FBP. For FBP, the initial values were determined as a function of the effect at fixed concentrations of the two substrates.

By fitting the data to the Hill cooperative model, the turnover number (k_{cat}), the $S_{0.5}$ value (defined as the substrate concentration at 1/2 V_{max} in Hill model) and the Hill coefficient n_H were determined (Table 2.2).

Table 2.2 **Kinetic parameters determined for *E. coli* wild-type PK1.** *Results are means ± standard errors.*

PEP							
FBP(-)				**2 mM FBP**			
k_{cat} s^{-1}	$S_{0.5}^{PEP}$ mM	n_H	$k_{cat}/S_{0.5}$ s^{-1}/mM	k_{cat} s^{-1}	$S_{0.5}^{PEP}$ mM	n_H	$k_{cat}/S_{0.5}$ s^{-1}/mM
243 ± 2	1.5 ± 0.1	3.1 ± 0.6	162	268 ± 4	0.06 ± 0.002	1.0 ± 0.04	4467
ADP							
FBP(-)				**2 mM FBP**			
k_{cat} s^{-1}	$S_{0.5}^{ADP}$ mM	n_H	$k_{cat}/S_{0.5}$ s^{-1}/mM	k_{cat} s^{-1}	$S_{0.5}^{ADP}$ mM	n_H	$k_{cat}/S_{0.5}$ s^{-1}/mM
241 ± 12	0.54 ± 0.22	0.8 ± 0.07	446	309 ± 19	0.34 ± 0.07	1.0 ± 0.08	909

When FBP was absent from the assay solution, strong positive cooperativity was evident with respect to PEP (n_H = 3.1 ± 0.6) (Figure 2.6), consistent with PEP being a homotropic effector for PK1. This value agreed well with data obtained in a previous study to investigate the regulation of *E. coli* PK1 (n_H = 3.2 ± 0.06) (Valentini *et al.* 2000). The $S_{0.5}^{PEP}$ increased dramatically (1.5 ± 0.1 mM), as compared to the titration done in the presence of FBP.

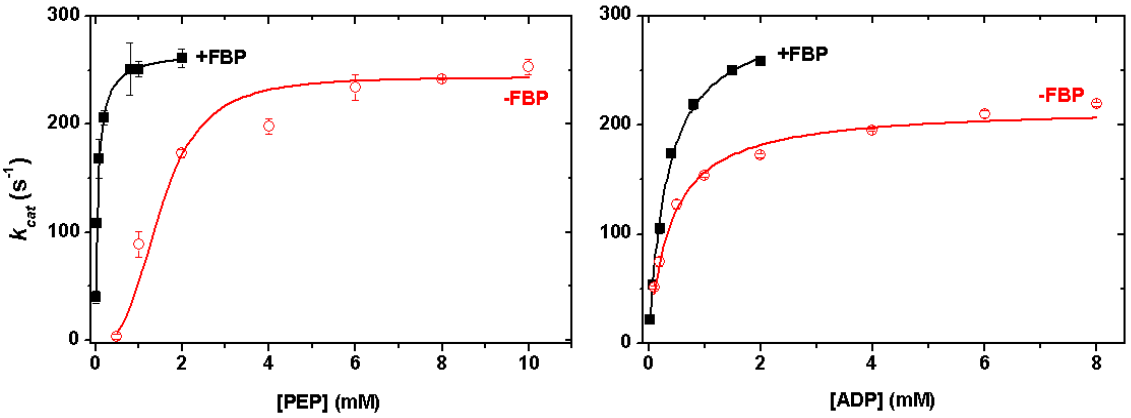

Figure 2.6 **Kinetic properties of wild-type PK1.** The activity of wild-type PK1 was measured at varying concentrations of substrates (PEP and ADP) and allosteric activator (FBP) (Section 6.4.2). Varying concentrations of PEP and ADP are in the absence (○) or presence (■) of 2 mM FBP. To obtain PEP response plots PEP was varied at constant 2 mM ADP, and to obtain ADP response plots ADP was varied at constant 2 mM PEP. Plots represent the best fit by non-linear regression to the Hill equation.

In the presence of 2 mM FBP, the K_M values for PEP and ADP were 0.06 ± 0.001 mM and 0.3 ± 0.03 mM, respectively. The k_{cat} values were 268 ± 4 s^{-1} (k_{cat}^{PEP}) and 309 ± 19 s^{-1} (k_{cat}^{ADP}), which were similar.

Although no study has found FBP to have any regulatory interaction with ADP on the wild-type PK1, an ADP titration assay in the presence and absence of FBP was performed (Figure 2.6). An n_H^{ADP} value of 0.8 ± 0.07 was obtained, which represented a slightly negative cooperativity. However, the data also fitted the Michaelis-Menten model well, with similar k_{cat}^{ADP} and $S_{0.5}^{ADP}$ values (R^2 = 0.98, by Origin fitting). This is again in agreement with previous studies (Valentini *et al.* 2000), and implied that FBP binding influenced PEP binding, as discussed in several earlier studies (Fenton & Blair 2002; Friesen *et al.* 1998a; Mattevi *et al.* 1996; Mattevi *et al.* 1995). ADP binding was not affected, as indicated by similar $S_{0.5}^{ADP}$values of 1.0 and 0.8, with and without FBP (Table 2.2).

These data support the previous findings that FBP does not affect the k_{cat}, but does affect the mode of PEP binding.

2.5 Biophysical Characterisation of wild-type PK1

2.5.1 Circular dichroism spectroscopy

Circular dichroism spectroscopy (CD) gives information about the secondary structure of a protein (Johnson 1999; Kelly *et al.* 2005). In addition, information relevant to protein folding and binding properties can be rapidly established by this method (Greenfield 2006). This technology utilises the handedness of circular polarized light. Asymmetric molecules interact with light and may absorb the right- and left-handed circularly polarized light to different extents. Data are usually recorded as the difference in the absorbance of the right- and left-handed lights and further processed as degrees of ellipticity. Ellipticity describes the shape the rotated light traces on the plane

of light (Greenfield 2006). In terms of protein, where amide chromophores of the polypeptide backbone are aligned, their optical transitions are changed (Greenfield 1996). Each alignment has its characteristic shape and degree of ellipticity, which is used to define the secondary structure. For instance, the CD spectra of α-helical proteins is characterised by the two negative peaks at 222 nm and 208 nm. CD spectra are processed by comparing the data with existing protein reference libraries, so that content of α-helix, β-sheet and random coils in the protein of interest can be determined. Conformational changes of the protein due to temperature, mutations, denaturants and bindings can be monitored by CD (Greenfield 2006). The secondary structures of the protein derived from the CD spectra are largely dependent on the spectral magnitude effect (Miles *et al.* 2005). Calibration of the instrument, the spectral cell length and the protein concentration needs to be accurately determined to obtain meaningful results (Greenfield 2006).

The secondary structure of wild-type PK1 was evaluated by circular dichroism (CD) spectroscopy using a Jasco-815 CD spectropolarimeter (Section 6.5.2). CD spectra were processed with 3 algorithms (SELCON3, CONTIN-LL and CDSSTR) on the DICHROWEB website and the results were compared (Compton & Johnson 1986; Sreerama *et al.* 1999; van Stokkum *et al.* 1990) (Table 2.3). These algorithms can be used in conjunction with any of the seven reference datasets on the DICHROWEB website (Sreerama *et al.* 2000). The quality of the fit was judged by the normalised root mean square deviation (n.r.m.s.d.) value, which is a goodness-of-fit parameter used to measure the correspondence between the calculated and the experimental spectra (Wallace *et al.* 2003). Among all the algorithms applied in DICHROWEB, CDSSTR is the least sensitive to the magnitude effect, with an overall low n.r.m.s.d. in all measurements (Miles *et al.* 2005). Dataset 7 was chosen because the data collected by the spectropolarimeter fell into the dataset range of 190 to 240 nm.

The CDSSTR algorithm requires a minimum number of reference proteins in a good

analysis, and follows four criteria: (1) the sum of the secondary structures are between 0.95 and 1.05, (2) fractions of the secondary structures should be above -0.03, (3) the re-constructed CD spectrum fits the original CD spectra well, with a low n.r.m.s.d. value, (4) the fraction of α-helices should be similar to that obtained using all reference proteins (Johnson 1999).

The n.r.m.s.d. showed that the CDSSTR algorithm best fitted the data using dataset 7 (Figure 2.7), as judged by the n.r.m.s.d. (0.017). Therefore, CDSSTR was chosen for data interpretation and comparison.

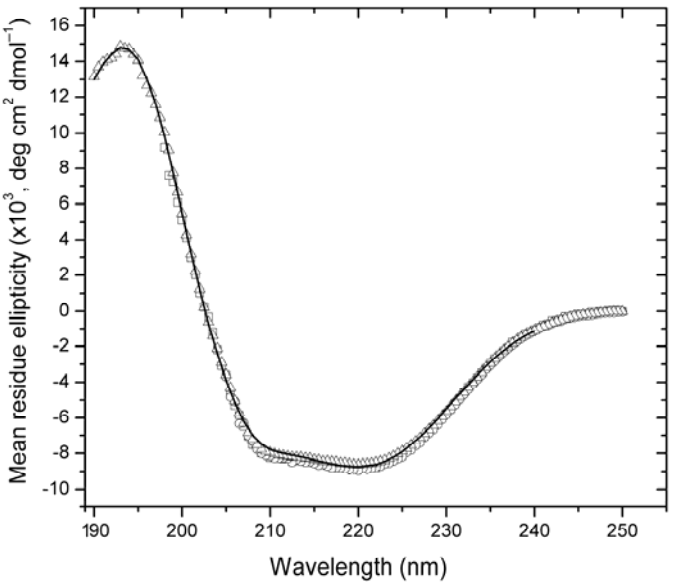

Figure 2.7 **Circular dichroism spectroscopy of wild-type PK1.** Mean residue ellipticity ([θ]) is plotted as a function of wavelength from 190 nm to 250 nm. The symbols show the raw data (□=0.47 mg/ml, O=0.23 mg/ml, and △=0.16 mg/ml) and the line shows fitting with CDSSTR algorithm (reference set 7) from DICHROWEB using 0.16 mg/ml enzyme.

In the experiment, the measurement of wavelengths ranged from 190 nm to 250 nm, using only data where the HT voltage was below 600 V. When the HT voltage exceeds 600 V, the signal-to-noise ratio greatly diminishes, making the data noisy and unreliable (Greenfield 2006).

The spectrum obtained for wild-type PK1 was comprised of two absorbance minima at approximately 208 nm and 222 nm, characteristic of α-helices (Figure 2.7). This result is consistent with the crystal structures obtained from several sources of pyruvate kinase, that the protein has a high content of α-helices (Larsen *et al.* 1998; Mattevi *et al.* 1995; Rigden *et al.* 1999). Although it does not give the residue-specific information that can be obtained by X-ray crystallography or NMR (Greenfield 2006), it suggests that the enzyme is well structured, with primarily α-helix and β-sheet secondary content.

Table 2.3 **Comparison of the wild-type CD fitting parameters using three different algorithms**

Parameters	***SELCON3***	***CONTIN-LL***	***CDSSTR***
n.r.m.s.d.	0.161	0.072	0.017
α-helix(1)	0.132	0.11	0.14
α-helix(2)	0.121	0.116	0.10
β-strand(1)	0.16	0.24	0.16
β-strand(2)	0.089	0.096	0.1
Turn	0.204	0.2	0.2
uncoiled	0.287	0.238	0.30
Total	**0.993**	**1**	**1**
Helix segments per 100 residues:	3.0	2.9	2.6
Ave helix length per segment:	8.4	7.8	9.3
Strand segments per 100 residues:	4.5	4.8	4.7
Ave strand length per segment:	5.6	7.0	5.2

Six secondary structures have been estimated, which are the regular α-helix (1), distorted α-helix (2), regular β-strand (1), distorted β-strand (2), turns and uncoiled structure. The number of α-helical and β-strand segments in the protein gives valuable information regarding distortion of the protein, that on average four residues per α-helix and two residues per β-strand may be considered to distort in protein (Sreerama *et al.* 1999). In the situation of wild-type PK1, the protein appeared to be well folded, as the lengths

(residues) per segment of the α-helix and the β-strand were 9.3 and 5.2, respectively.

2.5.2 Mass spectrometry

Electrospray ionisation (ESI) mass spectrometry (MS) accurately determines the mass of a molecule by generating a mass spectrum that is represented as ion intensity versus the mass-to-charge ratio (m/z) of sample components. Biological samples with large molecular weights are often multiply charged in positive or negative ionisation states. In addition, salt adducts may be present in the protein sample, resulting in different peaks of m/z on the histogram. A Gaussian-type distribution with multiple charged states in the ES/MS spectra is usually observed (Domon & Aebersold 2006).

The m/z distribution is used to estimate the molecular weight of the sample, by applying the equation:

$$m/z = (MW + nH^{+})/n$$

where m/z is the mass-to-charge ratio of the sample, MW is the molecular mass, n is the integer number of charges on the ions and H is the mass of a proton Domon & Aebersold 2006). In the situation where n is not known, an assumption is made that any two adjacent members in the series of multiply charged ions differ by one charge, so that molecular weight may be estimated.

For carrying out the mass spectrometric analysis, purified wild-type PK1 was directly injected into the mass spectrometer at various time points with the solution of acetonitrile in water combined with formic acid, at 0.25 ml/min (Section 6.5.1). Data were collected using the mass spectrometer with an electrospray ionising (ESI) source coupled to an Agilent 1100 LC system (Agilent, Palo Alto, CA).

The deconvoluted mass of the wild-type PK1 monomer was estimated to be 50729.34 Da (Figure 2.8), which is consistent with the isotopically averaged molecular weight of 50729.28 Da by amino acid (Valentini *et al.* 1979). There were two other adducts (+17

and +37 Da) associated with the main peak. A search of the ABRF DeltaMass database (a database of protein post-translational modifications, at http://www.abrf.org/), suggested the two adducts were most likely to be a sodium derivative (+22 Da) and a potassium salt adduct (+37 Da).

There was another peak (50805.18 Da) and two sub-peaks further away from the main peak, with a repeated pattern to the main peak. This peak was +76 Da heavier than the main peak and is consistent with a β-mercaptoethanol adduct. During protein purification, β-mercaptoethanol was added into buffer solution at every purification step. Therefore, it is likely that β-mercaptoethanol binds to the protein post purification.

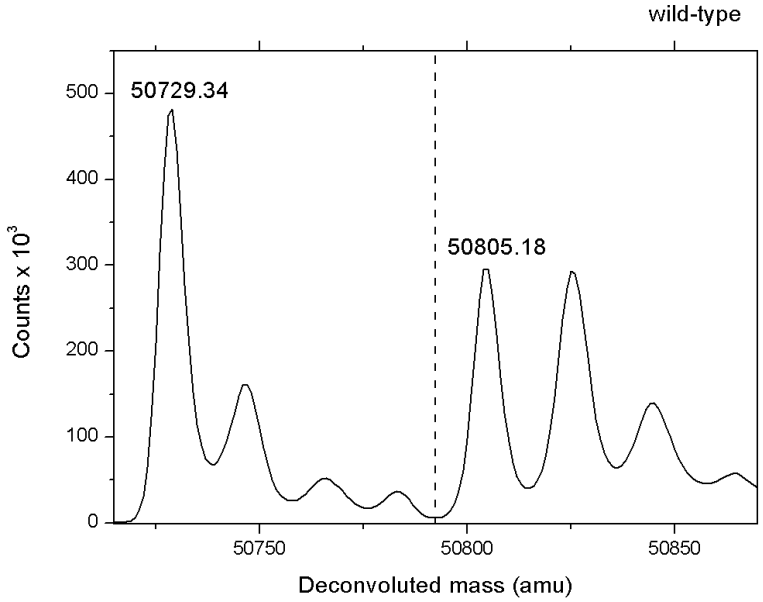

Figure 2.8 **Counts versus deconvoluted mass (amu) graph of wild-type PK1.** The peak with amu equal to 50729.34 represented a wild-type PK1 monomer, the following two peaks (50746.47 Da (+17) and 50766.04 Da (+37)) represented a PK1 monomer with different adducts. The peak with mass 50805.18 Da is consistent with the PK1 monomer plus β-mercaptoethanol.

2.5.3 Analytical ultracentrifugation

Generally, XL-I (or the older XL-A) ultracentrifuge instruments are used for carrying out

AUC experiments. These are equipped with optical systems that scan the solute concentration during the ultracentrifugation process. The technique of AUC has been improved largely by the development of new instruments and computational data analysis tools (Lebowitz *et al.* 2002). AUC sedimentation velocity experiments have been performed in this study to characterise the biophysical properties of wild-type PK1 and the variants.

At a large centrifugal force, protein leaves the meniscus and forms a boundary that moves towards the bottom of the cell as a function of time. The speed of movement through the solution is determined primarily by the size, but also the shape of the protein. Other factors that affect the sedimentation rate include protein concentration, solvent ionic strength (i.e. density) and solvent viscosity (Cole *et al.* 2008). In addition, there is a sample concentration distribution around the boundary, which is caused by diffusion.

Data obtained from a sedimentation velocity experiment can be analysed by various methods (Cole *et al.* 2008). The *c(s)* distribution method implemented in the SEDFIT software interface and based on the assumption of a non-interacting molecules (Schuck 2000) was used in this study.

The hydrodynamic properties of wild-type PK1 were examined by sedimentation velocity studies in the analytical ultracentrifuge. The wild-type PK1 was initially examined at 1.0 mg/ml (19.7 μM based on the monomeric mass of 50,729 Da) at 35,000 rpm and 20 °C. The data were collected at 236 nm with a step size 0.001 cm and fitted to a continuous sedimentation coefficient distribution (*c(s)*) model and to a continuous mass distribution (*c(M)*) model using the program SEDFIT (Schuck 2000). Continuous sedimentation distribution (*c(s)*) was plotted as a function of sedimentation coefficient (Svedberg, S) (Figure 2.9).

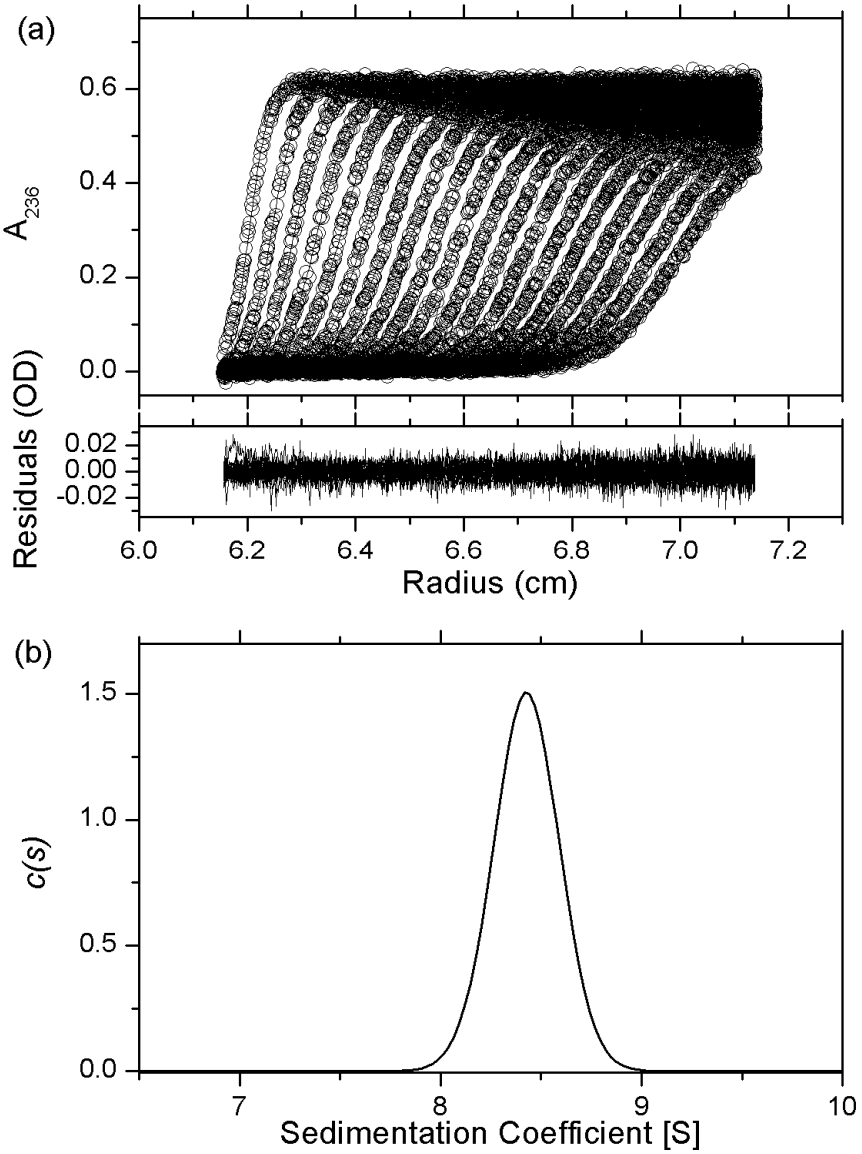

Figure 2.9 **Sedimentation velocity analysis of wild type PK1 at 1.0 mg/ml (19.7 μM) protein.** (a) Absorbance at 236 nm as a function of radius (cm) from the axis of rotation is plotted. The raw data are presented as open circles and are overlaid with the nonlinear least squares best-fit to a continuous-size distribution model (Lamm equation) by SEDFIT. Residuals for the nonlinear least squares best-fit are also shown. (b) The continuous sedimentation coefficient [*c(s)*] distribution as a function of sedimentation coefficient (Svedberg, S). The fit had a resolution of 150 species between s_{min} of 0.1 S and s_{max} of 14 S with P = 0.95, v-bar = 0.7413, ρ = 1.00117 g/ml, η = 0.010066 p, and f/f_0 = 1.31. The r.m.s.d. and runs test-Z score for the fit were 0.0068 and 6.5, respectively.

Data were fitted at a high resolution of 150 with an s value ranging between 0.1 S and 14 S. SEDNTERP was used to calculate the partial-specific volume of wild-type PK1 (0.7413 ml/g, based on the amino acid sequence), solvent density (1.00117 g/ml) and viscosity (0.010066 poise). The frictional ratio (f/f_0) of wild-type PK1, which indicates the maximum shape asymmetry of the enzyme (Lebowitz *et al.* 2002), was allowed to float during the fit, resulting in a f/f_0 of 1.31. The fit resulted an r.m.s.d. of 0.0068 and a runs test-Z score of 6.5, both of which indicated a good fit (Lebowitz *et al.* 2002). A continuous mass distribution fit of the same data was performed (data not shown here), and the results indicated that wild-type PK1 is a single species with molar mass approximately 200 kDa, which agreed well with the theoretical mass of the tetrameric mass of wild-type PK1 (203 kDa).

AUC of the wild-type PK1 was further performed at 1/10 concentration of previous analysis (i.e. at 0.1 mg/ml (1.97 μM)). At lower concentrations, the macromolecule may dissociate into smaller species (such as dimers) as the solute sediments to the bottom of the cell (Lebowitz *et al.* 2002). The dissociation constant (k_D) can be calculated using this information and further sedimentation equilibrium experiments (Cole *et al.* 2008).

However, in this experiment, the dissociation did not occur, as indicated on the *c(s)* distribution plot, where a single peak at ~8.5 S was observed (Figure 2.10). This experiment was performed under the same conditions as for that at 1.0 mg/ml (19.7 μM), and resulted in an r.m.s.d. and runs-Z test score for the fit of 0.0048 and 4.7, respectively, indicating a good fit.

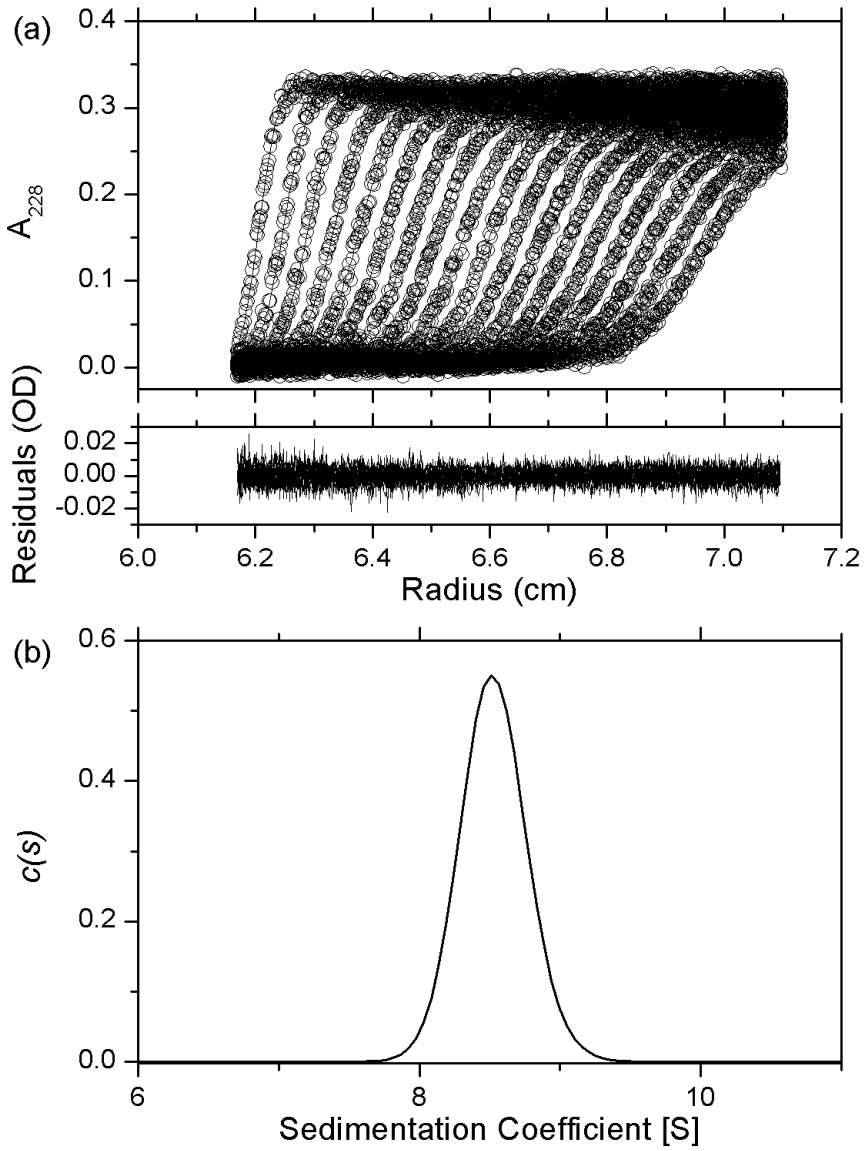

Figure 2.10 **Sedimentation velocity analysis of wild type PK1 at 0.1 mg/ml (1.97 μM) protein.** (a) Absorbance at 228 nm as a function of radius (cm) from the axis of rotation plotted. The raw data are presented as open circles and are overlaid with the nonlinear least squares best-fit to a continuous-size distribution model (Lamm equation) by SEDFIT. Residuals for the nonlinear least squares best-fit are also shown. (b) The continuous sedimentation coefficient [*c(s)*] distribution as a function of sedimentation coefficient (Svedberg, S). The fit had a resolution of 150 species between s_{min} of 0.1 S and s_{max} of 14 S with P = 0.95, v-bar = 0.7413, ρ = 1.00117 g/ml, η = 0.010066 p, and f/f_0 = 1.34. The r.m.s.d. and runs test-Z score for the fit were 0.0048 and 4.7, respectively.

2.5.4 Fluorescence detection system coupled with analytical ultracentrifugation: a new tool for analysing proteins at low concentrations

Protein and nucleic acid concentrations ranging from 10 μg/ml to 5 mg/ml are suitable for traditional AUC analyses (Cole & Hansen 1999). The addition of a fluorescence detection system is a new technology developed that extends the detectable concentration of macromolecules into the picomolar range (MacGregor *et al.* 2004). A trace quantity of the molecule of interest can be detected in solution, even in the presence of a high level of background molecules, which makes this technology very powerful for characterising low concentrations of molecules in solution, and for observing the metabolites in a similar-to-matrix background (Laue 2005).

The distribution of the radial concentration is a critical measurement in sedimentation velocity analysis. The absorbance optical system in a normal AUC will measure the absorbance of the samples at each radial position at a given wavelength from 190 nm to 800 nm. The intensity of the signal (A) is a direct reflection of (in this case) the protein concentration, as represented by the Beer-Lambert law:

$$A = \varepsilon \cdot c \cdot l,$$

where ε is the solute's weight extinction coefficient, c is the solute weight concentration and l is the sample pathlength (Cole *et al.* 2008). Fluorescence detection systems require a laser light source to achieve sufficient radial resolution (20-50 μm). The AUC-FDS measures a single wavelength at 488 nm; therefore, the protein must be labelled with a fluorescent label, so that an extrinsically acquired fluorescence signal can be measured (Cole *et al.* 2008). The intensity of AUC-FDS (F) is can be expressed as:

$$F = I_o \cdot Q \cdot \varepsilon \cdot c,$$

where ε is the extinction coefficient, c is the concentration of the solute, I_o is the intensity of the beam light and Q is the quantum field. The quantum field is largely affected by

degree of labelling and presence of quenchers, therefore, it is difficult to relate the intensity of the signal to concentration of the solute (Cole *et al.* 2008).

Although it is more difficult to run AUC-FDS in terms of sample preparation, experimental operation and data interpretation, as compared to the traditional absorbance analysis (Laue 2005), this novel technique has its advantages. First of all, the concentration detectable in the experiment is much lower; therefore a very dilute solute can be studied and allows one to study molecules with a very tight association. Secondly, the molecule can be examined in a very complex environment, as the fluorescence signal can be easily distinguished from the non-fluorescent absorbance signal. This makes it possible to examine the molecule in an environment that mimics the cell matrix, which is useful to characterise a molecule in near physiological conditions. Thirdly, the broad range of analysis from picomolar to micromolar range allows the concentration range where molecular association becomes significant.

Although AUC-FDS is an excellent technology for studying the structural and hydrodynamic properties of a protein at extremely low concentration, analysis of the *E. coli* PK1 by AUC-FDS (or AUC for that matter) has never been applied in previous studies. This analysis is novel, and is critical for this study, as it gives information about how this enzyme behaves in a highly diluted environment, with a concentration approaching the physiological level, and with the effectors.

Recent studies with dihydrodipicolinate synthase have shown that the substrate pyruvate may regulate enzyme activity by promoting an active dimer from an inactive monomer (Burgress *et al.* 2008). In an early paper it was found that FBP helped the association of a cytosolic thyroid hormone-binding protein (monomer) which shared 97% similarity with human PKM2 at amino acid level to tetrameric form (Fanjul & Farias 1993).

More strikingly, a study demonstrated the propensity of rabbit kidney PKRK to undergo

reversible subunit assembly and disassembly ($K_D^{\text{dimer-tetramer}}$ = 0.6 μM) using analytical gel filtration combined with stimulated sedimentation velocity experiment (Friesen *et al.* 1998b). It was proposed, according to the analytical gel filtration data, that the assembly of the tetramer was favoured by binding of PEP and FBP, whereas ADP and phenylalanine shifted the equilibrium towards disassembly to a dimer (Friesen *et al.* 1998b).

Since AUC with absorbance optics was not able to show dissociation of the wild-type *E. coli* PK1 enzyme, AUC-FDS was employed. The experimental aim was to estimate how tightly associated the tetramer of PK1 was, and to examine the effect of substrates (PEP and ADP) and the effector FBP on the oligomeric state.

In order to utilise AUC-FDS, the enzyme was labelled with a fluorescent tag. Wild-type PK1 was labelled with Alexa Fluor® 488 succinimidyl ester dye at 2.4 mg/ml (i.e. 1.2 x 10^{-5} M) (Section 6.5.4). The labelled protein was separated from the dye by passage through a Sephadex G-25 Column. A pale green band separated from the bright green dye could be visualised. Fractions containing the labelled protein were collected at 1.5 ml portions and pooled. The protein concentration and degree of labelling were determined spectrophotomically (Section 6.5.4).

AUC-FDS sedimentation velocity experiments with wild-type PK1 at 0.01 mg/ml (197 nM) were performed (Figure 2.11). Additional experiments followed the sedimentation of wild-type PK1 at 0.001 mg/ml (19.7 nM) (Figure 2.12), with and without 1.8 mM of substrates (PEP (Figure 2.13) and ADP (Figure 2.14)) and effector (FBP) (Figure 2.15) (Section 6.5.4). Subsequently, wild-type PK1 at a much diluted 0.0005 mg/ml (9.9 nM) (Figure 2.16) were analysed by AUC-FDS, which required the presence of 0.1 mg/ml ovalbumin as a loading protein (Cole *et al.* 2008; MacGregor *et al.* 2004). Different laser intensities and PMT voltages were set, adjusted for the protein concentration and the intensity of the fluorescence signal at the initial run (MacGregor *et al.* 2004).

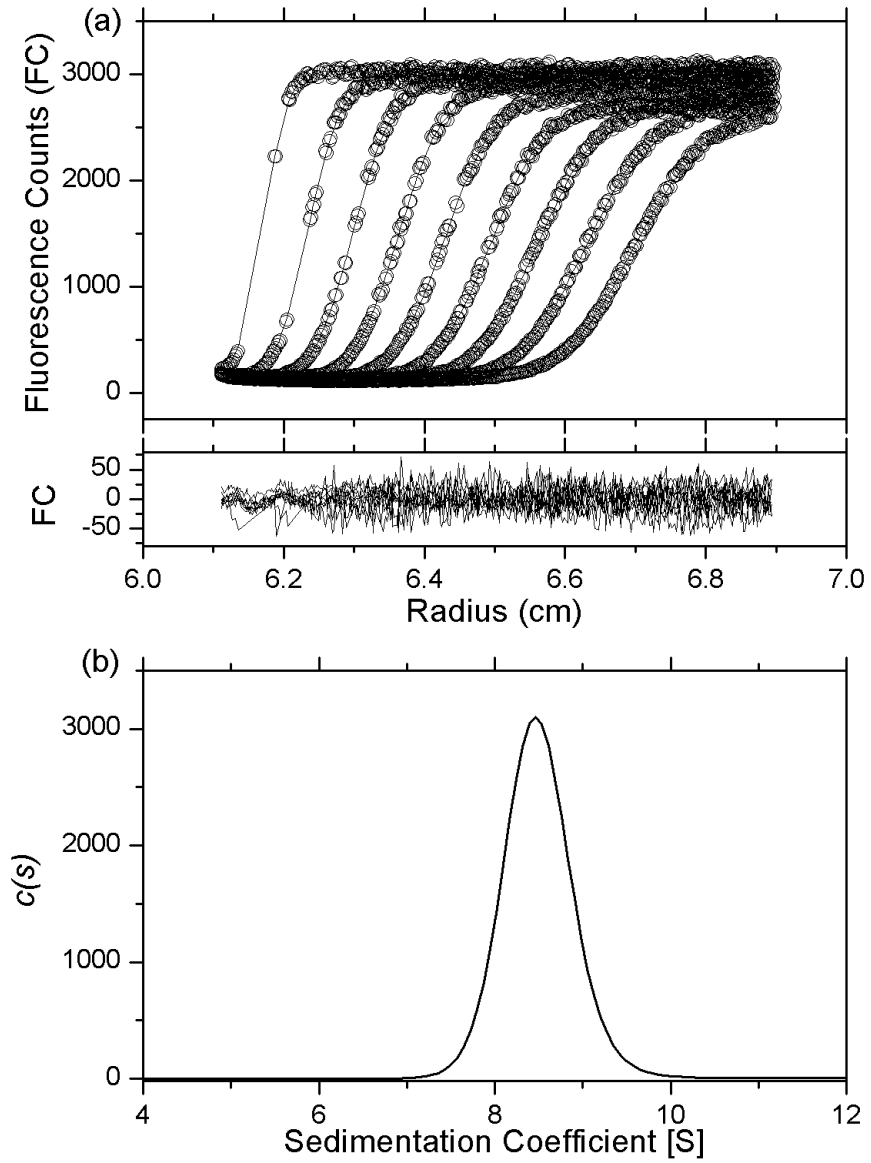

Figure 2.11 **AUC-FDS analysis of wild-type PK1 at 0.01 mg/ml (197 nM) protein with gains set at 2 × 84%.** (a) Fluorescence counts at 488 nm as a function of radius (cm) from the axis of rotation plotted. The raw data are presented as open circles and overlaid with the nonlinear least squares best-fit to a continuous-size distribution model (Lamm equation) by SEDFIT. Residuals for the nonlinear least squares best-fit are also shown. (b) The continuous sedimentation coefficient [*c(s)*] distribution as a function of sedimentation coefficient (S). The fit had a resolution of 150 species between s_{min} of 0.1 S and s_{max} of 15 S with P = 0.95, v-bar = 0.7436, ρ = 1.00117 g/ml, η = 0.010066 p, and f/f_0 = 1.45. The r.m.s.d. and runs test-Z score for the fit were 19 and 24, respectively.

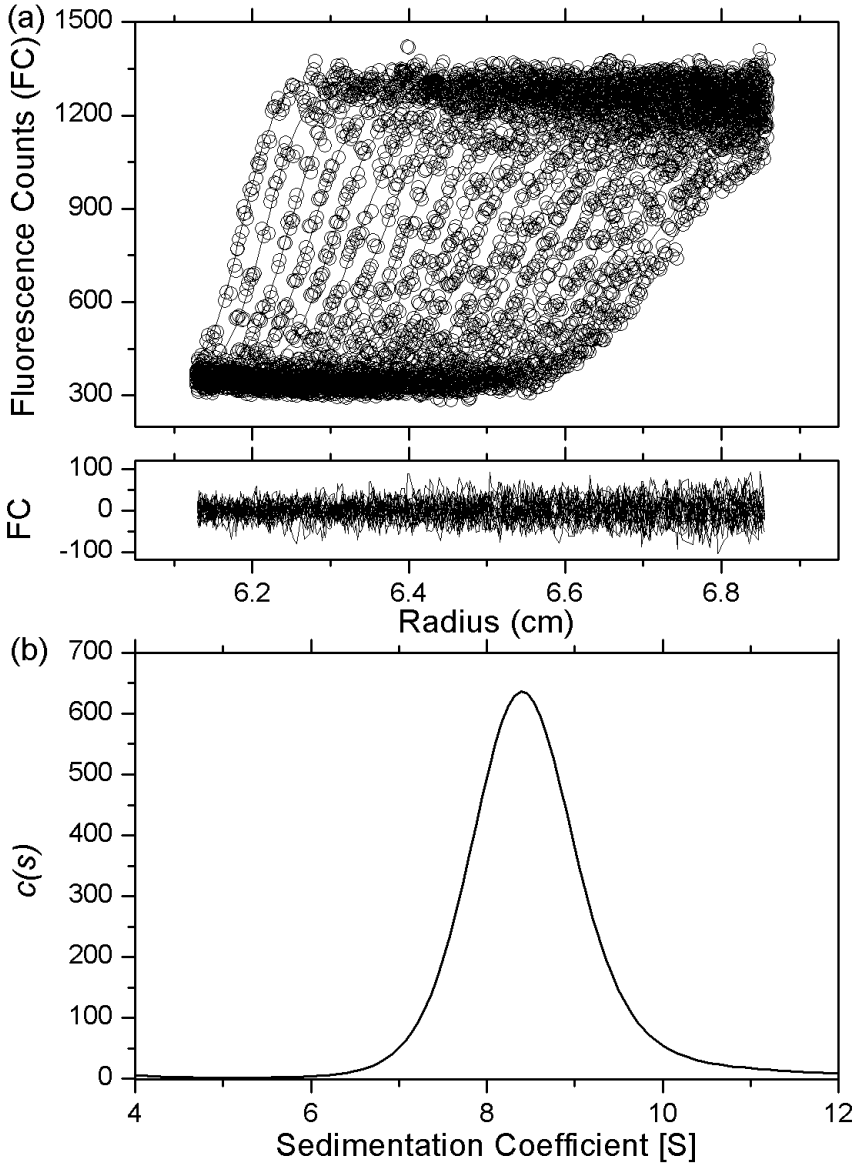

Figure 2.12 **AUC-FDS analysis of wild-type PK1 at 0.001 mg/ml (19.7 nM) protein with gains set at 8 × 95%.** (a) Fluorescence counts at 488 nm as a function of radius (cm) from the axis of rotation plotted. The raw data are presented as open circles and are overlaid with the nonlinear least squares best-fit to a continuous-size distribution model (Lamm equation) by SEDFIT. Residuals for the nonlinear least squares best-fit are also shown. (b) The continuous sedimentation coefficient [*c(s)*] distribution as a function of sedimentation coefficient (S). The fit had a resolution of 150 species between s_{min} of 0.1 S and s_{max} of 15 S with P = 0.95, v-bar = 0.7436, ρ = 1.00117 g/ml, η = 0.010066 p, and f/f_0 = 1.63. The r.m.s.d. and runs test-Z score for the fit were 26 and 22, respectively.

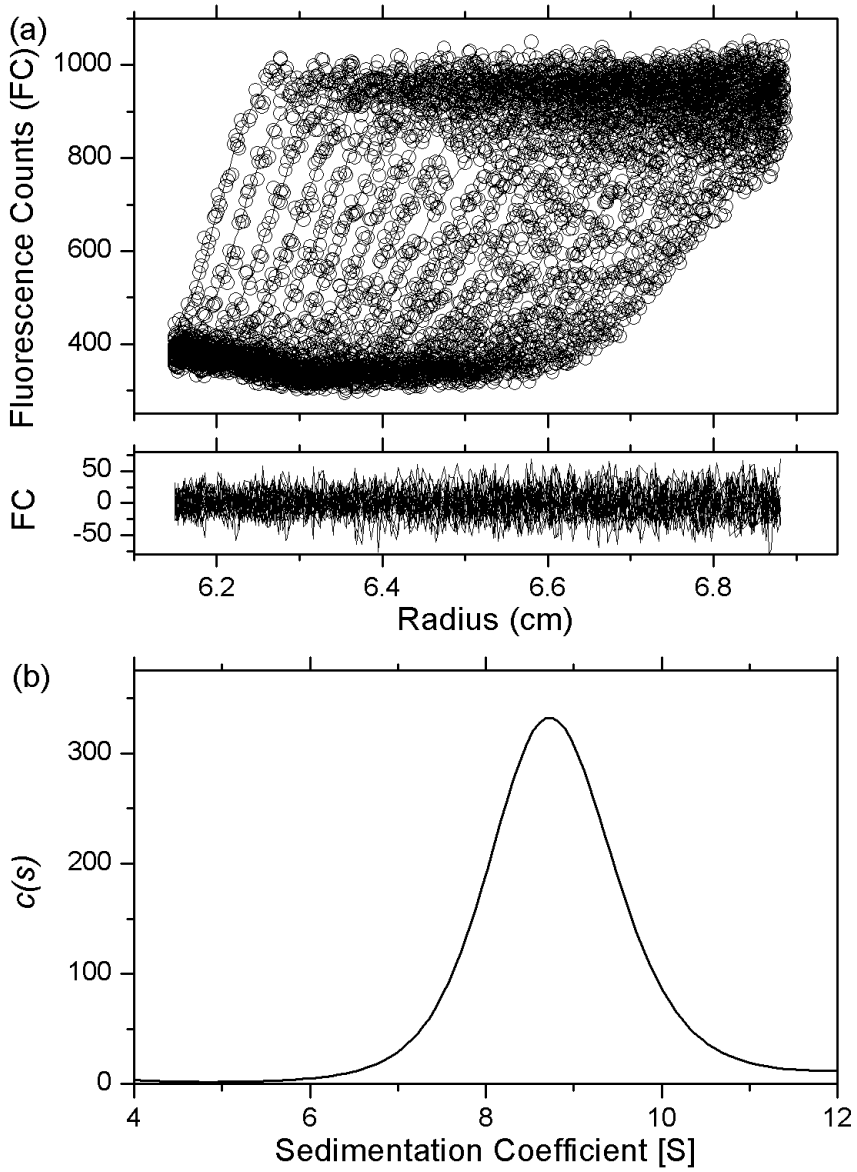

Figure 2.13 **AUC-FDS analysis of wild- type PK1 at 0.001 mg/ml (19.7 nM) protein with 1.8 mM PEP added, with gains set at 2 × 84%.** (a) Fluorescence counts at 488 nm as a function of radius (cm) from the axis of rotation plotted. The raw data are presented as open circles and are overlaid with the nonlinear least squares best-fit to a continuous-size distribution model (Lamm equation) by SEDFIT. Residuals for the nonlinear least squares best-fit are also shown. (b) The continuous sedimentation coefficient [*c(s)*] distribution as a function of sedimentation coefficient (S). The fit had a resolution of 150 species between s_{min} of 0.1 S and s_{max} of 15 S with P = 0.95, v-bar = 0.7413, ρ = 1.00117 g/ml, ŋ = 0.010066 p, and f/f_0 = 1.71. The r.m.s.d. and runs test-Z score for the fit were 21 and 18, respectively.

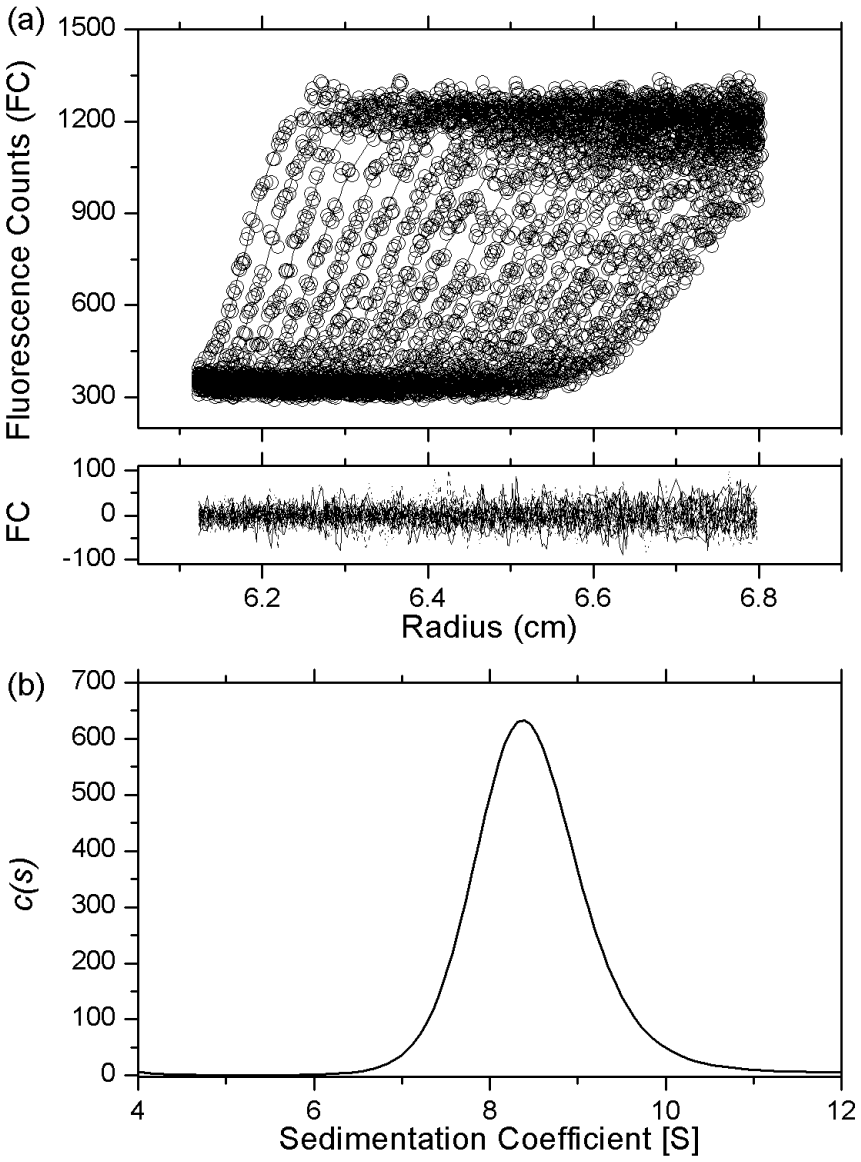

Figure 2.14 **AUC-FDS analysis of wild- type PK1 at 0.001 mg/ml (19.7 nM) protein with 1.8 mM ADP added, with gains set at 1 × 63%.** (a) Fluorescence counts at 488 nm as a function of radius (cm) from the axis of rotation plotted. The raw data are presented as open circles and are overlaid with the nonlinear least squares best-fit to a continuous-size distribution model (Lamm equation) by SEDFIT. Residuals for the nonlinear least squares best-fit are also shown. (b) The continuous sedimentation coefficient [*c(s)*] distribution as a function of sedimentation coefficient (S). The fit had a resolution of 150 species between s_{min} of 0.1 S and s_{max} of 15 S with P = 0.95, v-bar = 0.7436, ρ = 1.00117 g/ml, ŋ = 0.010066 p, and f/f_0 = 1.60. The r.m.s.d. and runs test-Z score for the fit were 23 and 19, respectively.

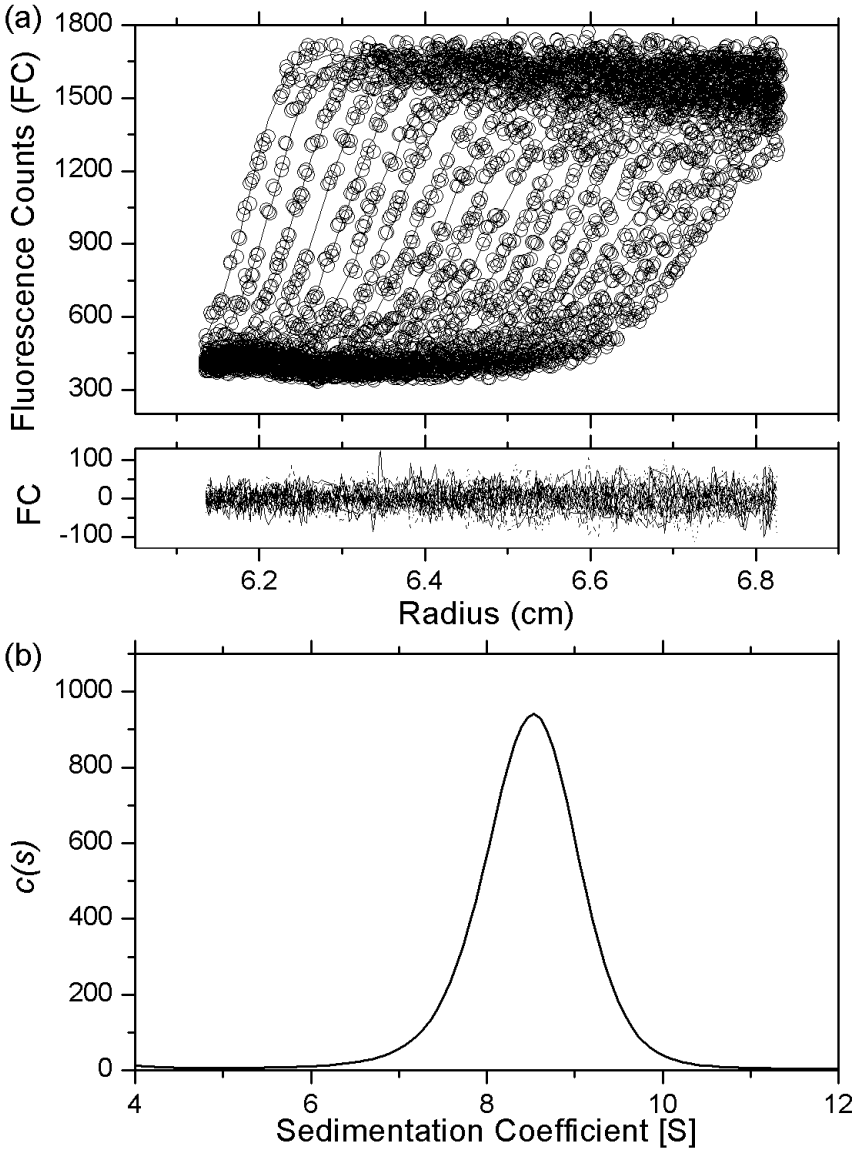

Figure 2.15 **AUC-FDS analysis of wild-type PK1 at 0.001 mg/ml (19.7 nM) protein with 1.8 mM FBP added, with gains set at 8 × 95%.** (a) Fluorescence counts at 488 nm as a function of radius (cm) from the axis of rotation plotted. The raw data are presented as open circles and are overlaid with the nonlinear least squares best-fit to a continuous-size distribution model (Lamm equation) by SEDFIT. Residuals for the nonlinear least squares best-fit are also shown. (b) The continuous sedimentation coefficient [*c(s)*] distribution as a function of sedimentation coefficient (S). The fit had a resolution of 150 species between s_{min} of 0.1 S and s_{max} of 15 S with P = 0.95, v-bar = 0.7436, ρ = 1.00117 g/ml, ŋ = 0.010066 p, and f/f_0 = 1.59. The r.m.s.d. and runs test-Z score for the fit were 29 and 23, respectively.

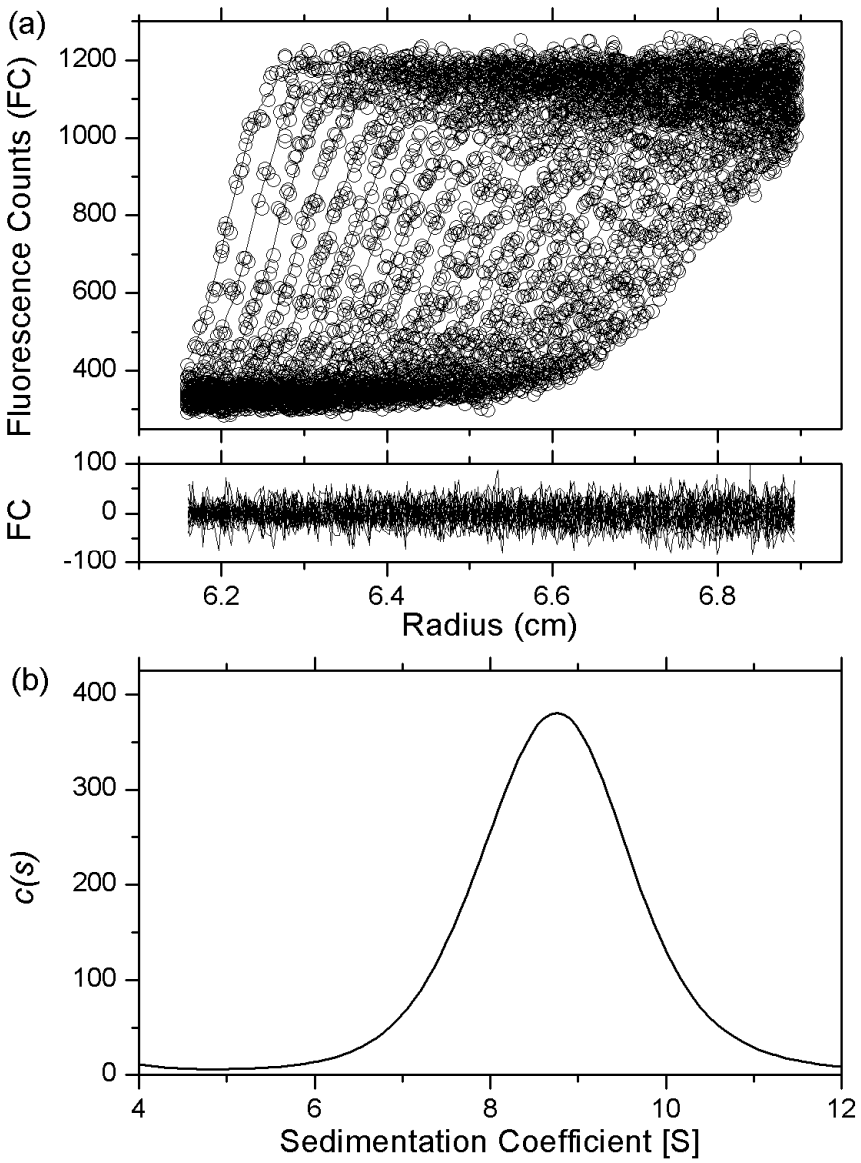

Figure 2.16 **AUC-FDS analysis of wild- type PK1 at 0.0005 mg/ml (9.9 nM) protein with 0.1 mg/ml OVA added, with gains set at 8 × 95%.** (a) Fluorescence counts at 488 nm as a function of radius (cm) from the axis of rotation plotted. The raw data are presented as open circles and are overlaid with the nonlinear least squares best-fit to a continuous-size distribution model (Lamm equation) by SEDFIT. Residuals for the nonlinear least squares best-fit are also shown. (b) The continuous sedimentation coefficient [*c(s)*] distribution as a function of sedimentation coefficient (S). The fit had a resolution of 150 species between s_{min} of 0.1 S and s_{max} of 15 S with P = 0.95, v-bar = 0.7413, ρ = 1.00117 g/ml, ŋ = 0.010066 p, and f/f_0 = 1.77. The r.m.s.d. and runs test-Z score for the fit were 23 and 19, respectively.

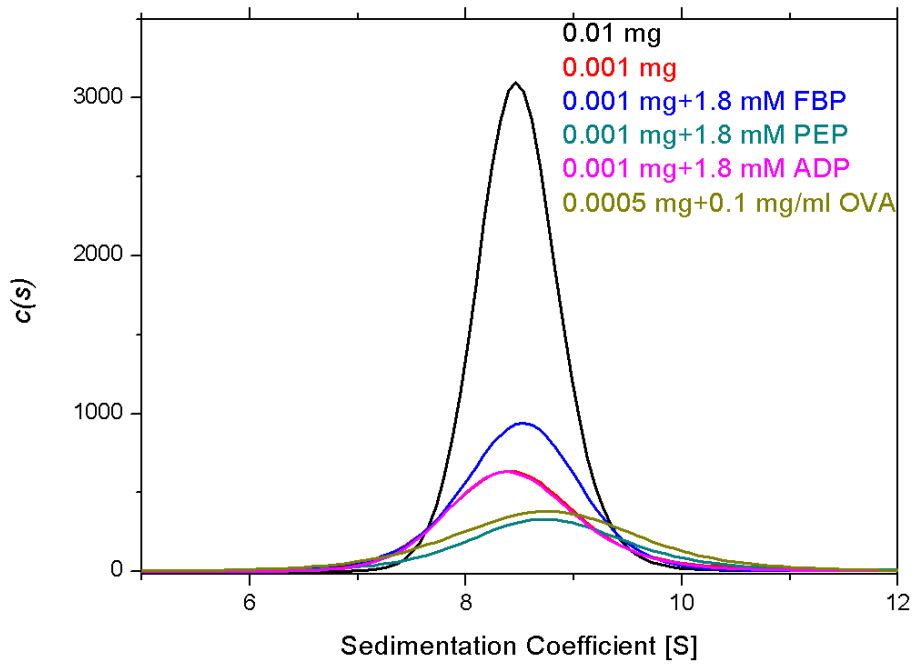

Figure 2.17 **AU-FDS *c(s)* distributions of the wild-type PK1.** This graph was re-generated from the individual *c(s)* distribution plots.

The S value for the labelled protein at various concentrations was unchanged compared to the AUC with absorbance optics, suggesting that the enzyme is unaffected by the presence of the label. An LDH assay revealed that 118% of the activity of the labelled enzyme was retained compared to the unlabelled protein, which confirmed this view. Figure 2.17 showed that the *c(s)* distribution overlaid well at different concentrations, with and without substrates and effector binding. This indicated that a single species was present in every solution, at the S value corresponding to a tetramer.

AUC-FDS data of wild-type PK1 were processed using SEDFIT. At 0.01 mg/ml (197 nM), the *c(s)* distribution showed a clear peak at around 8.5 S corresponded to a single species (Figure 2.11). This indicated that the enzyme remained tetrameric when labelled with Alexa Fluor® 488. Further analyses of wild-type PK1 at an even lower concentration at 0.001 mg/ml (19.7 nM), with and without the substrates (PEP and ADP)

and the allosteric effector (FBP) showed a similar single species corresponding to the tetramer (Figures 2.12-2.15). Although the signal-to-noise ratio decreased dramatically with the decrease of protein concentration, the data still showed a good fit, as indicated by the r.m.s.d. values. In addition, a slight broadening of the peak on the *c(s)* distribution curve at low concentrations was observed, which suggested some dissociation of the tetramer was occurring. To further test the strength of association of the PK1 tetramer, sedimentation velocity run of AUC-FDS was performed again, at a very low concentration of 0.0005 mg/ml (9.9 nM) protein. Pure ovalbumin at 0.1 mg/ml was added at this point as a loading protein to stabilise the labelled wild-type PK1 protein and to prevent the stickiness of protein to the centrepiece wall (MacGregor *et al.* 2004). When the sedimentation coefficient distribution was examined (Figure 2.16), a much broadened peak at 8.5 S was observed, with an increased friction ratio 1.77 (compare to $f/f_0 = 1.31$, observed in PK1 at 0.1 mg/ml), indicated that the tetramer may have changed shape in the solution, or may reflect an average f/f_0 of two species, one of which is highly asymmetric. A smaller species may be evident; however, no conclusion can be drawn at this point, due to the high noise level. What is clear is that the dissociation constant (K_D) for the tetramer is very low (picomolar range).

The AUC-FDS experiments detailed here confirmed the results obtained by AUC with absorbance optics and suggest that wild-type PK1 has a very low dissociation constant (K_D) in the picomolar range. The addition of the substrates PEP and ADP and allosteric effector FBP did not affect enzyme dissociation at the concentrations tested.

2.6 Summary

The *E. coli* PK1 wild-type enzyme has been structurally and functionally characterised. Kinetic studies revealed that this enzyme showed cooperative binding with the substrate PEP, and was allosterically activated by the effector FBP. This finding was consistent with earlier studies (Mattevi *et al.* 1996; Valentini *et al.* 2000). Structural properties of the PK1 wild-type were characterised by different techniques. The secondary structure

was investigated by circular dichroism, suggesting that the structure was highly ordered, with mainly α-helices and β-sheets present and consistent with the crystal structure (PDB accession number 1pky). The solution structure and subunit association/dissociation were probed by AUC and further by the new technology AUC-FDS at much lower concentration. From the results it can be concluded that wild-type PK1 forms a very tight tetramer, which does not dissociate even when concentration decreases to nanomolar range. Some early studies indicated that binding effector and substrates may affect protein subunit assembly or disassembly (Burgress *et al.* 2008; Fanjul & Farias 1993; Friesen *et al.* 1998b). In the AUC-FDS experiment, the effects of the enzyme substrates (PEP and ADP) and effector FBP on quaternary structure were examined. It was concluded that at the enzyme concentrations used, these molecules do not alter the quaternary structure of the enzyme.

2.7 References

Bradford MM. 1976. A rapid and sensitive method for the quantitation of microgram quantities of protein utilizing the principle of protein-dye binding. *Anal Biochem* 72:248-54

Bücher T, Pfeiderer G. 1955. Pyruvate kinase from muscle. *Methods Enzymol* 1:435-40

Burgress BR, Dobson RC, Bailey MF, Atkinson SC, Griffin MDW, Jameson, JB, Parker, MW, Gerrard, JA, Perugini, MA. 2008. Structure and evolution of a novel dimeric enzyme from a clinically-important bacterial pathogen. *JBC* Paper in press

Cole JL, Hansen JC. 1999. Analytical ultracentrifugation as a contemporary biomolecular research tool. *J Biomolecular Techniques* 10:163-76

Cole JL, Lary JW, Moody PT, Laue TM. 2008. Analytical ultracentrifugation: sedimentation velocity and sedimentation equilibrium. *Methods Cell Biol* 84:143-79

Compton LA, Johnson WC, Jr. 1986. Analysis of protein circular dichroism spectra for secondary structure using a simple matrix multiplication. *Anal Biochem* 155:155-67

Domon B, Aebersold R. 2006. Mass spectrometry and protein analysis. *Science* 312:212-7

Fanjul AN, Farias RN. 1993. Cold-sensitive cytosolic 3,5,3'-triiodo-L-thyronine-binding protein and pyruvate kinase from human erythrocytes share similar regulatory properties of hormone binding by glycolytic intermediates. *J Biol Chem* 268:175-9

Fenton AW, Blair JB. 2002. Kinetic and allosteric consequences of mutations in the subunit and domain interfaces and the allosteric site of yeast pyruvate kinase. *Arch Biochem Biophys* 397:28-39

Friesen RH, Castellani RJ, Lee JC, Braun W. 1998a. Allostery in rabbit pyruvate kinase: development of a strategy to elucidate the mechanism. *Biochemistry* 37:15266-76

Friesen RH, Chin AJ, Ledman DW, Lee JC. 1998b. Interfacial communications in recombinant rabbit kidney pyruvate kinase. *Biochemistry* 37:2949-60

Greenfield NJ. 1996. Methods to estimate the conformation of proteins and polypeptides from circular dichroism data. *Anal Biochem* 235:1-10

Greenfield NJ. 2006. Using circular dichroism spectra to estimate protein secondary structure. *Nat Protoc* 1:2876-90

Hill AV. 1910. The possible effects of the aggregation of the molecules of hemoglobin on its dissociation curves. *J Physiol (Lond)* 40:iv-vii

Johnson WC. 1999. Analyzing protein circular dichroism spectra for accurate secondary structures. *Proteins* 35:307-12

Kelly SM, Jess TJ, Price NC. 2005. How to study proteins by circular dichroism. *Biochim Biophys Acta* 1751:119-39

Larsen TM, Benning MM, Rayment I, Reed GH. 1998. Structure of the bis(Mg^{2+})-ATP-oxalate complex of the rabbit muscle pyruvate kinase at 2.1 A resolution: ATP binding over a barrel. *Biochemistry* 37:6247-55

Laue TM. 2005. Analytical Ultracentrifugation: A powerful "new" technology in drug discovery.

Lebowitz J, Lewis MS, Schuck P. 2002. Modern analytical ultracentrifugation in protein science: a tutorial review. *Protein Sci* 11:2067-79

Lovell SC, Mullick AH, Muirhead H. 1998. Cooperativity in *Bacillus stearothermophilus* pyruvate kinase. *J Mol Biol* 276:839-51

MacGregor IK, Anderson AL, Laue TM. 2004. Fluorescence detection for the XLI analytical ultracentrifuge. *Biophys Chem* 108:165-85

Malcovati M, Valentini G. 1982. AMP- and fructose 1,6-bisphosphate-activated pyruvate kinases from *Escherichia coli*. *Methods Enzymol* 90 Pt E:170-9

Mattevi A, Bolognesi M, Valentini G. 1996. The allosteric regulation of pyruvate kinase. *FEBS Lett* 389:15-9

Mattevi A, Valentini G, Rizzi M, Speranza ML, Bolognesi M, Coda A. 1995. Crystal structure of *Escherichia coli* pyruvate kinase type I: molecular basis of the allosteric transition. *Structure* 3:729-41

Miles AJ, Whitmore L, Wallace BA. 2005. Spectral magnitude effects on the analyses of secondary structure from circular dichroism spectroscopic data. *Protein Sci* 14:368-74

Munoz ME, Ponce E. 2003. Pyruvate kinase: current status of regulatory and functional properties. *Comp Biochem Physiol B Biochem Mol Biol* 135:197-218

Ponce E, Flores N, Martinez A, Valle F, Bolivar F. 1995. Cloning of the two pyruvate kinase isoenzyme structural genes from *Escherichia coli*: the relative roles of these enzymes in pyruvate biosynthesis. *J Bacteriol* 177:5719-22

Rigden DJ, Phillips SE, Michels PA, Fothergill-Gilmore LA. 1999. The structure of pyruvate kinase from *Leishmania mexicana* reveals details of the allosteric transition and unusual effector specificity. *J Mol Biol* 291:615-35

Schuck P. 2000. Size-distribution analysis of macromolecules by sedimentation velocity ultracentrifugation and lamm equation modeling. *Biophys J* 78:1606-19

Sreerama N, Venyaminov SY, Woody RW. 1999. Estimation of the number of alpha-helical and beta-strand segments in proteins using circular dichroism spectroscopy. *Protein Sci* 8:370-80

Sreerama N, Venyaminov SY, Woody RW. 2000. Estimation of protein secondary structure from circular dichroism spectra: inclusion of denatured proteins with native proteins in the analysis. *Anal Biochem* 287:243-51

Valentini G, Chiarelli L, Fortin R, Speranza ML, Galizzi A, Mattevi A. 2000. The allosteric regulation of pyruvate kinase. *J Biol Chem* 275:18145-52

Valentini G, Iadarola P, Somani BL, Malcovati M. 1979. Two forms of pyruvate kinase in *Escherichia coli.* A comparison of chemical and molecular properties. *Biochim Biophys Acta* 570:248-58

Valentini G, Mattevi A, Barilla D, Galizzi A, Speranza ML. 1997. Recombinant pyruvate kinase type I from *Escherichia coli*: overproduction and revised C-terminus of the polypeptide. *Biol Chem* 378:719-21

van Stokkum IH, Spoelder HJ, Bloemendal M, van Grondelle R, Groen FC. 1990. Estimation of protein secondary structure and error analysis from circular dichroism spectra. *Anal Biochem* 191:110-8

Wallace BA, Lees JG, Orry AJ, Lobley A, Janes RW. 2003. Analyses of circular dichroism spectra of membrane proteins. *Protein Sci* 12:875-84

Chapter 3

Mutagenesis, over-expression, purification and kinetic studies of the PK1 mutants

3.1 Introduction

The seven PK1 mutants investigated in this study originated from a long-term evolutionary system aimed to address the nature of adaptation in biological systems (Lenski *et al.* 1991) (Section 1.1). It was found that the populations of *E. coli* carrying these mutations, which were evolved in a stable glucose-limited environment, showed generally improved fitness and changed morphology (Lenski *et al.* 1998; Lenski & Travisano 1994). Further studies investigated the parallel changes in the gene expression profiles (Cooper *et al.* 2003) and found these unique mutations in the *pykF* gene, which codes for PK1 in *E. coli* (Woods *et al.* 2006).

The aim of the work in this chapter was to: (1) obtain pure mutated PK1 enzymes; (2) collect data on the kinetic properties of the seven mutants and compare these to the wild-type PK1 (Chapter 2); and (3) address the question of whether the replicate populations evolved in the same way at the function level; that is, by parallel evolution at the enzyme function level. To the author's knowledge, no previous study has characterised the molecular basis for adaptation in an *in vivo* context.

This study is pivotal to Lenski's long-term evolution study, since it begins to extend the previous population description of the evolved bacteria (e.g. Cooper *et al.* 2003; Woods *et al.* 2006) to examine how evolved populations adapt at a molecular level. In addition, this work attempts to enhance and/or challenge the understanding of how allostery operates in pyruvate kinase.

It is hypothesised here that the evolved populations have adapted to the low glucose

environment by altering the way in which PK1 is regulated. The mutations that will be described are implicated in the allosteric models in Section 1.3.6 (Christofk *et al.* 2008; Fenton & Blair 2002; Friesen *et al.* 1998a; Friesen *et al.* 1998b; Jurica *et al.* 1998; Lovell *et al.* 1998; Mattevi *et al.* 1996; Valentini *et al.* 2000). Understanding the mechanisms of allosteric regulation of enzyme function has been an ongoing challenge. Surprisingly, a firm account of the allosteric activation of PK1 (by FBP and the substrate PEP) has been elusive, despite over 50 years of biochemical and structural study on this enzyme.

3.2 Mutagenesis, over-expression and purification of the mutated PK1 enzymes

3.2.1 Site-directed mutagenesis of *pykF* gene

Synthetic oligonucleotide primers containing the desired mutations were designed to be used in the site-directed mutagenesis experiments (Section 6.2.9). The primer design process is illustrated using the P70T mutation as an example. The *pykF* sequence around P70 (which is underlined) is shown below:

```
                5'CTGCTTGATACCAAAGGTACGGAAATCCGCACC 3'
181     GCCGCTATCCTGCTTGATACCAAAGGTCCGGAAATCCGCACCATGAAACTGGAAGGCGGT
                3'GACGAACTATGGTTTCCATGCCTTTAGGCGTGG 5'
```

The designed primer for P70T (in both directions) was 33 base pairs in length (shown in red), with the melting temperature at 82 °C (Section 6.2.9.1). GC content of the primer was 51%.

The plasmid pGV5A (containing the *pykF* gene coding for the wild-type PK1) served as the template for PCR-based site-directed mutagenesis (Section 6.2.9). The resulting PCR products were confirmed on agarose gels (Figure 3.1).

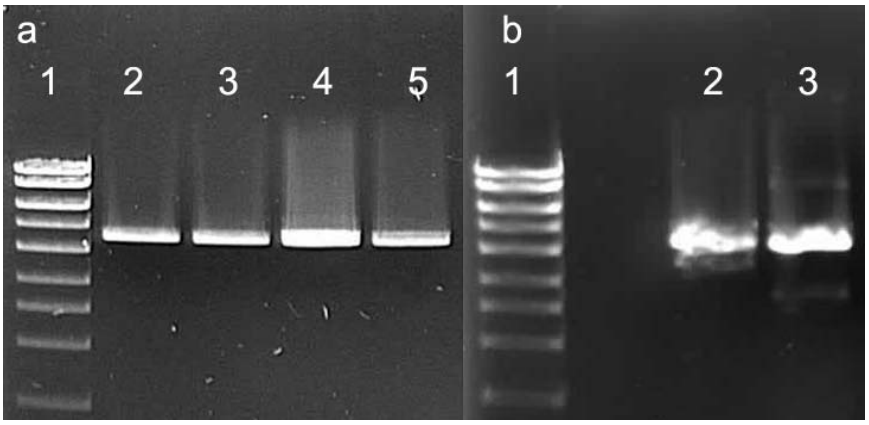

Figure 3.1 **PCR products with pGV5A derivatives embedding PK1 mutations obtained from site-directed mutagenesis.** (a) Lane 1: DNA ladder; lane 2: pGV5A-D127N; lane 3: pGV5A-A301S; lane 4: pGV5A-A301T; lane 5: pGV5A-G381A. (b) Lane 1: DNA ladder; lane 2: pGV5A-P70T; lane 3: pGV5A-P70Q.

The modified pGV5A plasmids with the desired mutations were used to transform competent *E. coli* XL1-Blue cells (Section 6.2.9.4). The process was found to be successful by DNA sequencing of the plasmid prepared from these cells (Section 6.2.14). Plasmids with the mutated PK1 were then used to transform *E. coli* BL21 (DE3) cells (Section 6.2.15) for over-expression and purification.

3.2.2 Over-expression and purification of PK1 mutants

E. coli BL21 (DE3) cells transformed with pGV5A derived plasmids were cultured and the PK1 enzymes over-expressed using IPTG induction (Section 6.3.3). The cell lysate was loaded onto a SDS-PAGE gel (Figure 3.2, lane 2 shows the cell lysate of PK1-P70T). A clear band at approximately 50 kDa was seen on the gel, among other impurities. This band is consistent with the molecular mass of an *E. coli* PK1 monomer (Mattevi *et al.* 1996) and confirmed the over-expression of the protein. Activity of the whole cell lysate was tested by the LDH coupled assay (Section 6.5.1), which further confirmed the expression. Over-expression of all the mutant proteins was comparable to the wild-type.

Purification of the PK1 mutants was performed according to the method developed by Valentini and colleagues (2000) for the wild-type PK1. *E. coli* BL21 (DE3) cells, transformed with pGV5A mutated plasmids, were cultured and the cells were harvested after induction by IPTG (Section 6.3.3). Cells were lysed by ultrasonication followed by

centrifugation. A three-step purification procedure, including ion-exchange (step 1), phenyl-Sepharose hydrophobic interaction (step 2) and size-exclusion chromatography (step 3) was performed to obtain pure protein. SDS-PAGE analysis was performed to check the purity of the proteins (Figure 3.2 shows a typical SDS-PAGE for PK1-P70T). All protein purification yields were calculated by using the Bio-Rad protein assay based on the Bradford method (Bradford 1976) (Section 6.3.1) to determine the protein concentration and the LDH coupled activity assay for determining PK1 activity (Table 3.1).

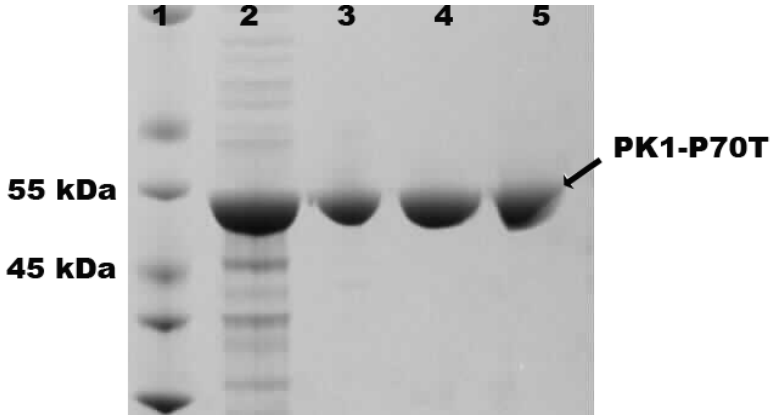

Figure 3.2 **SDS-PAGE gel of PK1-P70T mutant protein expression.** Lane 1: Protein marker; lane 2: the cell free crude extract of the BL21 (DE3) with PK1-P70T over-expressed; lane 3: the pooled fractions after ion exchange chromatography; lane 4: the pooled fractions after phenyl-Sepharose chromatography; lane 5: the pooled fractions after size-exclusion chromatography.

This procedure appeared to be an effective method for purifying both the wild-type PK1 enzyme and its derivatives. All the proteins eluted at a similar position, with a similar salt content and conductivity in the column. This indicated that the structure (or at least the pIs) of the mutants were similar. A major protein band at ~50 kDa was observed in all active eluents (Figure 3.3). This band corresponds to the monomeric molecular weight of *E. coli* PK1 (Mattevi *et al.* 1995). Only trace impurities were seen on SDS-PAGE gels after size-exclusion chromatography. In addition, the specific activities of PK1 derivatives usually increased three-fold during purification (Table 3.1).

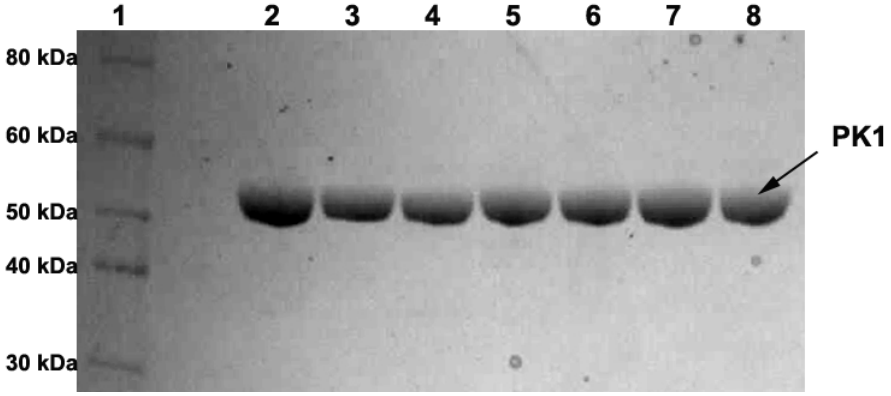

Figure 3.3 **SDS-PAGE gel of the purified wild-type PK1 and its derivatives following size-exclusion chromatography.** Lane 1: Protein marker. Lane 2: Wild-type PK1. Lane 2-8: P70T, P70Q, D127N, I264F, A301T, A301S and G381A PK1 mutants. In each lane, 6 μg of protein was loaded.

Table 3.1 **Purification of the wild-type PK1 and its derivatives**

Sample	Purification Procedure	Total protein (mg)	Total activity[a] (U)[b]	Specific activity (U/mg)	% Yield	Relative purity (fold)
P70T	**crude extract**	122	154	1.3	-	-
	Step 1	87	86	0.98	55	**0.8**
	Step 2	33	160	4.9	104	**3.9**
	Step 3	21	66	3.2	43	**2.5**
P70Q	**crude extract**	161	156	0.97	-	-
	Step 1	57	76	1.3	49	**1.4**
	Step 2	36	95	2.6	61	**2.7**
	Step 3	20	50	2.6	32	**2.7**
D127N	**crude extract**	131	1.4	0.01	-	-
	Step 1	100	0.9	0.009	69	**0.9**
	Step 2	57	1.3	0.02	97	**2.2**
	Step 3	28	1.1	0.04	80	**3.8**
I264F	**crude extract**	110	108	0.98	-	-
	Step 1	91	93	1.0	86	**1.0**
	Step 2	47	76	1.6	70	**1.7**
	Step 3	20	63	3	58	**3.2**
A301T	**crude extract**	206	92	0.5	-	-
	Step 1	200	96	0.5	104	**1.1**
	Step 2	73	85	1.2	93	**2.6**
	Step 3	11	23	2.0	25	**4.5**
A301S	**crude extract**	194	105	0.5	-	-
	Step 1	192	106	0.6	101	**1.0**
	Step 2	38	68	1.8	65	**3.3**
	Step 3	12	31	2.6	30	**4.9**
G381A	**crude extract**	132	93	0.7	-	-
	Step 1	109	97	0.9	105	**1.1**
	Step 2	37	73	2.0	79	**2.8**
	Step 3	31	77	2.5	83	**3.6**

[a] Activity was determined using the LDH coupled assay.

[b] 1 unit is defined as the oxidation of 1 μmol of NADH per second. Assays were performed at 30 °C at pH 7.5, with 2 mM of PEP, ADP and FBP, 0.12 mM NADH and with 22 units of LDH.

3.3 Steady-state kinetics of the PK1 mutants

A kinetic study of the PK1 variants was performed using a method adapted from Valentini (2000), (Section 6.4.2), and was essentially the same as that used for the wild-type.

PEP titrations were performed for all seven mutants in the presence and absence of FBP (Figures 3.4 & 3.5, Table 3.2) in order test the activity of the mutants and the allosteric regulation pattern in response to FBP. Without FBP present in the assay, the saturating concentrations of PEP for the majority of the enzymes were higher than 2 mM, except for the wild-type and PK1-I264F enzymes. Despite that, ADP titrations were performed with and without FBP, at 2 mM PEP constant. Therefore, for ADP titrations, the k_{cat}^{ADP} values were dependent on both PEP and ADP concentrations. The $S_{0.5}^{PEP}$ for A301T was 20 mM in the absence of FBP. Not surprisingly, this mutant enzyme did not show detectable activity with up to 10 mM ADP, at constant 2 mM PEP, when FBP was not present in the assay (Figure 3.5, Table 3.2).

FBP titrations were also performed. The FBP titrations were dependent on two factors, which are, the FBP affinity to the enzyme, and the extent to which FBP influences PEP affinity (Fenton & Blair 2002). Therefore, k_{cat} values relative to FBP activation were represented in the results (Figure 3.6, Table 3.3).

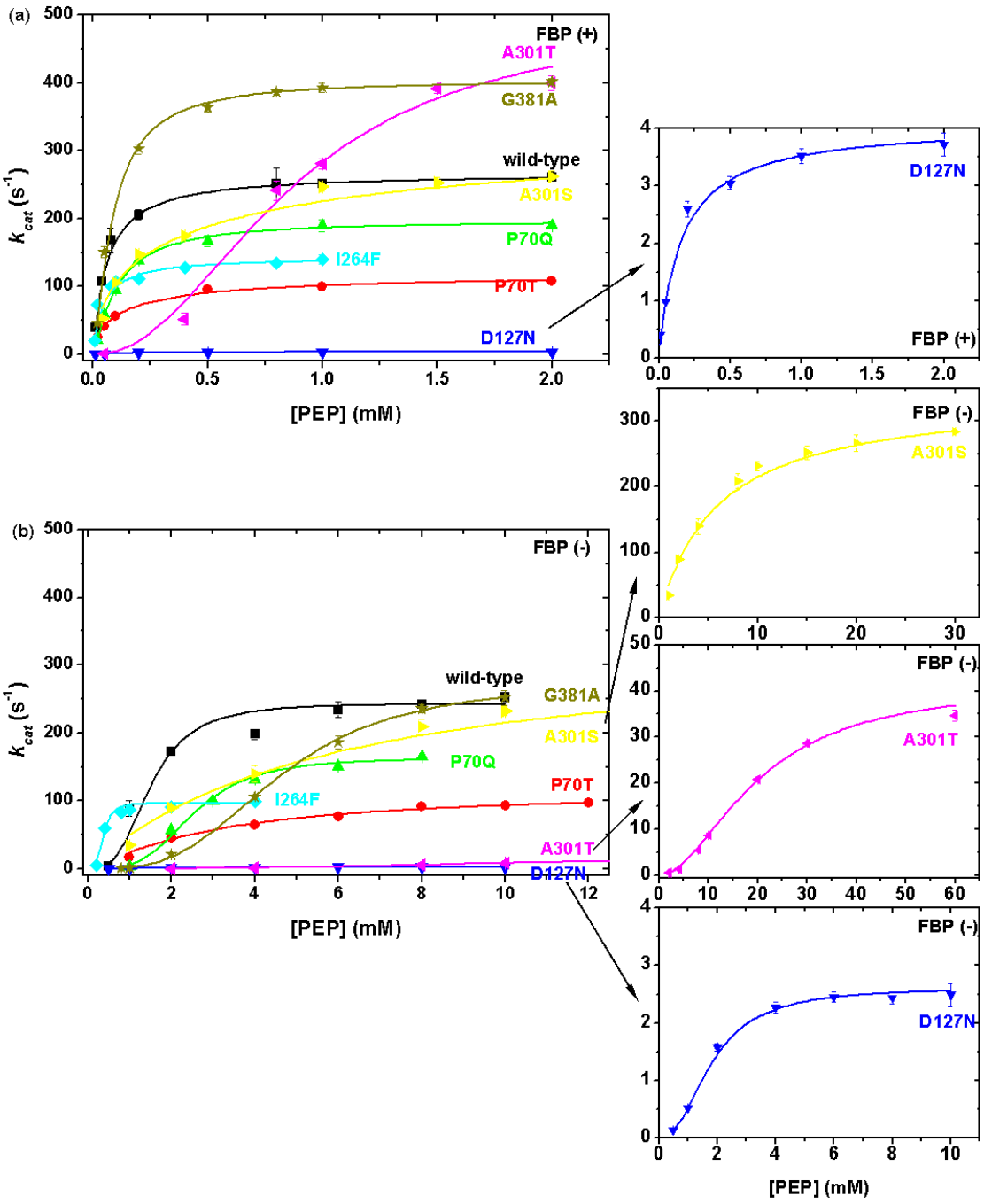

Figure 3.4 **PEP titration curves for the wild-type PK1 and the mutants P70T, P70Q, D127N, I264F, A301T, A301S and G381A.** Enzyme activity was assayed at 30 °C and pH 7.5, as described in Section 6.4.2 with ADP present at 2 mM. (a) The titration in the presence of 2 mM FBP and (b) in the absence of FBP: wild-type (■, black), P70T (●, red), P70Q (▲, green), D127N (▼, blue), I264F (◆, cyan), A301T (◀, pink), A301S (▶, yellow) and G381A (★, olive). Error bars represent the standard error of the mean for two replicates. The insets highlight those curves difficult to distinguish in the main plot.

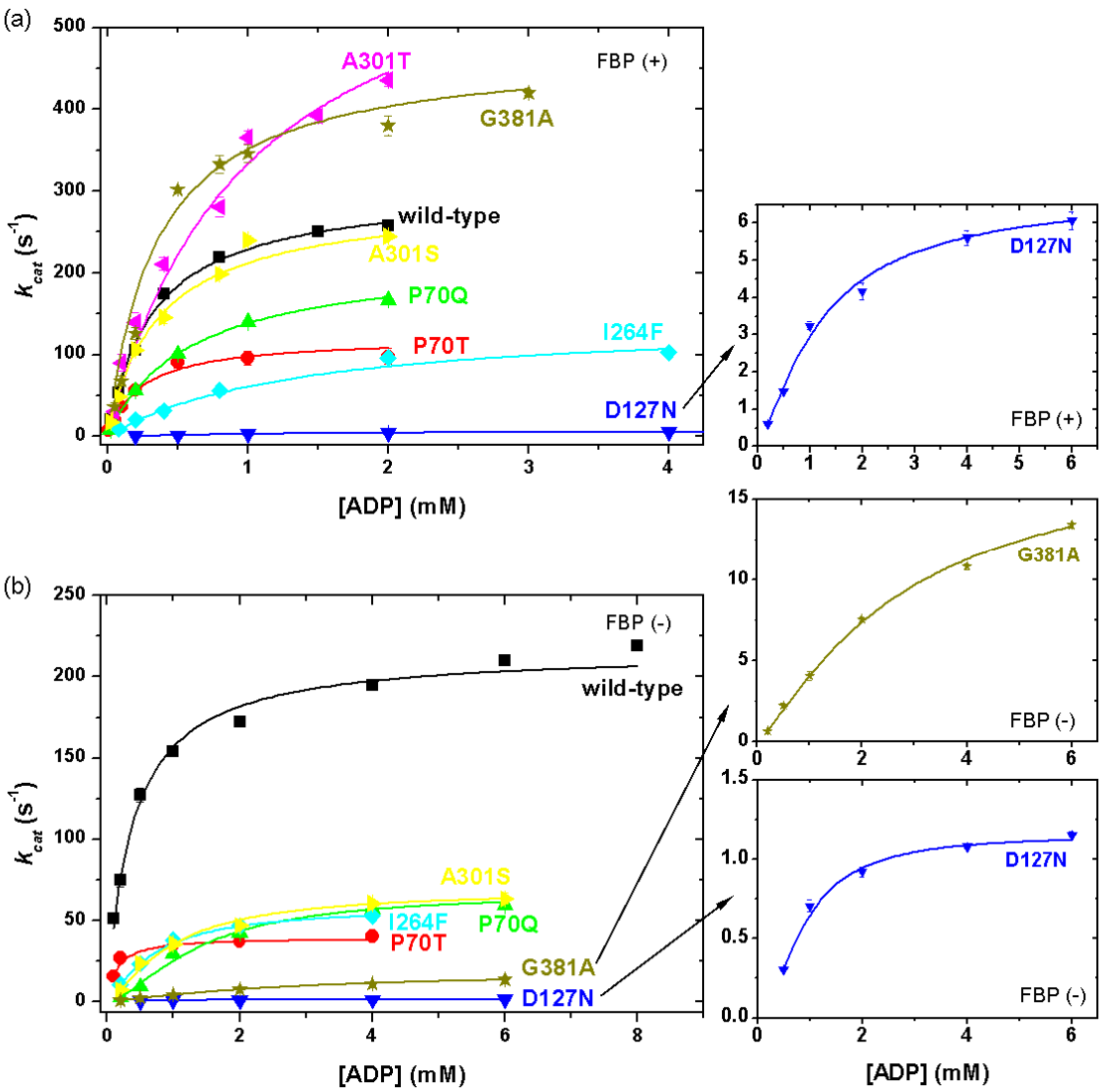

Figure 3.5 **ADP titration curves for the wild-type PK1 and the mutants P70T, P70Q, D127N, I264F, A301T, A301S and G381A.** Enzyme activity was assayed at 30 °C and pH 7.5, as described in Section 6.4.2 with PEP present at 2 mM. (a) The titration was performed in the presence of 2 mM FBP; (b) the titration was performed in the absence of FBP: wild-type (■, black), P70T (●, red), P70Q (▲, green), D127N (▼, blue), I264F (◆, cyan), A301T (◀, pink), A301S (▶, yellow) and G381A (★, olive). A301T was not active with the absence of FBP, when a fixed 2 mM PEP was present in the solution. Error bars represent the standard error of the mean for two replicates. The insets highlight those curves difficult to distinguish in the main plot. Note that ADP titrations were performed at 2 mM PEP (constant) for both assays, at this concentration is not the saturating concentration for most enzymes at the situation when FBP is absent, except the wild-type and the PK1-I264F mutant (as adjusted by $S_{0.5}^{PEP}$, FBP(-). Therefore, only the $S_{0.5}^{ADP}$ values were discussed here.

Table 3.2 **Kinetic parameters of the wild-type and mutant *E. coli* PK1 by fitting the Hill equation (Hill 1910) (Equation 2.1b).** Results are mean values ± standard errors for duplicate measurements.

		PEP							
		FBP (-)				FBP (+)			
		k_{cat}	$S_{0.5}^{PEP}$	n_H	$k_{cat}/S_{0.5}$	k_{cat}	$S_{0.5}^{PEP}$	n_H	$k_{cat}/S_{0.5}$
		s^{-1}	*mM*			s^{-1}	*mM*		
wt		243 ± 2	1.5 ± 0.1	3.1 ± 0.6	162	268 ± 4	0.06 ± 0.002	1.0 ± 0.04	4467
P70T	*Active site mutant*	116 ± 17	3.1 ± 0.9	1.2 ± 0.3	37	124 ± 3	0.12 ± 0.01	0.7 ± 0.03	1033
P70Q	*Active site mutant*	163 ± 6	2.5 ± 0.2	3.6 ± 0.5	65	197 ± 6	0.1 ± 0.006	1.3 ± 0.03	1970
D127N	*Active site mutant*	3 ± 0.1	1.8 ± 0.08	2.3 ± 0.1	2	4 ± 0.4	0.14 ± 0.04	1.3 ± 0.2	29
I264F	*A/A' interface mutant*	114 ± 3	0.4 ± 0.03	3.7 ± 1	285	154 ± 7	0.03 ± 0.006	1.3 ± 0.2	5133
A301T	*A/A' interface mutant*	42 ± 3	20 ± 1.8	1.9 ± 0.07	2	496 ± 46	0.9 ± 0.1	2.1 ± 0.1	551
A301S	*A/A' interface mutant*	301 ± 6	3.9 ± 0.3	1.4 ± 0.1	77	292 ± 27	0.2 ± 0.06	0.7 ± 0.1	1460
G381A	*FBP binding site mutant*	274 ± 17	4.6 ± 0.2	3.2 ± 0.07	60	402 ± 9	0.09 ± 0.009	1.4 ± 0.1	4467
		ADP							
		FBP (-)				FBP (+)			
		k_{cat}	$S_{0.5}^{ADP}$	n_H	$k_{cat}/S_{0.5}$	k_{cat}	$S_{0.5}^{ADP}$	n_H	$k_{cat}/S_{0.5}$
		s^{-1}	*mM*			s^{-1}	*mM*		
wt		241 ± 12	0.54 ± 0.11	0.75 ± 0.07	446	309 ± 19	0.34 ± 0.07	1.0 ± 0.08	909
P70T	*Active site mutant*	39 ± 1	0.15 ± 0.02	1.1 ± 0.2	260	120 ± 11	0.24 ± 0.06	1.0 ± 0.1	500
P70Q	*Active site mutant*	67 ± 3	1.4 ± 0.2	1.6 ± 0.08	48	223 ± 7	0.6 ± 0.04	1.0 ± 0.02	372
D127N	*Active site mutant*	1 ± 0.04	0.9 ± 0.08	1.8 ± 0.2	1	7 ± 0.7	1.2 ± 0.2	1.3 ± 0.1	6
I264F	*A/A' interface mutant*	69 ± 1	0.7 ± 0.03	1.3 ± 0.06	99	183 ± 4	1.6 ± 0.7	0.9 ± 0.1	114
A301T[a]	*A/A' interface mutant*	--[a]	--[a]	--[a]	--[a]	494 ± 47	0.5 ± 0.1	1.2 ± 0.1	988
A301S	*A/A' interface mutant*	68 ± 3	1.0 ± 0.06	1.4 ± 0.1	68	292 ± 6	0.4 ± 0.02	1.0 ± 0.04	730
G381A	*FBP binding site mutant*	18 ± 1	2.8 ± 0.4	1.2 ± 0.05	6	430 ± 9	0.3 ± 0.02	1.6 ± 0.1	1433

[a] A301T is essentially inactive with 2 mM PEP up to 10 mM ADP, in the absence of FBP (refer to Section 3.3.1 text).

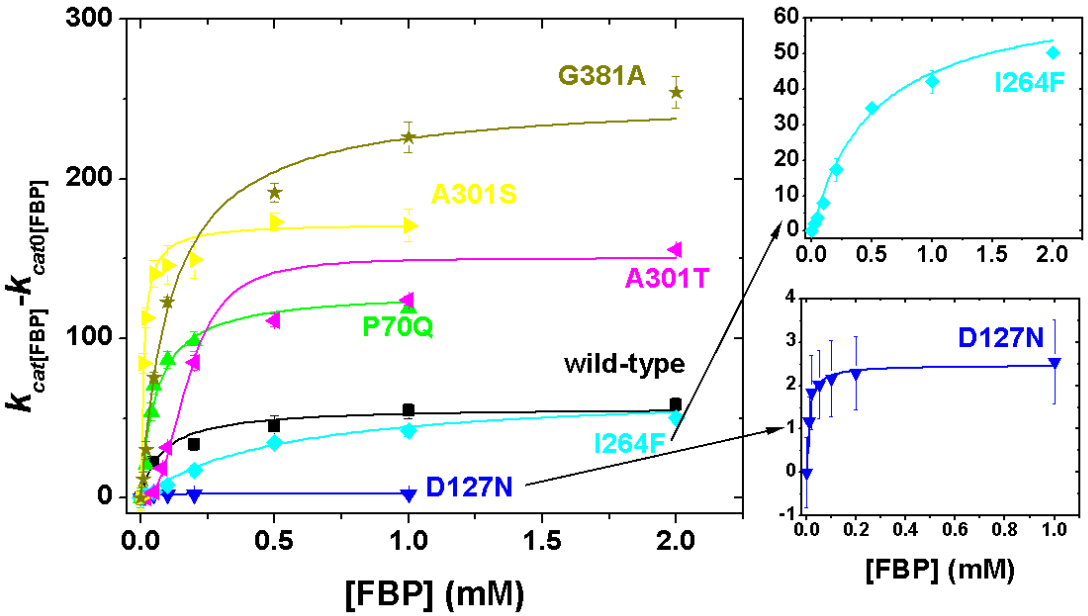

Figure 3.6 **Enzyme activity relative to FBP for the wild-type PK1 and the enzymes with P70Q, D127N, I264F, A301T, A301S and G381A mutations.** Enzyme activity was assayed at 30 °C and pH 7.5, with the absence of FBP as background ($V_{0[FBP]}$). The assay was then performed at various FBP concentrations, as described in Section 6.4.2. Relative enzymatic activities in the presence of FBP are shown here by subtracting the background activity ($V_{0[FBP]}$). PEP and ADP were present at 2 mM respectively: wild-type (■, black), P70Q (▲, green), D127N (▼, blue), I264F (◆, cyan), A301T (◄, pink), A301S (►, yellow) and G381A (★, olive). Titration for P70T was not performed. Error bars represent the standard error of the mean of the k_{cat} between two replicates. The insets highlight those curves difficult to distinguish in the main plot.

Table3.3 **The relative k_{cat} with respect to FBP (i.e. $k_{cat[FBP]}$-$k_{cat0[FBP]}$).** Parameters were determined in the presence of 2 mM PEP and 2 mM ADP using Michaelis-Menten model (Equation 2.1a). A301T was fitted using Hill cooperative model (Hill 1910) (Equation 2.1b). P70T was not examined. Results are mean values ± standard errors for duplicate measurements unless stated.

		$k_{cat[FBP]}$-$k_{cat0[FBP]}$ s^{-1}	K_M mM	n_H
Wild-type		57 ± 4	0.08 ± 0.01	1
P70T[a]	*Active site mutant*	n/a[a]	n/a[a]	n/a[a]
P70Q	*Active site mutant*	130 ± 11	0.06 ± 0.01	1
D127N	*Active site mutant*	2.5 ± 0.08	0.01 ± 0.001	1
I264F	*A/A' interface mutant*	67 ± 6	0.5 ± 0.1	1
A301T	*A/A' interface mutant*	150 ± 6	0.2 ± 0.03	2.7 ± 0.5
A301S	*A/A' interface mutant*	172 ± 3	0.01 ± 0.001	1
G381A	*FBP binding site mutant*	250 ± 11	0.1 ± 0.01	1

[a] FBP titration for PK1-P70Q was not performed.

3.4 Kinetic properties of the mutants

Generally, the mutated enzymes showed altered kinetic properties compared to the wild-type. When FBP was present in the reaction, some of the mutated enzymes were more active than the wild-type when titrated against PEP (PK1-A301T, PK1-A301S and PK1-G381A) and ADP (PK1-A301T and PK1-G381A), while others were less active (PK1-P70T, PK1-P70Q, PK1-D127N and PK1-I264F) (Figures 3.4 & 3.5). In addition, some mutants showed altered substrate affinity in response to FBP in terms of allosteric cooperativity, as judged by the n_H values (Table 3.2). The degree of the FBP activation was also examined (Figure 3.6, Table 3.3).

All mutants except PK1-D127N showed activities much higher than the residual PK1 activity, which was estimated using the LDH coupled assay early on in the *E. coli* BL21 (DE3) whole cell lysate (0.2% of wild-type activity) (Section 2.3). PK1-D127N is highly inactive (1.5% of wild-type activity) with a distinct ADP titration pattern from the wild-type. Given the low activity, the possibility of wild-type contamination cannot be excluded; however, we note that $S_{0.5}^{ADP}$ in the presence of FBP (Table 3.2) is quite different to that of the wild-type, which would not be the case if the measured activity was due to residual wild-type enzyme alone. That the activity is still affected by FBP, precludes the possibility that the residual activity is from *E. coli* PK type 2, which is regulated AMP and monophosphorylated sugars (Mattevi *et al.* 1995).

As mentioned in Section 1.4, the seven mutations fall loosely into three groups with respect to the PK structure (Figures 1.11 & 3.7), those are, P70T, P70Q and D127N belonging to the active site mutation group; I264F, A301T and A301S belonging to A/A' subunit interface mutation group; and G381A at the FBP binding site. The mutations at the active site were predicted to have an effect on catalysis, while those at the FBP binding site was possible to affect FBP binding.

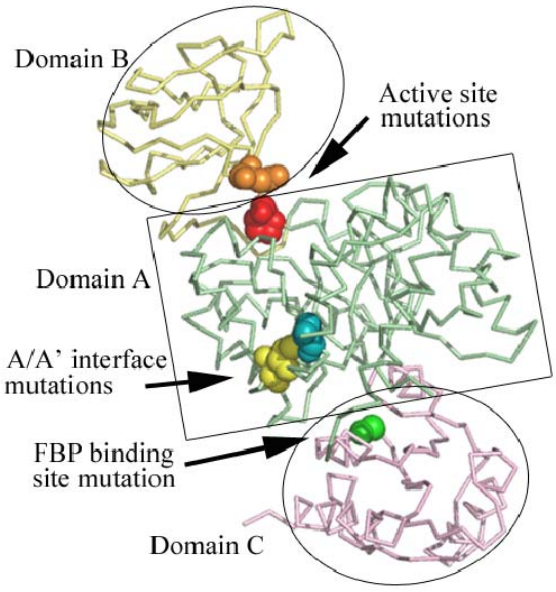

Figure 3.7 **Mutations in evolved PK1 enzymes.** Mutated residues are represented as spheres. The active site residue P70 is in red, and D127 in orange; the A/A' subunit interface residue I264 is in blue, and A301 in yellow; the FBP binding site residue G381 is in green. Figure was generated by Pymol (DeLano 2002) using PDB file 1pky (*E. coli* PK1) (Mattevi *et al.* 1995).

3.4.1 The active site

The residues P70 and D127 are situated within or close to the active site, which lies in a pocket between domains A and B (Figure 3.7) (Muirhead *et al.* 1986). Thus, it was predicted that mutations at these positions would affect the catalytic activity of the mutant enzymes compared to the wild-type enzyme. However, because the regulatory mechanism of PK1 is unclear, we could not predict whether the regulation would also be affected.

Both mutations at position 70 exchanged the nonpolar side-chain of proline for more polar side-chains. Kinetic data showed that the P70T and P70Q mutants were less active than the wild-type (Table 3.2, Figure 3.8). Interestingly, P70Q showed similar cooperative activation with respect to PEP titration (n_H = 3.6 ± 0.5) compared to n_H = 3.1 ± 0.6 for the wild-type, while P70T showed little PEP cooperativity (n_H = 1.2 ± 0.3). P70 is positioned on an extended loop connecting the A and B domains. The proline produces a kink in the loop and a number of residues about this position are thought to be responsible for binding the K^+ ion (Figure 3.9). In addition, P70 is close to S192, which is thought to interact with both PEP and ADP (Munoz & Ponce 2003).

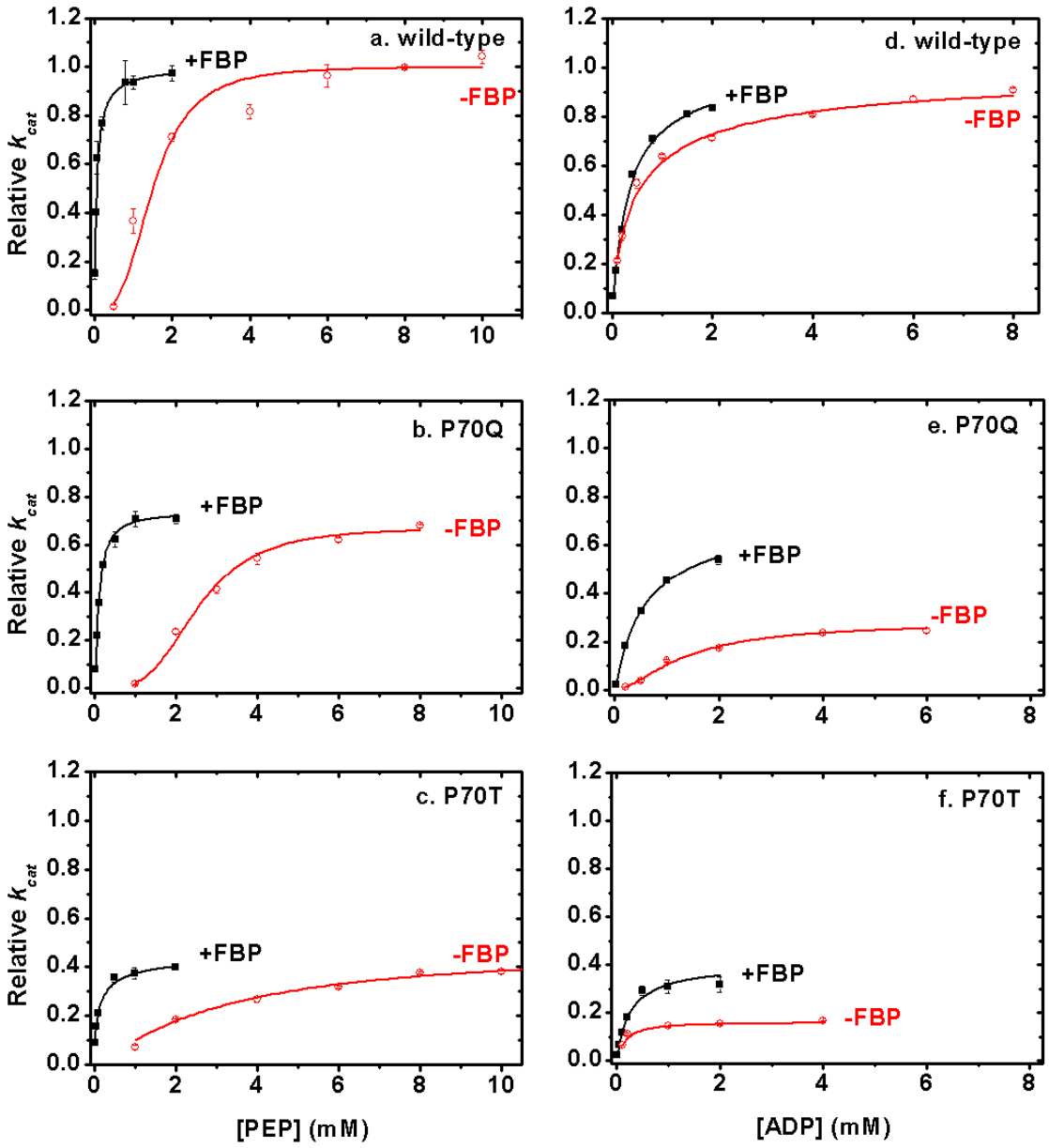

Figure 3.8 **Kinetic properties of wild-type, PK1-P70T and PK1-P70Q enzymes.** a-c: The relative k_{cat} of wild-type, PK1-P70T and PK1-P70Q enzymes with respect to the wild-type enzyme measured at varying concentrations of PEP (Section 6.4.2). d-e: The relative k_{cat} of wild-type, PK1-P70T and PK1-P70Q enzymes with respect to the wild-type enzyme measured at varying concentrations of ADP. Titrations are in the absence (○) or presence (■) of 2 mM FBP. Curves represent the best fit to the Hill cooperative model (presented in Table 3.2). Error bars represent the standard error of the mean between two replicates.

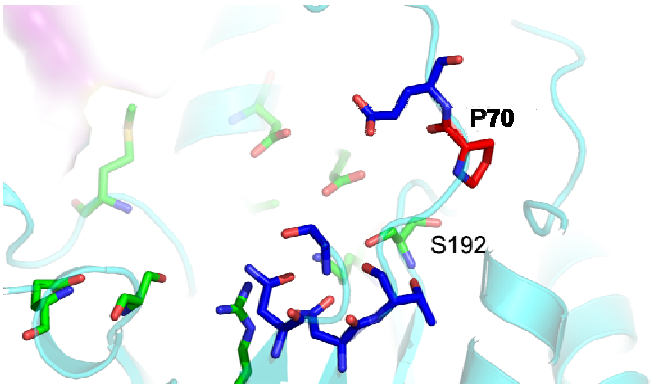

Figure 3.9 **The residues involved in K^+ and substrate binding in *E. coli* PK1.** Residues in blue are involved in binding K^+, while those in green bind ADP, PEP and Mg^{2+}. P70 and S192 are indicated in the figure from a view down to the barrel of the active site. Figure is generated by Pymol (DeLano 2002) using PDB file 1pky (Mattevi *et al.* 1995).

For rabbit muscle PKM1, the binding of ADP appears to facilitate a large movement of domain B, closing the active site, as demonstrated by the Bis(Mg^{2+})-ATP-oxalate complex (Figure 3.10). This complex represents the enzyme:product complex of the reaction between oxalylphosphate (the slow substrate of PK, (Kofron & Reed 1990)) and ADP. P116 (P70 in *E. coli* PK1 numbering) sits at one of the hinge points for this movement (Larsen *et al.* 1998). A structure overlay of the *E. coli* PK1 and rabbit muscle PKM1 (unbound form, free of Mg^{2+}-ATP) revealed high similarity between the two structures at domains A and B (Figure 3.11). Therefore, it is possible that a similar role for P70 exists in *E. coli* PK1 during the substrate binding transition.

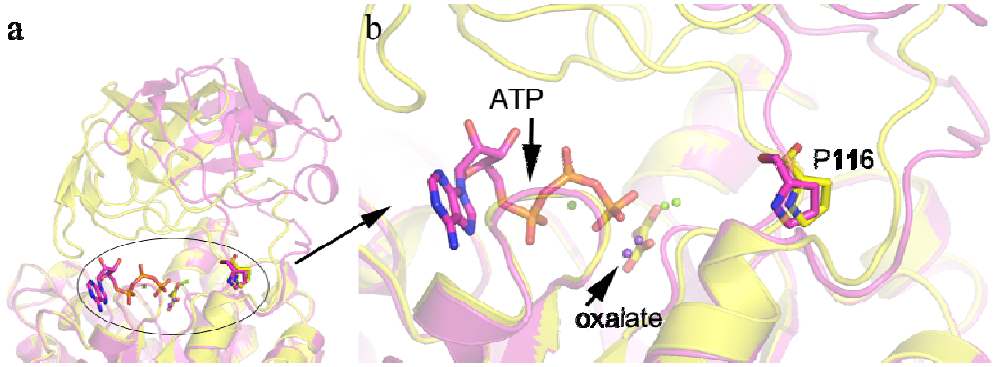

Figure 3.10 **ATP and oxalate defined the PK active site (orange yellow stick) for rabbit muscle PKM1.** a: an overall view and b: a close up view. P116 overlay is shown in stick form (pink and yellow). Pink, ATP unbound subunit; yellow, ATP bound subunit. This plot illustrates the 40° rotation of the B domain relative to the A domain. P116 is situated at the hinge of this rotation. Mg^{2+} cations are shown as green balls and K^+ as purple balls. Figure is generated by Pymol (DeLano 2002) using PDB file 1a49 (Larsen *et al.* 1998).

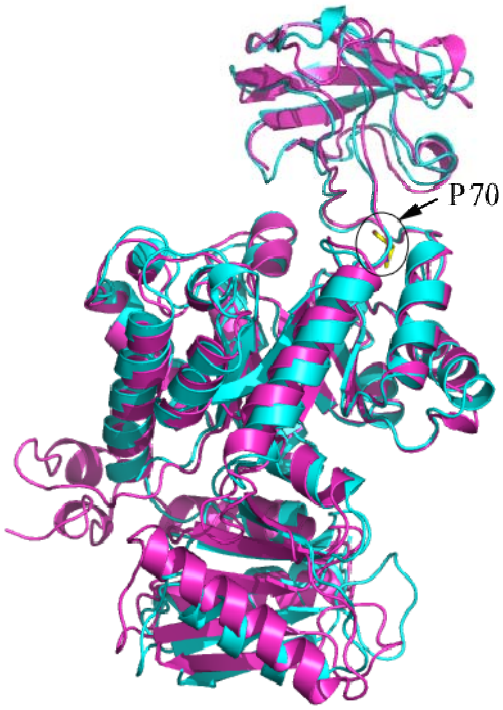

Figure 3.11 **Overlay of *E. coli* PK1 (blue) and rabbit muscle PKM1 (pink), unbound.** It shows that the A and B domains have excellent structural conservation, although this is not true for the allosteric FBP binding domain (C). The 2 proteins share 46% sequence identity (Mattevi, 1995). Figure was generated by Pymol (DeLano 2002) using PDB files 1pky (*E. coli* PK1) (Mattevi *et al.* 1995) and 1a49 (rabbit muscle PKM1) (Larsen *et al.* 1998), with r.m.s.d. of C_α overlay 1.7.

The lower activity observed for both enzymes with P70T and P70Q mutations compared to the wild-type (as judged by the specificity constant, $k_{cat}/S_{0.5}$) is perhaps because of altered K^+ (*via* adjacent residues) or substrate binding (*via* S192). Mutations at P70 may also affect the domain movement upon substrate binding. Presumably, the nature of the extended loop connecting domains A and B (to which P70 belongs) is to attenuate activity by modulating the domain movement upon ADP binding. Thus, mutations at P70 would have the effect of not positioning within the active site those residues at domain B important for catalysis, such as R119, K156, and D127. The lack of PEP cooperativity for PK1-P70T compared to the wild-type and PK1-P70Q is interesting, but more difficult to explain, given that a detailed and rational mechanism for such cooperativity has not been proposed. Future structural studies may be required to explain this behavior.

The residue D127 is situated on a loop of the B domain (Larsen *et al.* 1998; Mattevi *et al.* 1995). Like P70, D127 is also highly conserved across species (Munoz & Ponce 2003). It is proposed to have a critical role in forming a salt-bridge with the side chain of R292 from the adjacent subunit across the A/A' interface in the T- to R-state transition upon FBP binding (Mattevi *et al.* 1995). Moreover, a structural study of the rabbit PKM1 found that D177, which corresponds to D127 in *E. coli* PK1, moved substantially (6.8 Å) from the open conformation to the closed conformation in the Mg^{2+}-ATP binding state (Larsen *et al.* 1998), interacting with the hydration shell of Mg^{2+}. Thus, this residue appears to be involved in both allosteric and catalytic functions and this mutation tests both of these proposals.

The mutation D127N involved the change of aspartic acid to asparagine at position 127, exchanging the carboxylic acid moiety with a carbamoyl group and loss of the associated *-ve* charge. Consistent with it proposed role in catalysis, PK1-D127N shows severely attenuated catalytic activity ($k_{cat}/S_{0.5}$ ranging from 2-29) compared to the wild-type enzyme. Given this mutation is isosteric, it is reasonable to conclude that the carbamoyl group of N127 is not able to interact with the hydration shell of Mg^{2+} in the same way as the carboxyl may. Thus, D127 appears to have a critical role in catalysis which has not been reported for the *E. coli* enzyme.

In addition, the overall $S_{0.5}$ for the substrates is similar to the wild-type enzyme except for the $S_{0.5}$ for ADP, which is increased three-fold (Table 3.2, Figure 3.12), suggesting that the mutant binds substrates with similar affinity. The possibility of large structural changes cannot be excluded (which will be tested by CD in Chapter 4) and a crystal structure will be sought in the future.

It is interesting to note that in a human erythrocyte PK study, when D211, which occupies the same position as D127 in *E. coli* PK1 (Figure 1.5), is mutated to an asparagine and causes severe PK function deficiency (Fermo *et al.* 2005; Pendergrass *et al.* 2006; Zanella *et al.* 2005). This mutational study at this position begins to explain why this might be the case from a protein structure/function viewpoint.

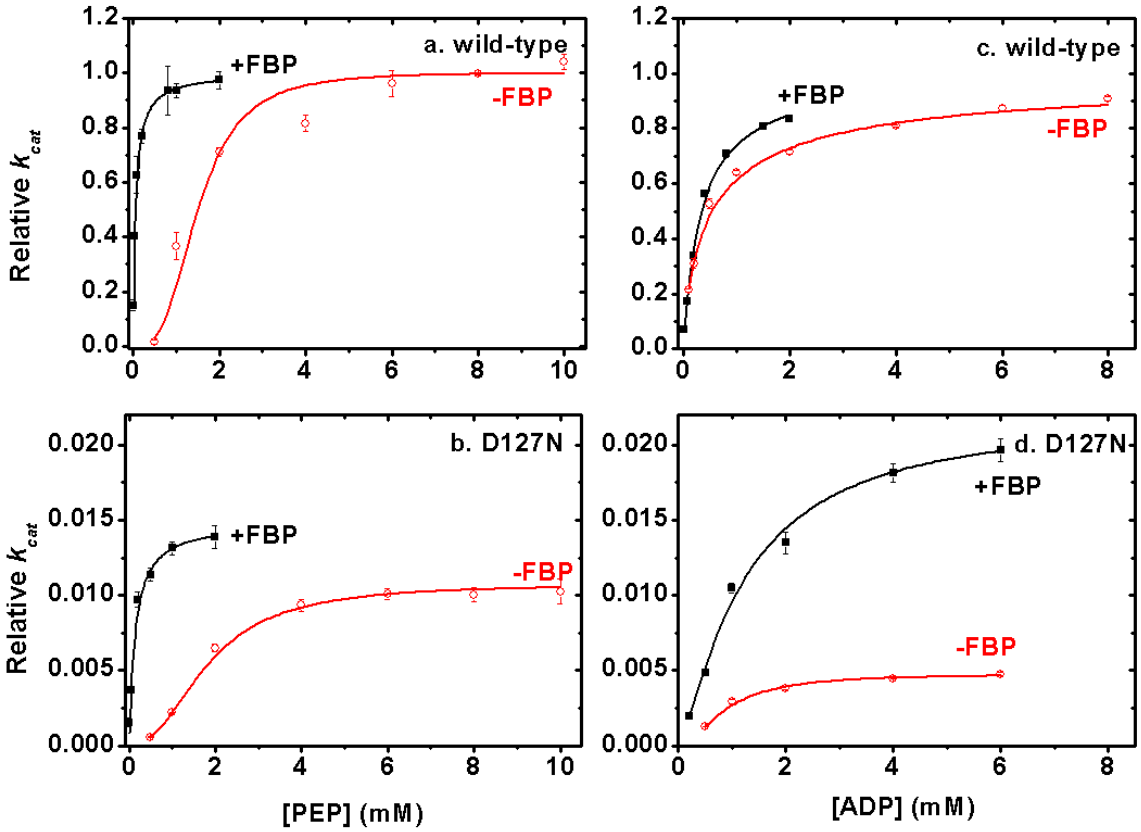

Figure 3.12 **Kinetic properties of the wild-type and PK1-D127N enzymes.** a & b: The relative k_{cat} of purified wild-type and PK1-D127N enzymes to the k_{cat} of the wild-type enzyme was measured at varying concentrations of PEP as described (Section 6.4.2). c & d: The relative k_{cat} of purified wild-type and PK1-D127N enzymes to the k_{cat} of the wild-type enzyme was measured at varying concentrations of ADP as described (Section 6.4.2). Varying concentrations of PEP and ADP are in the absence (○) or presence (■) of 2 mM FBP. Curves represent the best fit to the Hill equation. Kinetic parameters determined by fitting the results to the Hill equation are presented in Table 3.2. Error bars represent the standard error of the k_{cat} relevant to the wild-type k_{cat} between two replications. Note that the scales for the wild-type enzyme and for the PK1-D127N are not the same.

3.4.2 The A/A' interface

The residues I264 and A301 are near the A/A' interface (Figure 3.7). Both residues are very close to one another in space, being situated on adjacent α-helices, which make up the A/A' interface (Figure 3.13). A sequence alignment among PK1 enzymes from a variety of organisms showed that I264 and A301 are well conserved across species (Figure 1.5).

Mutations at both positions were of particular interest, since allosteric binding is thought to promote domain movements, interface rearrangements, or change in oligomeric states (Fenton & Blair 2002) and thus the PK mutants in this category may inform a new allosteric mechanism. In addition, four separate populations from Lenski's evolution experiment developed mutations at A301, suggesting a hitherto unknown function.

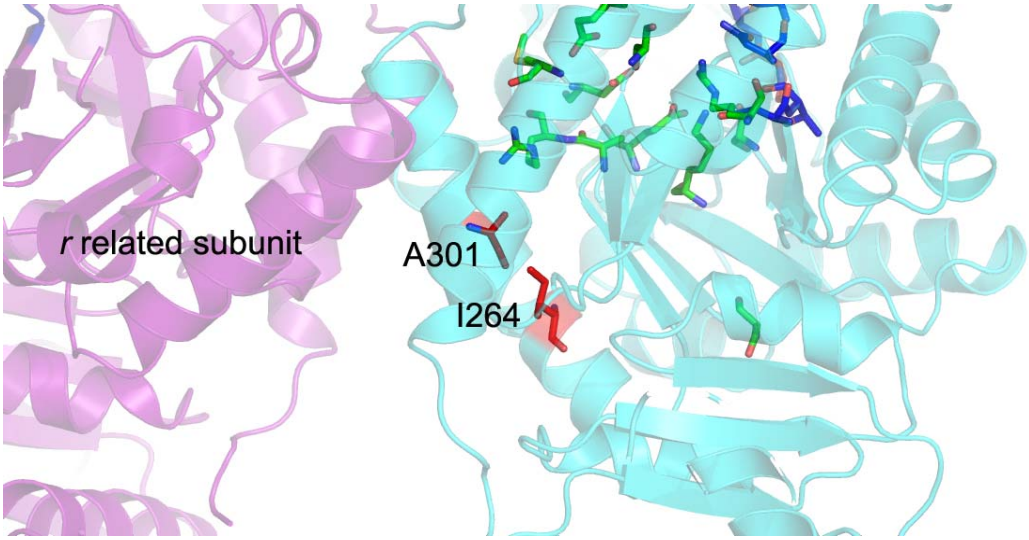

Figure 3.13 **Positions of I264 and A301 at A/A' interface of *E. coli* PK1.** The adjacent subunit is illustrated in purple. Ile264 and Ala301 are shown in red sticks. Figure was generated by Pymol (DeLano 2002) using PDB file 1pky (*E. coli* PK1) (Mattevi *et al.* 1995).

The mutation I264F replaces a nonpolar side group with a similarly hydrophobic, but sterically larger aromatic group. I264 is part of the Aα6 helix and the side chain sits in a largely hydrophic pocket with hydrophobic interactions with V274, I268, T306 and V242 (Figure 3.14). The A/A' interface is largely formed by contacts between helices Aα6 and Aα7. Given the juxtaposition of the helices, a bulkier mutation may interfere with the helical packing about the $(\beta/\alpha)_8$-barrel, and also the A/A' interface that these helices contribute to. This distortion may in turn affect a number of conserved contacts between

the helices, but specifically the conserved salt bridge between R244 of Aα6' and D297 of Aα7 (Fenton & Blair 2002; Jurica *et al.* 1998; Valentini *et al.* 2000). The short helix Aα6' sits in the loop (loop6) between Aβ6 and Aα6 and is highly conserved (Figure 1.5). It is proposed to play a role in both PEP binding and the FBP allosteric response (Mattevi *et al.* 1995). In addition, the *E. coli* structure in the T-state shows that D297 of Aα7 also contacts R292 of the adjacent monomer. Mutation of either D297 or R292 renders the enzyme completely inactive (Valentini *et al.* 2000).

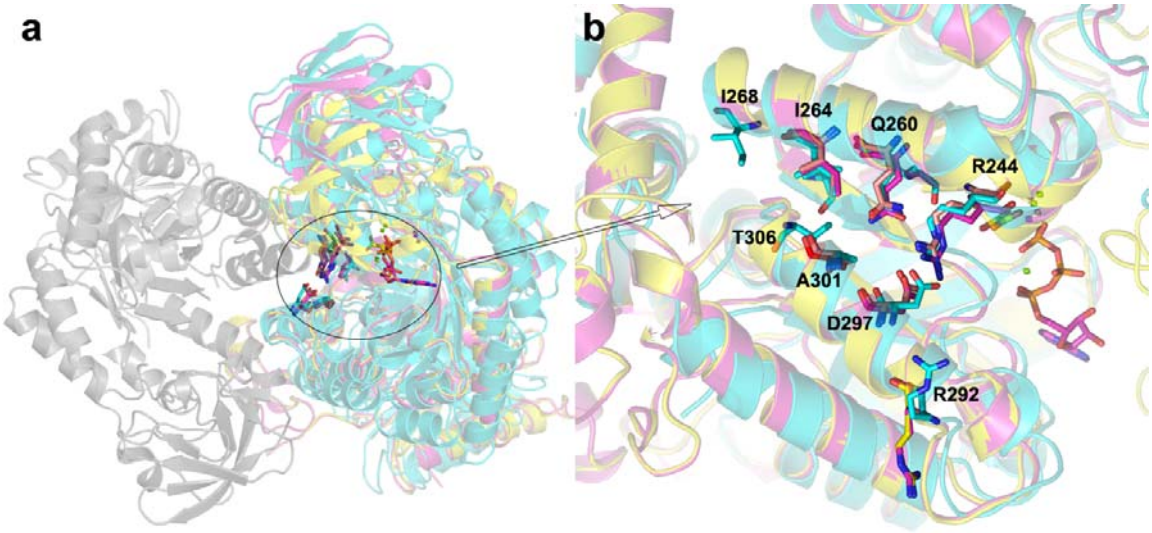

Figure 3.14 **Overlay of *E. coli* PK1 (blue), rabbit PKM1 (pink) and yeast PK (yellow) A/A' interface structures and the important residues.** (a) an overall view; (b) An expanded view with the overly of residues at the interfaces.

Kinetic analysis (Table 3.2, Figure 3.15) showed that PK1-I264F was less active than the wild-type PK1. PK1-I264F had similar substrate binding properties to the wild-type enzyme, although it showed greater affinity for PEP in the absence of FBP. Interestingly, the specificity constant ($k_{cat}/S_{0.5}$) for PEP increased compared to the wild-type (285 $s^{-1}mM^{-1}$ *vs.* 162 $s^{-1}mM^{-1}$ in the absence of FBP; 5133 $s^{-1}mM^{-1}$ *vs.* 4462 $s^{-1}mM^{-1}$ in the presence of FBP), suggesting that the enzyme had a more specific response to increasing PEP concentrations.

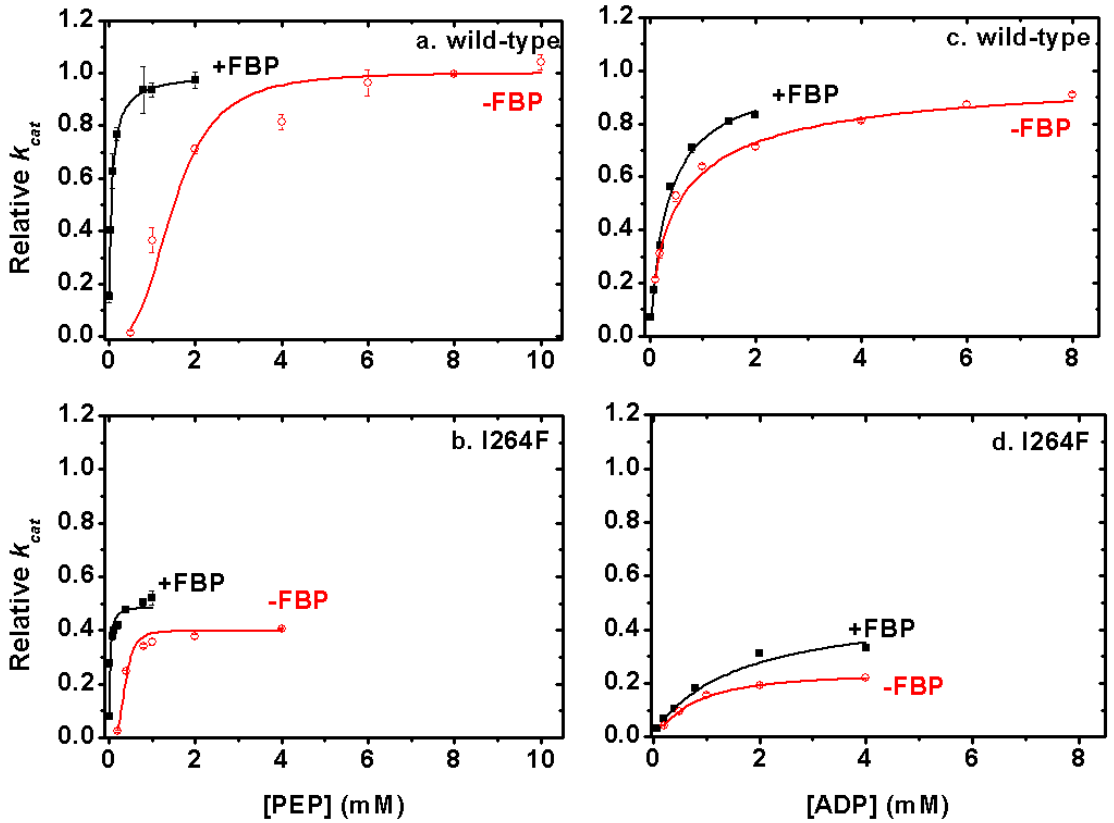

Figure 3.15 **Kinetic properties of the wild-type and PK1-I264F enzymes.** a & b: The relative k_{cat} of wild-type and PK1-I264F enzymes to the k_{cat} of the wild-type enzyme was measured at varying concentrations of PEP as described (Section 6.4.2). c & d: The relative k_{cat} of wild-type and PK1-I264F enzymes to the k_{cat} of the wild-type enzyme was measured at varying concentrations of ADP as described (Section 6.4.2). Varying concentrations of PEP and ADP are in the absence (○) or presence (■) of 2 mM FBP. Curves represent the best fit to the Hill equation. Kinetic parameters determined by fitting the results to the Hill equation are presented in Table 3.2. Error bars represent the standard error of the k_{cat} relevant to the wild-type k_{cat} between two replications.

With respect to allostery, I264F showed remarkably diminished binding of FBP (Figure 3.6, Table 3.3). This result suggests that the A/A' interface is critical for communicating the allosteric signal from domain C to the active site, *via* the Aα6 helix. Fenton and Blair (2002) have previously communicated this proposal when considering the results of a mutagenic study with the yeast PK enzyme (in their work helix Aα6 is called H10). This result is consistent with the proposal that FBP binding alters the activity *via* a signal through the Aα6 helix.

For the mutations A301T and A301S, a similar analysis was carried out. These mutations were interesting because of their high incidence in the evolutionary study (Section 1.1).

Residue A301 belongs to helix Aα7 (Figures 1.12 & 3.13), which holds a number of highly conserved residues (Figure 1.5). A301 sits at the top of the same hydrophobic pocket for which I264F is a part and is also close to R292 (4.8 Å) and D297 (5.4 Å) (Figure 3.14), both of which are involved in the A/A' interfacial transition and affect enzyme catalysis and, as discussed above, may be the link that connects the FBP binding site with the active site (Mattevi *et al.* 1996; Mattevi *et al.* 1995; Valentini *et al.* 2000). Both the A301S and A301T mutations introduce a hydroxyl moiety and moderate steric bulk to the side chain.

Given the similarity of the mutations (i.e. serine and threonine), the most surprising feature was how different they behaved kinetically. In the absence of FBP, both mutations were attenuated, but where PK1-A301S was still active, PK1-A301T showed essentially no activity at all (Figure 3.16). Although both were very active in the presence of FBP, PK1-A301T showed a greater k_{cat} than the wild-type.

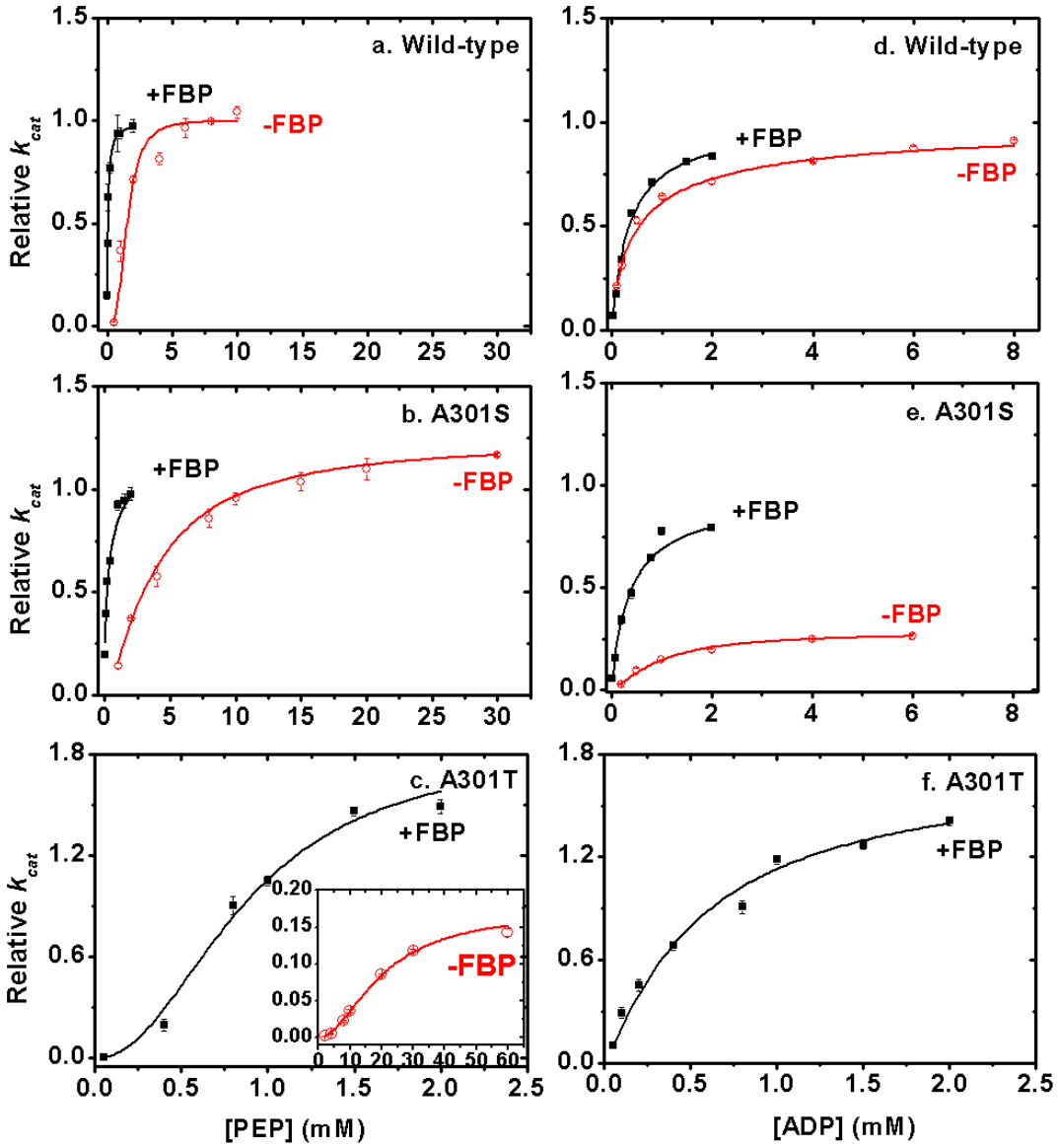

Figure 3.16 **Kinetic properties of the wild-type, PK1-A301T and PK1-A301S enzymes.** a - c: The relative k_{cat} of wild-type, PK1-A301T and PK1-A301S enzymes with respect to the wild-type enzyme measured at varying concentrations of PEP as described (Section 6.4.2). d - f: The relative k_{cat} of wild-type, PK1-A301T and PK1-A301S enzymes with respect to the wild-type enzyme measured at varying concentrations of ADP as described (Section 6.4.2). Titrations were in the absence (○) or presence (■) of 2 mM FBP. A301T is inactive at 2 mM PEP with ADP up to 10 mM. Curves represent the best fit to the Hill equation and are presented in Table 3.2. Error bars represent the standard error of the k_{cat} relevant to the wild-type k_{cat} between two replications. Note that the scales for the wild-type enzyme and for the PK1-A301T are not the same.

Perhaps the most intriguing result was that PK1-A301T showed activation by PEP even in the presence of FBP. It would seem that this mutation has disentangled the affect of allosteric FBP activation and PEP activation. The structure of these mutated enzymes

would be very helpful in understanding the processes of both FBP activation and PEP activation. Both enzymes showed decreased cooperativity to PEP when FBP was absent in the solution, as judged by the decreased n_H value (Table 3.2). Clearly, mutations at the A/A' interface have a profound affect on enzyme regulation. The results in this thesis are entirely consistent with the hypothesis put forward by Fenton and Blair (2002). However, structural studies of the mutated enzymes will be required to more fully explain the altered kinetic behaviour.

3.4.3 The FBP binding site

Residue G381 is the only residue situated at the FBP binding site that was found to have a mutation in the evolution study. G381 belongs to a stretch of conserved residues involved in the formation of FBP binding site (Munoz & Ponce 2003) and is adjacent to residues found to be crucial for the FBP binding to PK1 (Section 1.4.3, Figure 1.16). Figure 3.17 shows that G381 is within a loop joining Cβ1 and Cα3 of the C domain, and this loop region contributes to FBP binding (assuming the same FBP binding pocket for *E. coli* PK1). The mutation of a glycine to an alanine residue is a subtle change, although glycine residues are more conformationally tolerant and thus often found in loop regions. It was hypothesised that this mutation may affect FBP binding caused by a reorientation of the Cβ1 and Cα3 loop.

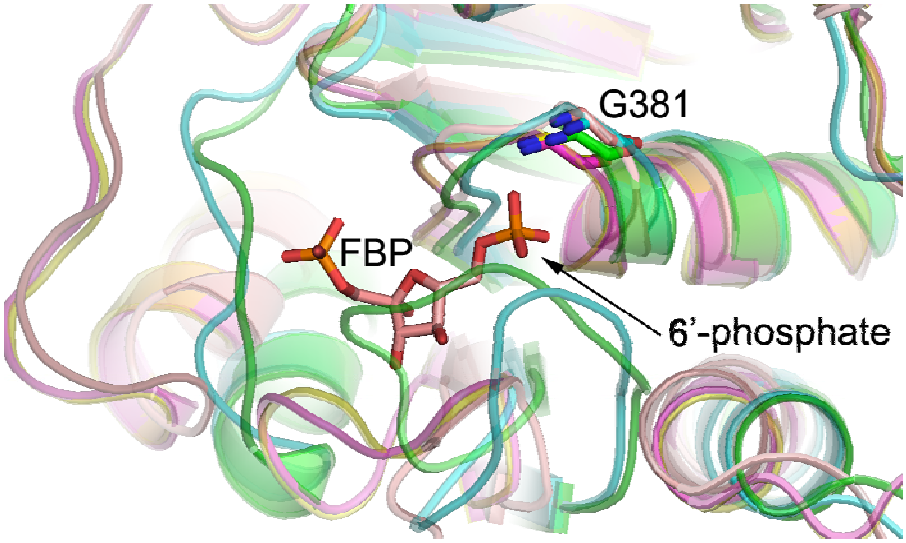

Figure 3.17 **Overlay of FBP binding site of *E. coli* PK1 (green), rabbit PKM1 (purple), yeast PK (blue) and *B. stearothermophilus* PK (yellow).** G381 (*E. coli* PK numbering) is labelled. FBP is shown in orange sticks, which shows the orientation as in yeast PK crystal.

The PK1-G381A enzyme showed similar kinetic profiles to the wild-type in the presence of FBP for both PEP and ADP titration experiments, with comparable $S_{0.5}$ and $k_{cat}/S_{0.5}$ ratios, but had a greater k_{cat} (Figure 3.18). When FBP is absent, however, the $S_{0.5}^{PEP}$ increased in comparison to the wild-type, which indicated some impairment in PEP binding (Figure 3.18b). G381 belongs to the pocket which binds to 6'-phosphate of FBP in the yeast PK (Fenton & Blair 2002; Jurica *et al.* 1998). Although the residues making the pocket are not completely conserved, G381 itself is absolutely conserved among the sequences (Figure 1.5) (Munoz & Ponce 2003). Mutation G381A probably distorts this pocket.

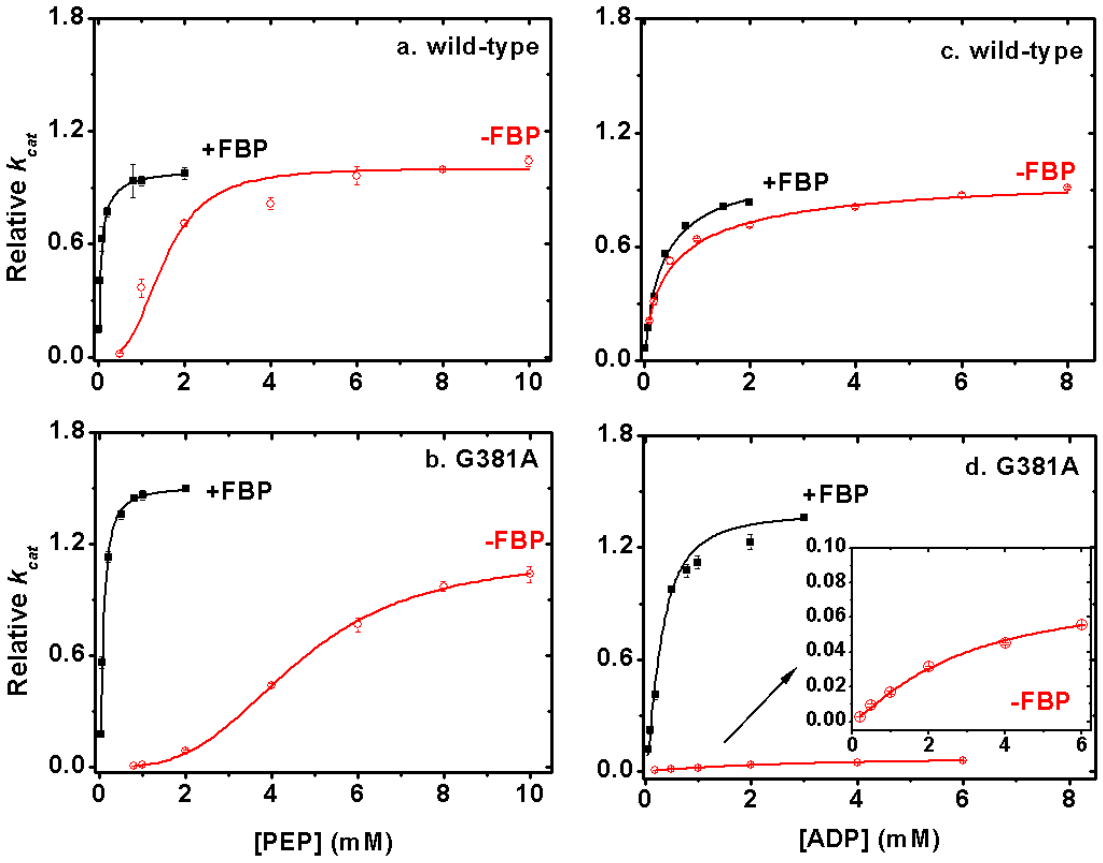

Figure 3.18 **Kinetic properties of the wild-type and PK1-G381A enzymes.** a & b: The relative k_{cat} of purified wild-type and PK1-G381A enzymes to the k_{cat} of the wild-type enzyme was measured at varying concentrations of PEP as described (Section 6.4.2). c & d: The relative k_{cat} of purified wild-type and PK1-G381A enzymes to the k_{cat} of the wild-type enzyme was measured at varying concentrations of ADP as described (Section 6.4.2). Varying concentrations of PEP and ADP are in the absence (○) or presence (■) of 2 mM FBP. Curves represent the best fit to the Hill equation. Kinetic parameters determined by fitting the results to the Hill equation are presented in Table 3.2. Error bars represent the standard error of the k_{cat} relevant to the wild-type k_{cat} between two replications.

3.5 Summary

In this chapter, the kinetic properties of the mutated PK1 enzymes were discussed in detail, along with the comparison with the wild-type enzyme. Mutations found in the previous evolutionary study (Woods *et al.* 2006), which were discussed in this thesis, were not random in that they all (apart from D127N) appeared to play a part in allosteric mechanisms. When mapped to the structure, P70T/Q and D127N are seen to be active site mutations, which affect substrate affinity and the catalysis (Larsen *et al.* 1998; Larsen *et al.* 1997); the mutations I264F and A301T/S belonged to the A/A' subunit interface, which was proposed to involve allosteric signal transition in previous studies (Fenton & Blair 2002; Friesen *et al.* 1998a); and G381A was a mutation that caused a subtle change at the FBP binding site, which affected FBP binding (Fenton & Blair 2002; Jurica *et al.* 1998). G381 was also close to the A/C domain interface, which may therefore be involved in the allosteric signal transition (Mattevi *et al.* 1996; Mattevi *et al.* 1995).

PK1 with mutations at different positions showed distinct kinetics to the wild-type enzyme. Some of the mutations led to activation of the enzyme, as judged by $S_{0.5}$ and k_{cat} values, such as A301T and G381A mutations. Others caused the enzyme to be less active, such as P70 mutations, D127N and I264F. A301S had similar activity when FBP was present in the assay, however, became less active in response to ADP, partly due to a non-saturating PEP level. The most surprising finding was that although A301T and A301S differed by only one methyl group, their kinetic profiles were significantly different with respect to both the catalysis and allosteric regulation pattern. PK1-A301T was the only mutated enzyme exhibiting sigmoidal type kinetics to PEP, even with FBP present in the assay. Clearly, the populations have not evolved parallel PK1 function.

These results generally support the study carried out by Fenton and colleagues (2002) on yeast PK. Some of the results (e.g. kinetic results for PK1-A301T) highlighted the important role of A/A' subunit interface in the allosteric regulation in *E. coli* PK1 (Fenton & Blair 2002), and the role of Aα6 loop involved in the allosteric signal transition under the "network mechanism" (Friesen *et al.* 1998a).

3.6 References

Bradford MM. 1976. A rapid and sensitive method for the quantitation of microgram quantities of protein utilizing the principle of protein-dye binding. *Anal Biochem* 72:248-54

Christofk HR, Vander Heiden MG, Wu N, Asara JM, Cantley LC. 2008. Pyruvate kinase M2 is a phosphotyrosine-binding protein. *Nature* 452:181-6

Cooper TF, Rozen DE, Lenski RE. 2003. Parallel changes in gene expression after 20,000 generations of evolution in *Escherichia coli*. *Proc Natl Acad Sci U S A* 100:1072-7

DeLano WL. 2002. *The PyMOL molecular graphics system.* SanCarlos, CA, USA: DeLano Scientific

Fenton AW, Blair JB. 2002. Kinetic and allosteric consequences of mutations in the subunit and domain interfaces and the allosteric site of yeast pyruvate kinase. *Arch Biochem Biophys* 397:28-39

Fermo E, Bianchi P, Chiarelli LR, Cotton F, Vercellati C, Writzl K, Baker K, Hann I, Rodwell R, Valentini G, Zanella A. 2005. Red cell pyruvate kinase deficiency: 17 new mutations of the PK-LR gene. *Br J Haematol* 129:839-46

Friesen RH, Castellani RJ, Lee JC, Braun W. 1998a. Allostery in rabbit pyruvate kinase: development of a strategy to elucidate the mechanism. *Biochemistry* 37:15266-76

Friesen RH, Chin AJ, Ledman DW, Lee JC. 1998b. Interfacial communications in recombinant rabbit kidney pyruvate kinase. *Biochemistry* 37:2949-60

Hill AV. 1910. The possible effects of the aggregation of the molecules of hemoglobin on its dissociation curves. *J Physiol (Lond)* 40:iv-vii

Jurica MS, Mesecar A, Heath PJ, Shi W, Nowak T, Stoddard BL. 1998. The allosteric regulation of pyruvate kinase by fructose-1,6-bisphosphate. *Structure* 6:195-210

Kofron JL, Reed GH. 1990. Synthesis of oxalyl phosphate and processing of the acyl phosphate by phosphoenolpyruvate-dependent enzymes. *Arch Biochem Biophys* 280:40-4

Larsen TM, Benning MM, Rayment I, Reed GH. 1998. Structure of the bis(Mg^{2+})-ATP-oxalate complex of the rabbit muscle pyruvate kinase at 2.1 A resolution: ATP binding over a barrel. *Biochemistry* 37:6247-55

Larsen TM, Benning MM, Wesenberg GE, Rayment I, Reed GH. 1997. Ligand-induced domain movement in pyruvate kinase: structure of the enzyme from rabbit muscle with Mg^{2+}, K^{+}, and L-phospholactate at 2.7 A resolution. *Arch Biochem Biophys* 345:199-206

Lenski RE, Mongold JA, Sniegowski PD, Travisano M, Vasi F, Gerrish PJ, Schmidt TM. 1998. Evolution of competitive fitness in experimental populations of *E. coli*: what makes one genotype a better competitor than another? *A. V. Leeuwenhoek* 73:35-47

Lenski RE, Rose MR, Simpson SC, Tadler SC. 1991. Long-term experimental evolution in *Escherichia coli*. I. Adaptation and divergence during 2,000 generations. *Am Nat* 138:1315-41

Lenski RE, Travisano M. 1994. Dynamics of adaptation and diversification: a 10,000-generation experiment with bacterial populations. *Proc Natl Acad Sci U S A* 91:6808-14

Lovell SC, Mullick AH, Muirhead H. 1998. Cooperativity in *Bacillus stearothermophilus* pyruvate kinase. *J Mol Biol* 276:839-51

Mattevi A, Bolognesi M, Valentini G. 1996. The allosteric regulation of pyruvate kinase. *FEBS Lett* 389:15-9

Mattevi A, Valentini G, Rizzi M, Speranza ML, Bolognesi M, Coda A. 1995. Crystal structure of *Escherichia coli* pyruvate kinase type I: molecular basis of the allosteric transition. *Structure* 3:729-41

Muirhead H, Clayden DA, Barford D, Lorimer CG, Fothergill-Gilmore LA, Schiltz E, Schmitt W. 1986. The structure of cat muscle pyruvate kinase. *EMBO J* 5:475-81

Munoz ME, Ponce E. 2003. Pyruvate kinase: current status of regulatory and functional properties. *Comp Biochem Physiol B Biochem Mol Biol* 135:197-218

Pendergrass DC, Williams R, Blair JB, Fenton AW. 2006. Mining for allosteric information: natural mutations and positional sequence conservation in pyruvate kinase. *IUBMB Life* 58:31-8

Valentini G, Chiarelli L, Fortin R, Speranza ML, Galizzi A, Mattevi A. 2000. The allosteric regulation of pyruvate kinase. *J Biol Chem* 275:18145-52

Woods R, Schneider D, Winkworth CL, Riley MA, Lenski RE. 2006. Tests of parallel molecular evolution in a long-term experiment with *Escherichia coli*. *Proc Natl Acad Sci U S A* 103:9107-12

Zanella A, Fermo E, Bianchi P, Valentini G. 2005. Red cell pyruvate kinase deficiency: molecular and clinical aspects. *Br J Haematol* 130:11-25

Chapter 4

Biophysical characterisation of the PK1 mutants

4.1 Introduction

The biophysical properties of an enzyme are reflected in its structure, hydrodynamic and thermodynamic properties. The altered kinetic properties of the mutants seen in Chapter 3 may have resulted from altered structure, reflecting the protein structure-function relationship of this enzyme. Secondary structure, quaternary structure and the hydrodynamic properties of the mutant PK1 enzymes were compared to the wild-type enzyme. In addition, X-ray crystallography was attempted, however, crystals of several mutated PK1 enzymes diffracted only weakly and data has not been collected.

4.2 Circular Dichroism

The secondary structure of the seven PK1 mutants was examined by circular dichroism (CD) using the same conditions as for the wild-type (Section 2.5.1). Similar to the wild-type enzyme, the results were processed using software on DICHROWEB (Whitmore & Wallace 2004) using the analysis algorithms SELCON3, CONTIN-LL and CDSSTR (Section 6.5.2) (Compton & Johnson 1986; Sreerama *et al.* 1999; van Stokkum *et al.* 1990) and dataset 7, with the quality of the fit judged by the n.r.m.s.d. value. CD plots have been drawn according to the CDSSTR fit (with lowest n.r.m.s.d. value) (Table 4.1, Figure 4.1), and the parameters had been listed (Table 4.1).

In the analysis, data with a HT voltage above 600 mV, observed in some samples to 190 nm, were not included. Parameters for the mutant enzymes were compared with those of the wild-type, which showed that the α and β contents of the wild-type and mutated enzymes were not identical. This indicated changed secondary structures of mutants.

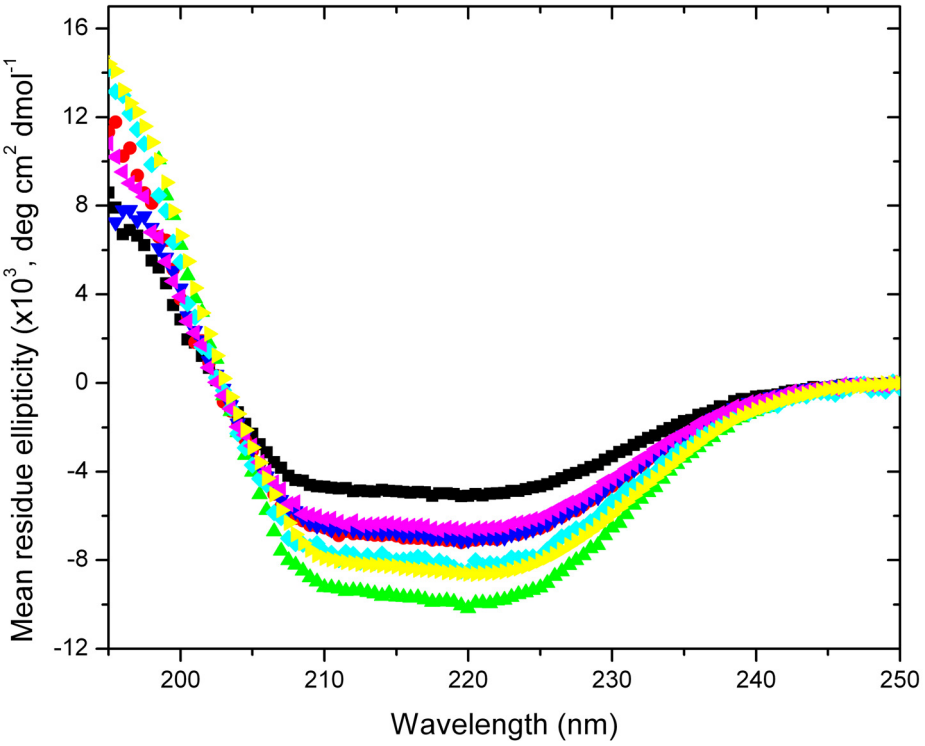

Figure 4.1 **Comparison of the mutated PK1 enzymes with the wild-type.** (Enzymes of wild-type 0.15 mg/ml, ▲; A301T 0.15 mg/ml, ▲; G381A 0.2 mg/ml, ▲; P70T 0.2 mg/ml, ●; D127N 0.25 mg/ml, ▲; A301S 0.2 mg/ml, ▲; and I264F 0.22 mg/ml, ■); CD was performed in a Jasco-815 CD spectropolarimeter at 20 ºC. Wavelength scans were recorded from 240 to 195 nm in 0.5 nm pitch using step scan method. The HT voltage was below 600 mV.

The mutated enzymes have similar CD plots compared to the wild-type, except enzymes with mutations I264F and G381A. PK1-I264F has lower α-helical content than the wild-type enzyme. Residue I264, which belonged to helix Aα6, was mutated to a phenylalanine with a bulker side chain. This may have affected the helical structure at Aα6, as suggested by the CD result. PK1-G381A, on the other hand, had higher α-helical content compared to the wild-type. G381 is part of a loop at the FBP binding site. Given that alanine is less flexible than glycine, it may have affected the protein structure in a way that the helices are packed differently around the FBP binding site.

Table 4.1 **Fitted parameters of the PK1 enzymes using CDSSTR software on DICHROWEB.** [a] CD for PK1-P70Q was not performed.

	Wild-type	**P70T**	**P70Q[a]**	**D127N**	**I264F**	**A301T**	**A301S**	**G381A**
n.r.m.s.d.	***0.017***	***0.034***	***n/a*** [a]	***0.042***	***0.046***	***0.028***	***0.026***	***0.044***
α-helix(1)	0.14	0.08	n/a [a]	0.06	0.05	0.09	0.07	0.15
α-helix(2)	0.10	0.09	n/a [a]	0.09	0.07	0.1	0.08	0.13
β-strand(1)	0.16	0.19	n/a [a]	0.21	0.23	0.18	0.21	0.14
β-strand(2)	0.1	0.11	n/a [a]	0.11	0.12	0.11	0.11	0.08
Turn	0.2	0.22	n/a [a]	0.24	0.21	0.24	0.23	0.21
uncoiled	0.30	0.3	n/a [a]	0.3	0.33	0.28	0.29	0.29
Total	**1**	**0.99**	**n/a** [a]	**1.01**	**1.01**	**1**	**0.99**	**1**
Helix segments per 100 residues	2.6	2.3	n/a [a]	2.2	1.6	2.4	2.0	3.3
Ave helix length per segment	9.3	7.7	n/a [a]	6.5	7.1	7.7	7.5	8.6
Strand segments per 100 residues	4.7	5.3	n/a [a]	5.5	5.8	5.5	5.7	4.1
Ave strand length per segment	5.2	5.7	n/a [a]	5.8	6.1	5.3	5.7	5.4

4.3 Mass spectrometry

Electrospray mass spectrometry (ES-MS) was performed for all the seven mutants, as for the wild-type (Section 6.5.1). Molecular weights of the mutants obtained by mass spectrometry were compared with the previously predicted isotopically averaged molecular weights by protein calculator v 3.3 (from the Scripps research institute, La Jolla, CA). The results are shown in Figure 4.2 and Table 4.2.

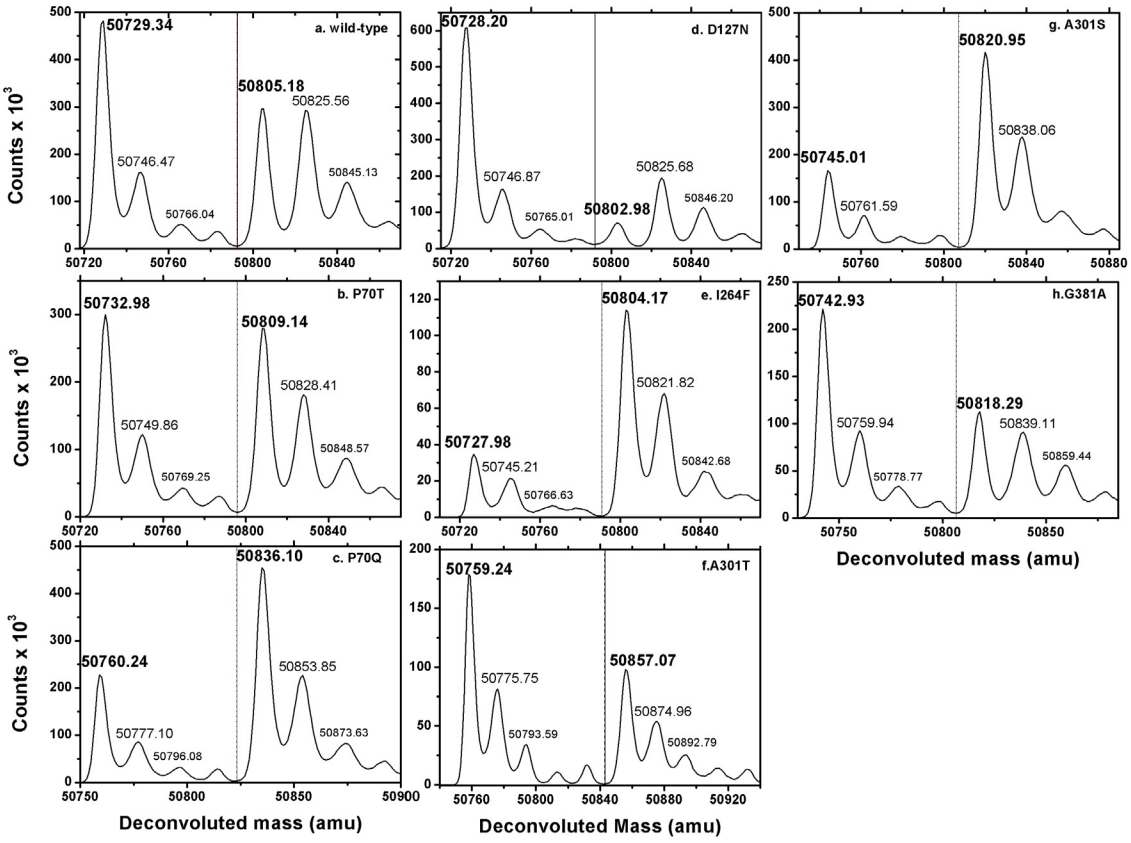

Figure 4.2 **Counts *vs.* Deconvoluted mass (amu) of the wild-type PK1 and the mutants.** (a) Wild-type PK1 with the main peaks labelled. (b) PK1-P70T mutant. (c) PK1-P70Q mutant. (d) PK1-D127N mutant. (e) PK1-I264F mutant. (f) PK1-A301T mutant. (g) PK1-A301S mutant. (h) PK1-G381A mutant.

Table 4.2 **Comparison of the molecular weights of the wild-type PK1 and the mutated enzymes obtained from mass spectrometry and the isotopically averaged molecular weights.**

	Isotopically Averaged MW (Da)	MW obtained by MS (Da)
Wild-type	50729.28	50729.34
P70T	50733.27	50732.98
P70Q	50760.29	50760.24
D127N	50728.29	50728.20
I264F	50763.29	50766.63
A301T	50759.30	50759.24
A301S	50745.28	50745.01
G381A	50743.30	50742.93

MS data were consistent with the isotopically averaged molecular weights, which further confirmed the identities of the mutated enzymes obtained by mutagenesis. In all the mutants, several adducts similar to those found in wild-type were observed (Figure 4.2). One adduct with a molecular weight of ~76 Da was found in the MS data of the wild-type (i.e. 50805.18 Da - 50729.34Da = 75.84 Da) and all the mutants. The molecular weight is consistent with β-mercaptoethanol molecule (76 Da) (estimated using ABRF DeltaMass mass finder from http://www.abrf.org/index.cfm/dm.home). β-Mercaptoethanol (2 mM) was added into all buffer solutions during the protein purification procedure, which made it likely that the ethoxythiol group was attached to the protein covalently, however, the mechanism is unknown. Two adducts associated with the main peak were also observed, with molecular weights ~18 Da (i.e. 50746.47 Da - 50729.34 Da = 17.13 Da for the wild-type PK1) and ~37 Da (i.e. 50766.04 Da- 50729.34 Da = 36.7 Da for the wild-type PK1), respectively, which are consistent with the molecular weights of sodium (22 Da) and potassium (37 Da) (http://www.abrf.org/index.cfm/dm.home), which are present in the buffer (Section 6.3.3).

4.4 Analytical ultracentrifugation (AUC)

The quaternary structure and the hydrodynamic properties of the mutants were studied by analytical ultracentrifugation (AUC), as for the wild-type (Section 6.5.3). At 1.0 mg/ml (19.7 μM) (graphs not shown) and 0.1 mg/ml (1.97 μM) (Figures 4.3-4.9), respectively, all the mutants had sedimentation coefficients around 8.5 S, which corresponded to a single tetrameric species. There were subtle differences with the friction ratios; however, these do not indicate an altered quaternary structure. The results were generally consistent with

the wild-type PK1, thus indicating that the quaternary structure in solution was the same for the wild-type PK1 and the mutants.

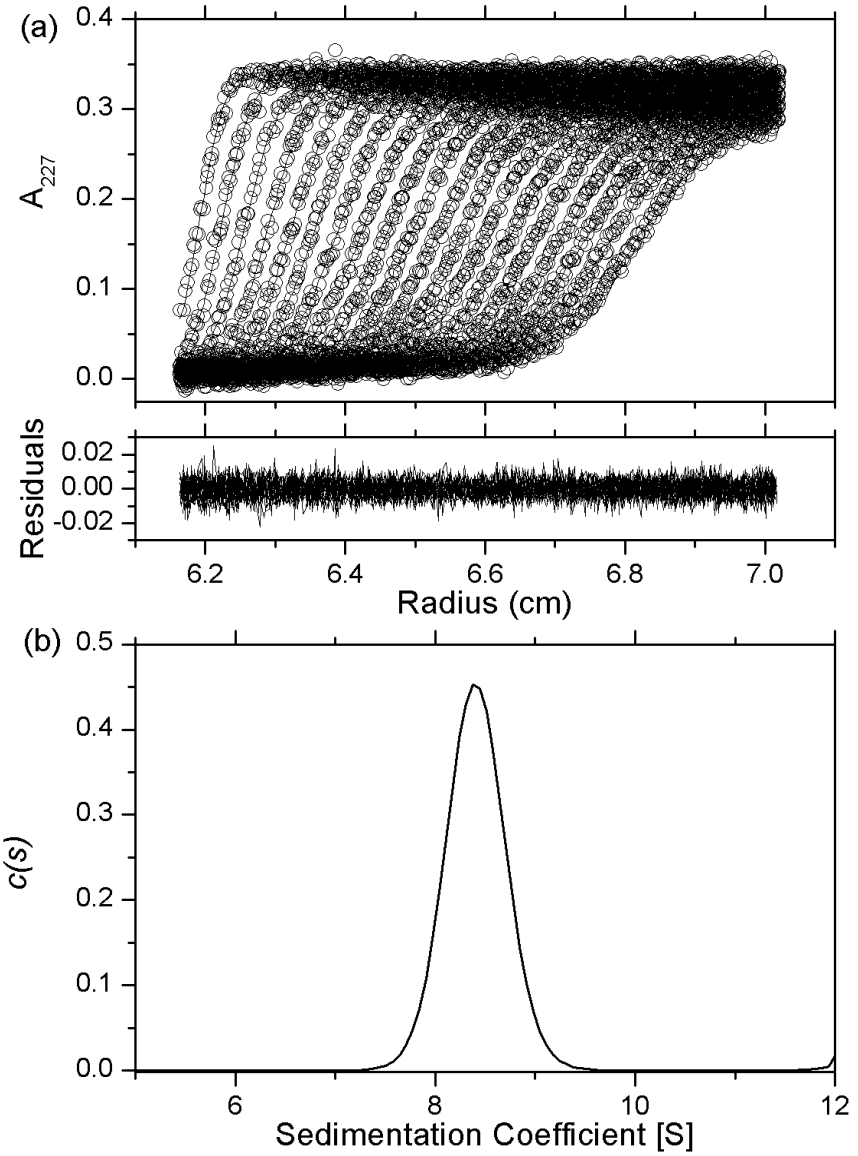

Figure 4.3 **Sedimentation velocity analysis of PK1-P70T at 0.1 mg/ml (1.97 μM).** (a) Absorbance at 227 nm as a function of radius (cm) from the axis of rotation is plotted. The raw data are presented as open circles and are overlaid with the nonlinear least squares best-fit to a continuous-size distribution model (Lamm equation) by SEDFIT. Residuals for the nonlinear least squares best-fit are also shown. (b) The continuous sedimentation coefficient [*c(s)*] distribution as a function of sedimentation coefficient (Svedberg, S). The fit had a resolution of 150 species between s_{min} of 0.1 S and s_{max} of 14 S with P = 0.95, v-bar = 0.7413, ρ = 1.00117 g/ml, η = 0.010066 p, and f/f_0 = 1.38. The r.m.s.d. and runs test-Z score for the fit were 0.0052 and 1.71, respectively.

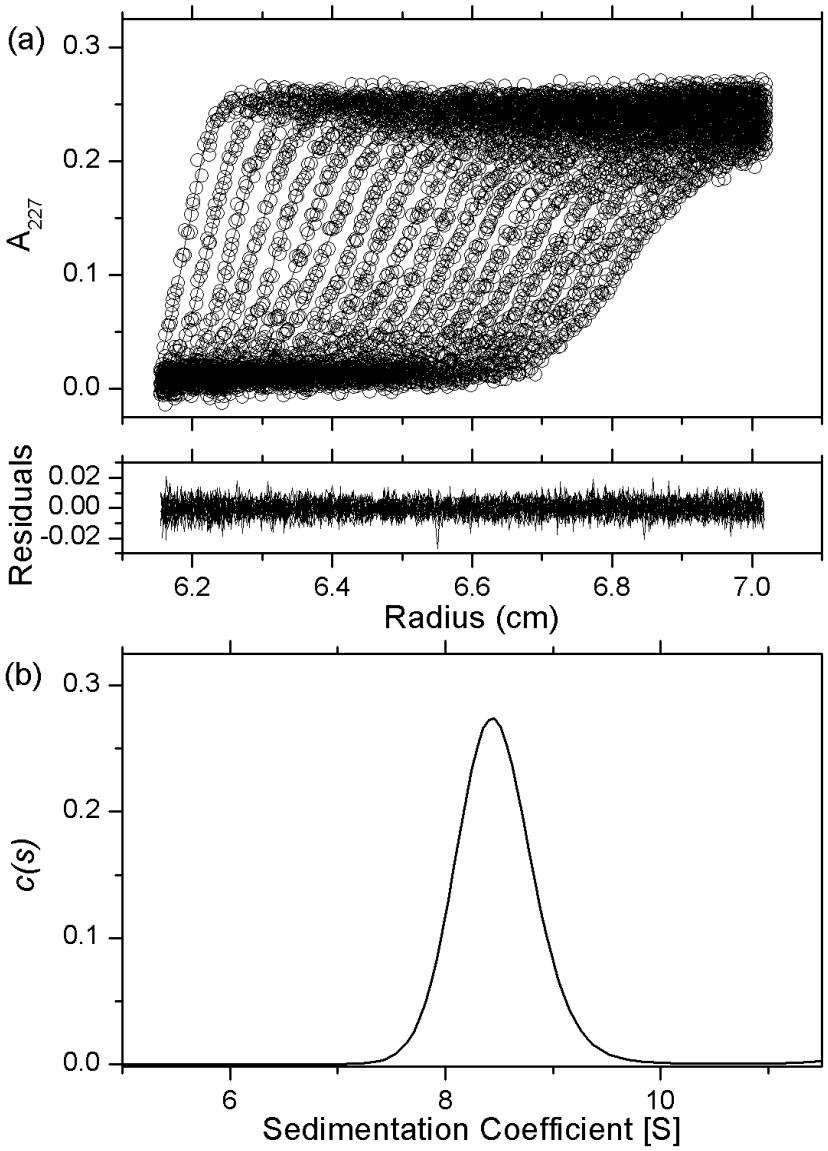

Figure 4.4 **Sedimentation velocity analysis of PK1-P70Q at 0.1 mg/ml (1.97 μM).** (a) Absorbance at 227 nm as a function of radius (cm) from the axis of rotation is plotted. The raw data are presented as open circles and are overlaid with the nonlinear least squares best-fit to a continuous-size distribution model (Lamm equation) by SEDFIT. Residuals for the nonlinear least squares best-fit are also shown. (b) The continuous sedimentation coefficient [*c(s)*] distribution as a function of sedimentation coefficient (Svedberg, S). The fit had a resolution of 150 species between s_{min} of 0.1 S and s_{max} of 14 S with P = 0.95, v-bar = 0.7413, ρ = 1.00117 g/ml, η = 0.010066 p, and f/f_0 = 1.45. The r.m.s.d. and runs test-Z score for the fit were 0.0051 and 1.07, respectively.

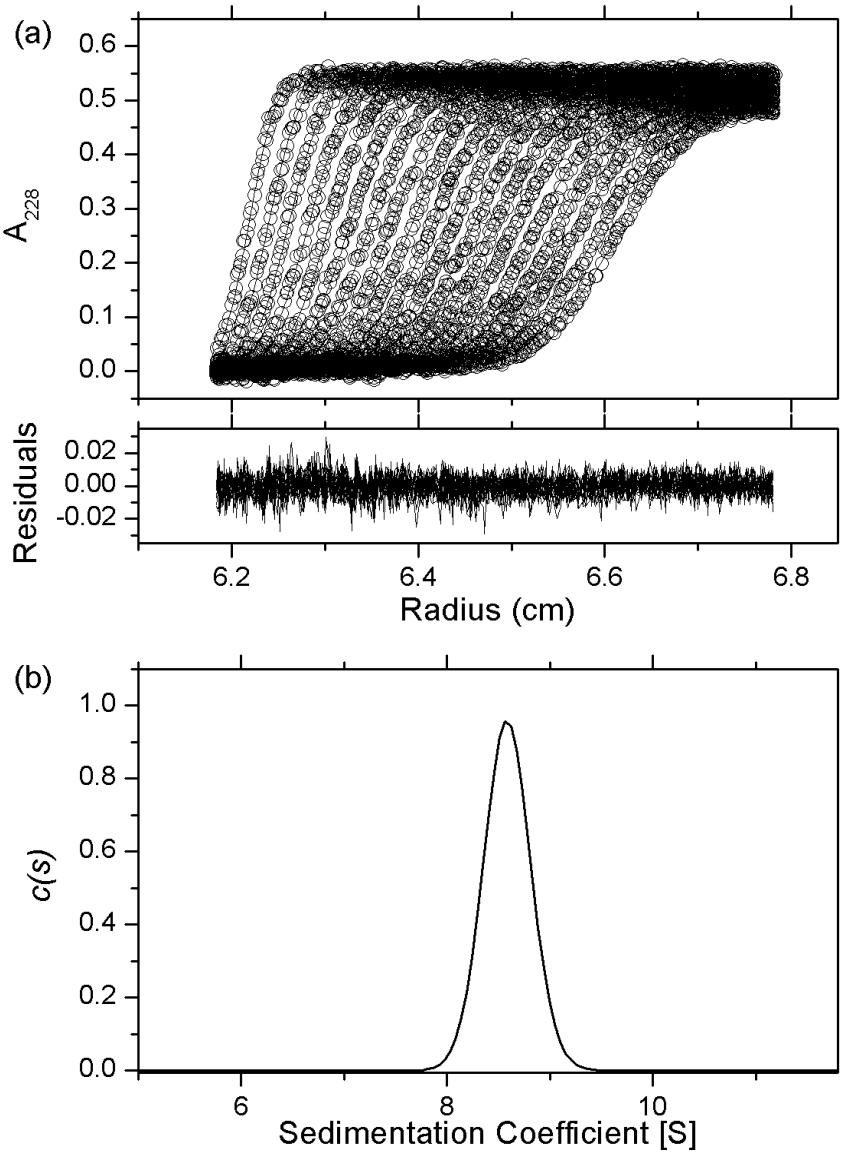

Figure 4.5 **Sedimentation velocity analysis of PK1-D127N at 0.1 mg/ml (1.97 μM).** (a) Absorbance at 227 nm as a function of radius (cm) from the axis of rotation is plotted. The raw data are presented as open circles and are overlaid with the nonlinear least squares best-fit to a continuous-size distribution model (Lamm equation) by SEDFIT. Residuals for the nonlinear least squares best-fit are also shown. (b) The continuous sedimentation coefficient [*c(s)*] distribution as a function of sedimentation coefficient (Svedberg, S). The fit had a resolution of 150 species between s_{min} of 0.1 S and s_{max} of 14 S with P = 0.95, v-bar = 0.7413, ρ = 1.00117 g/ml, η = 0.010066 p, and f/f_0 = 1.34. The r.m.s.d. and runs test-Z score for the fit were 0.0062 and 6.27, respectively.

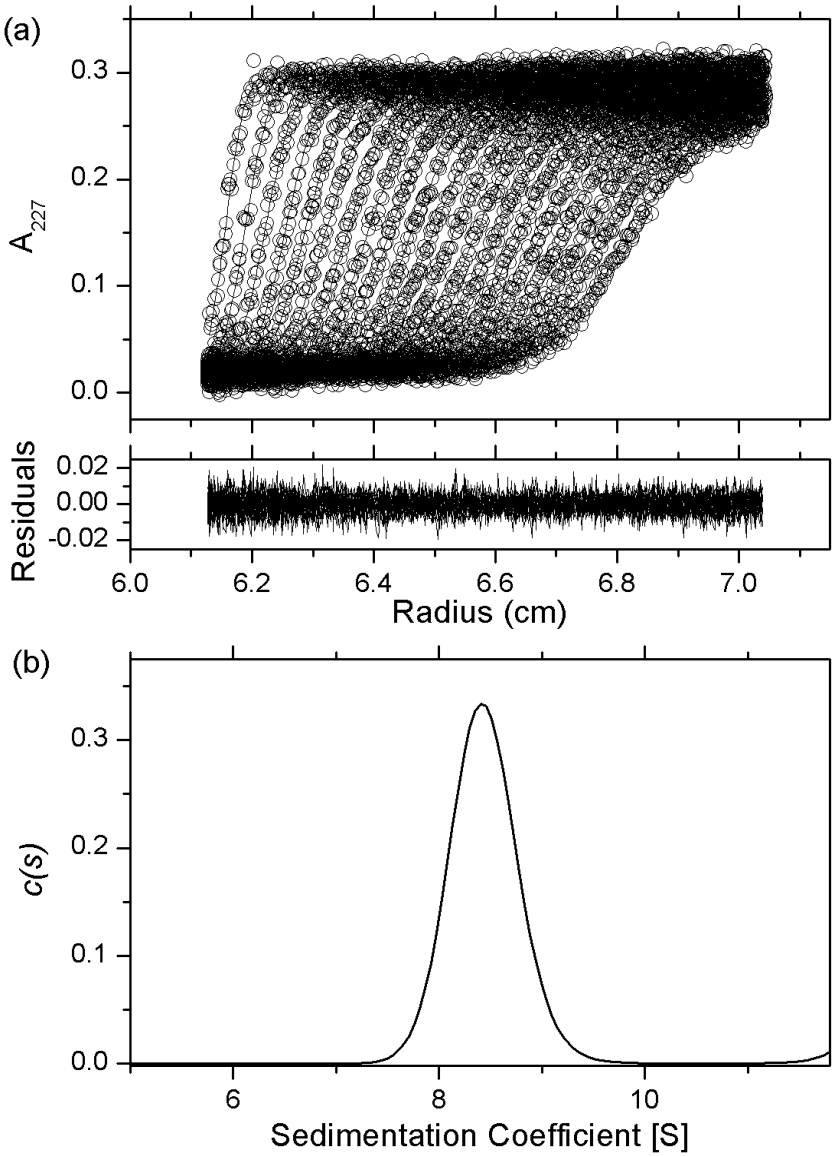

Figure 4.6 **Sedimentation velocity analysis of PK1-I264F at 0.1 mg/ml (1.97 μM).** (a) Absorbance at 227 nm as a function of radius (cm) from the axis of rotation is plotted. The raw data are presented as open circles and are overlaid with the nonlinear least squares best-fit to a continuous-size distribution model (Lamm equation) by SEDFIT. Residuals for the nonlinear least squares best-fit are also shown. (b) The continuous sedimentation coefficient [*c(s)*] distribution as a function of sedimentation coefficient (Svedberg, S). The fit had a resolution of 150 species between s_{min} of 0.1 S and s_{max} of 14 S with P = 0.95, v-bar = 0.7413, ρ = 1.00117 g/ml, η = 0.010066 p, and f/f_0 = 1.45. The r.m.s.d. and runs test-Z score for the fit were 0.0053 and 0.01, respectively.

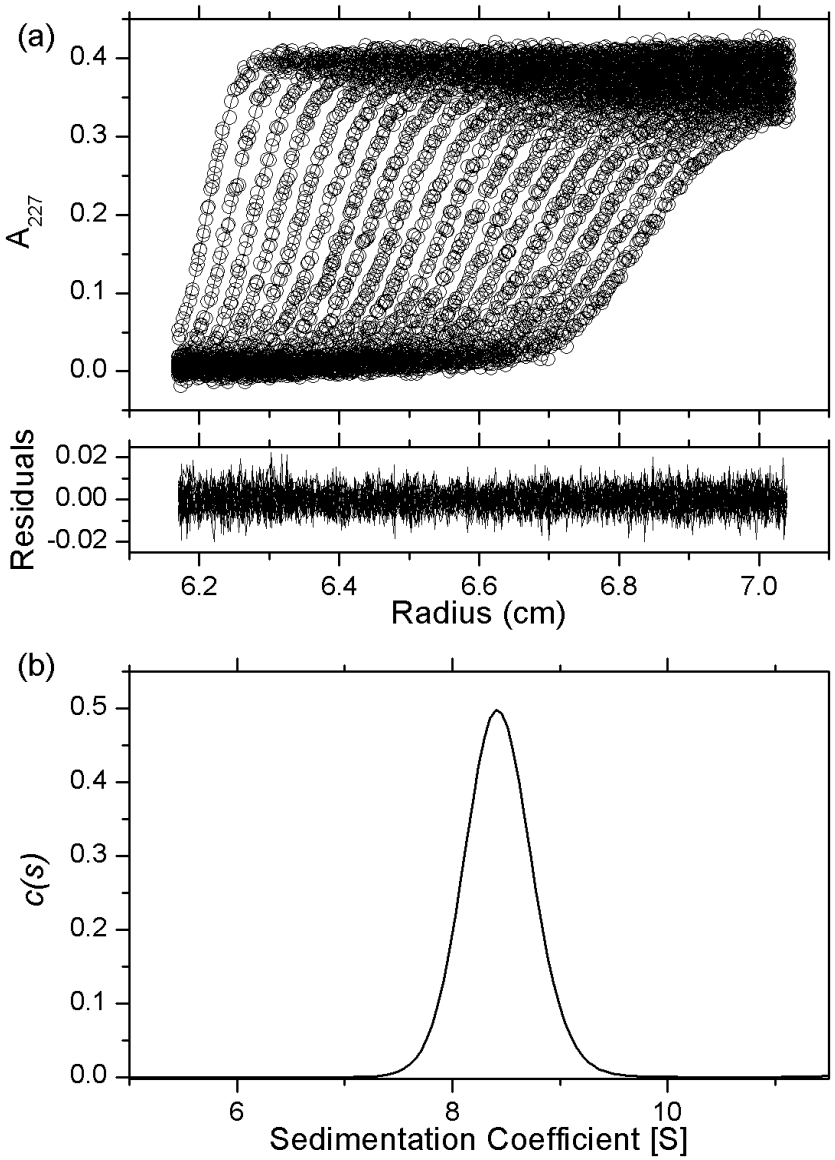

Figure 4.7 **Sedimentation velocity analysis of PK1-A301T at 0.1 mg/ml (1.97 μM).** (a) Absorbance at 227 nm as a function of radius (cm) from the axis of rotation is plotted. The raw data are presented as open circles and are overlaid with the nonlinear least squares best-fit to a continuous-size distribution model (Lamm equation) by SEDFIT. Residuals for the nonlinear least squares best-fit are also shown. (b) The continuous sedimentation coefficient [*c(s)*] distribution as a function of sedimentation coefficient (Svedberg, S). The fit had a resolution of 150 species between s_{min} of 0.1 S and s_{max} of 14 S with P = 0.95, v-bar = 0.7413, ρ = 1.00117 g/ml, η = 0.010066 p, and f/f_0 = 1.44. The r.m.s.d. and runs test-Z score for the fit were 0.0054 and 1.51, respectively.

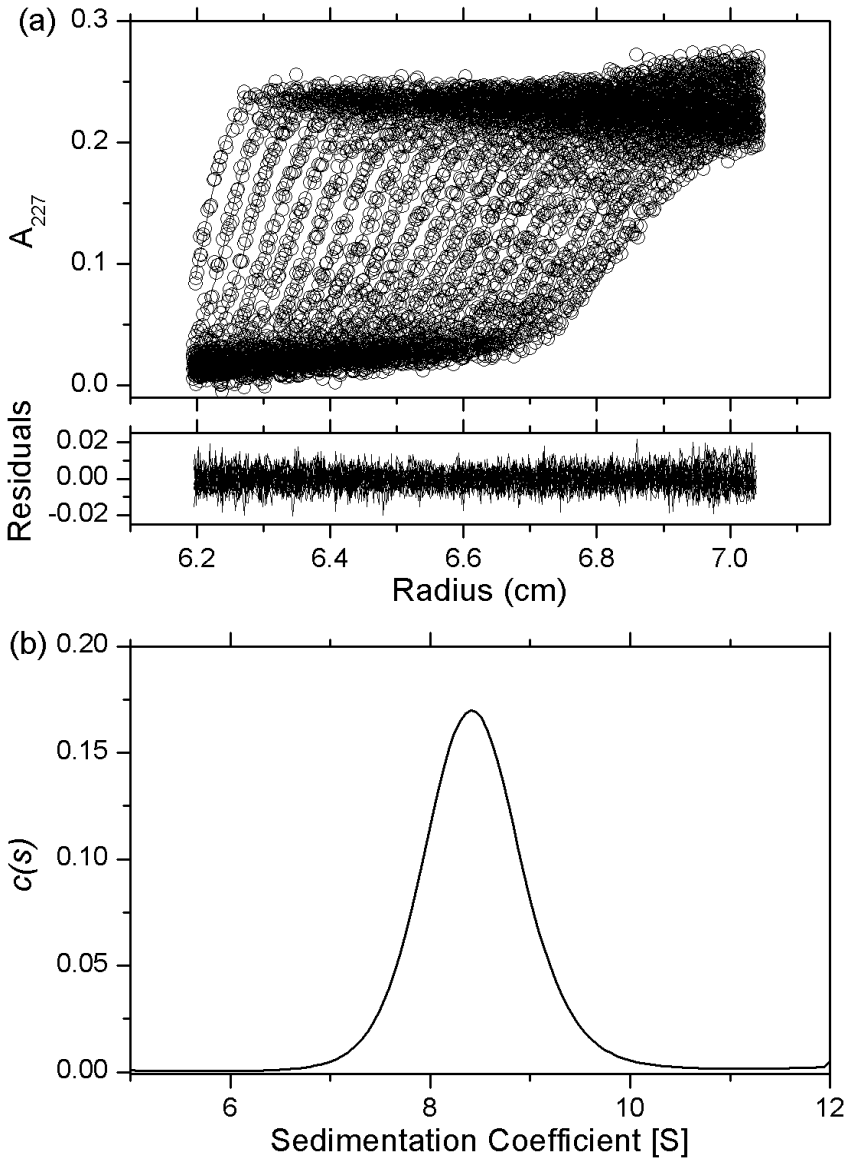

Figure 4.8 **Sedimentation velocity analysis of PK1-A301S at 0.1 mg/ml (1.97 μM).** (a) Absorbance at 227 nm as a function of radius (cm) from the axis of rotation is plotted. The raw data are presented as open circles and are overlaid with the nonlinear least squares best-fit to a continuous-size distribution model (Lamm equation) by SEDFIT. Residuals for the nonlinear least squares best-fit are also shown. (b) The continuous sedimentation coefficient [*c(s)*] distribution as a function of sedimentation coefficient (Svedberg, S). The fit had a resolution of 150 species between s_{min} of 0.1 S and s_{max} of 14 S with P = 0.95, v-bar = 0.7413, ρ = 1.00117 g/ml, η = 0.010066 p, and f/f_0 = 1.57. The r.m.s.d. and runs test-Z score for the fit were 0.0053 and 5.66, respectively.

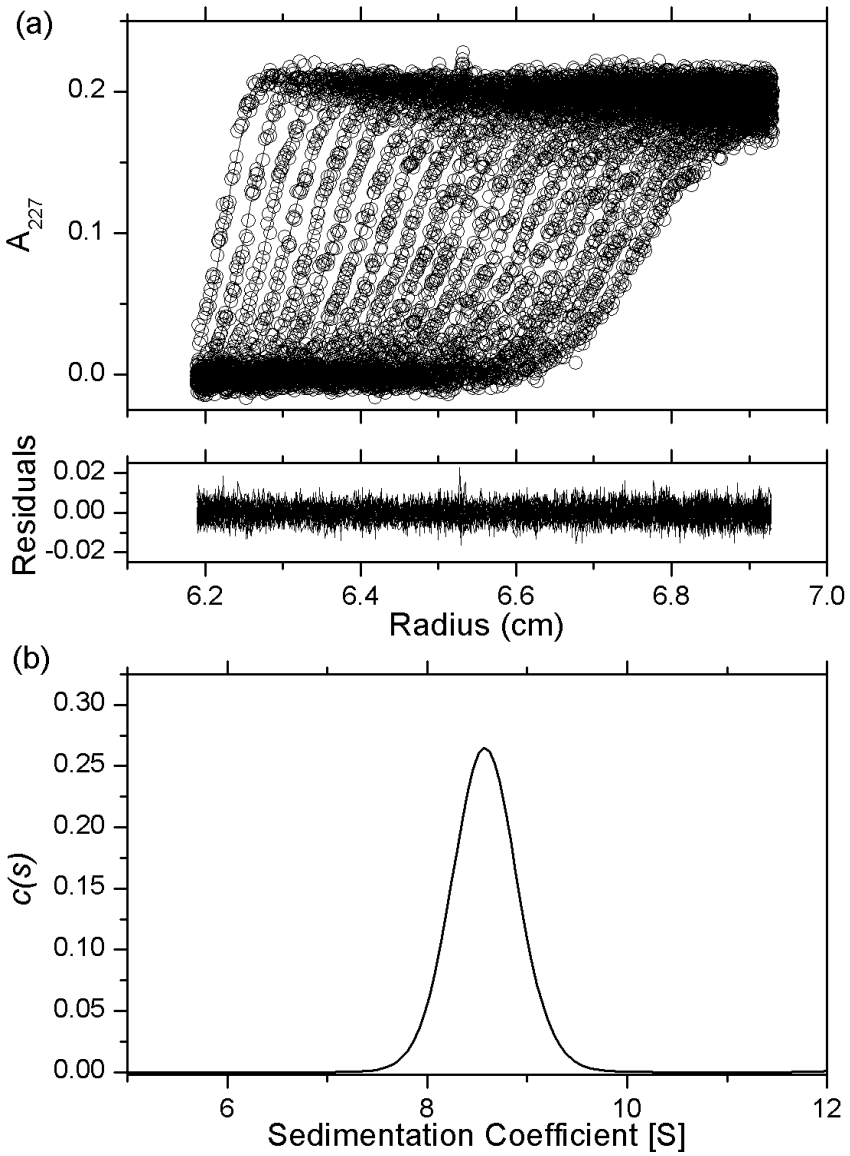

Figure 4.9 **Sedimentation velocity analysis of PK1-G381A at 0.1 mg/ml (1.97 μM).** (a) Absorbance at 227 nm as a function of radius (cm) from the axis of rotation is plotted. The raw data are presented as open circles and are overlaid with the nonlinear least squares best-fit to a continuous-size distribution model (Lamm equation) by SEDFIT. Residuals for the nonlinear least squares best-fit are also shown. (b) The continuous sedimentation coefficient [*c(s)*] distribution as a function of sedimentation coefficient (Svedberg, S). The fit had a resolution of 150 species between s_{min} of 0.1 S and s_{max} of 14 S with P = 0.95, v-bar = 0.7413, ρ = 1.00117 g/ml, η = 0.010066 p, and f/f_0 = 1.36. The r.m.s.d. and runs test-Z score for the fit were 0.0045 and 1.85, respectively.

4.5 Analytical ultracentrifugation coupled with fluorescence detection system (AUC-FDS)

To further examine the association/dissociation limit of PK1, AUC-FDS experiments were performed. This technology utilises traditional AUC principles and integrates a novel fluorescence detection unit onto the ultracentrifuge equipment (Schmidt *et al.* 1990). By labelling the protein using a fluorescent dye, the fluorescence emission intensity is monitored by a photomultiplier (Schmidt *et al.* 1990). For detecting trace amount of materials, this technology is advantageous over absorbance and interference detections where the detection limit is within picomolar (pM) range (MacGregor *et al.* 2004).

Three mutants were selected for AUC-FDS analysis. Of the seven mutated PK1 found in the previous evolutionary study (Lenski 1991), two were mutated at position 301 along the amino acid chain, namely PK1-A301T and PK1-A301S (Cooper *et al.* 2003). A301 belongs to Aα7, which is an important loop at the A/A' interface (Figures 1.12 & 3.12) crucial for the enzyme catalysis and is involved in the allosteric regulation (Section 3.4.2). Moreover, PK1-A301T showed distinct kinetic behaviour to the wild-type. These make it a good candidate for AUC-FDS analysis for the investigation of the possible quaternary structural changes or an altered dissociation strength caused by these mutations at low concentration. The PK1-A301S enzyme was found in three independently evolved populations, which further emphasised the importance of this mutation (Cooper *et al.* 2003). PK1-G381A was also examined by AUC-FDS, as it belongs to the FBP binding site (Mattevi *et al.* 1996). It was suspected that the quaternary structure of G381A might be sensitive to the presence of FBP.

Pure protein samples of PK1-A301T, PK1-A301S and PK1-G381A were labelled as for the wild-type enzyme (Section 2.5.4) and the degree of labelling (DOL) was determined (Section 6.5.4). The DOL of the three protein samples is shown in Table 4.3.

Table 4.3 **Protein concentrations and DOL for Alexa Fluor® 488 dye labelled proteins.**

	A_{280}	A_{max}	$A_{protein}$	[protein] (mg/ml)	DOL
PK1-A301T	0.33	0.46	0.28	1.9	0.17
PK1-A301S	0.63	1.3	0.48	3.3	0.29
PK1-G381A	0.080	0.041	0.076	0.51	0.057

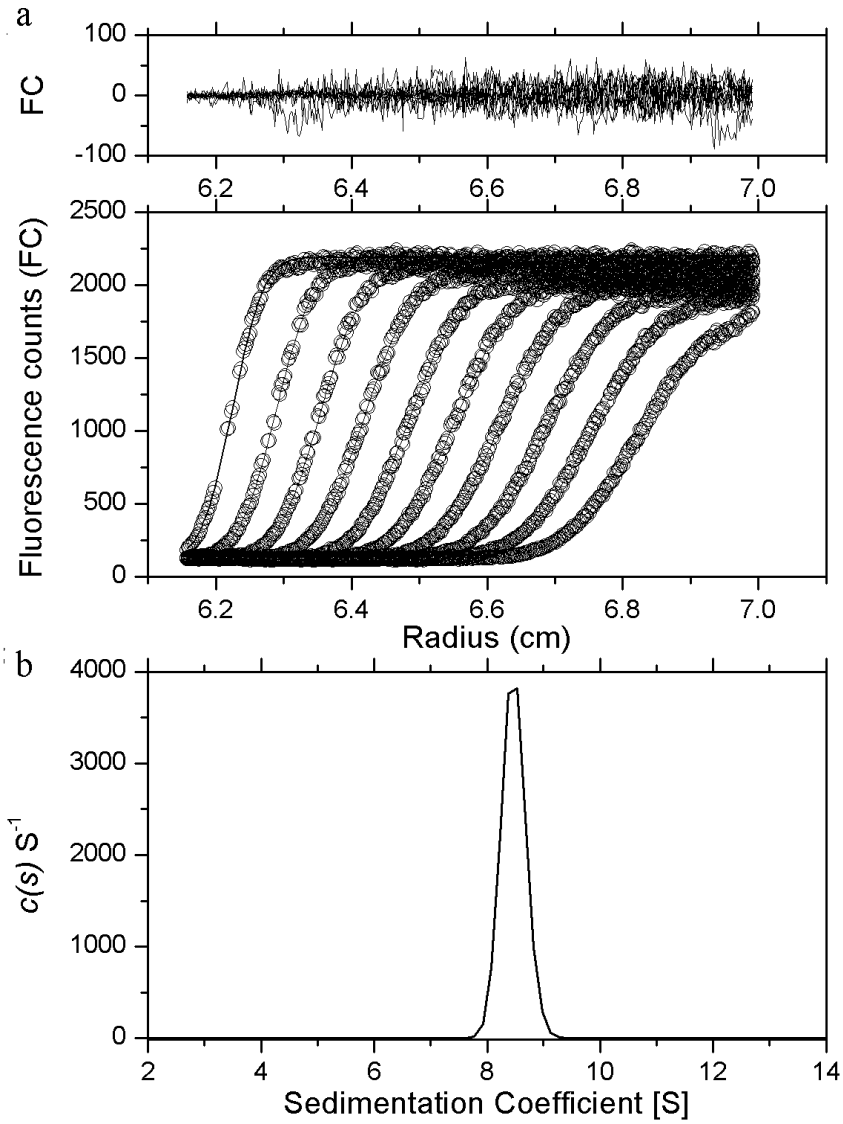

Figure 4.10 **AUC-FDS analysis of PK1-A301T at 0.01 mg/ml (197 nM), with gains set at 2 × 84%.** (a) Fluorescence counts at 488 nm as a function of radius (cm) from the axis of rotation plotted. The raw data are presented as open circles and are overlaid with the nonlinear least squares best-fit to a continuous-size distribution model (Lamm equation) by SEDFIT. Residuals for the nonlinear least squares best-fit are also shown. (b) The continuous sedimentation coefficient [*c(s)*] distribution as a function of sedimentation coefficient (Svedberg, S). The fit had a resolution of 100 species between s_{min} of 0.1 S and s_{max} of 15 S, with P = 0.95, v-bar = 0.7413, ρ = 1.00117 g/ml, η = 0.010066 p, and f/f_0 = 1.42. The r.m.s.d. and runs test-Z score for the fit were 15 and 17.3, respectively.

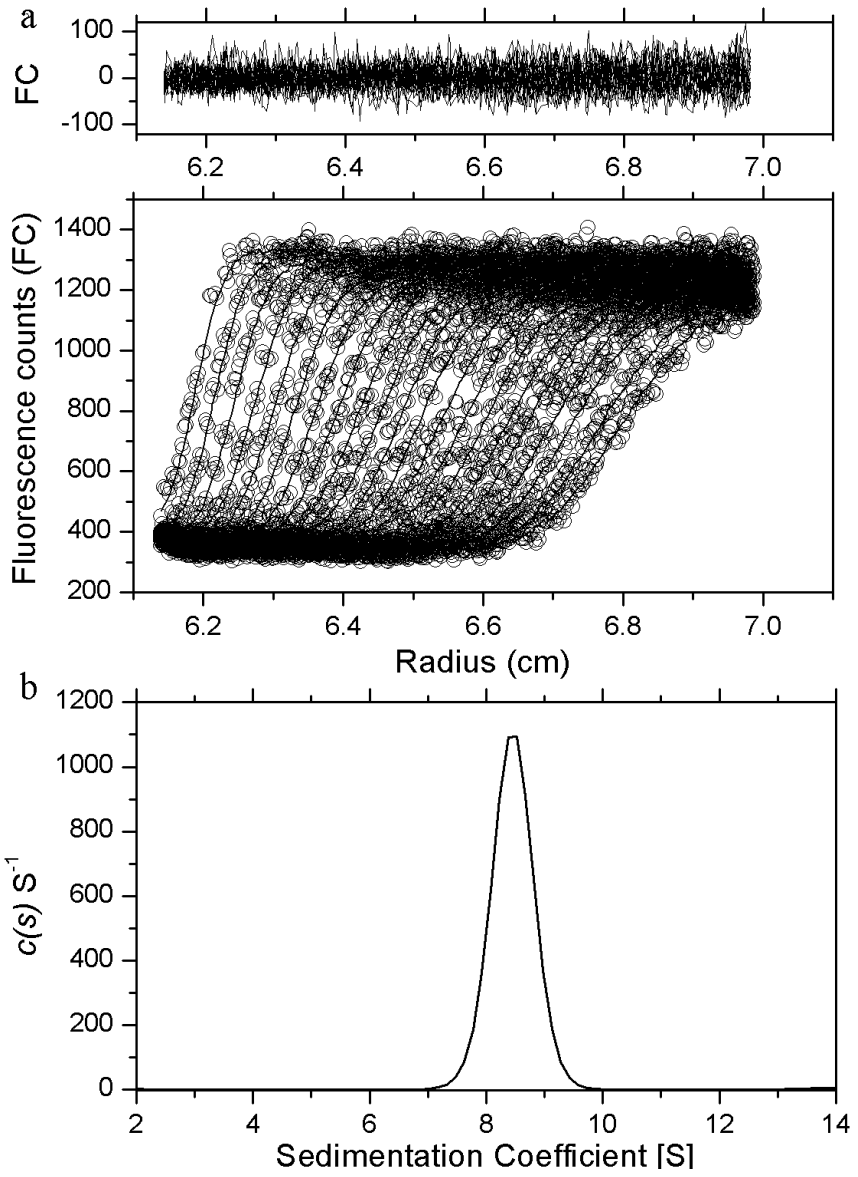

Figure 4.11 **AUC-FDS analysis of PK1-A301T at 0.001 mg/ml (19.7 nM), with gains set at 8 × 95%.** (a) Fluorescence counts at 488 nm as a function of radius (cm) from the axis of rotation plotted. The raw data are presented as open circles and are overlaid with the nonlinear least squares best-fit to a continuous-size distribution model (Lamm equation) by SEDFIT. Residuals for the nonlinear least squares best-fit are also shown. (b) The continuous sedimentation coefficient [*c(s)*] distribution as a function of sedimentation coefficient (Svedberg, S). The fit had a resolution of 100 species between s_{min} of 0.1 S and s_{max} of 15 S with P = 0.95, v-bar = 0.7413, ρ = 1.00117 g/ml, η = 0.010066 p, and f/f_0 = 1.43. The r.m.s.d. and runs test-Z score for the fit were 25 and 26.0, respectively.

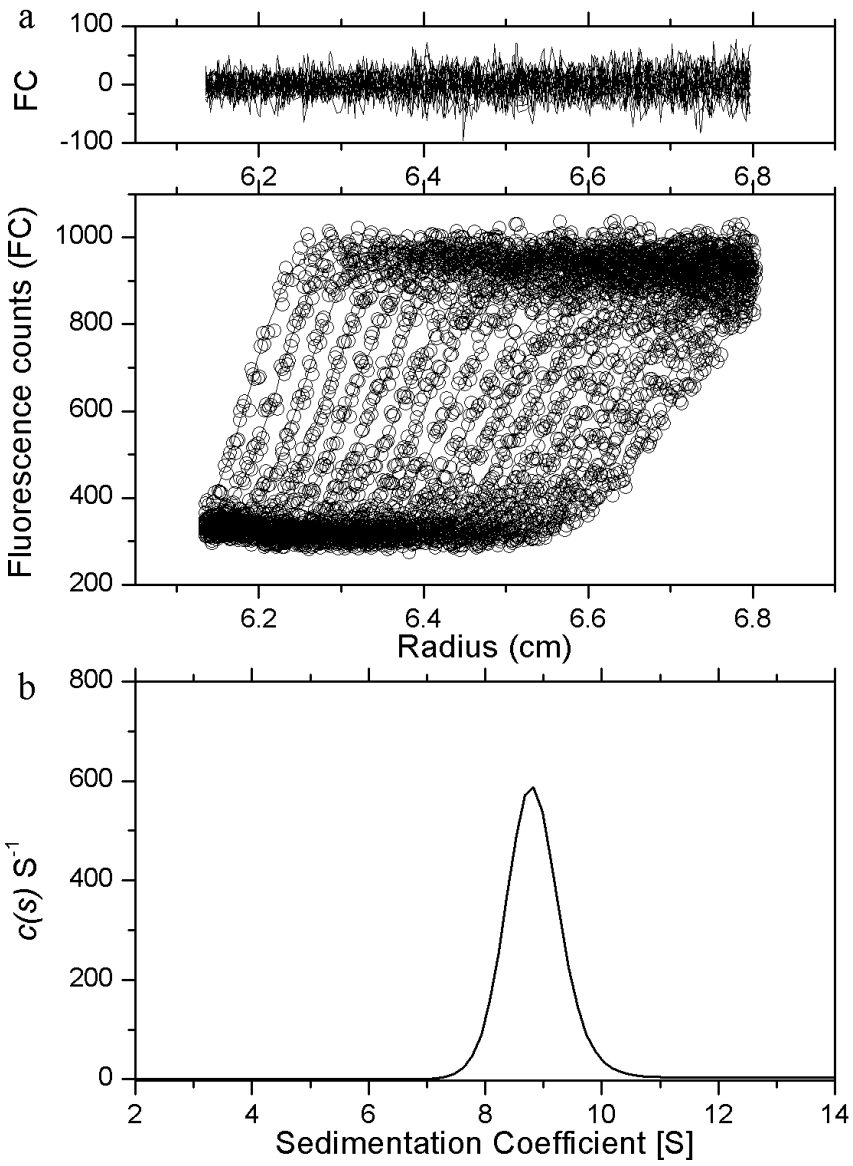

Figure 4.12 **AUC-FDS analysis of PK1-A301T at 0.001 mg/ml (19.7 nM) with 1.8 mM PEP added, with gains set at 1 × 63%.** (a) Fluorescence counts at 488 nm as a function of radius (cm) from the axis of rotation plotted. The raw data are presented as open circles and are overlaid with the nonlinear least squares best-fit to a continuous-size distribution model (Lamm equation) by SEDFIT. Residuals for the nonlinear least squares best-fit are also shown. (b) The continuous sedimentation coefficient [*c(s)*] distribution as a function of sedimentation coefficient (Svedberg, S). The fit had a resolution of 100 species between s_{min} of 0.1 S and s_{max} of 15 S with P = 0.95, v-bar = 0.7413, ρ = 1.00117 g/ml, η = 0.010066 p, and f/f_0 = 1.46. The r.m.s.d. and runs test-Z score for the fit were 20 and 25.5, respectively.

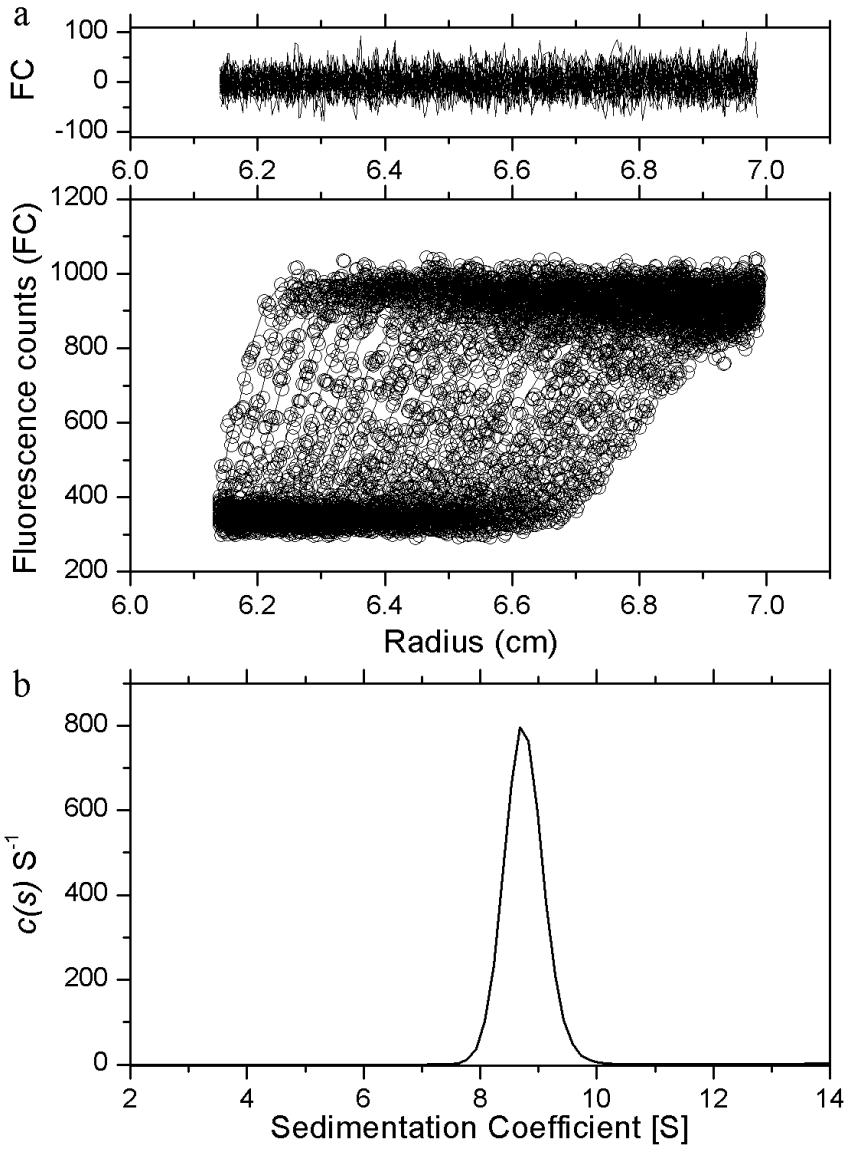

Figure 4.13 **AUC-FDS analysis of PK1-A301T at 0.001 mg/ml (19.7 nM) with 1.8 mM ADP added, with gains set at 8 × 95%.** (a) Fluorescence counts at 488 nm as a function of radius (cm) from the axis of rotation plotted. The raw data are presented as open circles and are overlaid with the nonlinear least squares best-fit to a continuous-size distribution model (Lamm equation) by SEDFIT. Residuals for the nonlinear least squares best-fit are also shown. (b) The continuous sedimentation coefficient [*c(s)*] distribution as a function of sedimentation coefficient (Svedberg, S). The fit had a resolution of 100 species between s_{min} of 0.1 S and s_{max} of 15 S with P = 0.95, v-bar = 0.7413, ρ = 1.00117 g/ml, η = 0.010066 p, and f/f_0 = 1.40. The r.m.s.d. and runs test-Z score for the fit were 23 and 26.8, respectively.

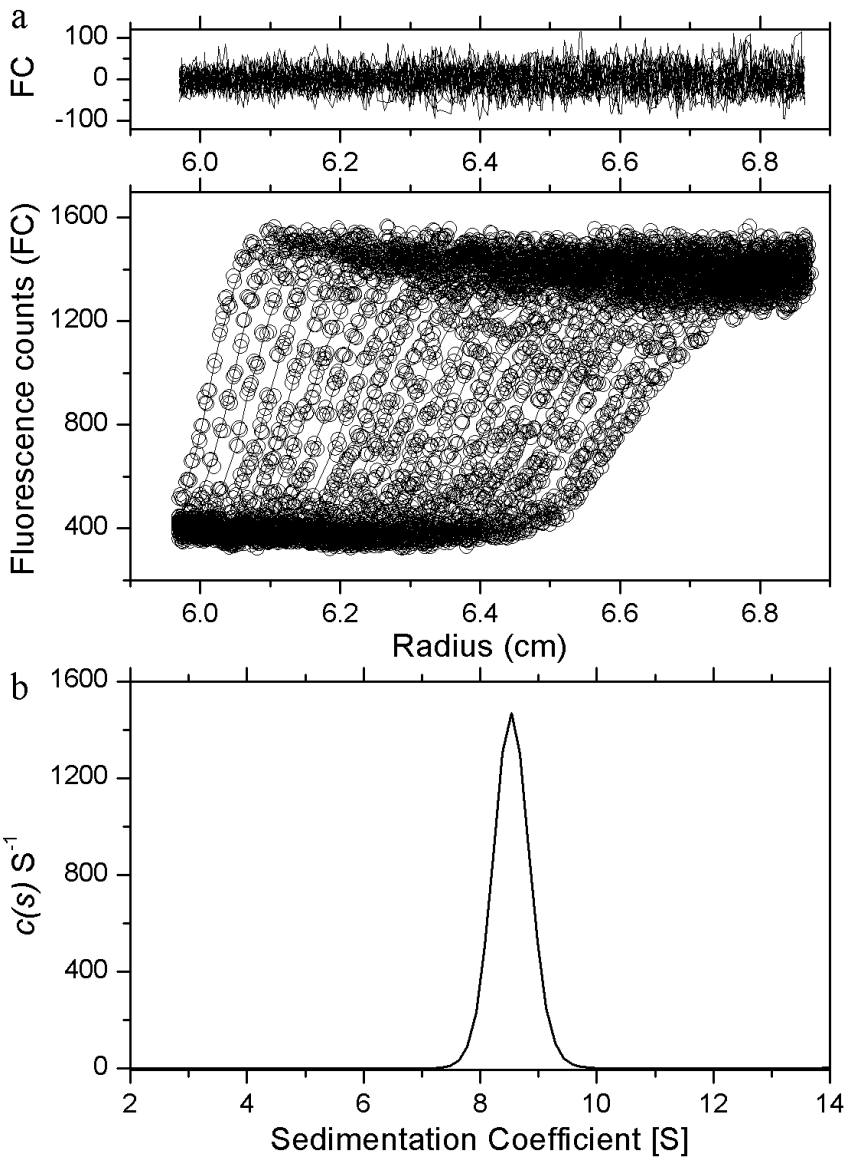

Figure 4.14 **AUC-FDS analysis of PK1-A301T at 0.001 mg/ml (19.7 nM) with 1.8 mM FBP added, with gains set at 8 × 95%.** (a) Fluorescence counts at 488 nm as a function of radius (cm) from the axis of rotation plotted. The raw data are presented as open circles and are overlaid with the nonlinear least squares best-fit to a continuous-size distribution model (Lamm equation) by SEDFIT. Residuals for the nonlinear least squares best-fit are also shown. (b) The continuous sedimentation coefficient [*c(s)*] distribution as a function of sedimentation coefficient (Svedberg, S). The fit had a resolution of 100 species between s_{min} of 0.1 S and s_{max} of 15 S with P = 0.95, v-bar = 0.7413, ρ = 1.00117 g/ml, η = 0.010066 p, and f/f_0 = 1.43. The r.m.s.d. and runs test-Z score for the fit were 27 and 31.0, respectively.

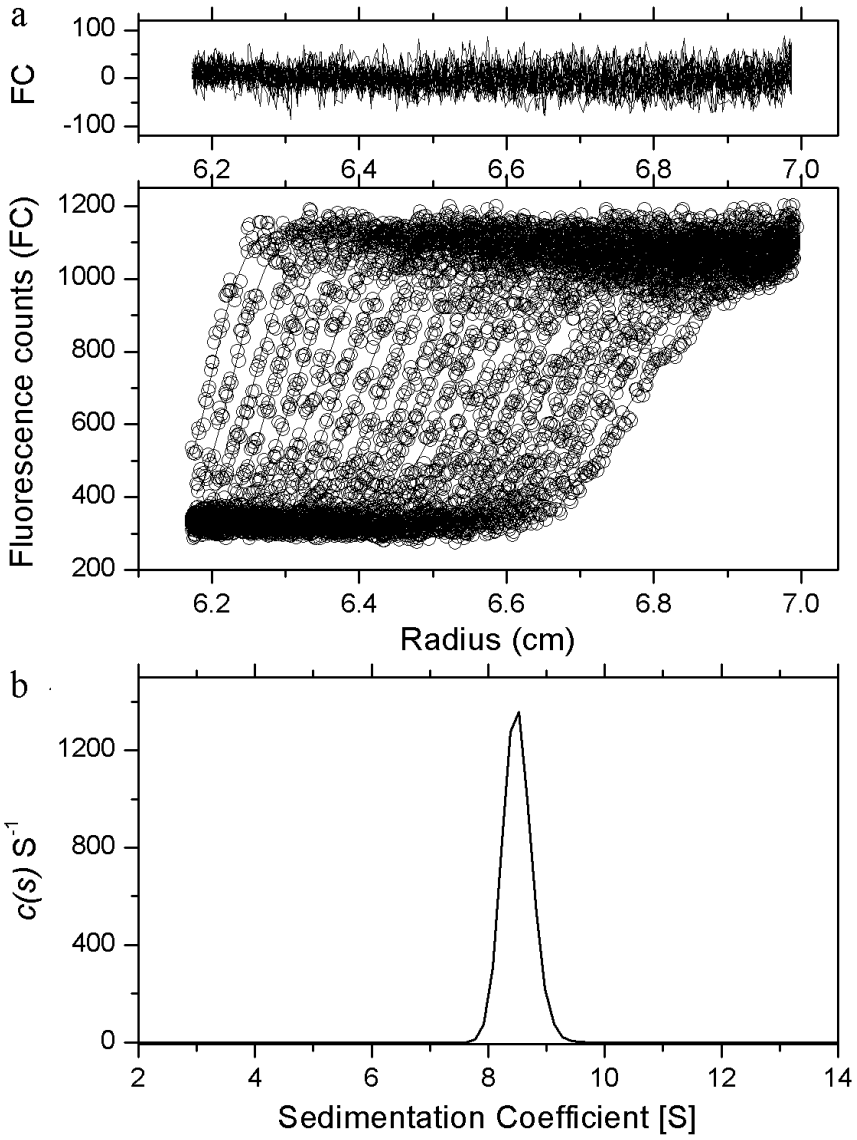

Figure 4.15 **AUC-FDS analysis of PK1-A301T at 0.0005 mg/ml (9.9 nM) with 0.1 mg/ml ovalbumin added, with gains set at 2 × 84%** (a) Fluorescence counts at 488 nm as a function of radius (cm) from the axis of rotation plotted. The raw data are presented as open circles and are overlaid with the nonlinear least squares best-fit to a continuous-size distribution model (Lamm equation) by SEDFIT. Residuals for the nonlinear least squares best-fit are also shown. (b) The continuous sedimentation coefficient [*c(s)*] distribution as a function of sedimentation coefficient (Svedberg, S). The fit had a resolution of 100 species between s_{min} of 0.1 S and s_{max} of 15 S with P = 0.95, v-bar = 0.7413, ρ = 1.00117 g/ml, η = 0.010066 p, and f/f_0 = 1.40. The r.m.s.d. and runs test-Z score for the fit were 23 and 28.4, respectively.

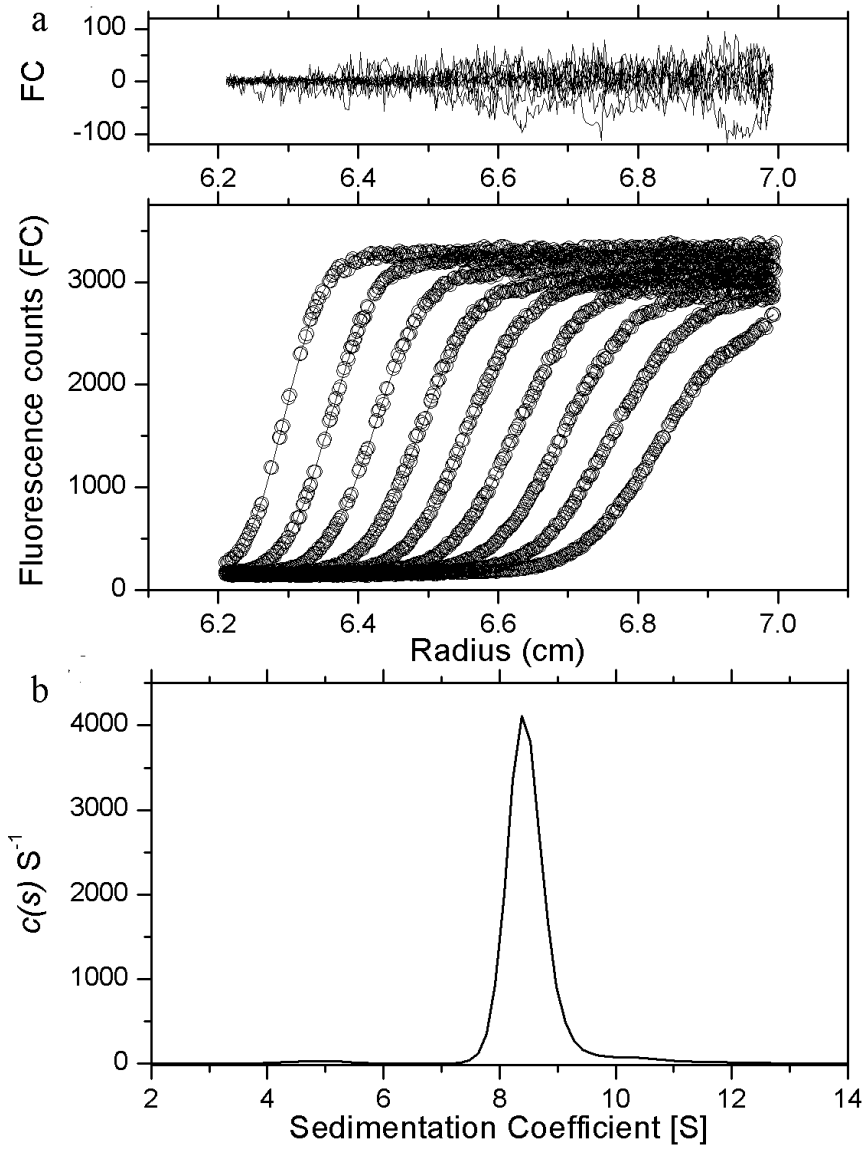

Figure 4.16 **AUC-FDS analysis of PK1-A301S at 0.01 mg/ml (197 nM), with gains set at 2 × 84%.** (a) Fluorescence counts at 488 nm as a function of radius (cm) from the axis of rotation plotted. The raw data are presented as open circles and are overlaid with the nonlinear least squares best-fit to a continuous-size distribution model (Lamm equation) by SEDFIT. Residuals for the nonlinear least squares best-fit are also shown. (b) The continuous sedimentation coefficient [*c(s)*] distribution as a function of sedimentation coefficient (Svedberg, S). The fit had a resolution of 100 species between s_{min} of 0.1 S and s_{max} of 15 S with P = 0.95, v-bar = 0.7413, ρ = 1.00117 g/ml, η = 0.010066 p, and f/f_0 = 1.46. The r.m.s.d. and runs test-Z score for the fit were 21 and 20.4, respectively.

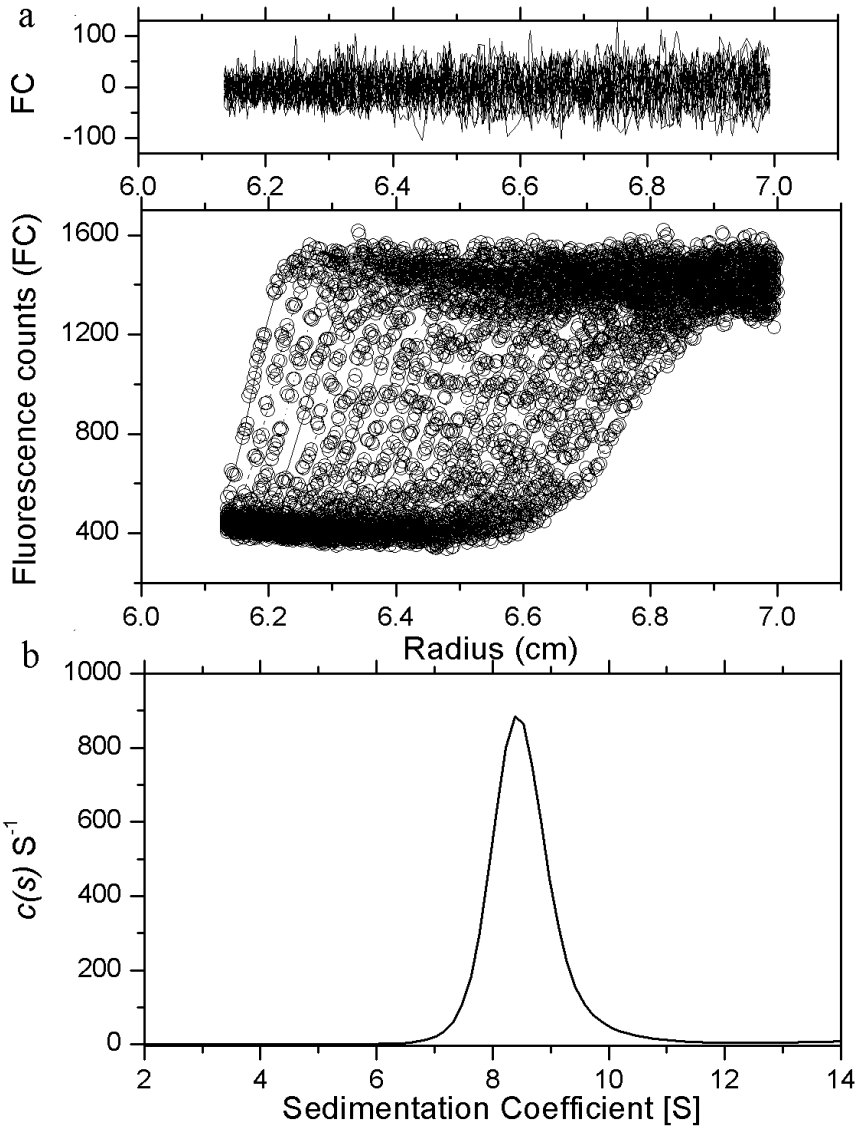

Figure 4.17 **AUC-FDS analysis of PK1-A301S at 0.001 mg/ml (19.7 nM), with gains set at 8 × 95%.** (a) Fluorescence counts at 488 nm as a function of radius (cm) from the axis of rotation plotted. The raw data are presented as open circles and are overlaid with the nonlinear least squares best-fit to a continuous-size distribution model (Lamm equation) by SEDFIT. Residuals for the nonlinear least squares best-fit are also shown. (b) The continuous sedimentation coefficient [*c(s)*] distribution as a function of sedimentation coefficient (Svedberg, S). The fit had a resolution of 100 species between s_{min} of 0.1 S and s_{max} of 15 S with P = 0.95, v-bar = 0.7413, ρ = 1.00117 g/ml, η = 0.010066 p, and f/f_0 = 1.47. The r.m.s.d. and runs test-Z score for the fit were 30 and 33.0, respectively.

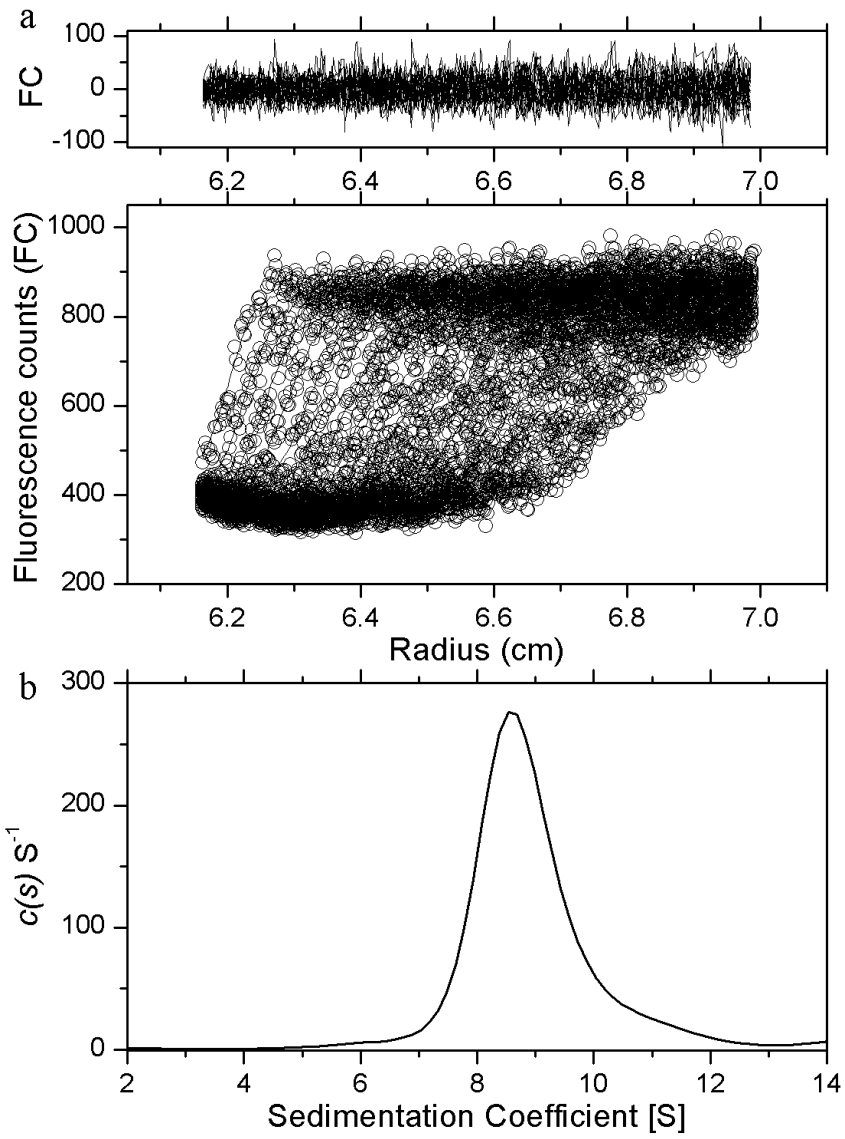

Figure 4.18 **AUC-FDS analysis of PK1-A301S at 0.001 mg/ml (19.7 nM) with 1.8 mM PEP added, with gains set at 2 × 84%.** (a) Fluorescence counts at 488 nm as a function of radius (cm) from the axis of rotation plotted. The raw data are presented as open circles and are overlaid with the nonlinear least squares best-fit to a continuous-size distribution model (Lamm equation) by SEDFIT. Residuals for the nonlinear least squares best-fit are also shown. (b) The continuous sedimentation coefficient [*c(s)*] distribution as a function of sedimentation coefficient (Svedberg, S). The fit had a resolution of 100 species between s_{min} of 0.1 S and s_{max} of 15 S with P = 0.95, v-bar = 0.7413, ρ = 1.00117 g/ml, η = 0.010066 p, and f/f_0 = 1.73. The r.m.s.d. and runs test-Z score for the fit were 24 and 27.9, respectively.

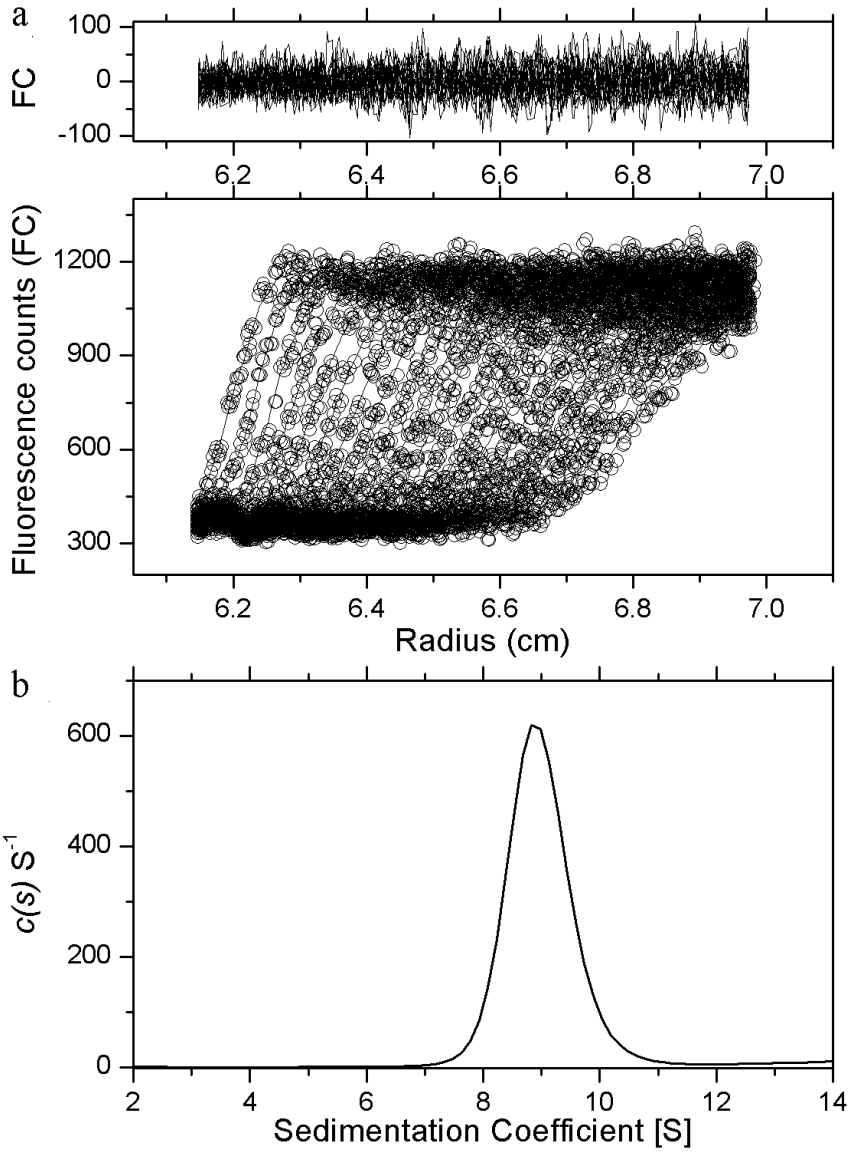

Figure 4.19 **AUC-FDS analysis of PK1-A301S at 0.001 mg/ml (19.7 nM) with 1.8 mM ADP added, with gains set at 1 × 63%.** (a) Fluorescence counts at 488 nm as a function of radius (cm) from the axis of rotation plotted. The raw data are presented as open circles and are overlaid with the nonlinear least squares best-fit to a continuous-size distribution model (Lamm equation) by SEDFIT. Residuals for the nonlinear least squares best-fit are also shown. (b) The continuous sedimentation coefficient [*c(s)*] distribution as a function of sedimentation coefficient (Svedberg, S). The fit had a resolution of 100 species between s_{min} of 0.1 S and s_{max} of 15 S with P = 0.95, v-bar = 0.7413, ρ = 1.00117 g/ml, η = 0.010066 p, and f/f_0 = 1.52. The r.m.s.d. and runs test-Z score for the fit were 26 and 28.3, respectively.

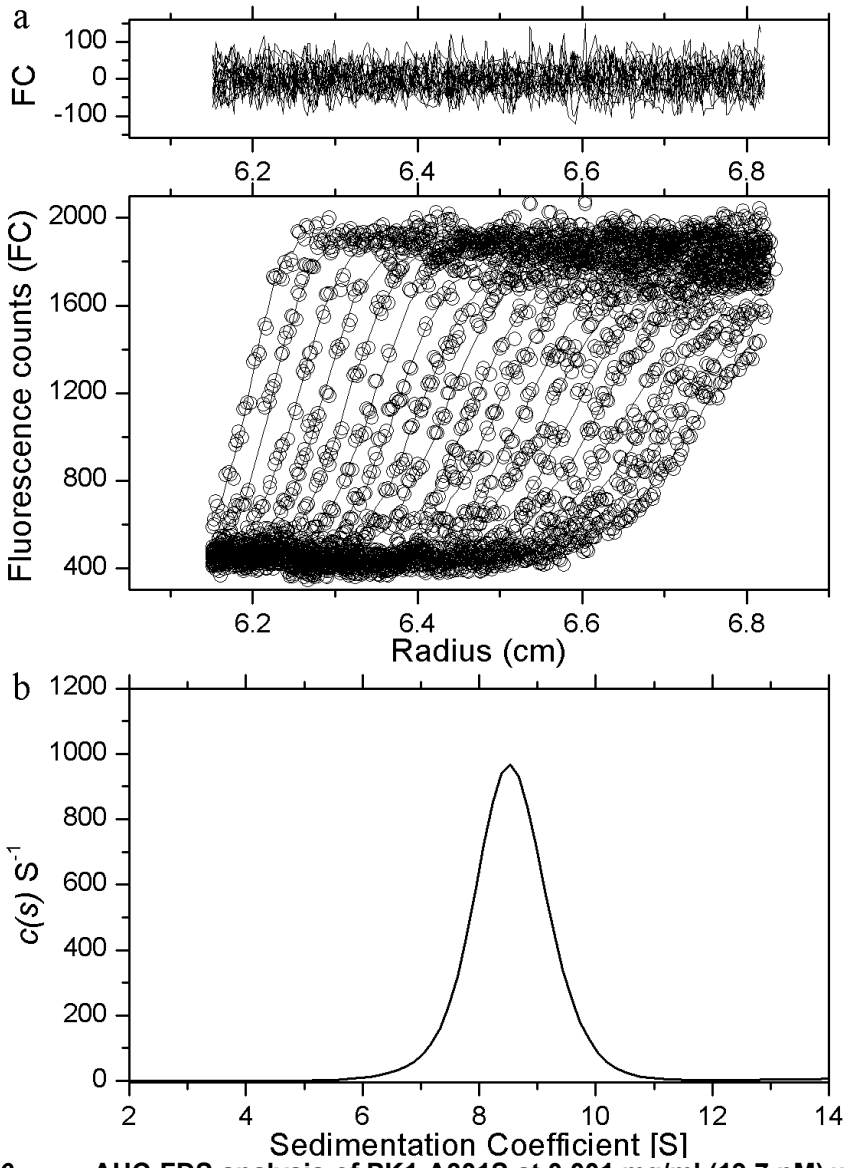

Figure 4.20 **AUC-FDS analysis of PK1-A301S at 0.001 mg/ml (19.7 nM) with 1.8 mM FBP added, with gains set at 8 × 95%.** (a) Fluorescence counts at 488 nm as a function of radius (cm) from the axis of rotation plotted. The raw data are presented as open circles and are overlaid with the nonlinear least squares best-fit to a continuous-size distribution model (Lamm equation) by SEDFIT. Residuals for the nonlinear least squares best-fit are also shown. (b) The continuous sedimentation coefficient [*c(s)*] distribution as a function of sedimentation coefficient (Svedberg, S). The fit had a resolution of 100 species between s_{min} of 0.1 S and s_{max} of 15 S with P = 0.95, v-bar = 0.7413, ρ = 1.00117 g/ml, η = 0.010066 p, and f/f_0 = 1.45. The r.m.s.d. and runs test-Z score for the fit were 37 and 36.8, respectively.

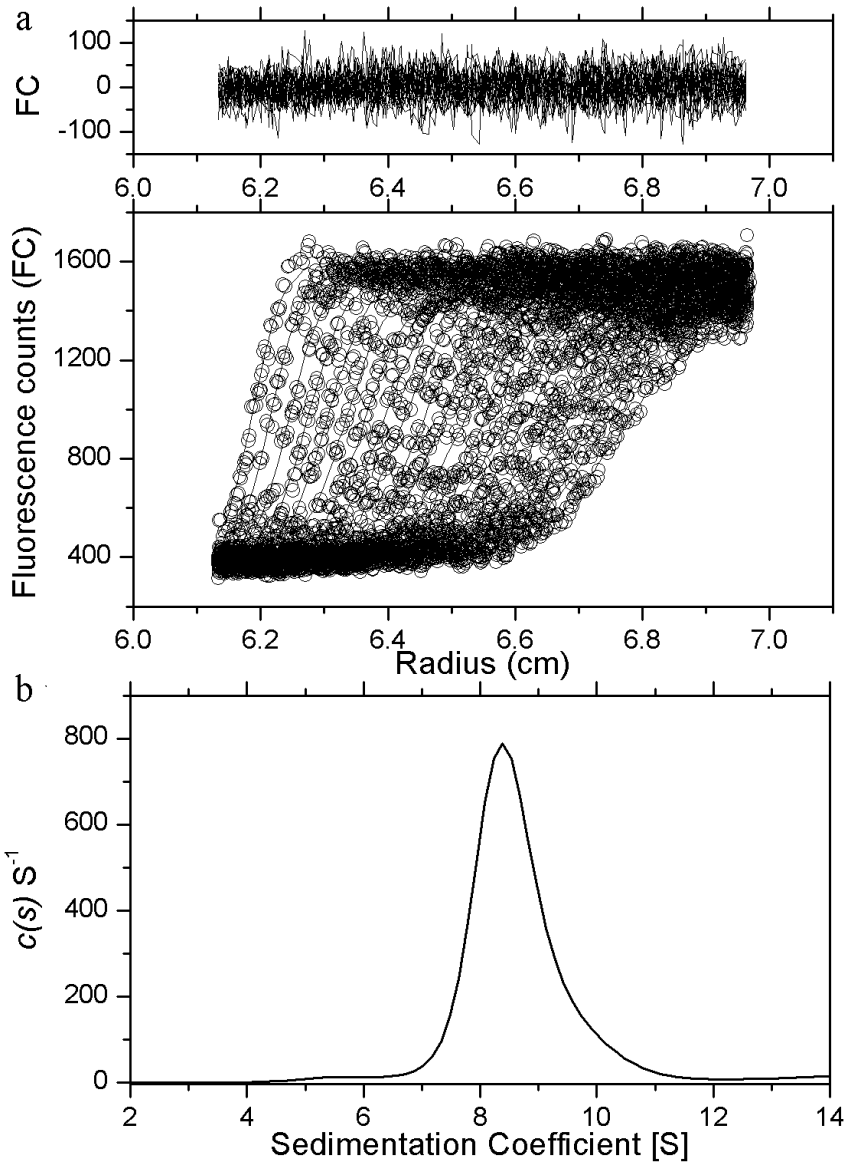

Figure 4.21 **AUC-FDS analysis of PK1-A301S at 0.0005 mg/ml (9.9 nM) with 0.1 mg/ml ovalbumin added, with gains set at 2 × 84%.** (a) Fluorescence counts at 488 nm as a function of radius (cm) from the axis of rotation plotted. The raw data are presented as open circles and are overlaid with the nonlinear least squares best-fit to a continuous-size distribution model (Lamm equation) by SEDFIT. Residuals for the nonlinear least squares best-fit are also shown. (b) The continuous sedimentation coefficient [*c(s)*] distribution as a function of sedimentation coefficient (Svedberg, S). The fit had a resolution of 100 species between s_{min} of 0.1 S and s_{max} of 15 S with P = 0.95, v-bar = 0.7413, ρ = 1.00117 g/ml, η = 0.010066 p, and f/f_0 = 1.48. The r.m.s.d. and runs test-Z score for the fit were 31 and 24.9, respectively.

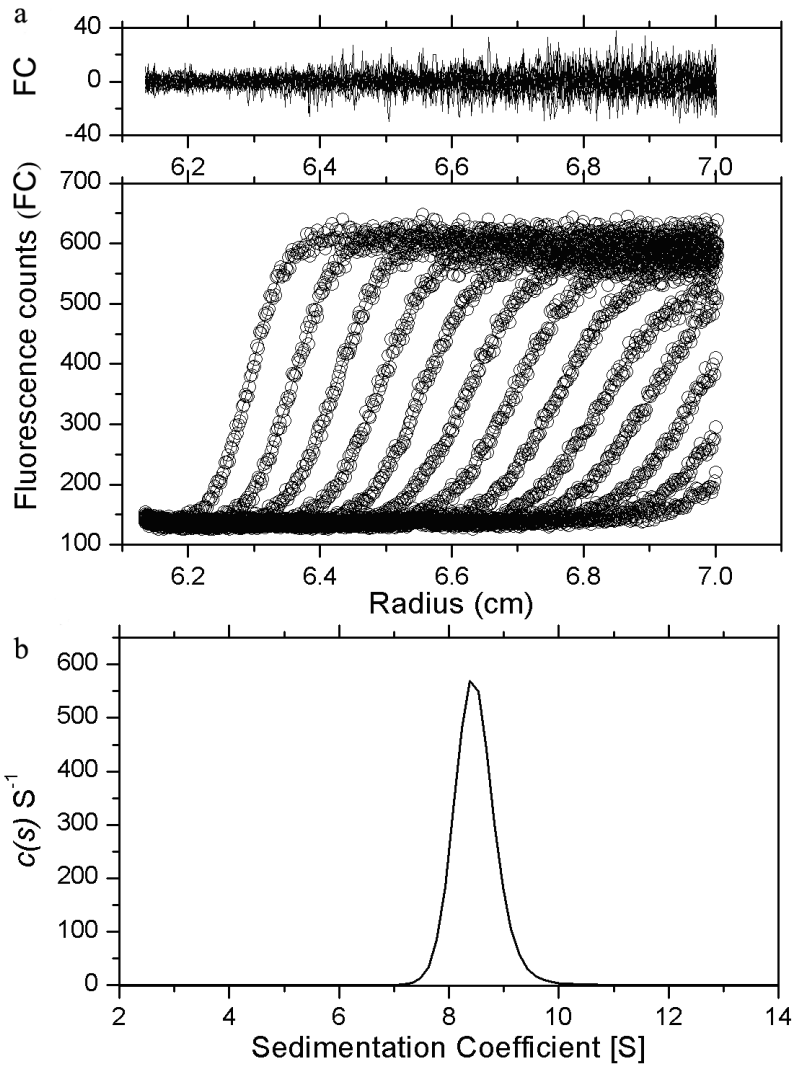

Figure 4.22 **AUC-FDS analysis of PK1-G381A at 0.01 mg/ml (197 nM), with gains set at 2 × 84%.** (a) Fluorescence counts at 488 nm as a function of radius (cm) from the axis of rotation plotted. The raw data are presented as open circles and are overlaid with the nonlinear least squares best-fit to a continuous-size distribution model (Lamm equation) by SEDFIT. Residuals for the nonlinear least squares best-fit are also shown. (b) The continuous sedimentation coefficient [*c(s)*] distribution as a function of sedimentation coefficient (Svedberg, S). The fit had a resolution of 100 species between s_{min} of 0.1 S and s_{max} of 15 S with P = 0.95, v-bar = 0.7413, ρ = 1.00117 g/ml, η = 0.010066 p, and f/f_0 = 1.43. The r.m.s.d. and runs test-Z score for the fit were 18 and 25.6, respectively.

The DOL for PK1-A301T and PK1-A301S was 17.1% and 28.9%, respectively (Table 4.3). It was sufficient to perform AUC-FDS, even at a very low concentration (0.0005 mg/ml or 9.9 nM), and high fluorescent signals were observed (Figures 4.15 & 4.21). The recommended protein concentration for amine labelling was above 2 mg/ml; however, the

concentration of the PK1-G381A protein before labelling was much lower than the recommended level. This affected the yield of labelling, with a low DOL of 0.06 achieved for the PK1-G381A sample, which led to a low yield of FDS signal.

At 0.01 and 0.001 mg/ml (197 nM and 19.7 nM), both PK1-A301T and PK1-A301S had a single maximum of sedimentation coefficient around 8.5 S, which indicated the single protein species of the tetrameric form (Figures 4.10 & 4.11; Figures 4.16 & 4.17). PK1-G381A had a similar sedimentation coefficient maximum at around 8.5 S at 0.01 mg/ml (197 nM) (Figure 4.22); however, the signal was not reliable for 0.001 mg/ml (19.7 nM) or lower concentrations for AUC-FDS detection due to the low DOL.

At a much lower concentration, 0.0005 mg/ml (9.9 nM), a single maximum at 8.5 S were observed for PK1-A301T and PK1-A301S with a spread of the peak, which might indicate the merge between the symmetric tetramer and a highly asymmetric species in solution (Cole *et al.* 2008). To prevent the loss of sample material to the cell surfaces, 0.1 mg/ml ovalbumin was added to the solution as the carrier protein at 0.0005 mg/ml (9.9 nM) sedimentation velocity runs (Cole *et al.* 2008; MacGregor *et al.* 2004) (Figures 4.15 & 4.21).

PEP, ADP and FBP were added to the buffer with 0.001 mg/ml (19.7 nM) protein concentration for both PK1-A301T and PK1-A301S, to test the effects of the substrate and allosteric effector binding to the quaternary structure of the protein (Figures 4.12-4.15; Figures 4.18-4.20). When 1.8 mM PEP was added into the PK1-A301S protein, a high f/f_0 ratio of 1.73 was again observed. This is comparable to the wild-type enzyme centrifuged with FDS at the same condition (f/f_0 = 1.71, Figure 2.14), and is higher than the f/f_0 ratio obtained by normal AUC at 0.1 mg/ml (1.97 μM) or higher. The increment in the f/f_0 ratio at 19.7 nM for the wild-type enzyme and PK1-A301S may indicate that the quaternary structures of these enzymes have changed, as compared to the structure at a higher concentration, or that an asymmetric species is present in the solution (Figure 4.18). However, no smaller peaks were observed on the *c(s)* distribution besides the mean peak with maximal s around 8.5 S. This indicates that the mutant enzymes were all tetrameric under the conditions. As the concentration of the proteins lowered, signal-to-noise ratio decrease dramatically, the result became unreliable (Cole *et al.* 2008), therefore, analysis at

lower concentrations was not performed.

These results, combined with circular dichroism, suggest that the mutated enzymes have the same quaternary structure as the wild-type enzyme and that the impact of the ligands (PEP, ADP and FBP) on the quaternary structure of the PK1 wild-type and the mutant enzymes was minimal. A structural characterisation of the PK1 mutants may provide more information.

4.6 Attempted X-ray crystallography

Protein crystallisation was performed using both handing-drop method for the wild-type enzyme (Mattevi *et al.* 1995) and robotic crystallisation screening for the mutants (Newman *et al.* 2005) (Section 6.6). Three mutants formed crystals, each in different conditions to the wild-type enzyme and to each other. Crystallisation trials were performed using the pH-, anion- and cation-testing (PACT) screen and the diffraction experiments were conducted at the Australian Synchrotron, beamline 3BM1, to no better than 3.5 Å.

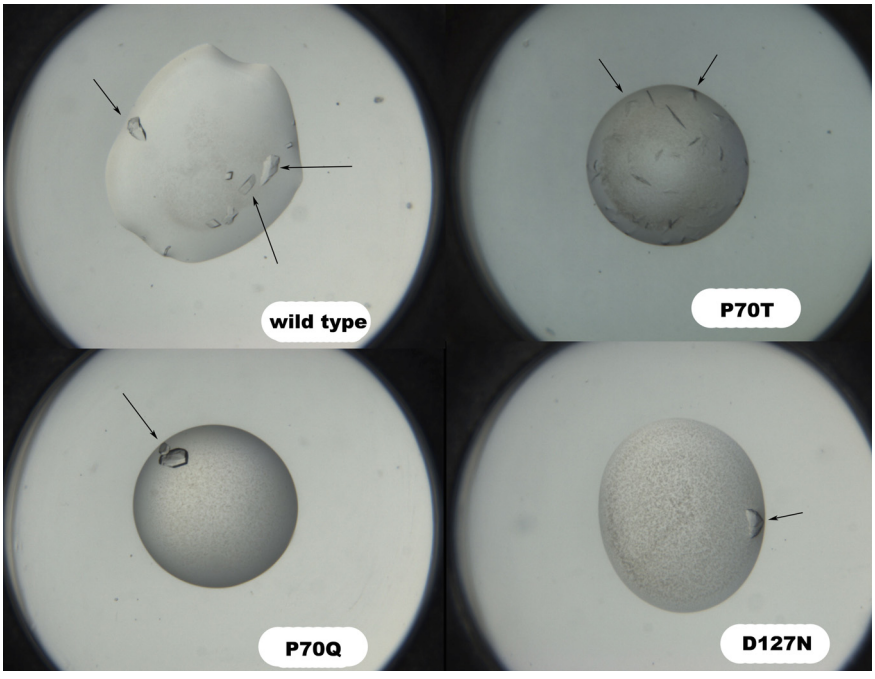

Figure 5.1 **Crystals obtained at the Bio21 Collaborative Crystallisation Centre.** The crystals were grown from the PACT screen and diffracted to < 3.5 Å at beamline 3BM1 at the Australian synchrotron.

4.7 Summary

In this chapter, the structural properties of the mutated enzymes were tested, and compared to those of the wild-type enzyme (discussed in Chapter 2). In addition, the effect of the substrates (PEP and ADP) and the allosteric effector FBP to subunit assembly and disassembly of PK at very low concentrations were investigated.

The mutated PK1 enzymes were examined by circular dichroism, which revealed some changes in the secondary structure, whereby different α-helix and β-sheet contents among themselves and compared to the wild-type enzyme were found. The increased α-helix content of PK1-G381A may be consistent with the mutation allowing an extension to an α-helix in the FBP binding domain, perhaps explaining the altered affect of FBP on this mutant enzyme (Chapter 3). In addition, PK1-I264F showed decreased α-helix content, suggesting that this mutation had affected the structure of Aα6.

The molecular masses of the mutated PK1 enzymes were confirmed by electrospray mass spectrometry. Results indicated that a molecule, probably β-mercaptoethanol with or without K^+ salt, which was used as a reducing agent during protein purification, was attached to the enzyme.

AUC experiments showed that all mutated enzymes had similar friction ratios around 1.34, and a sedimentation coefficient about 8.5 S, which indicated a tight tetrameric form in very dilute solution (nanomolar range). To further investigate the dissociation thresholds of the enzymes, AUC coupled with FDS was performed on three selected mutated enzymes. This was the first time that this novel technology has been performed on pyruvate kinase. In this experiment, although an increase in the friction ratio has been observed in some experiments, no clear sign of dissociation was evident, even at low concentrations (low nanomolar range). These results indicated the tight association of the tetramer of the mutated enzymes and the overall similarity with the wild-type, and the dissociation constant (K_D) of the wild-type and mutant enzyme are at picomolar range, below the concentrations tested.

Protein crystals of the wild-type enzyme and some of the mutants were obtained. The

wild-type enzyme crystallised using conditions described by Mattevi and colleagues (1995). The mutants crystallised at conditions different to the wild-type. Unfortunately, these crystals did not diffract to better than 3.5 Å resolution.

The changed kinetics of the mutated enzymes is not due to altered quaternary structure, but may be the consequences of the secondary structure change or some subtle changes affecting substrate/effector binding or the allosteric signal transition. This awaits further investigation by protein crystallography.

4.8 References

Cole JL, Lary JW, Moody PT, Laue TM. 2008. Analytical ultracentrifugation: sedimentation velocity and sedimentation equilibrium. *Methods Cell Biol* 84:143-79

Compton LA, Johnson WC, Jr. 1986. Analysis of protein circular dichroism spectra for secondary structure using a simple matrix multiplication. *Anal Biochem* 155:155-67

Cooper TF, Rozen DE, Lenski RE. 2003. Parallel changes in gene expression after 20,000 generations of evolution in *Escherichia coli*. *Proc Natl Acad Sci U S A* 100:1072-7

Lenski RE. 1991. Quantifying fitness and gene stability in microorganisms. *Biotechnology* 15:173-92

MacGregor IK, Anderson AL, Laue TM. 2004. Fluorescence detection for the XLI analytical ultracentrifuge. *Biophys Chem* 108:165-85

Mattevi A, Bolognesi M, Valentini G. 1996. The allosteric regulation of pyruvate kinase. *FEBS Lett* 389:15-9

Mattevi A, Valentini G, Rizzi M, Speranza ML, Bolognesi M, Coda A. 1995. Crystal structure of *Escherichia coli* pyruvate kinase type I: molecular basis of the allosteric transition. *Structure* 3:729-41

Newman J, Egan D, Walter TS, Meged R, Berry I, Ben Jelloul, M, Sussman, JL, Stuart, DI, Perrakis, A. 2005. Towards rationalization of crystallization screening for small- to medium-sized academic laboratories: the PACT/JCSG+ strategy. *Acta Crystallogr D Biol Crystallogr* 61:1426-31

Schmidt B, Rappold W, Rosenbaum V, Fischer R, Riesner D. 1990. A fluorescence detection system for the analytical ultracentrifuge and its application to proteins, nucleic acids and viruses. *Colloid Polym Sci* 268:45-54

Sreerama N, Venyaminov SY, Woody RW. 1999. Estimation of the number of alpha-helical and beta-strand segments in proteins using circular dichroism spectroscopy. *Protein Sci* 8:370-80

van Stokkum IH, Spoelder HJ, Bloemendal M, van Grondelle R, Groen FC. 1990. Estimation of protein secondary structure and error analysis from circular dichroism spectra. *Anal Biochem* 191:110-8

Whitmore L, Wallace BA. 2004. DICHROWEB, an online server for protein secondary structure analyses from circular dichroism spectroscopic data. *Nucleic Acids Res* 32:W668-73

Chapter 5

Summary and Conclusions

This chapter summarises the research findings of this thesis, which builds on a previous study that found mutations in PK1 in the evolved *E. coli* populations (Woods *et al.* 2006). This is the first study to examine these mutations at a biochemical level, in an effort to relate the molecular changes to the phenotype that emerged during adaptive evolution. Given pyruvate kinase has a crucial role in carbohydrate metabolism, it was of interest to explore how mutations in this enzyme may account for the improved fitness observed in the descendent populations compared to the ancestor. The findings firstly address the degree of parallel adaptation at a molecular level for the first time (previously observed at the cell physiology, gene expression and genetic levels among the evolved populations) and secondly contribute to the understanding of the allosteric regulation of pyruvate kinase.

In this study, seven mutated PK1 enzymes were obtained by site-directed mutagenesis. Steady-state kinetic experiments were performed to examine the function of the mutated enzymes. This was followed by structural studies involving circular dichroism to study the secondary structure and AUC (including AUC-FDS) to study the quaternary structure of the enzymes as well as the effects of PEP, ADP and FBP on subunit association. Crystallisation trials were also performed in an attempt to explain the structural basis of the mutation effect on enzyme function.

5.1 Insights into the enzymology of PK1

5.1.1 Catalysis

The mutated PK1 enzymes exhibited quite different catalytic competencies (k_{cat}) and altered affinity to the substrates ($S_{0.5}$). The patterns of change for each enzyme were distinct, making interpretation of the data complex. The mutated enzymes all adopted a similar quaternary structure to the wild-type, with a very tight association between subunits ($K_D < 1 \times 10^{-8}$ M). However, some mutant enzymes showed differences in the secondary structure, as judged by circular dichroism.

Mutations at residue P70 resulted in enzymes with lower turnover numbers compared to the wild-type enzyme. While a similar cooperative binding pattern to PEP between PK1-P70Q and the PK1 wild-type was observed, a hyperbolic pattern was shown for PK1-P70T. These results implied that P70 was a critical residue involved in interactions at the active site and PEP binding during catalysis. This is consistent with a previous observation that P70 serves as a "kink" at the loop connecting domains A and B, thus undergoing a large movement during catalysis.

Another mutation at the active site (D127N) resulted in an enzyme with less than 2% activity compared to the wild-type enzyme. That the affinity of the substrates did not change, suggests that D127 is essential in a catalytic step, likely *via* interactions with the solvent shell of Mg^{2+} (Larsen *et al.* 1998; Larsen *et al.* 1997).

Mutations found at the subunit interface also showed altered catalytic properties; however, the more striking results were their effect on the regulation patterns of PK1 (Section 5.1.2). The mutation G381A, at the FBP binding site, caused elevated enzymatic activity compared to the wild-type and a similar substrate affinity when FBP was present.

5.1.2 Regulation

PK is usually tightly regulated due to its core role in glycolysis. The regulation in *E. coli* is mainly achieved *via* the allosteric effector FBP. Although several mechanisms have been put forward regarding the mechanism of FBP allostery (Christofk *et al.* 2008; Friesen *et al.* 1998b; Mattevi *et al.* 1996; Mattevi *et al.* 1995; Rigden *et al.* 1999), a definite conclusion is elusive. This is mainly due to the lack of protein crystals from the same source in both the low affinity T-state and the high affinity R-state (Mattevi *et al.* 1995). Therefore, PK crystals at each state from different sources were compared to gain insight into the conformational changes during catalysis, and hence the allosteric regulation pattern (Jurica *et al.* 1998; Mattevi *et al.* 1996; Valentini *et al.* 2000).

For *E. coli* PK1, the "domain rotation" model has been proposed (Mattevi *et al.* 1996; Mattevi *et al.* 1995). This model depicts PK1 as a modular enzyme, undergoing conformational changes by a combination of domain rotations and movements among subunits within the tetramer, upon FBP binding, whereas the movements within domains are minimal (Mattevi *et al.* 1995). The key prediction of this model is that residues at the interfaces are involved in transfer of the allosteric signal from the allosteric binding site and the active site, which are over 40 Å apart (Jurica *et al.* 1998; Mattevi *et al.* 1996; Mattevi *et al.* 1995; Valentini *et al.* 2000). Another model, namely "the network mechanism", was proposed by Friesen *et al.* (1998b) and further supported by Fenton *et al.* (2002) in studying the yeast PK. This mechanism hypothesised the formation of salt bridges across the subunit interface to transfer the allosteric signal to the active site.

In this study, the wild-type *E. coli* PK1 showed typical allosteric regulation by FBP, with PEP affinity increasing in response to FBP binding ($S_{0.5}^{PEP}$ changed from 1.5 mM to 0.06 mM). The mutated enzymes showed a different response to FBP binding compared to the wild-type PK1. The most striking finding was that A301T was the only mutation that caused the PEP binding pattern of the enzyme to change from hyperbolic to a sigmoidal

pattern when FBP was present. Residue A301 belongs to helix Aα7 at A/A' subunit interface, next to helix Aα6, which was proposed be part of the allosteric signal transmitting pathway at the subunit interface (Friesen *et al.* 1998a; Friesen *et al.* 1998b). The kinetic data implied a crucial role of the residues at the A/A' interface in relaying the allosteric signal between the active centre and the allosteric binding site. Despite the similarity in the structure between PK1-A301T and the wild-type PK1 (as judged by CD and AUC), the mutation may have distorted the interfacial communication pathway between the active site and the allosteric regulation site, thus altering the allosteric regulation pattern. Another mutated enzyme (PK1-I264F) where the mutation was at the subunit interface (specifically α-helix Aα6) had an altered secondary structure (as judged by CD) with a lower α-helical content. The enzyme showed diminished FBP binding. Combining the above results, distortion of the interfacial structure and, therefore, transmission of the allosteric signal may be possible. However, more detailed structural information (such as from X-ray crystallography) is needed for further study of this mutation. Nevertheless, these results are in general agreement with the study carried out by Fenton and colleagues (2002).

5.2 Impact on glycolysis

Glycolysis is an essential energy producing pathway for bacterial survival. During this process, glucose is consumed to generate energy, in the form of ATP and NADH. Meanwhile, pyruvate is generated, which further feeds into various metabolic pathways. In the experimental environment defined in the evolutionary study (Lenski *et al.* 1991), bacteria grow in an environment with a limited amount of glucose for several hours, before the glucose is depleted. It is hypothesised that in the initial conditions, cells utilise glucose for cell growth and reproduction, which also feeds into the glycogen synthesis pathway, whereas at later stages, when glucose depletes, it is necessary for the cells to release the stored energy for a series of cellular functions.

Previously, it was found that the descendent populations showed improved fitness in a

competition assay with the ancestor by having a shorter lag-phase in the growth period (Cooper & Lenski 2000; Lenski *et al.* 1998). It has also been demonstrated in previous studies that glycogen synthesis and glycolysis are co-regulated, with several enzymes involved in regulation (Dietzler *et al.* 1979a; Dietzler *et al.* 1979b). Glycogen biosynthesis was found to be regulated by the cellular level of ADP-glucose in the bacteria (Kumar *et al.* 1989).

Although the mutated PK1 enzymes investigated in this study behaved differently to each other, and to the wild-type, in terms of substrates and allosteric regulator binding, the fact that all the mutants still functioned confirmed that the glycolysis pathway was not shut down in any of the twelve populations.

5.3 Is the evolution of *E. coli* parallel at an enzyme structure/function level?

The molecular basis of adaptation is a major focus in evolutionary biology (Wichman *et al.* 1999). This study was born from Lenski's evolutionary experiment (Woods *et al.* 2006), which is designed to study adaptation and evolutionary reproducibility. In previous studies it was found that parallel adaptation occurred at the phenotypic level (larger cells and improved fitness) (Cooper & Lenski 2000; Lenski *et al.* 1998; Lenski *et al.* 1991; Lenski & Travisano 1994) and at the genome level (gene expression) (Cooper *et al.* 2003; Elena & Lenski 2003). Woods *et al.* (2006), by showing mutations in *pykF* and *nadR* loci in all twelve populations, concluded that although there was extensive parallel adaptation at the genetic level (i.e. the same genes had mutations in each of the twelve populations) at a base pair level the mutations of the genes were only rarely parallel. However, this work did not exclude the possibility that different mutations on the gene (e.g. *pykF*) produced the same biochemical phenotype. The work in this thesis directly tested this by performing kinetic and biophysical analyses on the mutant enzymes and comparing them with the wild-type enzyme.

The mutated enzymes investigated in this study exhibited distinct kinetic behaviour and response to FBP regulation, compared to the wild-type enzyme and to each other. Therefore, it is concluded that no parallel adaptation at the level of PK1 function had occurred. However, the gene expression and protein analyses performed for this evolutionary experimental system to date cannot alone explain the overall changes in the cell. Further work involving structural studies and *in vivo* metabolic studies will help to investigate this system further.

5.4 Ongoing biological questions & future experiments

5.4.1 Structural studies of PK1 and mutants

Structural changes may have taken place in the mutated PK1, as suggested by the differences observed in CD (Section 4.2). These changes may be responsible for the altered kinetic properties and the regulation patterns observed in the kinetic experiments (Section 3.3). X-ray crystallography trials were attempted on the wild-type enzyme as well as the mutated enzymes. However, no diffraction patterns were found (3.5 Å). This work continues to look into the structural changes of the mutants.

5.4.2 The role of mutations in other genes

This study was not able to test whether altered function in PK1 has been coupled with other effects in the metabolic pathway, with the combined effect resulting in improved fitness to the glucose-limited environment over the ancestor. How do the mutations in other genes contribute to the improved fitness (e.g. *nadR*, which codes nadR, a negative protein regulates NAD biosynthesis pathway in *E. coli* (Raffaelli *et al.* 1999) and how are they related to one another? What changes do the mutations confer to the metabolic profile of the evolved bacteria? And what synergies are there between different enzymes in individual populations?

Perhaps one way to address this is to use metabolomics. Metabolomics is a comprehensive analysis in which all the metabolites of a biological system are identified and quantified (Fiehn *et al.* 2000). By studying the metabolic profiles of the evolved populations in combination with future research of PK1 and nadR and other altered genes in the various populations, a comprehensive view of the outcome of the parallel adaptation at the molecular level can be established.

5.5 References

Christofk HR, Vander Heiden MG, Wu N, Asara JM, Cantley LC. 2008. Pyruvate kinase M2 is a phosphotyrosine-binding protein. *Nature* 452:181-6

Cooper TF, Rozen DE, Lenski RE. 2003. Parallel changes in gene expression after 20,000 generations of evolution in *Escherichia coli*. *Proc Natl Acad Sci U S A* 100:1072-7

Cooper VS, Lenski RE. 2000. The population genetics of ecological specialization in evolving *Escherichia coli* populations. *Nature* 407:736-9

Dietzler DN, Leckie MP, Lais CJ, Henry DA, Rothert JH, Ferguson RM. 1979a. Periodic inventory review as a strategy for survival in *Escherichia coli*. The observation of precisely timed, rapid, and simultaneous shifts in glycogen synthesis and glucose utilization in the absence of an external stimulus during prolonged nitrogen starvation. *J Biol Chem* 254:8288-94

Dietzler DN, Leckie MP, Sternheim WL, Ungar JM, Crimmins DL, Lewis JW. 1979b. Regulation of glycogen synthesis and glucose utilization in *Escherichia coli* during maintenance of the energy charge. Quantitative correlation of changes in the rates of glycogen synthesis and glucose utilization with simultaneous changes in the cellular levels of both glucose 6-phosphate and fructose 1,6-diphosphate. *J Biol Chem* 254:8276-87

Elena SF, Lenski RE. 2003. Evolution experiments with microorganisms: the dynamics and genetic bases of adaptation. *Nat Rev Genet* 4:457-69

Fiehn O, Kopka J, Dormann P, Altmann T, Trethewey RN, Willmitzer L. 2000. Metabolite profiling for plant functional genomics. *Nat Biotechnol* 18:1157-61

Friesen RH, Castellani RJ, Lee JC, Braun W. 1998a. Allostery in rabbit pyruvate kinase: development of a strategy to elucidate the mechanism. *Biochemistry* 37:15266-76

Friesen RH, Chin AJ, Ledman DW, Lee JC. 1998b. Interfacial communications in recombinant rabbit kidney pyruvate kinase. *Biochemistry* 37:2949-60

Jurica MS, Mesecar A, Heath PJ, Shi W, Nowak T, Stoddard BL. 1998. The allosteric regulation of pyruvate kinase by fructose-1,6-bisphosphate. *Structure* 6:195-210

Kumar A, Ghosh P, Lee YM, Hill MA, Preiss J. 1989. Biosynthesis of bacterial glycogen. Determination of the amino acid changes that alter the regulatory properties of a mutant *Escherichia coli* ADP-glucose synthetase. *J Biol Chem* 264:10464-71

Larsen TM, Benning MM, Rayment I, Reed GH. 1998. Structure of the bis(Mg^{2+})-ATP-oxalate complex of the rabbit muscle pyruvate kinase at 2.1 A resolution: ATP binding over a barrel. *Biochemistry* 37:6247-55

Larsen TM, Benning MM, Wesenberg GE, Rayment I, Reed GH. 1997. Ligand-induced domain movement in pyruvate kinase: structure of the enzyme from rabbit muscle with Mg^{2+}, K^{+}, and L-phospholactate at 2.7 A resolution. *Arch Biochem Biophys* 345:199-206

Lenski RE, Mongold JA, Sniegowski PD, Travisano M, Vasi F, Gerrish PJ, Schmidt TM. 1998. Evolution of competitive fitness in experimental populations of *E. coli*: what makes one genotype a better competitor than another? *A. V. Leeuwenhoek international journal of general and molecular microbiology* 73:35-47

Lenski RE, Rose MR, Simpson SC, Tadler SC. 1991. Long-term experimental evolution in *Escherichia coli*. I. Adaptation and divergence during 2,000 generations. *Am Nat* 138:1315-41

Lenski RE, Travisano M. 1994. Dynamics of adaptation and diversification: a 10,000-generation experiment with bacterial populations. *Proc Natl Acad Sci U S A* 91:6808-14

Mattevi A, Bolognesi M, Valentini G. 1996. The allosteric regulation of pyruvate kinase. *FEBS Lett* 389:15-9

Mattevi A, Valentini G, Rizzi M, Speranza ML, Bolognesi M, Coda A. 1995. Crystal structure of *Escherichia coli* pyruvate kinase type I: molecular basis of the allosteric transition. *Structure* 3:729-41

Raffaelli N, Lorenzi T, Mariani PL, Emanuelli M, Amici A, Ruggieri S, Magni G. 1999. The *Escherichia coli* NadR regulator is endowed with nicotinamide mononucleotide adenylyltransferase activity. *J Bacteriol* 181:5509-11

Rigden DJ, Phillips SE, Michels PA, Fothergill-Gilmore LA. 1999. The structure of pyruvate kinase from *Leishmania mexicana* reveals details of the allosteric transition and unusual effector specificity. *J Mol Biol* 291:615-35

Valentini G, Chiarelli L, Fortin R, Speranza ML, Galizzi A, Mattevi A. 2000. The allosteric regulation of pyruvate kinase. *J Biol Chem* 275:18145-52

Wichman HA, Badgett MR, Scott LA, Boulianne CM, Bull JJ. 1999. Different trajectories of parallel evolution during viral adaptation. *Science* 285:422-4

Woods R, Schneider D, Winkworth CL, Riley MA, Lenski RE. 2006. Tests of parallel molecular evolution in a long-term experiment with *Escherichia coli*. *Proc Natl Acad Sci U S A* 103:9107-12

Chapter 6

Experimental

6.1 Materials

General chemicals were purchased from the Sigma-Aldrich Chemicals Company, unless otherwise stated. Bacterial culture media, SDS-PAGE gels and site-directed mutagenesis kit were purchased from Invitrogen. Bio-Rad protein assay kit was purchased from Bio-Rad Laboratories.

6.2 Microbiology and molecular biology methods

'Molecular Cloning: A laboratory Manual, 3rd edition' (Sambrook & Russell 2001) was used as a general reference for manipulating bacterial strains and DNA.

6.2.1 Bacterial Strains

Two bacterial strains were used in this study. *E. coli* XL-1 Blue strain (genotype: *recAl endA1 gyrA96 thi-1 hsdR17 supE44 relA1 lac* [F' *proAB lacl* ZΔM15]) was used for mutagenesis as part of the QuikChange site-directed mutagenesis kit from Stratagene. *E. coli* BL21 (DE3) strain (genotype: *E. coli* BF^- *dcm ompT hsdS* ($r_B^-m_B^-$) *gal* λ (DE3)) was used for protein expression and purification.

6.2.2 Plasmids

The pyruvate kinase type 1 gene (*pykF*) had been previously cloned into a pBluescript II KS+ vector. This plasmid (pGV5A) was kindly donated by Professor Mattevi (University of Pavia, Italy) (Mattevi *et al.* 1996). Point mutations were made using pGV5A as a template and the resulted plasmids with PK1 mutation are listed below:

Plasmids	Relevant genotype
pGV5A	::*pyk*F, Amp^r
pP70T	::*pyk*F-pro70thr, Amp^r
pP70Q	::*pyk*F-pro70gln, Amp^r
pD127N	::*pyk*F-asp127asn, Amp^r
pI264F	::*pyk*F-ile264phe, Amp^r
pA301T	::*pyk*F-ala301thr, Amp^r
pA301S	::*pyk*F-ala301ser, Amp^r
pG381A	::*pyk*F-gly381ala, Amp^r

6.2.3 Bacterial cultures

Media for bacterial cultures were sterilised by autoclaving at 121 °C for 15 minutes. Equipment for handling the bacterial culture was either autoclaved or purchased sterile. Solutions were prepared with sterilised distilled water (ddH_2O) or distilled water (dH_2O) filtrated by 0.22 μm syringe driven filter units (Millipore). Standard sterile techniques were used for each experiment and any possible contamination was monitored by controls.

6.2.4 Media

6.2.4.1 Luria-Bertani medium (LB)

LB base was purchased from Invitrogen in ready-to-use powder form. 2% w/v of LB medium was prepared by mixing 20 g LB powder with every litre of dH_2O and autoclaved.

6.2.4.2 SOB medium

SOB medium was prepared in ddH_2O with 2% w/v tryptone, 0.5% yeast extract, 10 mM NaCl with pH adjusted and autoclaved. 10 ml/l of filter-sterilised 1 M $MgCl_2$ and 10 ml/l of filter-sterilised 1 M $MgSO_4$ were added prior to use.

6.2.4.3 SOC medium

SOC medium was prepared immediately before use, by adding 2 ml of filter-sterilised 20% (w/v) glucose into 98 ml of SOB medium.

6.2.5 Antibiotics

Ampicillin was the main antibiotic marker in this study. A 1000 × concentrated stock solution was prepared by adding 100 mg/ml of ampicillin in dH_2O, followed by filtration using the 0.22 μm syringe driven filter units (Millipore). Ampicillin stocks were stored in 1.5 ml aliquots at -20 °C.

6.2.6 Agar plate preparation

6.2.6.1 LB agar plates

2% w/v LB powder and 1.6% w/v bacterial grade agar were dissolved in dH_2O and sterilised by autoclaving. Appropriate antibiotics were added into the molten media at about 50 °C and mixed by gentle swirling. 20 ml of media was then poured into each sterile Petri dish in a sterile laminar flow hood. The plates were cooled in the hood for 30 minutes before being covered with lids and sealed in plastic bags. The plates were stored in the fridge up to one week.

6.2.6.2 Agar plates for blue-white colour screening

For the blue-white colour screening, 8 μl of 100 mg/ml isopropyl-1-thio-β-D-galactopyranoside (IPTG) in ddH_2O and 40 μl of 20 mg/ml 5-bromo-4-chloro-3-inolyl-β-D-galactopyranoside (X-gal) in dimethylformamide (DMF) were spread onto a LB plate with ampicillin and dried 30 minutes prior to plating.

6.2.7 Inoculating bacterial culture

Bacteria from a glycerol freeze stock solution were streaked on LB plates with ampicillin using flame-sterilised nichrome wire and incubated at 37 °C overnight. Each colony was used to inoculate a 10 ml LB medium with antibiotics. This starter culture was then incubated in a 37 °C water bath with moderate shaking (175-200 rpm) for at least 4 hours (until cloudy). It was then used to inoculate 1 l of LB medium containing appropriate

antibiotics and incubated at 37 °C with shaking overnight.

6.2.8 Strain storage using glycerol freeze stocks

1.5 ml of overnight bacterial culture was centrifuged at 4,000 *g* for 2 minutes in Eppendorf tubes and most of the supernatant removed. The pellet was resuspended in fresh LB medium and transferred into a 1.5 ml screw-top cryo-storage tube. A 1:1 volume of 50% glycerol was added and mixed gently. The tubes were snap frozen in liquid nitrogen and stored at -80 °C freezer.

6.2.9 QuikChange Site-directed mutagenesis

Site-directed mutagenesis was carried out as described in the Stratagene QuikChange site-directed mutagenesis manual.

6.2.9.1 Primer Design

Site-directed mutagenesis introduces specific alterations (changed nucleotides) into the template DNA by incorporating mutated primers into the plasmid during the PCR reaction. Primers were designed based on the QuikChange site-directed mutagenesis manual (Stratagene).

Both primers contained the required mutation and annealed to opposite strands of the plasmid at the same point in the sequence. The primers were between 25 and 45 bases in length and had a melting temperature (T_m) > 78 °C. The equation for calculating the melting temperature was as follows:

$$T_m = 81.5 + 0.41\ (\%\ GC) - 675/N - \%\ mismatch$$

where % GC is the GC content, N is the number of base pairs and % mismatch is the unpaired base content, as compared to all the primer bases. The above equation is specifically used to calculate melting temperature in 1 M Na^+, as the melting temperature is highly affected by salt concentration. The substituted bases were placed in the middle

of the primer with 10 to15 bases at each end. Ideally, the % GC should be over 40% with one or more GC pair at each terminus of the primer for stronger hydrogen bonding. In addition, self-complementary for each primer should be avoided.

6.2.9.2 PCR Reaction

PCR reactions were performed with 20 ng and 50 ng template DNA per tube. The pWhitescript plasmid and the mutagenic primers were used as a control. pWhitescript has a point mutation at the *lacZ* gene (which codes for β-galactosidase) to generate a stop codon that is exchanged to a glutamine by the mutagenic primers and β-galactosidase activity is restored when the mutagenesis reaction is successful. Bacteria expressing β-galactosidase activity form blue colonies on IPTG/X-gal plate. In this way, the mutation efficiency can be determined by the ratio of blue/white colonies on an IPTG/X-gal plate.

In this study, site-directed mutagenesis was performed on pGV5A. Template DNA was quantified using a Nano-Drop spectrophotometer by measuring absorbance at 260 nm and 280 nm. PCR reactions were carried out in a DNA Engine PTC-200 Peltier thermal cycler (MJ research). All PCR reaction used thin-wall PCR tubes from Eppendorf.

Reagents for the PCR reaction mixture of *pyk*F-P70T site-directed mutagenesis are listed below:

	Initial conc.	**Volume** (μl)	**Amount** (ng)
Reaction buffer (10 ×)		5	
pGV5A plasmid (3.0 kb)	10 ng/μl	2 and 5	20 and 50
P70T #1 (forward)	100 ng/μl	1.25	125
P70T #2 (backward)	100 ng/μl	1.25	125
dNTP mix		1	
PCR water (ddH_2O)		8.5 and 35.5	
P*fu* Turbo DNA polymerase	2.5 units/μl	1	

Reagents for the reaction mixture of pWhitescript mutagenesis control are shown below:

	Initial conc.	**Volume** (µl)	**Amount** (ng)
Reaction buffer (10x)		5	
pWhitescript plasmid (4.5kb)	5 ng/µl	2	10
Oligonucleotide control primer #1	100 ng/µl	1.25	125
Oligonucleotide control primer #2	100 ng/µl	1.25	125
dNTP mix		1	
PCR water (ddH_2O)		38.5	
P*fu* Turbo DNA polymerase	2.5 units/µl	1	

PCR cycling condition is listed as follow:

Step	**Temperature** (°C)	**Time** (min)
1. Initiation	95	0.5
2. Denaturing	95	0.5
3. Annealing	55	1
4. Final annealing	68	12
5. Cycles	Steps 2-4 were repeated 15 times	

Agarose gel electrophoresis was performed to confirm the amplification of the DNA, with 10 µl of reaction product loaded into each well.

6.2.9.3 Enzymatic digestion of the old templates

After PCR amplification, 1 µl of *Dpn*I at 10 units/µl was added into each tube and mixed gently. The tubes were incubated at 37 °C for 1 hour to fully digest the template DNA. *Dpn*I specifically targets methylated and hemi-methylated parental template DNA and does not affect the new mutated cDNA.

6.2.9.4 Transformation of XL1-Blue sub-cloning grade competent cells

Transformation was performed by adding 1 µl of each mutated plasmid DNA into 50 µl of competent XL1-Blue cells. 100 pg of pUC18 plasmid was transformed into 50 µl of XL1-Blue cells as a control. The solutions were mixed gently and incubated on ice for 30 minutes followed by a 45-second heat shock at 42 °C and cooled on ice for 2 minutes. 1

ml of SOC medium pre-heated at 42 °C was added into each tube and the tubes were incubated at 37 °C with vigorous shaking (225-250 rpm) for 1 hour. The transformation mixtures were then centrifuged to remove excess medium and less than 200 µl of each mixture was plated on LB agar plates with appropriate antibiotics. For the pUC18 control reaction, 100 µl of transformation mixture was plated on LB-ampicillin agar plates.

6.2.10 Plasmid preparation by alkaline lysis

Solutions required for performing the plasmid preparation by the alkaline lysis are listed as follow:

Solution 1	50 mM glucose 10 mM EDTA 25 mM Tris-HCl, pH 8.0
Solution 2	0.2 M sodium hydroxide 1% SDS
Solution 3	3 M sodium acetate, pH 4.8 11.5% v/v glacial acetic acid

An agar plate streaked with XL1-Blue cells containing a plasmid with desired mutation was grown at 37 °C overnight. A single colony was transferred into 10 ml LB medium with ampicillin in 37 °C water bath shaker (175-200 rpm) for approximately 4 hours. Cells were then harvested by centrifugation at 12,000 *g* at 4 °C for 30 seconds. The supernatant was aspirated and the pellet was resuspended in 100 µl of ice-cold solution 1 with gentle vortex. 200 µl of freshly made solution 2 was added into the tube and mixed by inverting the tube 5 times and stored on ice. 150 µl of solution 3 was added, the tube vortexed for 10 seconds and stored on ice for 3 to 5 minutes. The tube was then centrifuged at 12,000 *g* at 4 °C for 5 minutes, and the supernatant was transferred to a new Eppendorf tube. dsDNA was precipitated out with two volume equivalents of pure ethanol (analytical grade) at room temperature, vortexed and allowed to stand for 2 minutes. It was then centrifuged at 12,000 *g* at 4 °C for 5 minutes. After the

supernatant was discarded, the pellet was rinsed with 1 ml of ice-cold 70% ethanol and the pellet was dried for 10 minutes in a sterile laminar hood. The dsDNA pellet was rehydrated in 30 µl of sterile water at 4 °C overnight and stored at -20 °C. Alternatively, the plasmid was further purified (Section 6.2.11).

6.2.11 Plasmid purification by RNA removal and phenol/chloroform protein extraction

A 10 mg/ml RNAse solution was made by dissolving pancreatic RNAse in a buffer containing 10 mM Tris-HCl buffer at pH 7.5 and 15 mM NaCl. The solution was then incubated at 100 °C for 15 minutes and allowed to cool to room temperature slowly. 1 µl of this RNAse solution was added into 30 µl of the DNA solution obtained by the alkaline lysis method (Section 6.2.10) and incubated at 37 °C for 1 hour. 70 µl of ddH_2O was then added, together with 1/8 volume of 2 M potassium acetate. 100 µl of phenol and 100 µl chloroform:isopropanol solution were added and the mixture was centrifuged at 12,000 *g* for 5 minutes. The aqueous layer was then transferred into a new tube with 100 µl chloroform:isopropanol and 100 µl phenol and centrifuged again. The aqueous layer was transferred into a tube containing 2 volumes of cold ethanol, incubated on ice for 10 minutes and centrifuged at 12,000 *g* at 4 °C for 10 minutes. The DNA was precipitated out to form a pellet. The pellet was rinsed with 70% ice-cold ethanol and dried in a sterile laminar hood. Finally, the purified DNA pellet was rehydrated in 10 µl sterile water and stored at -20 °C.

6.2.12 Plasmid preparation by Purelink™ Quick Plasmid Miniprep Kit

Alternatively, plasmids were prepared using Purelink quick plasmid miniprep kit (Invitrogen). According to the protocol, 5 ml of overnight culture of *E. coli* BL21 (DE3) were pelleted by centrifugation. The pellet was then resuspended in 250 µl resuspension

buffer (R3) with RNase. 250 µl of the lysis buffer (L7) was added and mixed well by inverting 5 times. The tube was incubated at room temperature for 5 minutes before 350 µl of the precipitation buffer (N4) was added. The solution was mixed thoroughly to homogeneity, and the lysis debris was removed by centrifugation at 12,000 *g* for 10 minutes at room temperature. The supernatant was loaded onto a spin column.

For plasmid clean up, the spin column containing the supernatant was placed into a wash tube and centrifuged at 12,000 *g* for 1 minute. The flow through was discarded, and 500 µl of the wash buffer (W10) with ethanol was added to the column to wash the remaining lysis solution. The plasmid was washed again with 700 µl wash buffer (W9) with ethanol and then centrifuged to remove any residual wash buffer (W9).

The plasmid DNA was then eluted with TE buffer. The spin column was placed into a recovery tube and 75 µl of preheated TE buffer (65-70 °C) was added to the centre of the column. The column was incubated for 1 minute at room temperature, followed by centrifugation at 12,000 *g* for 2 minutes. The recovering tube contained the purified plasmid, which was stored at -20 °C for downstream applications. The plasmid concentration was quantified using a Nano-Drop spectrophotometer (Section 6.3.1.2). The purity of the pGV5A plasmid and its derivatives was tested by electrophoresis (Section 6.2.13).

6.2.13 Agarose gel electrophoresis

Reagents required for agarose gel electrophoresis is listed below:

Loading dye	30% v/v glycerol 0.25% w/v bromophenol blue 0.25% w/v xylene cyanol
TAE buffer	40 mM Tris-acetate, pH 8.0 1 mM EDTA

An agarose gel was made by melting 1.5% w/v agarose in 30 ml of TAE buffer, cooled down to about 50 °C and poured into a gel casting tray with the comb inserted. The gel was left to set for at least 30 minutes. When set, the comb was removed and the tray was transferred into a gel tank containing ice-cold TAE buffer. DNA fragments were mapped on a 1.5% w/v agarose gel against a 1 kb+ ladder, by adding 8 µl DNA solution with 2µl loading dye into each well. The gel was run at 80 V for approximately one hour, until the loading dye nearly reached the bottom of the gel. The gel was then stained with 0.5 mg/ml ethidium bromide for 30 minutes and DNA fragments were visualised under UV radiation in a CHEMI GENIUS bio-imaging system (Syngene).

6.2.14 DNA sequencing

DNA sequencing was carried out at the Genomics Unit in University of Auckland. Plasmids obtained by mutagenesis which contained the mutated *pykF* gene were quantified using a Nano-Drop spectrophotometer with the purity checked. Approximately 200 ng/µl of purified plasmid in sterile water was prepared for sequencing. Each reaction required 5 µl of such plasmid as the DNA template. The sequencing reactions were carried out using BigDye dye terminator version 3.1 on a 9700 thermal cycler (Applied Biosystems) with T7 and T3 primers. Fragments were separated by a 3130XL capillary sequencer (Applied Biosystems) by capillary electrophoresis.

6.2.15 Transforming BL21 (DE3) cells by the calcium chloride method

6.2.15.1 $CaCl_2$ solution

A 1 M $CaCl_2$ solution was sterilised by filtering through a 0.22 µm syringe driven filter unit and stored in 10 ml aliquots at -20 °C. Upon usage, the calcium chloride stock solution was diluted 10 fold using distilled water and filtered. The solution was then stored on ice.

6.2.15.2 $MgCl_2$-$CaCl_2$ solution

8 ml of a 1 M $MgCl_2$ stock solution and 2 ml of a 1 M $CaCl_2$ solution were mixed and diluted 10 times. The solution was then filtered and chilled on ice.

6.2.15.3 Preparation of competent cells

BL21 (DE3) cells were streaked onto an LB plate and incubated at 37 °C overnight. A colony (2-3 mm) was transferred into a 1 litre flask containing 100 ml sterilised LB medium. The flask was then incubated in a 37 °C water bath with vigorous shaking (200-225 rpm) until the OD_{600} reached 0.4. The cells were then transferred into sterile 50 ml Falcon tubes and incubated on ice for 10 minutes. Cells were centrifuged at 2,700 *g* at 4 °C for 10 minutes and the supernatant was discarded. The pellets were drained and resuspended in 30 ml ice-cold $MgCl_2$-$CaCl_2$ solution by gentle vortexing and then centrifuged. Finally, the pellets were resuspended in 2 ml of ice-cold calcium chloride solution for each 50 ml of bacterial culture (cells are now competent) and stored in 200 µl aliquots at -80 °C.

6.2.15.4 Transformation

200 µl of competent BL21 (DE3) cells were thawed on ice. 50 ng of plasmid DNA in a volume of 10 µl or less was added, mixed by swirling and kept on ice for 30 minutes. Subsequently, cells were heat-shocked at 42 °C for 90 seconds and cooled on ice for 2 minutes. 800 µl SOC medium was then added into each tube and incubated at 37 °C for 45 minutes with slow shaking (150 rpm). The cell culture was centrifuged to remove excess medium, and less than 200 µl of cell culture was plated onto a LB plate with ampicillin.

6.3 Biochemistry general methods

Enzymes were stored at -20 °C in 100 µl aliquots. All enzymes were manipulated at 4 °C or kept on ice, unless otherwise stated. Centrifugation was carried out in an Eppendorf centrifuge 5810 R (maximum speed 12,000 rpm) using an EL082 rotor for small scale

(≤1.5 ml), or a DL091 rotor (maximum speed 6,000 rpm) for larger scale (<50 ml) centrifugations. Alternatively, swing rotor A-4-81 (maximum speed 4,000 rpm) was used for cell harvesting (<400 ml). All centrifugations for protein purification were performed at 4 °C. Protein purification was carried out in several chromatography columns using an AKTA purifier system (Amersham Biosciences) at 4 °C. Frac-950 fraction collector (Amersham) with 96-well plates was used for fraction collection. SDS-PAGE was carried out with a Bio-Rad gel electrophoresis unit using Bio-Rad 300 power pack. pH of all solution was measured using a standard pH meter equipped with an UltraBasic electrode (type number 300729.1).

6.3.1 Determination of protein concentration

6.3.1.1 Bio-Rad protein assay

Bio-Rad protein assay, which was based on the method of Bradford (Bradford 1976), was used to determine the protein concentrations in each purification step. The microassay procedure was performed. Firstly, 5 dilutions of a BSA protein standard were prepared within the linear range of the assay (1.2-10.0 μg/ml). 800 μl of each the diluted BSA solution and the protein sample solution were added into 200 μl of the protein assay dye reagent concentrate (Bio-Rad) in a cuvette and mixed thoroughly. The solutions were then incubated at room temperature for exactly 10 minutes for the time-dependent colour development of the dye. Absorbance at 595 nm was measured in a Hewlett Packard diode array spectrophotometer (model 8452A), and compared to the calibration curve. 800 μl of distilled water was added into the cuvette instead of the protein sample to serve as a blank. Protein samples were assayed in duplicate.

6.3.1.2 Spectrophotometry

Pure protein solutions in 20 mM Tris buffer were quantified by measuring absorbance at 280 nm using a Nano-Drop ND-1000 UV-Vis spectrophotometer. Fluorescently labelled protein (Section 6.5.4) was quantified by performing a wavelength scan from 800 nm to 200 nm in a UV-Vis spectrophotometer.

6.3.2 NuPAGE® SDS-PAGE (Poly-Acrylamide Gel Electro-phoresis)

The reagents used in the sample preparation are listed:

Reagent	Reduced Sample
Sample	x µl
Sample Buffer (4x)	2.5 µl
Reducing Agent (10x)	1 µl
Deionised water	up to 6.5 µl
Total Volume	**10 µl**

The NuPAGE® MOPS SDS running buffer contains reagents listed as follow:

Reagent	Concentration
MOPS	50 mM
Tris Base, pH 7.7	50 mM
SDS	0.1%
EDTA	1 mM

The reagents for Stain and destain solutions are listed:

Coomassie blue stain	1% w/v Coomassie blue 50% v/v methanol 10% v/v glacial acetic acid
Destain	5% v/v methanol 10% v/v glacial acetic acid

Samples were heated in a 70 °C water bath for 10 minutes and cooled on ice. An SDS-PAGE gel chamber was set with a NuPAGE® 10-well 4-12% Bis-Tris gel (Invitrogen) and filled with MOPS SDS running buffer. 10 µl of each sample was loaded into the well, with 5 µl of Novex® sharp pre-stained protein standard (3.5-260 kDa) loaded in the first well. Electrophoresis was run at 200 V (constant) for 50 minutes. The gel was then

stained with Coomassie blue stain for 30 minutes and destained in the destain solution overnight. Finally, the gel was visualized in the CHEMI GENIUS bio-imaging system (Syngene).

6.3.3 Over-expression and purification of the wild-type and mutant PK1 enzymes

6.3.3.1 Growth of E. coli *BL21 Star™ (DE3) with pGV5A and its derivatives*

Crude extract buffer
1 mM EDTA
2 mM Mercaptoethanol
10 mM Tris, pH 8.5 at 4 °C
100 mM KCl
10 mM $MgCl_2$

Glycerol freeze cultures of *E. coli* BL21 (DE3) containing pGV5A and its derivatives were streaked onto LB plates with appropriate antibiotics and incubated at 37 °C overnight. For each strain, a single colony was used to inoculate 10 ml LB broth with antibiotics and incubated in a 37 °C water bath shaker with moderate shaking (175-200 rpm) for at least 4 hours. This culture was used to inoculate 1 litre of LB medium, which was then incubated at 37 °C for 20 hours (with shaking). 0.16 mM of isopropylthio-β-D-galactoside (IPTG) was added into the culture 3 hours prior to harvest to induce protein expression. Cells were harvested by centrifugation at 4,000 *g* at 4 °C for 15 minutes. The supernatant was discarded and the cell pellet was resuspended in the crude extract buffer and centrifuged again to wash off the residual LB. Finally, the cell pellet was suspended in 40 ml of ice-cold crude extract buffer.

6.3.3.2 Purification of PK1 from E. coli *BL21 (DE3)*

The protocol for the purification of PK1 from BL21 (DE3) was adapted from the procedure used by Mattevi and colleagues (Mattevi *et al.* 1996) and involved ion-exchange, hydrophobic interaction and size-exclusion chromatography to obtain pure and functional

enzymes.

6.3.3.3 Preparation of cell free crude extract by ultrasonication

Cells suspended in crude extract buffer were sonicated for 5 minutes using the Sonics cell vibrates amplifier in cycles of 1 second bursts and 2 seconds pauses. Sonication was performed on ice. The solution was then centrifuged at 6,000 *g* for 15 minutes to precipitate cell debris. The supernatant containing soluble protein was collected.

6.3.3.4 Ion exchange chromatography

Ion-exchange buffer A	1 mM EDTA 2mM Mercaptoethanol 10 mM Tris, pH 8.5 at 4 °C 100 mM KCl
Ion-exchange buffer B	1 mM EDTA 2mM Mercaptoethanol 10 mM Tris, pH 8.5 at 4 °C 500 mM KCl

The supernatant collected from the ultrasonication was loaded on to a Q-sepharose ion exchange column (bed volume 106 ml, 2.6 × 20 cm) that had been pre-equilibrated with 200 ml of ion-exchange buffer A. The column was then washed with 100 ml of buffer A and the enzyme was eluted with ion-exchange buffers A and B in an increasing salt gradient (100-500 mM KCl). Eluted fractions were collected and the UV peaks were tested for PK1 activity using a LDH-coupled assay (Section 6.4.1). All the active fractions were pooled and tested by SDS-PAGE (Section 6.3.2).

6.3.4.5 Phenyl-Sepharose chromatography

Pooled fractions of protein sample from the ion-exchange column were pre-equilibrated with 1.17 M ammonium sulphate before the hydrophobic-interaction chromatography was performed.

Phenyl-Sepharose buffer A	1 mM EDTA 2 mM Mercaptoethanol 50 mM Tris, pH 7.5 at 4 °C 100 mM KCl 1.17 M $(NH_4)_2SO_4$
Phenyl-Sepharose buffer B	1 mM EDTA 2 mM Mercaptoethanol 50 mM Tris, pH 7.5 at 4 °C 100 mM KCl

The phenyl-Sepharose column (bed volume 80 ml, 2.6 × 15 cm) was pre-equilibrated with 160 ml of phenyl-Sepharose buffer A. After the solution had been loaded on to the column, 80 ml of buffer A was used to wash the column and then the enzyme was eluted with increasing phenyl-Sepharose buffer B in a decreasing concentration of ammonium sulphate 1.17-0 M. Again, the fractions with high UV absorbance were tested for activity (Section 6.3.1) and the SDS-PAGE (Section 6.3.2).

6.3.4.6 Gel filtration chromatography

Buffer containing 10 mM Tris (pH 7.5) and 1 mM EDTA and 2 mM β-mercaptoethanol at 4 °C was used as the gel filtration buffer.

A Hi-Load Superdex 200 column (bed volume 120 ml, 60 × 1.6 cm) pre-equilibrated with the gel filtration buffer was used as the size-exclusion column. Up to 2 ml (maximum amount of protein 50 mg) of pre-concentrated pooled sample from the previous purification step (Section 6.3.3) was loaded onto the column and eluted. Finally, the activity assay and SDS-PAGE were performed on the eluted fractions.

6.4 Kinetic study

6.4.1 LDH coupled activity assay

A LDH-coupled activity assay (Malcovati & Valentini 1982) was used to test the activity of fractions collected in the protein purification procedure. The LDH catalysed reaction is illustrated:

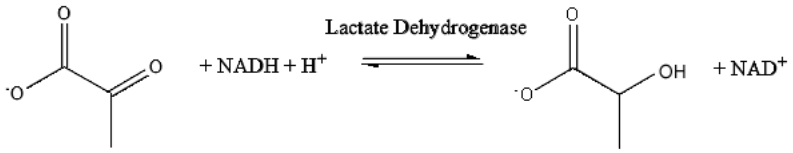

Pyruvate Lactate

The reaction was initiated by the addition of 10 µl from the eluted fractions into the assay mixture, which had been pre-incubated at 30 °C for 10 minutes. Activity was measured by monitoring the decrease of NADH absorbance at 340 nm, which was caused by the reaction between NADH and pyruvate, catalysed by LDH, producing NAD^+ and lactate. The decrease of NADH corresponded to PK1 activity. 1 unit of PK1 enzymatic activity (U) was determined to be 1 µmole NADH per second per mg of enzyme.

The reagents for carrying out the LDH-coupled activity assay are listed as follow:

	[Initial] (mM)	**Volume (µl)**	**[Final] (mM)**
Hepes (pH 7.5)	100	100	10
KCl	500	100	50
$MgCl_2$	100	100	10
PEP	200	10	2
ADP	200	10	2
FBP	200	10	2
NADH	12	10	0.12
LDH		10	22 (unit/cell)
ddH_2O		640	
Total volume		**990**	

6.4.2 Steady state kinetic study of PK1 wild-type and the mutants

Steady state kinetics of the enzyme was performed by the same LDH coupling assay method as did for activity test (Section 6.4.1). The reaction mixture contained 10 mM Hepes at pH 7.5, 50 mM KCl, 10 mM $MgCl_2$, 22 unit/ml LDH, 0.12 mM NADH and varying amount of PEP, ADP and FBP. Five sets of conditions were examined, so as to determine the mutation effects on PEP binding, ADP binding and FBP regulation. Firstly, enzymatic activity was measured in the presence of 2 mM FBP, 2 mM ADP and varying concentrations of PEP. Secondly, the assay was performed with 2 mM FBP, 2 mM PEP and varied amount of ADP. The above two assays were then performed with the absence of FBP. Finally, FBP titration experiments were performed at fixed 2 mM PEP and ADP. Each reaction mixture was incubated in 30 °C water bath for 10 minutes. The reaction was initiated by addition of enzyme. The total volume of reaction solution (including the enzyme) was 1 ml.

6.5 Biophysical methods

6.5.1 Mass spectrometry

Mass spectrometry was performed in the Bio21 Molecular Science and Biotechnology Institute, University of Melbourne, Australia, using an Agilent 6510 LC/Q-TOF mass spectrometer with an electrospray ionising (ESI) source coupled to an Agilent 1100 LC system (Agilent, Palo Alto, CA). Data were collected and processed with the program Mass Hunter (Agilent).

The enzyme was directly injected (5 µl) into the mass spectrometer at various time points with 25% *v/v* acetonitrile in water with 0.1% *v/v* formic acid at 0.25 ml/min. Mass spectrometric data were collected using the Agilent 6510 LC/Q-TOF mass spectrometer

with an electrospray ionising (ESI) source coupled to an Agilent 1100 LC system (Agilent, Palo Alto, CA). All data were acquired and reference mass corrected *via* a dual-spray ESI source. Each scan or data point on the total ion chromatogram was an average of 10,000 transients, producing a scan every second. Spectra were created by averaging the scans across each peak. Data for the enzyme without inhibitor were also collected. The conditions for the mass spectrometer were**:** positive mode; drying gas flow was 7 l/min; nébuliser was 30 psi; drying gas temp was 300 °C; Vcap was set to 3000 V; the fragmentor was set to 225 V; the skimmer was set to 60 V; the OCT RFV was 750 V; and the scan range acquired was 100-2500 m/z.

6.5.2 Circular dichroism spectroscopy (CD)

Circular dichroism (CD) spectra of the wild-type and the mutant PK1 enzymes were recorded on a Jasco-815 CD spectropolarimeter in a rectangular quartz cuvette with 0.2 cm path length. Protein samples with appropriate ligands were dissolved in 10 mM sodium phosphate buffer at pH 8.0 (CD buffer).

6.5.2.1 Sample preparation

Wild-type PK1 and its mutants kept in Tris buffer were run through a HiTrap™ 5 ml desalting column (GE Healthcare Life Science) for buffer exchange to phosphate buffer. CD buffer was degassed for one hour in prior, as oxygen was an UV light quencher (Greenfield 2006). Protein samples were concentrated to approximately 1.0 mg/ml, with concentration accurately determined by a Nano-Drop spectrophotometer with published molar extinction coefficient of pyruvate kinase. This stock solution was then diluted for CD measurement.

6.5.2.2 CD Experiment

Before starting theinstrument, the optics compartment was flushed with nitrogen for 15-20 minutes as to remove the oxygen. Subsequently, CD spectra were done by UV scanning from 250 nm to 185 nm, with 0.5 nm bandwidth and 1 second intervals, and accumulated

for 131 seconds. Data were stored every second in wavelength (nm) versus millidegree (θ, mdeg). Simultaneously, a wavelength scan was performed in order to monitor the absorbance. Cells were rinsed thoroughly with ethanol and distilled water between experiments. Data were processed using SELCON3, CONTIN-LL and CDSSTR programs from DICHROWEB online analysis using reference data 7 (Whitmore & Wallace 2004).

6.5.3 Analytical ultracentrifugation (AUC)

Sedimentation velocity experiments of the wild-type and mutated PK1 enzymes were performed using an Optima™ XL-I analytical ultracentrifuge (Beckman-Coulter) equipped with absorption optical scanner (ABS). 20 mM Tris (pH 8.0) with 50 mM KCl was used as the AUC buffer. Addition of KCl to the buffer increased ionic strength thus prevented the primary charge effect, which is caused by long range electrostatic interactions (Schuck *et al.* 2002). Protein samples at 1.0 mg/ml and 0.1 mg/ml were examined. Centrifuge cells with Epon double-sector centrepieces and quartz windows were assembled before each experiment. 380 µl of sample and 400 µl of the reference solution (buffer) were loaded into the cells pre-tightened to 120 psi.

To optimise wavelength selection for the high speed centrifugation, an initial wavelength scan was performed at 3,000 rpm and 20 °C between 200-300 nm. Sedimentation velocity experiments were then performed at 35,000 rpm for 120 scans, and the data was recorded at step size 0.001 cm. Data were processed by SEDFIT software (which can be downloaded from www.analyticalultracentrifugation.com) using *c(s)* distribution analysis (Schuck 2000). SEDNTERP software was used for calculating the protein partial-specific volumes and extinction properties, as well as buffer density and viscosity. Graphs were drawn using Origin software (OriginLab, version 8E).

6.5.4 AUC-FDS: Analytical ultracentrifugation coupled with fluorescence detection system

Confocal fluorescence optics (Aviv Biochemical) was integrated into a Beckham Coulter Optima™ XL-1 analytical ultracentrifuge (Beckham-Coulter) the for fluorescence detection experiments. Centrifuge cells were assembled before each experiment from aluminium cell housing, a sapphire window, and an Epon two-sector centrepiece.

6.5.4.1 Protein labelling

Pure protein samples stored in Tris buffer were buffer exchanged with 0.1 M sodium bicarbonate (pH 8.3) and concentrated to about 2.0 mg/ml, as recommended in amine-reactive probe (Invitrogen).

Approximately 10 ml of acetonitrile (CH_3CN) was dehydrated using molecular sieves (3 Å beads, 4-8 mesh, Sigma-Aldrich) by pouring acetonitrile over the beads and left in the dark for 20 minutes. 1 mg of Alexa Fluor® 488 succinimidyl ester dye (Invitrogen) was centrifuged briefly to move all the dye to the bottom of the vial and added with 1 ml dehydrated acetonitrile. Various volumes of this dye suspension in acetonitrile were aliquotted into Eppendorf tubes, so that a 1:1 molar ratio of protein to dye was made. Specific volumes of the dye suspension solution required by each protein sample for the labelling are listed as follow:

	MW (Da)	**[protein]** [mg/ml]	**Volume** (ml)	**M** (mole/ml)	**Volume dye** (µl)
Wild-type	50729.3	2.36	0.8	4.652×10^{-5}	26
A301T	50759.3	1.42	0.8	2.798×10^{-5}	16
A301S	50745.3	2.65	1.0	5.222×10^{-5}	36
G381A	50743.3	0.30	1.0	5.912×10^{-6}	4.2

Acetonitrile in the tubes with the required amount of dye suspension for each protein was evaporated. Protein samples in 100 mM Na_2CO_3 buffer (pH 8.3) were then added and

mixed gently. The protein-dye solution was incubated on ice in the dark for 2 hours to allow the labelling reaction to proceed. The resulting solution had a fluorescent bright green colour.

A Sephadex G-25 column (bed volume 24 ml, 30 × 1.0 cm) was used for separating the labelled protein from the dye. The column was pre-equilibrated with 20 mM Tris, pH 8 and 50 mM KCl. The protein conjugated to the dye was separated from unreacted protein by monitoring the eluted fractions with UV at 280 nm (for unlabelled protein) and 495 nm (for labelled protein and the dye). Fractions with the labelled protein were collected in 1.5 ml Eppendorf tubes and pooled. The protein concentration was checked by measuring the absorbance of the protein-dye conjugate at 280 nm (A_{280}) and at the absorbance maximal wavelength (λ_{max}) for the dye (A_{max}). The λ_{max} for Alexa Fluor 488 dye is 495 nm (amine-reactive probes, Invitrogen). Corrected protein absorbance for the contribution of the dye to the absorbance at A_{280} was calculated as follows:

$$A_{protein} = A_{280} - A_{max} \times (CF),$$

where CF is ($A_{280\ free\ dye}/A_{max\ free\ dye}$). CF for the Alexa Fluor® 488 dye is 0.11, as listed in the appendix of the amine-reactive probes (Invitrogen).

The protein concentration ([protein]) was then calculated:

$$[Protein] = A_{protein} \times \epsilon_{protein},$$

where $\epsilon_{protein}$ is the extinction coefficient of *E. coli* PK1 at 280 nm and protein concentration is in mg/ml. $\epsilon_{protein}$ is 0.147 (without disulfides).

Degree of labelling (D.O.L) was calculated:

$$DOL = A_{max} \times MW / [protein] \times \epsilon_{dye},$$

where MW is the molecular weight of the protein, ϵ_{dye} is the extinction coefficient of the dye at its absorbance maximum and protein concentration is in mg/ml. ϵ_{dye} for Alexa Fluor® 488 dye is 71,000 as listed in the appendix of the Invitrogen amine-reactive probes.

Protein concentrations and degrees of labelling of Alexa Fluor® 488 dye labelled proteins are listed as follow:

	A_{280}	A_{max}	$A_{protein}$	[protein] (mg/ml)	DOL
Wild-type	0.3374	0.5621	0.276	1.875	0.214
A301T	0.3340	0.4599	0.283	1.928	0.171
A301S	0.6305	1.3303	0.484	3.294	0.289
G381A	0.0801	0.0412	0.076	0.514	0.057

6.5.4.2 AUC-FDS performance

350 µl of each sample comprising Alexa Fluor® 488 dye-labelled PK1 was initially centrifuged at 3,000 rpm and then 40,000 rpm at 20 °C. 50 µl heavy mineral oil and 2 µl light mineral oil, which included 0.1% bodipy fluorescent dye, were added into the cells in order to define the boundaries (meniscus of the solvent and bottom of the cell). 200 radial scans were collected continuously. Data were collected between 5.8 and 7.2 cm at 0.002 cm increments and represented the average of five scans. The excitation beam (488 nm output from a frequency-doubled 13 mW CW solid-state laser) was positioned directly above the sample and directed confocally to a small spot beneath the sapphire window. The sample emission was also recorded from directly above, reaching the photomultiplier tube (PMT) after passing through a dichronic mirror (to eliminate reflected excitation) and 505 nm cut-off filter (MacGregor *et al.* 2004). Sedimentation velocity data were analysed according to a continuous size distribution model using the program SEDFIT.

The AUC-FDS logsheet with protein name and location in the rotor, cell content and FGA gains specified is shown below:

Cell	Sample (mg/ml)	Volume (µl)	Light oil (µl)	Heavy oil (µl)	FGA Gains
1	Counter balance				
2A	G381A, 0.103	350	2	50	1×
2B	A301T, 0.096	350	2	50	63%
3A	G381A, 0.0103	350	2	50	2×
3B	A301T, 0.0096	350	2	50	84%
4A	G381A, 0.00103	350	2	50	8×
4B	A301T, 0.00096	350	2	50	90%
5	Counter balance				
6A	A301S, 0.103	350	2	50	1×
6B	Wild-typ, 0.1042	350	2	50	63%
7A	A301S, 0.0103	350	2	50	2×
7B	Wild-type, 0.01042	350	2	50	84%
8A	A301S, 0.00103	350	2	50	8×
8B	Wild-type, 1.00042	350	2	50	90%

AUC-FDS was performed at a lower concentration at 0.0005 mg/ml for the wild-type enzyme and enzymes with A301T and A301S mutations. Ovalbumin at 0.1 mg/ml was added into the AUC-FDS buffer to stabilise the enzymes. The sample volume and the amount of light oil (with 0.1% bodipy fluorescent dye) and heavy oil added was identical to those in the logsheet shown below, with the FGA gains set at 8 × 95%.

6.6 X-ray crystallography

Hanging drop vapour-diffusion method with conditions specified in the work done by Mattevi and colleagues (1995) was used in this study. 5 µl protein solution and 5 µl reservoir solution was pipetted onto the cover slide, without mixing. 500 µl of reservoir solution was used in each well.

Reservoir solution:

MES/NaOH, pH 6.2	100 mM
$MgSO_4$	100 mM
KCl	10 mM
NaN_3	0.02% (w/v)
PEG 8000	16% (w/v)

Protein solution:

Purified enzyme	10 mg/ml
Tris-HCl, pH 7.5	10 mM
β-mercaptoethanol	2 mM

For the mutated enzymes, robotic crystallisation screening was performed at Bio21 collaborative crystallisation centre, Melbourne, Australia, using sitting-drop method. A pH-, anion- and cation-testing (PACT) screen was performed, and diffraction trials were performed using beamline 3BM1 at the Australian synchrotron.

6.7 References

Bradford MM. 1976. A rapid and sensitive method for the quantitation of microgram quantities of protein utilizing the principle of protein-dye binding. *Anal Biochem* 72:248-54

Greenfield NJ. 2006. Using circular dichroism spectra to estimate protein secondary structure. *Nat Protoc* 1:2876-90

MacGregor IK, Anderson AL, Laue TM. 2004. Fluorescence detection for the XLI analytical ultracentrifuge. *Biophys Chem* 108:165-85

Malcovati M, Valentini G. 1982. AMP- and fructose 1,6-bisphosphate-activated pyruvate kinases from *Escherichia coli*. *Methods Enzymol* 90 Pt E:170-9

Mattevi A, Bolognesi M, Valentini G. 1996. The allosteric regulation of pyruvate kinase. *FEBS Lett* 389:15-9

Niesen FH, Berglund H, Vedadi M. 2007. The use of differential scanning fluorimetry to detect ligand interactions that promote protein stability. *Nat Protoc* 2:2212-21

Sambrook J, Russell DW. 2001. *Molecular cloning: A laboratory manual*: Cold Spring Harbor, N.Y. : Cold Spring Harbor Laboratory Press

Schuck P. 2000. Size-distribution analysis of macromolecules by sedimentation velocity ultracentrifugation and lamm equation modeling. *Biophys J* 78:1606-19

Schuck P, Perugini MA, Gonzales NR, Howlett GJ, Schubert D. 2002. Size-distribution analysis of proteins by analytical ultracentrifugation: strategies and application to model systems. *Biophys J* 82:1096-111

Whitmore L, Wallace BA. 2004. DICHROWEB, an online server for protein secondary structure analyses from circular dichroism spectroscopic data. *Nucleic Acids Res* 32:W668-73